

Université de Montréal

**The *C. elegans* primordial germline:  
a robust syncytial precursor for a thriving expansion**

*Par*

Jack Bauer

Programme de Biologie Moléculaire, Institut de recherche en immunologie et en  
cancérologie (IRIC), Faculté de Médecine

Thèse présentée en vue de l'obtention du grade de doctorat en Biologie Moléculaire  
option Biologie des Systèmes

Septembre 2021

© Jack Bauer, 2021



Université de Montréal

Programme de Biologie Moléculaire, Institut de recherche en immunologie et en  
cancérologie (IRIC), Faculté de Médecine

*Cette thèse intitulée*

**The *C. elegans* primordial germline: a robust syncytial precursor for a thriving  
expansion**

*Présentée par*

**Jack Bauer**

*A été évaluée par un jury composé des personnes suivantes*

**Marc Therrien**

Président-rapporteur

**Jean-Claude Labbé**

Directeur de recherche

**Alisa Piekny**

Membre du jury

**Lynn Cooley**

Examineur externe



## Résumé

La cellule est l'unité à la base de la vie. Elle est généralement délimitée par sa membrane et contient un noyau et du cytoplasme en plus d'autres composantes. Les cellules se divisent afin de maintenir et de perpétuer la vie par duplication de leur matériel génétique et par leur séparation en deux cellules physiquement distinctes durant la cytokinèse. Cependant, la division cellulaire est parfois modifiée et aboutit à la formation d'un tissu contenant plusieurs noyaux bordés d'une membrane unique appelé syncytium. Les syncytia sont fréquemment retrouvés chez les organismes vivants, bien que leurs fonctions et mode de formation restent peu compris. L'organisation en syncytium est conservée chez tous les animaux étudiés à ce jour au niveau de la lignée germinale dans laquelle les cellules partagent un cytoplasme commun par l'intermédiaire d'un pont intercellulaire stable. Dans la majorité des lignées germinales étudiées, les cellules sont directement connectées l'une à l'autre par un pont intercellulaire stable qui émerge de cytokinèses incomplètes. Cependant, certaines lignées germinales sont organisées autour d'une cavité commune à laquelle chaque cellule germinale est connectée. Dans ces lignées germinales, les mécanismes qui mènent à l'expansion du syncytium sont peu compris.

Ma thèse décrit l'utilisation de la lignée germinale primordiale de *C. elegans* à son premier stade larvaire pour mieux comprendre l'organisation, l'expansion et la fonction des lignées germinales syncytiales. En utilisant la microscopie électronique et confocale, j'ai découvert que l'organisation du syncytium est fixée au premier stade larvaire. En effet, les deux cellules germinales primordiales (CGP) sont chacune individuellement connectée à une cavité cytoplasmique centrale par le biais de ponts intercellulaires stables. Nous avons nommé cette cavité le proto-rachis car l'organisation des CGP est identique à l'organisation de la gonade adulte. Chez l'adulte, les ponts intercellulaires qui connectent les cellules germinales au rachis sont stabilisés par des régulateurs d'actomyosine. Nous avons vérifié si cela était également le cas dans la gonade au premier stade larvaire. Tous les régulateurs présents dans la gonade adulte, sont aussi présent dans les ponts intercellulaires des CGP, mais la lignée germinale primordiale est

réfractaire à la perturbation de la fonction de ces régulateurs. Ce résultat suggère que les régulateurs d'actomyosine sont organisés de manière très stable au premier stade larvaire.

Afin de mieux comprendre comment le syncytium se développe dans la lignée germinale de *C. elegans*, j'ai ensuite suivi la première division des CGP par microscopie à temps réel. J'ai mis en évidence que l'anneau de cytokinèse se stabilise, puis se déplace vers le proto-rachis jusqu'à qu'il s'y intègre. Ces résultats indiquent que le syncytium se développe par cytokinèse incomplète. De plus, mes résultats montrent que la connexion au proto-rachis est maintenue durant la division des CGP. C'est pourquoi nous proposons un modèle pour l'expansion du syncytium dans lequel l'anneau de cytokinèse stabilise pour connecter une des cellules filles au proto-rachis, tandis que l'autre cellule fille est connecté par l'anneau stable qu'elle aura hérité de la cellule mère. Enfin, pour s'assurer que les mécanismes d'expansion du syncytium observés durant la division des CGP sont conservés au cours du développement de la gonade, j'ai conceptualisé et créé un dispositif de micro-fluidique qui en théorie permettrait de suivre plusieurs séries de division des CGP.

En somme, mon travail de doctorat a fourni une caractérisation détaillée de la structure du syncytium dans la lignée germinale de *C. elegans* au premier stade larvaire, ainsi qu'un modèle pour l'expansion du syncytium. Mes découvertes indiquent que malgré des différences dans l'organisation des syncytia, la cytokinèse incomplète est un mécanisme conservé dans toutes les lignées germinales animales. Des travaux futurs seront nécessaires pour découvrir quelles voies de signalisation moléculaires sont sous-jacentes aux mécanismes de formation des syncytia, et ainsi de mieux comprendre quelle est la fonction de ces structures fascinantes.

**Mots-clés :** Syncytium, lignée germinale, Développement de *C. elegans*, pont intercellulaire stable, cytokinèse, cellules germinales primordiales, actomyosine

## Abstract

The cell constitutes the basic unit of life. It is generally delimited by its membrane and contains a nucleus and cytoplasm amongst other components. To maintain and perpetuate life, cells divide by duplicating their genetic material, and by physically separating into two distinct cells during the process called cytokinesis. However, cell division is sometimes modified and leads to the formation of a tissue in which several nuclei are delimited by a single membrane, called a syncytium. Syncytial tissues are common amongst living organisms, but why and how they form remains unclear. The syncytial architecture is conserved in all studied animal germlines where germ cells share a common cytoplasm through stable intercellular bridges. In most animal germlines, the germ cells are directly connected with one another, and the stable intercellular bridges that connect the cells are known to arise from regulated incomplete cytokinesis. However, some germlines are organized around a central common cavity to which each germ cell is connected. In such germlines, the mechanisms of syncytium expansions remain unknown.

My thesis describes the use of the *C. elegans* germline primordium at the first larval stage to better understand the organization, the expansion, and the function of germline syncytia. Using electron and confocal microscopy I found that the organization of the syncytium is established at the first larval stage. The two germ cells called the primordial germ cells (PGCs) each connect to a central cytoplasmic cavity through stable intercellular bridges. Because this organization is identical to the adult germline where each germ cell is connected to the central rachis, we termed the cavity between the PGCs proto-rachis. In the adult gonad, the intercellular bridges that connect the germ cells to the rachis are stabilized by actomyosin regulators, so I verified if this was also the case in the first larval stage gonad. All the regulators that localize to adult intercellular bridges were also present between the PGCs, but the primordial germ line is refractory to perturbation of these regulators. This suggests that the actomyosin regulators are organized in a very stable manner in the first larval stage germline.

I next tracked the first division of the PGCs with live imaging to better understand how the syncytium expands in the *C. elegans* germline. I found that the cytokinetic ring stabilizes, then displaces towards the proto-rachis until it integrates into the syncytial structures. This finding suggests the syncytium expands by incomplete cytokinesis. In addition, my results indicate that the connection to the proto-rachis was maintained during PGCs division. We therefore propose a model in which the cytokinetic ring stabilizes and connects one of the daughter cells to the proto-rachis while the other cell is connected through the inherited stable ring from the mother cell. Finally, I designed and created a microfluidic device that in theory would allow us to live image several rounds of PGCs division. This would confirm if the mechanisms of syncytium expansion that we observed during the first division of the PGCs are conserved in further development.

My work has provided a detailed characterization of the syncytial structure in the *C. elegans* germline primordium as well as a model for syncytium expansion. My findings indicate that despite differences in the organization of the syncytium, incomplete cytokinesis is conserved as the mechanism for syncytium expansion in all animal germlines. Further research will be necessary to bring to light the molecular pathways underlying syncytium formation to have a better understanding of the function of these fascinating structures.

**Keywords:** Syncytium, germline, *C. elegans* development, stable intercellular bridge, cytokinesis, primordial germ cells, actomyosin.



# Table of Content

<b>Résumé .....</b>	<b>5</b>
<b>Abstract.....</b>	<b>7</b>
<b>Table of Content.....</b>	<b>9</b>
<b>List of Figures and Tables.....</b>	<b>15</b>
<b>List of abbreviations .....</b>	<b>17</b>
<b>Acknowledgements .....</b>	<b>27</b>
<b>1. Introduction .....</b>	<b>29</b>
<i>1.1 The animal germline, an “immortal” cell lineage that is passed on to the progeny.....</i>	<i>30</i>
1.1.1 Specification of germlines.....	30
1.1.1.1 Specification by preformation in the <i>Drosophila</i> .....	32
1.1.1.2 Specification by induction in the mouse .....	33
1.1.2 Germline development .....	35
1.1.2.1 Germ cell migration and formation of the gonad primordium .....	35
1.1.2.2 Development of the gonad and establishment of germline stem cell.....	38
1.1.3. Gamete production.....	40
1.1.3.1 The <i>Drosophila</i> ovary, an assembly line for oocyte production.....	40
1.1.3.2 The mouse testis .....	43
1.2 Syncytium: cells that share .....	46
1.3 Animal intercellular bridges.....	50
1.3.1 Cytokinesis physically separates daughter cells.....	50
1.3.1.1 Cleavage furrow positioning .....	51
1.3.1.2 Contractile ring assembly and constriction.....	52
1.3.1.3 Midbody formation and abscission.....	53
1.3.2 Somatic syncytia .....	54
1.3.2.1 Intercellular bridges in blastoderm cells of squid <i>Loligo pealei</i> .....	54
1.3.2.1 Intercellular bridges in the epithelial follicle cells of <i>Drosophila</i> .....	56
1.3.3 Germline syncytia .....	57

1.3.3.1 The <i>Drosophila</i> egg chamber .....	57
1.3.3.2 The mouse testis .....	61
1.4 How do syncytia form? .....	64
1.4.1 Endoreplication (Bacteria, fungi, <i>Drosophila</i> embryo).....	64
1.4.1.1 Endocycle in the <i>Drosophila</i> nurse cells .....	64
1.4.1.2 Karyokinesis .....	65
1.4.2 Cell fusion .....	67
1.4.3 Cytokinesis failure.....	68
1.4.3.1 Megakaryocytes .....	68
1.4.3.2 Cardiomyocytes.....	69
1.4.4 Regulated cytokinesis incomplection .....	69
1.4.4.1 Stopping the cytokinetic furrow ingression in the <i>Drosophila</i> ring canals.....	70
1.4.4.2 Blocking abscission in the mouse testis. ....	70
1.5 Function of syncytia in animal tissues .....	73
1.5.1 Synchronous cellular mechanisms.....	73
1.5.2 Cytoplasmic exchange .....	74
1.5.3 Advantages of polyploidy.....	75
1.6 The nematode <i>C. elegans</i> as a model to study syncytium formation .....	77
1.6.1 The <i>C. elegans</i> germline.....	79
1.6.1.1 Germline specification .....	79
1.6.1.2 Germline development .....	80
1.6.1.3 Gamete production.....	83
1.6.2 The <i>C. elegans</i> germline is a syncytium .....	84
1.6.2.1 <i>C. elegans</i> syncytium maintenance.....	85
1.6.2.2 <i>C. elegans</i> syncytium genesis .....	91
1.6.2.3 Advantages of <i>C. elegans</i> to understand syncytial structures .....	94
1. 7 Objectives .....	95
<b>2. Article 1 - The initial expansion of the <i>C. elegans</i> syncytial germ line is coupled to incomplete primordial germ cell cytokinesis.....</b>	<b>97</b>
2.1 Author contributions.....	98
2.2 Abstract .....	99
2.3 Introduction .....	100

2.4 Results .....	103
2.4.1 Each <i>C. elegans</i> PGC possesses a stable intercellular bridge that opens to a common cytoplasmic compartment .....	103
2.4.2 The PGC cytokinetic ring is stabilized and integrates into the proto-rachis at the end of mitosis .....	109
2.4.3 The stable intercellular bridge permits cytoplasmic exchange during PGC cytokinesis .....	113
2.5 Discussion .....	116
2.6 Materiel and methods .....	119
2.6.1 Strains and alleles .....	119
2.6.2 Confocal microscopy.....	119
2.6.3 Bridge diameter and fluorecence intensity measurements .....	120
2.6.4 Fluorecence photobleaching.....	121
2.6.5 Dendra2 photoconversion .....	121
2.6.6 Transmission electron microscopy .....	122
2.7 Supplemental material .....	123
2.7.1 Online supplemental material .....	123
2.7.2 Tables and figures .....	124
2.8 Acknowledgements.....	132
<b>3. Article 2 - The primordial germ line is refractory to perturbations of actomyosin regulator function in <i>C. elegans</i> L1 larvae .....</b>	<b>133</b>
3.1 Author contributions.....	134
3.2 Abstract .....	135
3.3 Description.....	136
3.4 Methods.....	140
3.4.1 <i>C. elegans</i> strain maintenance.....	140
3.4.2 Imaging .....	140
3.4.4 Temperature-sensitive strain upshifts .....	140
3.4.5 dsRNA production.....	141
3.4.6 RNA Interference .....	141
3.4.7 Latrunculin A treatments .....	141
3.5 Supplementary material .....	142

3.6 Acknowledgements.....	143
<b>4. Article 3 - Following <i>C. elegans</i> first larval stage germline development.....</b>	<b>145</b>
4.1 Author contributions.....	146
4.2 Introduction.....	147
4.3 Results and Discussion.....	149
4.3.1 A genetic approach to track PGC divisions.....	149
4.3.2 Trapping worms in a viscous hydrogel for long-term imaging.....	151
4.3.3 Microfluidic chip design and creation for long-term immobilization of L1 animals.....	153
4.4 Material and methods.....	160
4.4.1 <i>C. elegans</i> strains and maintenance.....	160
4.4.2 Imaging and worm measurement.....	160
4.4.3 Hydrogel immobilization.....	161
4.4.4 Microfluidic device design.....	161
4.4.5 Master mold engineering.....	161
4.4.6 Chip fabrication.....	161
4.5 Supplementary material.....	162
<b>5. Discussion.....</b>	<b>165</b>
5.1 Preparing for syncytium expansion.....	166
5.1.1 The first larval stage PGCs: precursors to the adult syncytium.....	166
5.1.2 A robust syncytial organization.....	168
5.1.3 What about the membrane lobes?.....	171
5.1.4 Rewiring connections: formation of the rachis primordium.....	172
5.2 A model for syncytium expansion in <i>C. elegans</i> .....	173
5.2.1 It is just another incomplete cytokinesis.....	173
5.2.1.1 Different mechanisms for syncytium expansion in <i>C. elegans</i> ?.....	174
5.2.1.2 The rationale behind the incomplete cytokinesis model.....	174
5.2.1.3 More information is needed to complete the stable actomyosin ring bisection model... ..	176
5.2.1 An oriented furrow ingression.....	178
5.2.2 Stabilizing the furrow.....	179
5.3 Why be syncytial?.....	182
5.4 Concluding remarks.....	184

References ..... 185



# List of Figures and Tables

## 1. Introduction

Figure 1. 1 : Overview of germline specification and early development in <i>C. elegans</i> , <i>Drosophila</i> and mice. ....	31
Figure 1. 2: Different regulators of germline specification and somatic transcriptional quiescence in <i>C. elegans</i> , <i>Drosophila</i> and mice .....	34
Figure 1. 3: Establishment of the germline stem cells in the developing <i>Drosophila</i> ovary.....	36
Figure 1. 4: <i>Drosophila</i> ovaries are composed of several ovarioles which are linear arrays of developing oocytes...	37
Figure 1. 5: Timeline of mouse testis development .....	39
Figure 1. 6: Different models of oocyte selection in the <i>Drosophila</i> germline.....	41
Figure 1. 7: Models for stem-cell renewal in the mouse testis .....	45
Figure 1. 8: Different stages of tuberculosis observed by C. Radclyffe Hall .....	47
Figure 1. 9: Intercellular bridges in the male germline of several animal species.....	49
Figure 1. 10: The different steps of cytokinesis in animal cells .....	52
Figure 1. 11: Electron micrographs of the intercellular bridges connecting blastoderm cells in the squid embryo...	56
Figure 1. 12: Formation of syncytial structure in the <i>Drosophila</i> egg chamber and in the mouse testis.....	59
Figure 1. 13: Different mechanisms of syncytium formation .....	66
Figure 1. 14: Intercellular bridge comparison between somatic cells and mouse testis differentiating germ cells ...	72
Figure 1. 15: <i>C. elegans</i> life cycle and syncytial germline development .....	78
Figure 1. 16: <i>C. elegans</i> hermaphrodite gonadogenesis .....	82
Figure 1. 17: A model for the regulation of syncytial germline architecture in <i>C. elegans</i> .....	90
Figure 1. 18: A model for syncytium expansion in annelids .....	92

## 2. Article 1

Figure 2. 1: Both PGCs have an intercellular bridge in <i>C. elegans</i> first-stage larvae .....	105
Figure 2. 2: Actomyosin rings organize a functional proto-rachis in the <i>C. elegans</i> primordial germ line .....	108
Figure 2. 3: The cytokinetic ring integrates and expands the proto-rachis at the end of PGC division.....	112
Figure 2. 4: PGCs maintain their intercellular bridge to the proto-rachis during division.....	114
Figure 2. 5: Proposed model for initial expansion of the primordial <i>C. elegans</i> germ line by incomplete PGC cytokinesis .....	116

Figure S2. 1: .....	126
Figure S2. 2 : .....	127
Figure S2. 3: .....	128
Figure S2. 4: .....	129
Figure S2. 5: .....	130

### 3. Article 2

Figure 3. 1: Perturbation of actomyosin function in the <i>C. elegans</i> primordial germ line .....	138
--	-----

### 4. Article 3

Figure 4. 1: Tracking PGC division with a genetic approach or hydrogel immobilization.....	150
Figure 4. 2 : Design of a microfluidic device to immobilize L1 stage animals.....	154
Figure 4. 3 : Different variations of the microfluidic chamber design .....	156
Figure 4. 4 : Fabrication of the master mold and microfluidic setup .....	159

### 5. Discussion

Figure 5. 1: Cyst formation. ....	173
Figure 5. 2: Dividing germ cells in the adult germline and model for syncytium expansion .....	175

### Tables

Table S2. 1: Strains used in this study .....	124
Table S3. 1: Strains used in this study .....	142
Table S4. 1: Dimensions of the different microfluidic chips.....	162
Table S4. 2: Parameters for deep reactive ion etching .....	163



## List of abbreviations

AIDS : acquired immunodeficiency syndrome

ANI-1 : Anillin 1

ANI-2 : Anillin 2

ALIX : ALG-2-interacting protein X

AMH: anti-Mullerian hormone

APX-1 : anterior pharynx in excess

Arp2/3 : actin related protein 2/3

ATPase : adenosine triphosphatase

AVE : anterior visceral endoderm

BLMP1 : B-lymphocyte-induced maturation protein

BMP2 : Bone morphogenic protein 2

BMP4 : Bone morphogenic protein 4

BMP8b : Bone morphogenic protein 8b

CCM-3 : cerebral cavernous malformation 3

CDK : cyclin dependant kinase

Cdk1 : cyclin dependant kinase 1

CEP55 : centrosomal protein 55

CPC : chromosomal passenger complex

CTD : carboxyl-terminal repeat domain

CXCR4 : C-X-C motif chemokine receptor 4

CYK-1 : cytokinesis defect 1

CYK-4 : cytokinesis defect 4

CYK-7 : cytokinesis defect 7

DAZL : deleted in azoospermia like

DDH : developmental dysplasia of the hip

DMRT1 : doublesex and Mab-3 related transcription factor 1

DMYPT : *Drosophila* myosin binding subunit of myosin phosphatase

DNA : deoxyribonucleic acid

Dpp: Decapentaplegic

DPP3A : dipeptidyl peptidase 3

dsRNA : double strand RNA

DTC : distal tip cell

ECT-2 : epithelial cell transforming 2

EGF : epidermal growth factor

ESCRT-III : endosomal sorting complex required for transport III

ETV5 : ETS variant transcription factor 5

Exe : extraembryonic ectoderm

F-actin : filamentous actin

FBF-1 : Fem-3 mRNA binding factor 1

FBF-2 : Fem-3 mRNA binding factor 2

FGF : fibroblast growth factor

FOXD3 : forkhead box D3

FP : fluorescent protein

FRAP : fluorescence recovery after photobleaching

G-phase : growth phase

GAP : GTPase activating protein

GCK-1 : germinal center kinase family 1

GPCR : G protein-coupled receptor

GDP : guanosine diphosphate

GEF : GDP-GTP exchange

GFP : green fluorescent protein

GFR $\alpha$ 1 : GDNF family receptor alpha-1

GCL : germ-cell less

GLD-1 : defective in germline development 1

GLD-2 : defective in germline development 2

GLD-3 : defective in germline development 3

GLP-1 : abnormal germ line proliferation

GSC : Germline stem cell

GST : gonocytes to spermatogonia transition

GTP : Guanosine triphosphate

GTPase : guanine triphosphatase

HIV : human immunodeficient virus

HMGCR : 3-hydroxy-3-methylglutaryl coenzyme A reductase

HOXB1 : homeobox B1

HSF2 : Heat shock transcription factor 2

Hts : hu-li tai shao

ICB : intercellular bridge

ID4 : inhibitor of DNA binding 4

IFTM1 : interferon induced transmembrane protein 1

IFTM3 : interferon induced transmembrane protein 3

INCEP : inner centromere protein

MBR : midbody ring

MgcRacGap : male germ cell Rac GTPase-activating protein

MKLP1 : mitotic kinesin-like protein 1

MEL-11 : maternal effect lethal 11

MEX-5 : muscle excess 5

MEX-6 : muscle excess 6

mCh : mCherry

mNG : mNeonGreen

mRNA : messenger ribonucleic acid

Mucin-D : mucin *Drosophila*

NMY-1 : non-muscle myosin I

NMY-2 : non-muscle myosin II

NOS : *Nanos*

LAG-1 : Lin-12 and Glp-1 phenotype 1

LAG-2 : Lin-12 and Glp-1 phenotype 2

LAG-3 : Lin-12 and Glp-1 phenotype 3

Lat A : Latrunculin A

LCAM : L1 cell adhesion molecule

LST-1 : lateral signaling target 1

OCT4 : octamer-binding transcription factor 4

OMA-1 : oocyte maturation defective 1

OMA-2 : oocyte maturation defective 2

Otx2 : orthodenticle homeobox 2

P-TEFb : positive transcription elongation factor b

PAR-1 : abnormal embryonic partitioning of cytoplasm 1

PAR-2 : abnormal embryonic partitioning of cytoplasm 2

Pav-Klp : Pavarotti kinase like protein

PB : photobleaching

PH : pleckstrin-homology

PIE-1 : pharynx and intestine excess 1

POS-1 : posterior segregation 1

PP1 : protein phosphatase 1

PP2A : protein phosphatase 2A

PRDM14: PR-domain containing transcriptional regulator 14

PGC : primordial germ cell

Pgc : polar granule component

PY : phosphotyrosine

RA : retinoic acid

RGA-3/4 : Rho GTPase activating protein 2/4

Rho-1 : Rho family GTPase Rho-1

RhoA : Ras homology gene family member A

RNA : Ribonucleic acid

RNAi : RNA interference

RNApol II : ribonucleic acid polymerase II

ROCK : Rho-associated protein kinase

S-phase: synthesis phase

SDF-1 : stromal cell-derived factor 1

SEL-8 : suppressor/enhancer of Lin-12 8

SEPT2 : septin2

SPET7 : septin2

SEPT9 : septin2

SGP : somatic gonad precursor

SOHLH1 : spermatogenesis and oogenesis specific basic helix-loop-helix 1

SOHLH1 : spermatogenesis and oogenesis specific basic helix-loop-helix 2

SOX2 : SRY-box transcription factor 2

SOX9 : SRY-box transcription factor 9

SRY1: sex-determining region Y

SSC : spermatogonia stem cell

SYGL-1 : synthetic germline proliferation defective 1

TAF-4 : TBP-associated transcription factor

TagRFP : Tag red fluorescent protein

TEM : transmission electron microscopy

TEX14 : testis-expressed gene 14

Tre1 : trapped in endoderm 1

ts : thermo-sensitive

TSG 101 : tumor susceptibility gene 101

UNC-59 : uncoordinated 59

VE : visceral endoderm

Vps4 : vacuolar protein sorting 4

Wg : wingless

WNT3 : Wnt family member 3

ZEN-4 : zygotic epidermal enclosure defective 4

Zfp42 : zinc finger protein 42





*“Happiness can be found, even in the darkest of times,  
if one only remembers to turn on the light”*

*—Albus Dumbledore*

*“If you can’t love yourself, how in the hell you gonna love somebody else?”*


*—RuPaul Charles*



## Acknowledgements

Je remercie tout d'abord mon superviseur **Jean-Claude Labbé** de m'avoir accueilli dans son laboratoire et de m'avoir donné l'opportunité de travailler sur des questions biologiques qui me fascinent. Je me sens chanceux d'avoir passé ces années aux côtés d'un chercheur qui partage une vision de la science et de la recherche similaire à la mienne. Merci de m'avoir poussé tant bien que mal vers la ligne d'arrivée de cette aventure qu'est le doctorat.

Mention spéciale à **Eugénie Goupil** (U-gene), une scientifique extraordinaire et au grand cœur qui a naturellement pris une place de mentore tout au long de mon parcours au doctorat. Je te remercie infiniment pour ton soutien quotidien et sans faille, qu'il ait été pédagogique, technique, moral, ou « on the side ».

Merci à Herrmann, **Audrey Herrmann** , pour sa bonne humeur contagieuse, à **Léa Lacroix** d'avoir été la meilleure des cobayes pour ma première expérience de supervision, à **Vincent Poupart** de m'avoir suivi dans les plus beaux endroits du Québec et de mon inconscient, à **Réda Zellag** pour ta motivation inépuisable, ainsi qu'au reste des membres présents et passés du labo Labbé sans qui ces longues années de labeur n'auraient pas été autant le fun.

I would also like to thank all the members of my jury for taking the time to review my work, and especially **Marc Therrien** and **Alisa Piekny** for following my academic journey since year one and giving me quality advice and feedback.

Merci **Julie Mantovani** de rendre la vie des étudiants plus agréable et d'essayer de nous ouvrir des portes dans les murs auxquels nous faisons face. Merci à toi et à tous **les membres du groupe de rédaction** de m'avoir donné l'opportunité de soulager la charge émotionnelle et mentale qu'est la fin du parcours de doctorat.

Je suis extrêmement reconnaissant d'avoir eu la chance découvrir la science et la recherche avec quelques pas de recul, en dehors du contexte académique. Mes expériences en communication, en diplomatie et en art scientifique m'ont assurément apporté la motivation

nécessaire pour la réussite de mon parcours de doctorant. Je remercie tous les membres et organisateurs de **Dans les coulisses de la recherche, Science and Policy Exchange, ComSciCon-CAN, ComSciCon-QC**, et tant d'autres.

Je tiens à remercier tous mes amis, et toutes les belles rencontres faites durant mon parcours au Québec qui m'ont apporté joie de vivre et assouvissement. Merci à **la gang du 1605** d'avoir été mon premier noyau familial à Montréal. **I am very grateful for all of my IRIC related friends**, pour les escapades à Boston toute en légèreté 🧘, les campings agrémentés de jus de pickle à Charlevoix, les couchers de soleil-KD à Kamouraska, les Caribous/raclette au chalet l'hiver, les journées de berry picking, les journées vélo sans traversier; et bien entendu tous les partés d'Halloween, de Noël, de recrutement, les 5@7, the parties at the spicy house, the space house and in the future etc. Merci aux **coureurs du Zig-zag** 🏃, et aux **Hurricanes** 🌀🚣 de m'avoir maintenu en santé physique et mentale! Merci à **My fav' B** 🍷🐘 et **Sop-Sop** pour notre trio infernal qui nous a poussé au-delà des limites de la santé (le coin Côte-des-Neiges/Côte-Sainte-Catherine, les rooftop downtown et Jeanne s'en souviendront). Et enfin, merci à **PP & KK and baby C** for birds birds birds, bushtits and dickcissels 🐦, and especially for being my Montreal family and enduring me and loving me! The 245 times will definitely remain some of the bests.

Words cannot express how grateful I am for my partner **David**. Thank you for your love, your awesomeness, and for supporting me every single day. Thank you for teaching me that it is ok to be anxious in difficult times, that it is ok to be angry when we face injustices, and for helping me to put things in perspective. Thank you for our precious past and future times together, and finally, thank you for your family, for all the **Habs** and **Hars**(is that weird?) out there who took me as one of their own (and gave me delicious food, and an incredibly sweet niece).

Finalement, un énorme merci à **mes frères** et à **ma mère**, à **ma famille** qui se trouve sur un autre continent, gracias a **mi familia** un poco más al sur, or the ones right next door, para vuestro amor incondicional y vuestro apoyo que han hecho de mí la persona que soy.

# 1. Introduction

The work in this thesis aims to better understand how syncytial germlines form. I will describe how the *C. elegans* primordial germline is used here as a model to better characterize the syncytial structure and to uncover the mechanisms of syncytium expansion. Beforehand, I will use this introductory chapter to first introduce the general concepts of the formation of germlines. Then I will describe different syncytial tissues and what is known about their formation and their function. Finally, I will introduce the nematode *C. elegans* as a model to study germline syncytia.

## **1.1 The animal germline, an “immortal” cell lineage that is passed on to the progeny**

The germline in animals is essential for their sexual reproduction. The germline consists in population of cells, termed the germ cells, which are different from somatic cells as they ensure two specific functions: germ cells differentiate to pass on their genetic material to the progeny by forming gametes, and they maintain the potential to form all cell types after fertilisation to give rise to the progeny. The proper development and function of germlines is therefore crucial to ensure the formation of gametes and sustain progeny. Despite differences in how germlines arise and develop, multiple mechanisms are conserved from one species to another. In this section I will summarize what is currently known about animal germlines, their specification, development, and maintenance, focusing on the fruit fly *Drosophila melanogaster* and *Mus musculus* as examples for invertebrates and mammals, respectively.

### **1.1.1 Specification of germlines**

Germlines have been studied for over a hundred years and the mechanisms for germline specification in mouse and *Drosophila* have been reviewed and compared multiple times (Nakamura and Seydoux, 2008; Robert et al., 2015; Seydoux and Braun, 2006). The segregation of the germline precursor occurs relatively early during embryogenesis when the germline precursors, the Primordial Germ Cells (PGCs), segregate from the surrounding somatic cells (Saffman and Lasko, 1999). There are two different mechanisms observed for how PGCs are specified. One of them is preformation, like it is the case in *Drosophila*. Specification of the germline depends on cytoplasmic factors contained in germ granules, which are maternally inherited and segregated in the PGCs (Eddy, 1975). The other mechanism for germline specification is induction which is observed in mouse. In induced germlines, the PGCs emerge as the result of inductive signal from surrounding tissue (Extavour and Akam, 2003).

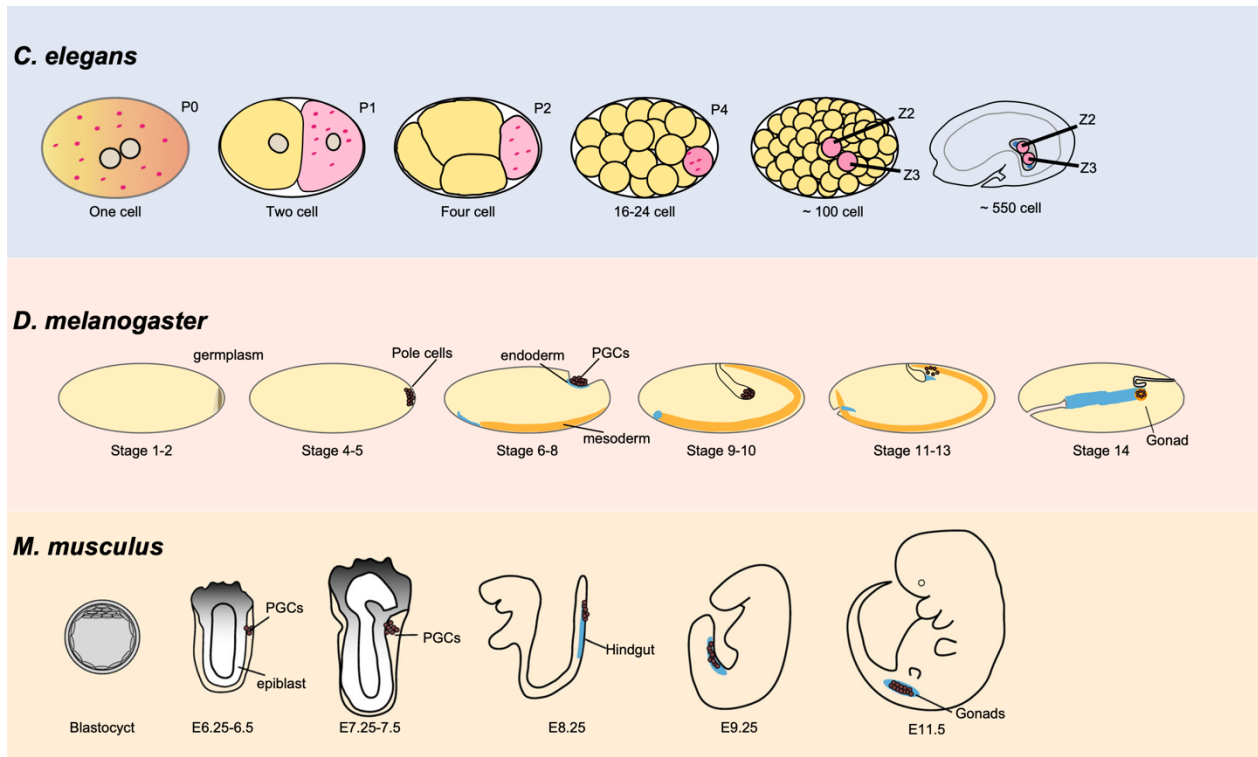


**Figure 1. 1 : Overview of germline specification and early development in *C. elegans*, *Drosophila* and mice.**

In *C. elegans*, the P-granules (magenta speckles) segregate in the one-cell blastomere. During the first zygotic division, asymmetric partitioning is established within the P1 blastomere (pink), and is maintained through successive divisions until P4 divides symmetrically to give rise to Z2 and Z3, which will form the gonad primordium. In *Drosophila*, the germ granules are formed during oogenesis and assemble in the posterior pole region. These granules are incorporated into the germ cells, which actively cross through the midgut epithelium, migrate towards the mesoderm, and join with somatic gonadal cells to form the final gonads. In mice, the germline is induced by ExE signaling, as well as signals from the VE to a set of epiblast cells. This signaling induces Blimp1 expression, leading to PGC proliferation which eventually take residence in the somatic gonad. Figure used with permission from (Robert *et al.*, 2015).

### 1.1.1.1 Specification by preformation in the *Drosophila*

In flies, the early embryo undergoes a series of synchronous nuclear divisions devoid of cellular membrane. Right before the nuclei cellularize (~100 min after fertilization) about 10 PGCs are formed at the posterior of the embryo (Figure 1.1). The relative position of the PGCs is already established during oogenesis and determined by the germ granules (also known as polar granules in *Drosophila*) that assemble at the posterior of the oocyte (Illmensee and Mahowald, 1974). Germ granules are maternally inherited cytoplasmic aggregates that have no surrounding membrane. The formation of the PGCs is dependent on maternally inherited proteins and mRNA and proteins present in the germ granules which are required for the formation of the germ granules and for PGC function (Dodson and Kennedy, 2020; Voronina et al., 2011).

The first discovered factor to be sufficient and necessary for germ granule formation is Oskar (Lehmann and Nusslein-Volhard, 1986). Before localizing at the germ granules in the oocyte, *oskar* mRNA is initially synthesized in the egg chamber by the surrounding nurse cells and actively transported to the oocyte via a microtubule dependant mechanism (Lehmann, 2016). When *oskar* mRNA reaches the posterior pole, it is translated and recruits Vasa, Aubergine, Tudor, and other known granule-enriched mRNA which, together, play a role in germ granule mRNA recruitment and integrity (Trcek and Lehmann, 2019). Oskar further localizes *nanos (nos)* mRNA at the posterior pole which plays a crucial role in germ cell specification as it is required to preserve germline identity.

Soon after their cellularization, the PGCs in flies become transcriptionally quiescent until the beginning of gastrulation (Figure 1.2). This quiescence correlates with a lack of transcriptionally active chromatin and the absence of transcriptionally active RNA polymerase II (RNAPol II), suggesting that the silencing is an active repression of transcriptional activation (Martinho et al., 2004; Schaner et al., 2003). The repression of transcription is mainly mediated by three germ granule components, *polar granule component (pgc)*, *nos*, and *germ-cell less (gcl)*. Pgc directly acts as a transcriptional repressor. It inhibits transcription by directly interacting with the P-TEFb kinase which prevents the phosphorylation of the carboxyl-terminal repeat domain (CTD) of RNA pol II at the Serine 2 position (Nakamura and Seydoux, 2008). In addition, Pgc may



play a role in ensuring the function of Nanos in the PGCs. Nanos is proposed to suppress somatic fate in germ cells by specifically repressing the expression of factors that promote somatic development (Trcek and Lehmann, 2019). Finally, GCL does not directly act as a transcriptional repressor, but rather regulates PGC cellularization. GCL controls the basal constriction of the membranes specifically around the PGCs to separate them from the somatic cells (Cinalli and Lehmann, 2013).

#### **1.1.1.2 Specification by induction in the mouse**

In contrast to flies, germline factors are not directly maternally inherited in the mouse zygote and the germline is specified later during embryogenesis from somatic inductive signals (figure 1.1). The first signs of germline induction appear between embryonic day 5 (E5) and E6, when the proximal epiblast receives Bone morphogenetic protein 4 (BMP4) and BMP8b signals from the extraembryonic ectoderm (ExE) and BMP2 signals from the visceral endoderm (VE). These BMP signals induce the expression of *Ifitm3* in the proximal epiblast (Saitou et al., 2002). At E6.25, about six of the epiblast cells that express *ifitm3* start expressing *Blimp1* (or *Prdm1*). These *Blimp1*-positive cells constitute the precursors for the PGCs as they start to lose the expression of mesodermal genes such as *Hoxb1* (Ohinata et al., 2005; Saitou et al., 2005). It is only by E7.25 when the *Blimp1*-positive precursors start expressing *Dpp3a* (or *Stella*) that the PGCs are specified (Yabuta et al., 2006; Yamaji et al., 2008). Concomitantly with the process of germline specification, the embryo polarises and Smad2 signals from the anterior visceral endoderm (AVE) restricts BMP signals to the posterior proximal epiblast where the PGCs are specified (Senft et al., 2019). The process of germline specification in mouse therefore involves both the production of signals from neighbouring cells and restriction of these signal to the posterior proximal epiblast.

During the formation of the mouse germline, the epiblast cells that will become the PGCs undergo drastic transcriptional change (Figure 1.2). These transcriptional changes are associated with different state of pluripotency necessary for PGC specification: naïve, formative, and primed pluripotency. As opposed to *Drosophila* PGCs that directly repress the somatic fate, cells in mouse first brush against a somatic commitment before swept into the pluripotent germline program. Before the VE and ExE express their first induction signals between E4.5 and E5.5, the expression

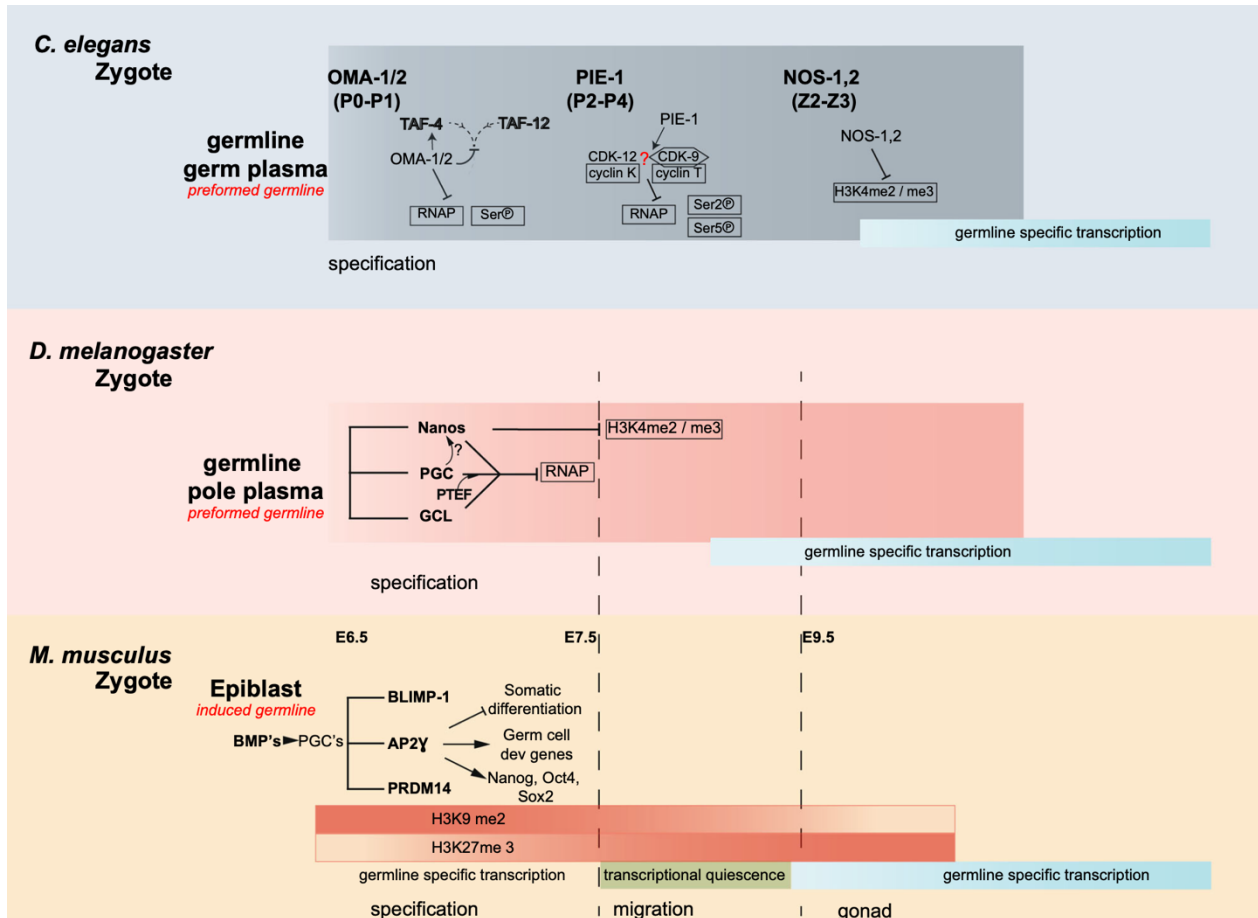


**Figure 1. 2: Different regulators of germline specification and somatic transcriptional quiescence in *C. elegans*, *Drosophila* and mice**

Figure used with permission from (Robert et al., 2015)

of pluripotency genes such as *Nanog* and *Prdm14* is downregulated in proximal epiblast cells, and expression of naïve pluripotency markers such as *Zfp42* or (*Rex1*) is lost (Mulas et al., 2017; Yang et al., 2019). This transition into the formative expression program is associated with expression of transcription factors that coordinate both the silencing of naïve pluripotency genes and activation of epiblast factors. *FOXD3* binds to enhancers to repress pluripotency genes, and *OTX2* and *ETV5* activate enhancers to implement the formative mesodermal program (Kalkan et al., 2019; Respuela et al., 2016). Around E6.25, the inductive signals of *BMP4* from the ExE and *WNT3* from the VE respectively repress *OTX2* and *FOXD3*, which stops the formative program to prevent induction of a somatic fate (Sumi et al., 2013; Zhang et al., 2018). Finally, these *WNT3* signals from the VE also induce the primed pluripotency program by activating PGC specifiers such as *BLIMP-*

1, AP2 $\gamma$  and PRDM14 (Aramaki et al., 2013; Robert *et al.*, 2015). At the same time, pluripotency genes such as *Nanog* are re-expressed in PGCs.

### **1.1.2 Germline development**

After the germline is established with the specification of the PGCs in the embryo, the PGCs generally migrate to their ultimate destination and associate with somatic cells called the somatic germ cells to form the gonad primordium (Kunwar et al., 2006). Together with the somatic germ cells, PGCs proliferate and differentiate to establish a functional gonad that will later produces gametes. Germline development both relies on specific germ cell identity and on somatic development because the soma sends patterning and proliferative signals to the germline. In this section I will focus on the development of the *Drosophila* ovary and the mouse testis because they are better characterized than their opposite sex counterpart. Despite differences in processes that rely in the distinct production of spermatozoa or oocytes, the fundamental mechanisms for gamete formation are conserved between sexes.

#### **1.1.2.1 Germ cell migration and formation of the gonad primordium**

As gastrulation initiates (embryonic stage 6-8), the germ cells in *Drosophila* migrate along different tissues to ultimately unite with the somatic germline (embryonic stage 9-14) (Figure 1.1). This process requires cellular changes in which multiple signaling pathways are involved (Boyle and Dinardo, 1995; Santos and Lehmann, 2004). During gastrulation, the germ cells are first internalized—probably passively—in the invaginating midgut endoderm epithelium (Saffman and Lasko, 1999). Then, the germ cells migrate through the midgut epithelium towards the overlying mesoderm. To migrate, the germ cells lose their cell-cell adhesion by downregulation of E-cadherin, mediated by the activation of the G protein-coupled receptor (GCPR) Tre1 (Kunwar et al., 2008). In addition, the remodeling of the endodermal epithelium to mesenchyme is necessary for the germ cells to gain access to the mesoderm (Seifert and Lehmann, 2012). Subsequently, the germ cells migrate in the mesoderm towards the somatic gonad precursors (SGPs). There are two different known cues that guide germ cells towards the SGPs. The first one is the expression of the genes encoding lipid phosphate phosphatase *wunen* (*wun*) and *wunen 2* (*wun2*) in the

tissues flanking the germ cell migratory route, which act as a repellant for germ cells to guide them towards the SGPs (Sano et al., 2005; Zhang et al., 1997). The second one is the expression of *hmgcr* (encoding for the 3-hydroxy-3-methylglutaryl coenzyme A reductase) by the SGPs, which is necessary and sufficient to attract the germ cells (Van Doren et al., 1998). Finally, once the germ cells have reached the SGPs, the SGPs assemble around the germ cells to form the gonad. The expression of *fear of intimacy (foi)* and *shotgun (shg)* in the SGPs is known to be required for this process. *foi*, which encodes for a transmembrane zinc transporter, has been proposed to regulate the levels of E-cadherin (encoded by *shg*) to control the assembly of the SGPs (Kunwar et al., 2006).

As in flies, after their specification, the mouse PGCs migrate through the endoderm towards the somatic gonadal mesoderm to form the gonad (figure 1.1) (Molyneaux and Wylie, 2004). Soon after the PGCs are specified, between E7.25 and 7.5, migratory behaviour is observed (Anderson et al., 2000). The PGCs first migrate from the posterior primitive streak to the adjacent

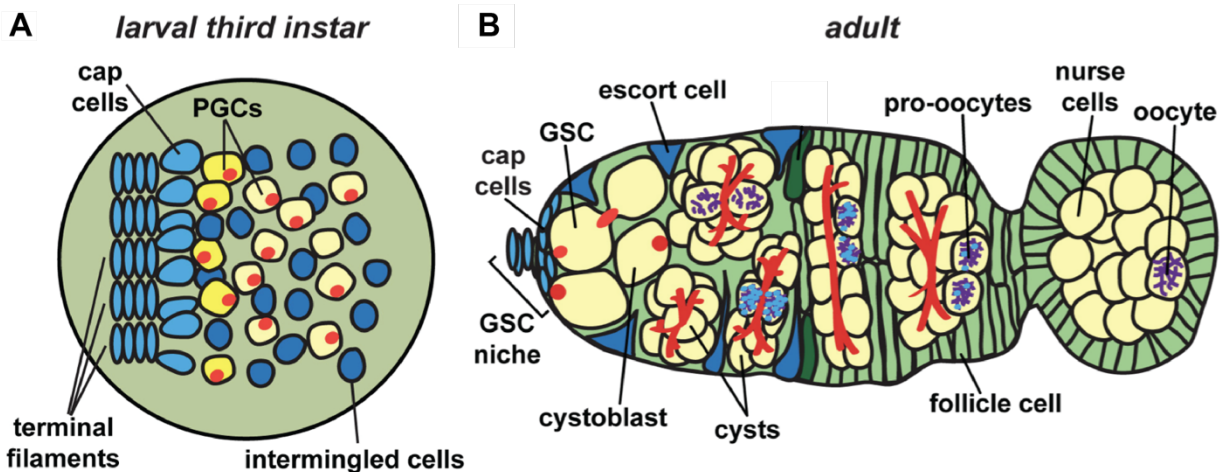


**Figure 1. 3: Establishment of the germline stem cells in the developing *Drosophila* ovary**

(A) The PGCs in contact with the cap cells differentiate into GSCs in the late third instar larvae. (B) In adult germarium, the niche send Dpp signaling to the GSCs to repress differentiation and preserve stem cell fate while the escort cells send Wnt/Wg and EGF signaling to the germ cells to promote differentiation. Red is fusome. Figure used with permission from (Hinnant et al., 2020).

endoderm, and this is proposed to be regulated by the expression of IFTM1 in the mesoderm that repulses the PGCs towards their destination (Tanaka et al., 2005). After initiation of the migration process, the PGCs migrate through the endoderm, and as in *Drosophila*, FGF-mediated E-Cadherin remodeling is shown to be important for the transepithelial migration of the PGCs towards the mesoderm (Takeuchi et al., 2005). At E9.5 the germ cells migrate towards the gonadal ridge as a network and interact using cytoplasmic extensions (Gomperts et al., 1994). This movement is regulated by the expression of the chemokine SDF1 in the genital ridges, and its receptor CXCR4 in germ cells (Ara et al., 2003; Molyneaux et al., 2003). Finally, around E11, the germ cells coalesce with the somatic gonadal cells to form the gonad primordium (Molyneaux et al., 2001).

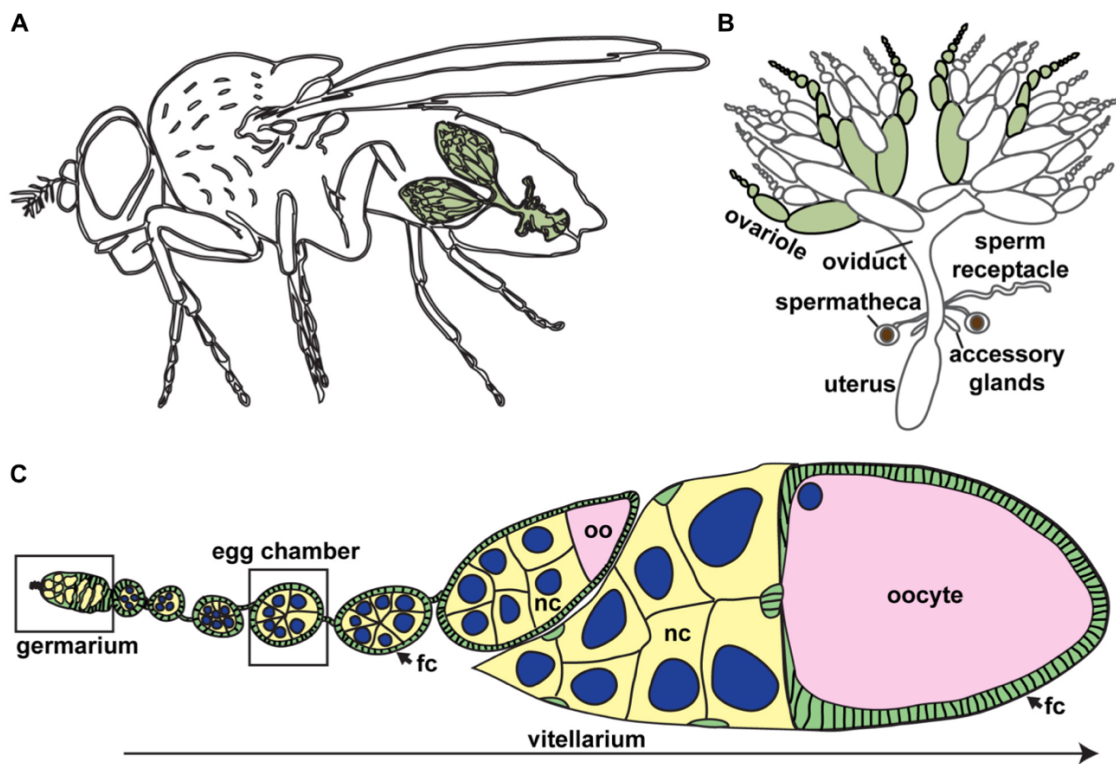


**Figure 1. 4: *Drosophila* ovaries are composed of several ovarioles which are linear arrays of developing oocytes**

(A) Ovaries of *Drosophila* are represented in green. (B) Each ovary contain 15-20 ovarioles (some examples represented in green) which are a linear chain of production for oocytes. (C) An ovariole is composed of a germarium and a vitellarium. Oogenesis starts in the germarium (shown in Figure 1.3 B), then egg chambers mature through the vitellarium. Germ cells, yellow; oocyte, pink; somatic cells, green; nuclei of germ cells, blue; fc, follicle cells; nc, nurse cells; oo, oocyte. Figure used with permission from (Hinnant et al., 2020).

### 1.1.2.2 Development of the gonad and establishment of germline stem cell

After establishment of the gonad primordium in the embryonic female *Drosophila*, the formation of the ovary requires the coordinated proliferation and differentiation of the PGCs with the SGPs during late larval development (Gilboa, 2015). First the SGPs differentiate into the intermingled cells which wrap the PGCs and the terminal filament. During later stages of larval development, the terminal filaments cells differentiate and extend into stacks termed the terminal filament at the anterior of the ovary (Lengil et al., 2015; Sahut-Barnola et al., 1996). Through Notch signaling, the terminal filaments recruit intermingled cells to form the cap cells at the anterior of the terminal filament (Figure 1.3A) (Song et al., 2007). Together the terminal filaments and the cap cells establish the stem cell niche and recruit the most anterior PGCs that differentiate into the germline stem cells (GSCs) in late third instar larvae (Figure 1.3B) (Asaoka and Lin, 2004). The establishment of the niche involves the anchoring of the GSCs to the cap cells through adherent junctions (Song and Xie, 2002). The remaining PGCs that are not in proximity with the cap cells and did not differentiate into GSCs go through oogenesis and will form the first oocytes produced by the animal. The number of functional differentiated GSCs determines the number of adult ovarioles, which are the oocyte producing units of the adult ovary (Figure 1.4A, B). The ovarioles are formed at the last stage of ovarian morphogenesis when a group of apical cells migrates between the terminal filaments to separate the gonad into the adult ovarioles (Sarikaya et al., 2012).

In mice, the development of the gonad is a complex and sex-specific series of processes involving the differentiation of the somatic cells in the gonadal ridge and the recruitment of several cell types that will form the testis (Figure 1.5). In parallel to the formation of the somatic gonad, the PGCs start their entry into their sex-specific pathway. Right after the formation of the gonad primordium at E11-E11.5, there is an upregulation of both XX and XY chromosome specific genes in the somatic gonadal cells (Stevant et al., 2018). This is followed by a wave of activation of male specific genes such as *Amh* and *Dhh* and the activation of the sex-determining region of the Y chromosome (*Sry*) gene and its downstream effector *sox9* (Hanley et al., 2000; Munger et al., 2013). SOX9 is a key regulator in testis development as it is essential for the differentiation of Sertoli cells (which are essential for spermatogenesis) and repression of the ovarian pathway

(Sekido and Lovell-Badge, 2008). By E12.5, Sertoli cells are differentiated and coordinate the differentiation of other somatic cells required for testis formation such as Leydig cells, which secrete testosterone and are required for masculinisation; and the peritubular myoid cells which are involved in the formation of the testis cord (Stevant and Nef, 2019). When *Sry* is induced around E12, the PGCs are incorporated into the testis chord and are referred to as gonocytes. Gonocytes proliferate exponentially until E14.5 when they enter a mitotic quiescence associated with downregulations and repression of pluripotency genes such as *nanog*, *sox2* and *oct4* (Campolo et al., 2013; Chambers et al., 2007; Kehler et al., 2004). It is only after birth that gonocytes resume their cell cycle and are referred to as spermatogonia (or spermatogonia stem cells), which are the germline stem cells responsible for gamete production (Nagano et al., 2000; Pui and Saga, 2017). The gonocytes to spermatogonia transition (GST) involves drastic changes in cell shape, position, and transcriptome which are induced in part by signaling from the Sertoli cells (Spiller et al., 2017). The maturation of the somatic gonad directly influences the GST and contributes to the establishment of the spermatogonia stem cell niche.

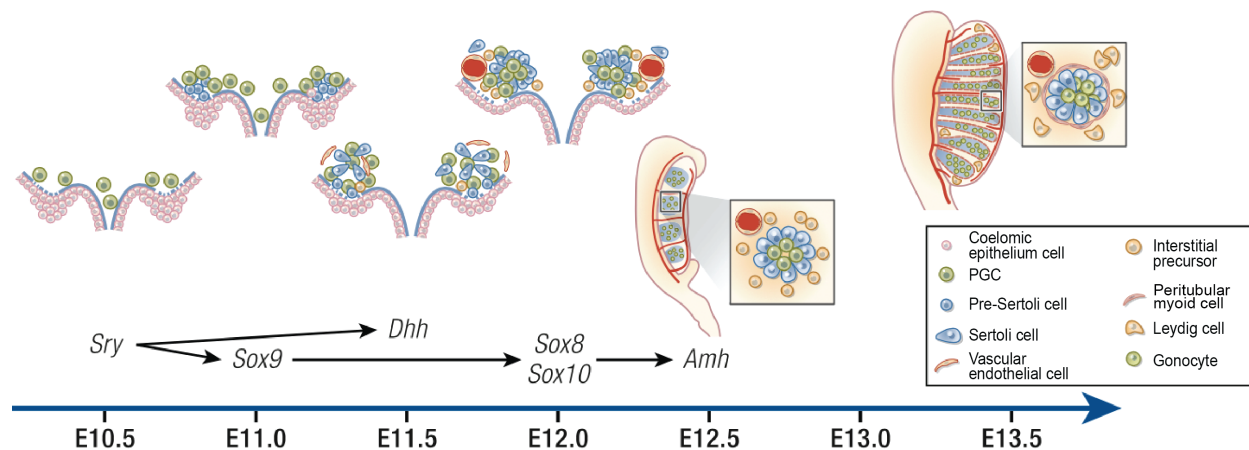


**Figure 1. 5: Timeline of mouse testis development**

The PGCs invade the gonadal ridge and start proliferating (E10.5-11.0). Sertoli cells differentiate and induce the formation of Leydig cells and peritubular myoid cells (E11.5-E12), which contribute to the formation of the testis cord in which PGCs are incorporated (E12.5-E13.5). Figure adapted with permission from (Makela et al., 2019).

### **1.1.3. Gamete production**

Once the stem cell niche is established, the assembly line for gamete production starts. Germline stem cells undergo a series of divisions and enter specific differentiation programs to form functional gametes. While dividing to produce gametes, germline stem cells must preserve their stem cell identity to keep feeding the assembly line. Germline stem cell renewal is generally ensured by surrounding somatic germ cells forming a microenvironment called “the niche”.

#### **1.1.3.1 The *Drosophila* ovary, an assembly line for oocyte production**

In the adult *Drosophila*, the ovary is composed of about 16 ovarioles which are essentially a production chain for oocytes. At the anterior tip of each ovariole lies the germarium which contains the stem cell niche (Figure 1.4). In the germarium, the GSCs undergo one asymmetric division giving rise to the cystoblast, which then proceeds with four successive rounds of synchronous divisions (Figure 1.6A) (Spradling, 1993). This cluster of 16 cells is packaged in a monolayer of somatic epithelial follicle cells to form the egg chamber. The oocyte is specified within the 16-cell cluster, and the remaining 15 cells become nurse cells (Robinson and Cooley, 1996). The nurse cells ensure support of the oocyte development by providing cytoplasmic components such as organelles, proteins, and RNA (Haglund et al., 2011; Mahajan-Miklos and Cooley, 1994). When the oocyte is specified, the egg chamber matures as it advances towards the posterior part of the ovariole called the vitellarium. In each germarium there are clusters of germ cells at different division stages and each vitellarium contains up to seven or eight maturing egg chambers.

#### ***Oocyte specification***

*Drosophila* germ cells display a specific structure that plays a central role in the specification of the oocyte: the fusome. The fusome is a branching cytoplasmic structure that connects the germ cells in the germarium as they divide and enables the synchronicity of germ cell division (more in section 1.3.3.1) (deCuevas et al., 1996). The determination of the oocyte starts after the second round of division when the two germ cells that bear the most fusome connections are selected as pro-oocyte and enter their own differentiation program (Figure 1.6A).



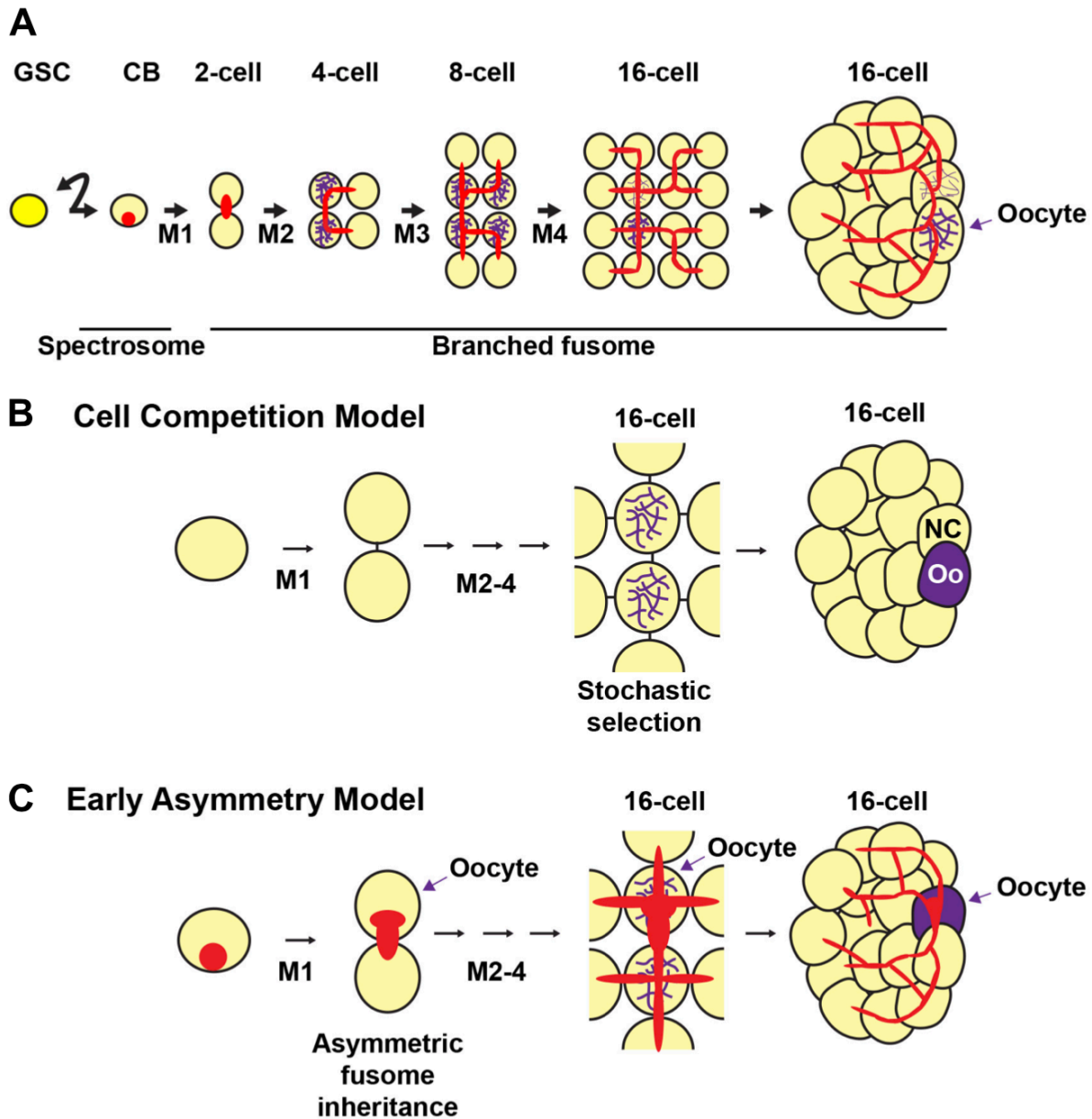


**Figure 1. 6: Different models of oocyte selection in the *Drosophila* germline**

(A) Formation of the 16-cell cluster connected by the fusome and specification of the oocyte. (B) Cell competition model: the oocyte is specified stochastically between the two cells that contain the most fusome material after all 4 rounds of division are complete. (C) Early asymmetry model: the oocyte is specified during the first mitotic division by receiving more fusome material. CB, cystoblast; GSC, Germline stem cell. Figure used with permission from (Hinnant *et al.*, 2020).

They can be distinguished from the nurse cells as they accumulate oocyte-specific factors that will enable them to go through meiosis (Huynh and St Johnston, 2004; Rubin et al., 2016). It is only when the egg chamber detaches from the germarium that a single oocyte is specified, pursues meiosis, and develops with the help of the nurse cells (Hughes et al., 2018). The other pro-oocyte differentiates into a nurse cell. It is proposed that the specification of the oocyte occurs stochastically between the two pro-oocytes after all rounds of mitosis are complete (Figure 1.6B). Another model suggests that determination of the oocyte is set from the first mitotic division (Figure 1.6C). This model relies on the observation that fusome material (spectrosome) is asymmetrically distributed from the first mitotic division, and it is proposed that this asymmetry is conserved and responsible for oocyte specification (de Cuevas and Spradling, 1998; Yue and Spradling, 1992).

### ***Germline stem cells: self-renewal and differentiation***

In *Drosophila*, oocyte production is ensured in adult females by the division and differentiation of the GSCs. However, to maintain gamete production, GSC also need to conserve their undifferentiated state. This balance between GSC self-renewal and differentiation is associated with specific regulation of the epigenetic landscape and is the result of GSC asymmetric division, ensured by the close association between the somatic germ cells (the niche) and the GSCs established during embryogenesis (Figure 1.3) (Flora et al., 2017; Lu et al., 2012). GSC self-renewal is regulated by extracellular signals that promote silencing of the differentiation program. The cap cells, which are in direct contact with the GSCs, secrete Decapentaplegic (Dpp) which binds to their receptors Punt, Thickveins, and Saxophone in the germ cells and induce the activation of the transcription factor Mad (Casanueva and Ferguson, 2004; Xie and Spradling, 1998). Mad then represses the transcription of *bag-of-marbles* which codes for a differentiation factor. The regulation of *bag-of-marbles* through Dpp signaling therefore ensures the repression of GSC differentiation in GSCs that are in proximity with cap cells. In opposition to the cap cells, the escort cells (which are germarium cells) send differentiation signals to the germ cells (Morris and Spradling, 2011). Through long cellular protrusions, the escort cells send Hedgehog, Wnt/Wg, Epidermal Growth Factor (EGF) signaling to the dividing cystoblast (Lu et al., 2015; Mottier-Pavie et al., 2016; Wang and Page-McCaw, 2018). These signals promote germ cell differentiation and

have been proposed to limit the range of undifferentiation signals from the cap cells (Gao et al., 2019).

### **1.1.3.2 The mouse testis**

The adult mouse testis is organized in seminiferous tubes surrounded by myoid cells, Leydig cells and blood vessels (Figure 1.5). The seminiferous tubes are delimited by a basement membrane and contain Sertoli cells wrapping around spermatogonia and developing spermatozoa. Spermatogonia stem cells are in close contact with the basement membrane while spermatogenesis occurs as cells displace towards the lumen of seminiferous tubes. Cells at all stages of spermatozoa development can be found along the basement membrane-lumen axis and, as a result, spermatozoa are formed constantly.

### ***Spermatogenesis***

For spermatozoa production, spermatogonia stem cells differentiate into spermatocytes then spermatids through mitotic and meiotic division accompanied with morphological transformation, with each step regulated by growth factors and hormones (Griswold, 2016). First, spermatogonia stem cells divide and form a pool of undifferentiated spermatogonia that consists of single chains of 2, 4, 8 or 16 interconnected cells (Makela and Toppari, 2018). Then these cells transition to a unidirectional differentiation pathway committing the cells to meiosis (Figure 1.7) (de Rooij and Griswold, 2012). Retinoic acid (RA) synthesized in Sertoli cells is an essential extrinsic factor that induces transcriptional changes in both Sertoli and germ cells and that are necessary for spermatogonia differentiation (Lin et al., 2008). In addition, germ cells that have initiated differentiation also synthesize RA, which may help the next generation of spermatogonia to differentiate (Davis et al., 2013). The regulators DAZL and DMRT1 also play an important role in differentiation. While DMRT1 (expressed in both Sertoli and germ cells) opposes the effect of RA, DAZL enables germ cells to respond to RA and enter differentiation (Lin et al., 2008; Matson et al., 2010). In addition, the SOHLH1 and SOHLH2 transcription factors suppress spermatogonia stem cell genes and induce expression of *kit*, necessary for differentiation (Suzuki et al., 2012). Once spermatogonia have differentiated into spermatocytes, they enter meiosis and further differentiate into spermatids. Finally, during spermiogenesis, the spermatids mature into

functional spermatozoa. During this process, the haploid cells undergo a hypercondensation of the chromatin, the construction of a flagellum, and a reduction in cytoplasm.

### ***Preserving the niche***

Similar to differentiation into a spermatozoon fate, spermatogonia stem cell self-renewal is influenced by the microenvironment where it is found: the niche. Although recent work continues to expand the understanding of self-renewal and stemness in the mouse testis, these mechanisms remain largely undefined (Makela and Hobbs, 2019). There are two existing models that propose different mechanisms for renewing the pool of stem cells. The classical model proposes that the stemness is restricted to single undifferentiated spermatogonium expressing high levels of *id4* and that undergoes complete cytokinesis instead of forming the single chain of 2, 4, 8 then 16 cells that would differentiate into spermatocytes (Figure 1.7) (Ernst et al., 2019; Lord and Oatley, 2017). In opposition, the dynamic model proposes that any of the undifferentiated spermatogonia that express NANOS and GFR $\alpha$ 1 within the chain of interconnected cells can physically detach and regain stem cell potential (Figure 1.7) (Hara et al., 2014; Nakagawa et al., 2010). Despite these contrasting views, the density and the size of the stem cell population is in part regulated by FGF signal secreted by the lymphatic endothelial cells (Kitadate et al., 2019). In addition, spermatogonia cell-autonomous transcription factors together with GDNF secreted by most testicular somatic cells (Sertoli cells, testicular endothelial cells and peritubular myoid cells) are essential for the maintenance of spermatogonia stem cell potential (Chen et al., 2016).

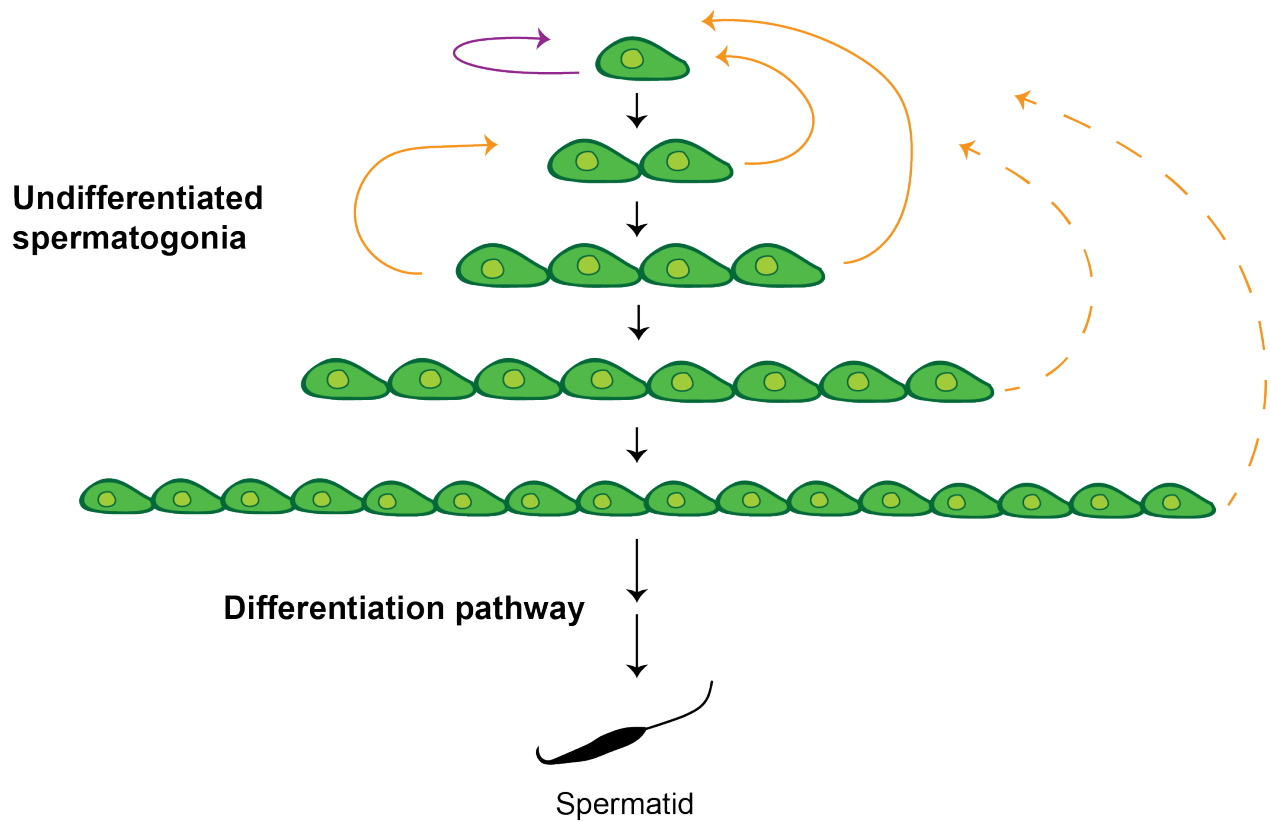


**Figure 1. 7: Models for stem-cell renewal in the mouse testis**

In the classical model, single spermatogonia undergo complete cytokinesis to renew the stem cell population (purple arrow). In the dynamic model, any spermatogonium can detach from the chain of interconnected spermatogonia to renew the pool of spermatogonia (orange arrow), however longer chain of cells rarely fragment (dashed orange arrow). Figure inspired from (Makela and Hobbs, 2019).

## 1.2 Syncytium: cells that share

The term syncytium is derived from “syn” and “kytos” in Greek and can be translated as “cells together”. A syncytium broadly defines a tissue or a cell in which several nuclei are found in a common pool of cytoplasm. Syncytia are relatively conserved in living organisms as they can be found in at least two domains of the living (eukaryotes and bacteria), in most eukaryotes and in all animal germlines. The organization of syncytia varies depending on the species and the type of tissue and can range from a single cavity comprising multiple nuclei to semi-closed membranous compartments separating nuclei from one another. The common point in syncytia is polyploidy in the tissue.

The first syncytial structure was described by Hall in 1855 when he discovered cells containing multiple nuclei in the pulmonary alveolae of patients suffering from tuberculosis (Figure 1.8) (Hall, 1855). He proposed that these cells came from the pulmonary epithelial cells that degenerated as the infection progressed. It became clear a few years later that these “giant cells” were not epithelial but rather “healing cells”, which are today known to be monocytes (Hektoen, 1898). Soon after that, osteoclasts were also shown to be multinucleated (Morison, 1873).

Around the same period, the first syncytial germline was described in animal testes. In 1865, Von la Vallette St. George observed that in several mammal species cells in the testis formed chains of cells that remain connected together. Later Sertoli in 1878 and von Ebner in 1888 found similar structures in cells undergoing spermatogenesis in mammal testis. The study of germline syncytia was limited by the technological advances in microscopy, and as such the precise organization of the connection between the germ cells remained obscure for a few decades. It is only after the development of electron microscopy that syncytial organizations were studied in more detail in germline tissues. Fawcett was the first to depict the structural details of the connection between the germ cells and named them intercellular bridges (ICBs). He found that ICBs were conserved in the male germline of multiple animal species: cat, *Drosophila*, pigeon, hamster, guinea pig, rabbit, monkey, hydra and human (Figure 1.9) (Burgos and Fawcett, 1955; Dym and Fawcett, 1971; Fawcett, 1950; 1970; 1973; Fawcett et al., 1959). In parallel to these

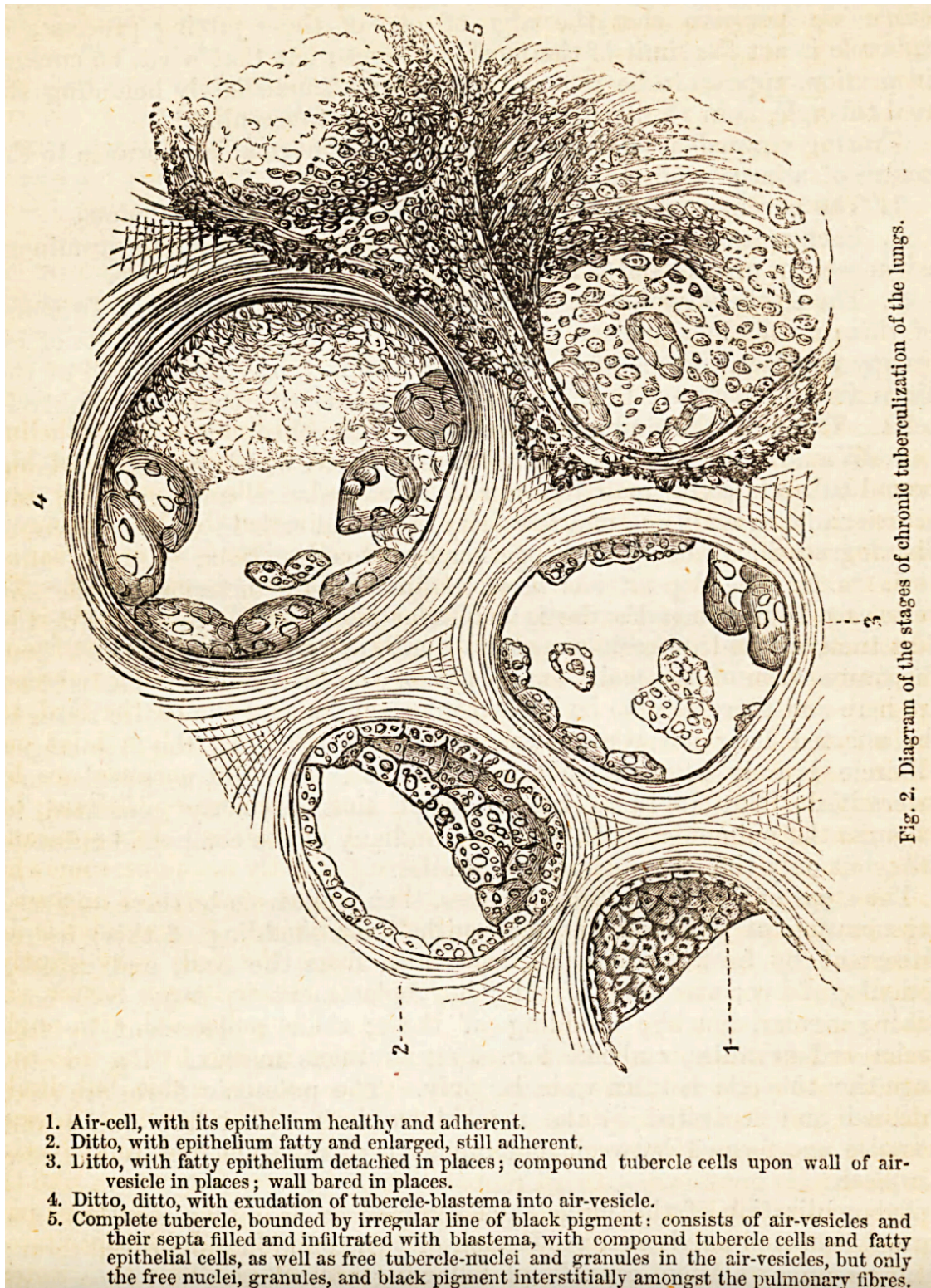


Fig. 2. Diagram of the stages of chronic tubercularization of the lungs.

**Figure 1. 8: Different stages of tuberculosis observed by C. Radclyffe Hall**

In 2, 3 and 4 C. Radclyffe Hall drew multinucleated cells in patients that contracted tuberculosis. Figure from (Hall, 1855).

studies in the male germline, ICBs were also found to connect germ cells in *Drosophila* and mammalian female germlines (Anderson and Huebner, 1968; Brown and King, 1964; Foor, 1967; Gondos and Conner, 1973; Zamboni and Gondos, 1968).

In the past 40 years the understanding of syncytial tissues has exponentially progressed. The development of more sophisticated gene editing tools and optical microscopy, together with the discovery of fluorescent proteins, has allowed a better understanding not only of the structure, the formation, and the maintenance and the significance of intercellular bridges in animal germlines, but also of non-germline syncytia (Greenbaum et al., 2011; Haglund et al., 2011; Lu et al., 2017; Swiatek and Urbisz, 2019).

Although stable ICBs in animal germlines are the focus of many syncytial studies, there is a large variety of syncytial structures that lack stable ICBs. Syncytial tissues devoid of stable ICBs exist in most phyla including animals, plants, fungi and even bacteria (Mela et al., 2020; Mendell et al., 2008; Plachno and Swiatek, 2011).



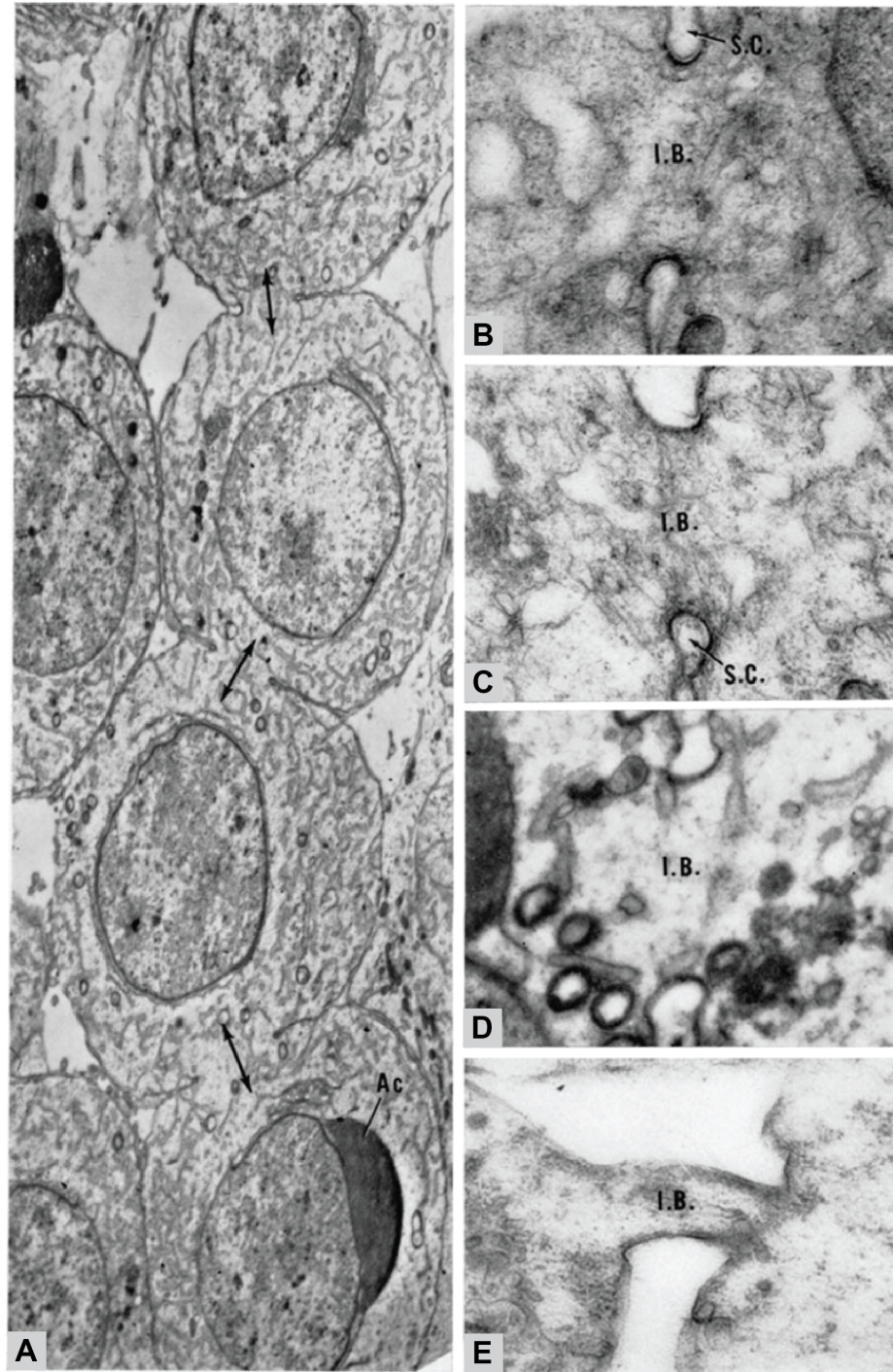


**Figure 1. 9: Intercellular bridges in the male germline of several animal species**

Electron micrographs of male germ cells. (A) Four guinea pig spermatids connected by three intercellular bridges (arrows) X 4,500. (B, C) Intercellular bridges between cat spermatids, X 35,000. (D) Intercellular bridges between guinea pig spermatids, X 35,000. (E) Intercellular bridges between guinea pig spermatids, X 48,000. I.B., Intercellular bridge; S.C, Sertoli cell. Adapted from (Fawcett et al., 1959)

## **1.3 Animal intercellular bridges**

The mechanisms of syncytium formation are best known in animal germlines where the regulation of ICBs that connect the germ cells have been extensively studied. The ICBs that connect the germ cells usually form during the last steps of cell division (cytokinesis), in which the daughter cells are physically separating from one another. Because cytokinesis usually leads to the formation of a transient ICB, cytokinesis is tightly linked to the process of ICB stabilization in syncytial tissues. To form the syncytial structure, these transient ICBs initially formed during cell division rearrange and mature to form stable ICBs that interconnect germ cells with one another. In this section I will first summarise the different mechanisms regulating cytokinesis, then I will describe the known actors required for ICB formation and stability in examples of both somatic and germline syncytia.

### **1.3.1 Cytokinesis physically separates daughter cells**

Cytokinesis is the last step of cell division during which the two daughter cells become physically separated (Figure 1.10). It starts at the onset of anaphase, when chromosomes segregate, with the formation of a cytokinetic furrow at the cell cortex. This cytokinetic furrow composed of a contractile actomyosin ring ingresses progressively to separate the mother cell into two daughter cells that are physically detached during cellular abscission. Cytokinesis is conserved in many organisms and essential to their proper growth and development. This process requires a timely regulation of a series of events that ensure the separation of both the genetic material and the cytoplasmic content. Any cytokinetic mis-regulation can cause chromosomal instability, which is directly linked to different diseases such as cancer (Lacroix and Maddox, 2012). Because cytokinesis is such a fundamental cellular process in living organisms it has been extensively studied over the years and is still the focus of many investigations, especially in animal species (Basant and Glotzer, 2018; D'Avino et al., 2015; Fremont and Echard, 2018; Glotzer, 2017; Green et al., 2012; Pollard and O'Shaughnessy, 2019).

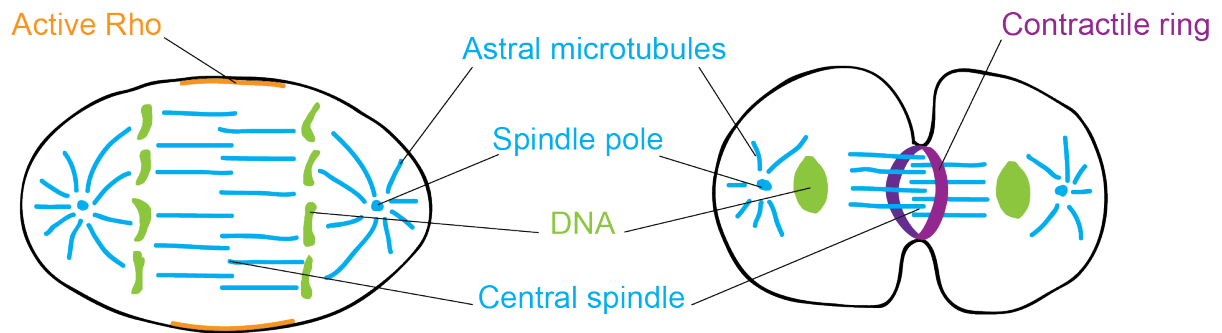
### 1.3.1.1 Cleavage furrow positioning

To ensure the correct segregation of the genetic and cytoplasmic material in each daughter cell after division, it is essential that the cleavage furrow is positioned correctly (Figure 1.10). The accuracy of cleavage furrow positioning is directly linked to the position of the spindle microtubules (Rappaport, 1961). At the onset of anaphase, the mitotic spindle rearranges in antiparallel crosslinked microtubules called the central spindle. Two protein complexes localize at the central spindle: the chromosomal passenger complex (CPC, composed of the kinase Aurora B, INCEP, Borealin and survivin) and the centralspindlin complex (composed of MKLP1 [or ZEN-4] and MgcRacGAP [or CYK-4]) (Carmena et al., 2012; Mishima et al., 2002; Nishimura and Yonemura, 2006). These two protein complexes are required both for microtubule crosslinking but also for specification of the cleavage furrow (Bringmann and Hyman, 2005; Cao and Wang, 1996; Dechant and Glotzer, 2003; Rappaport, 1996). In addition, the astral microtubules also contribute to the cleavage furrow positioning by contributing to polar relaxation (D'Avino et al., 2005; Glotzer, 2004; Lewellyn et al., 2010; Tse et al., 2011).

The degradation of cyclin B that allows the transition from metaphase to anaphase also allows the two central spindle protein complexes to form and localize at the equatorial cortex together with the Rho-GEF (ECT-2) through kinesin-dependant mechanisms (Hutterer et al., 2009; Nguyen et al., 2014; Niiya et al., 2005; Potapova et al., 2006). There, MgcRacGAP activates the Rho-GEF Ect2, which directly activates the Rho GTPase (RhoA) responsible for furrow formation (Prokopenko et al., 1999; Tatsumoto et al., 1999; Yuce et al., 2005). RhoA is considered the master regulator of cytokinesis because its local activation—RhoA is active when bound to GTP and inactive when bound to GDP—can induce the formation of a cytokinetic furrow anywhere at the cell cortex (Wagner and Glotzer, 2016).

## Cleavage furrow positioning

## Contractile ring ingress



## Midbody formation

## Abscission

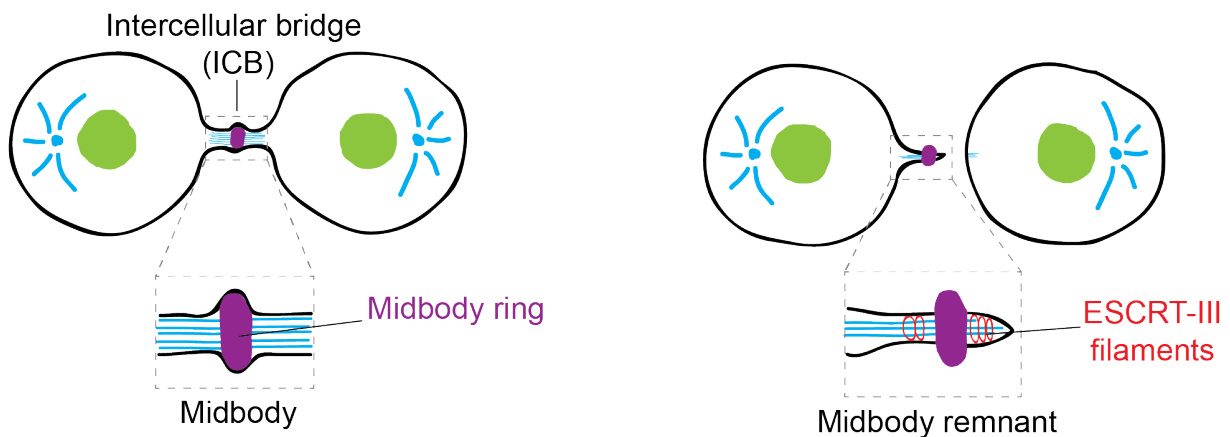


**Figure 1. 10: The different steps of cytokinesis in animal cells**

Figure inspired from (D'Avino et al., 2015)

### 1.3.1.2 Contractile ring assembly and constriction

The contractile ring (or cytokinetic ring) is formed from actomyosin filaments that assemble at the cleavage furrow and which are responsible for the mechanical constriction of the contractile ring (Figure 1.10). The assembly of the contractile ring is driven by active RhoA at the cleavage furrow (Piekny et al., 2005). Rho-kinase (ROCK), simultaneously activated by Rho-GTP, phosphorylates the regulatory light chains of myosin-II and formins, which are responsible for actin filament polymerization at the cleavage furrow (Jordan and Canman, 2012). The continuous

activity of RhoA is necessary during ring ingression to maintain proper actomyosin contraction (Bement et al., 2005; D'Avino *et al.*, 2005; Yuce *et al.*, 2005). Multiple other proteins implicated in contractile ring scaffolding and anchoring such as Anillin and citron kinase, have been shown to also be essential for properly-regulated cytokinesis (El-Amine et al., 2019; Kim et al., 2017; Matsuda et al., 2020; Piekny and Maddox, 2010).

### **1.3.1.3 Midbody formation and abscission**

The contractile ring constricts until it reaches the central spindle and generates a transient ICB, called the midbody (MB), that connects the two daughter cells (Figure 1.10) (Mierzwa and Gerlich, 2014). Because the MB derives from the central spindle, it contains microtubules compacted in a single bundle and proteins required for cytokinesis, such as the centralspindlin complex and the CPC. These complexes eventually play a role in recruiting the abscission machinery (Capalbo et al., 2012). The contractile ring stops constricting when it reaches a diameter of about 1  $\mu\text{m}$  and forms a structure at the middle of the MB called the midbody ring (MBR). The MBR contains Anillin, septins, citron kinase and RhoA. During MBR formation Anillin recruits septins involved in the formation of the constriction sites to ensure membrane stabilisation (Karasmanis et al., 2019; Renshaw et al., 2014). In addition, the maturation from contractile ring to MBR requires the action of citron kinase, Anillin and septins to remove the excess membrane from the nascent MBR (El Amine et al., 2013; Kechad et al., 2012).

Abscission is the process that mediates membrane severing at the end of cytokinesis, and consists of the continuous decrease in the diameter of the bridge on both sides of the MB (Figure 1.10). Little is known about this process but ESCRT-III, Vps4, and spastin are found to be three essential proteins leading to membrane scission. In vertebrates, CEP55 binds to the centralspindlin component MKLP1 and recruits ALIX and TSG101 to the MB (Carlton et al., 2008; Lee et al., 2008; Morita et al., 2007). ALIX and TSG101 then recruit ESCRT-III to the MB which polymerizes towards the site of abscission (Guizetti et al., 2011). It has recently been shown that to recruit ESCRT-III, ALIX interacts with Syndecan-4 and Syntenin for proper localization and abscission (Addi et al., 2020). ESCRT-III is essential to abscission because it directly constricts the membrane to mediate abscission (Wollert et al., 2009). In addition, the action of the ATPase Vps4

at the site of abscission is found to ensure the continuous turnover and constriction of ESCRT-III (Mierzwa et al., 2017). In parallel to ESCRT-III constriction, the microtubule severing enzyme spastin localizes at the MB to disassemble the microtubules and enable proper abscission (Connell et al., 2009; Yang et al., 2008).

### **1.3.2 Somatic syncytia**

Stable ICBs that arise of cytokinesis incompleteness have been mostly studied in animal germlines. However, stable ICBs have been described in multiple other somatic tissues such as in cytoplasts of hydra (Slautterback and Fawcett, 1959); in epithelial follicle cells of *Drosophila*, honeybee, mosquito, and stable flies (Giorgi, 1978; Meola et al., 1977; Ramamurty and Engels, 1977); in larval imaginal discs of *Drosophila* (Haglund et al., 2010; Kramerova and Kramerov, 1999); and in the blastoderm of the squid (Arnold, 1974). Somatic ICBs are largely represented in animal tissues but their structure and the mechanism underlying their formation remain poorly understood. Here I will describe what is known about somatic syncytial tissues in the blastoderm cells in the squid *Loligo pealei* and the epithelial follicle cells in *Drosophila*.

#### **1.3.2.1 Intercellular bridges in blastoderm cells of squid *Loligo pealei***

The study of somatic ICBs is not exhaustive in the squid since only a couple of articles have been published on the matter. The first evidence of connection between cells in the squid embryo was done by electrically stimulating cells in the embryo (Potter et al., 1966). It is only in 1974 that J.M. Arnold observed ICBs in the squid embryo for the first time. With transmission electron microscopy he showed that the future somatic cells in the blastoderm are connected to one another with ICBs (Figure 1.11A) (Arnold, 1974). These ICBs are bordered with electron dense structures typical of other ICBs observed in animal germlines. Further studies showed that the blastoderm cells form coiled chains of cells similarly to germ cells in the male germline (Cartwright and Arnold, 1980). To better understand the process of ICB formation, detailed observations of their structure were made over the course of cytokinesis. At the end of telophase, the electron dense contractile ring stops constricting to form a 400-700 nm ICB. In addition, the midbody forms normally, but is no longer present in late telophase. Meanwhile the ICB walls thicken and form a

sheath (50 nm) with an inner and an outer membrane (Cartwright and Arnold, 1981). These observations suggest that cell division in the squid blastomere are normal until the end of telophase, when the cytokinetic ring transitions into a stable ICB and the midbody disassembles without cellular abscission. Another observation of these stable ICBs suggests that they are occluded during mitosis by transverse membranous structures that were referred to as cisternae (Figure 1.11B) (Arnold, 1974; Cartwright and Arnold, 1981). The observation of multiple vesicles on the outer membrane of the ICB sheath suggests that the vesicles fuse together to form the longitudinal cisternae that occlude the ICB. Cisternae were proposed to serve as a diffusion barrier during mitosis, to prevent all the cells in the syncytium to enter concomitant mitosis. With electron microscopy, Arnold and Cartwright were able to show that the blastomere cells in the squid formed a syncytium which forms from incomplete cytokinesis by the modification of the cytokinetic furrow. Because no further studies were done on somatic syncytium of the squid, there is no molecular understanding of the processes required for formation of these ICBs.

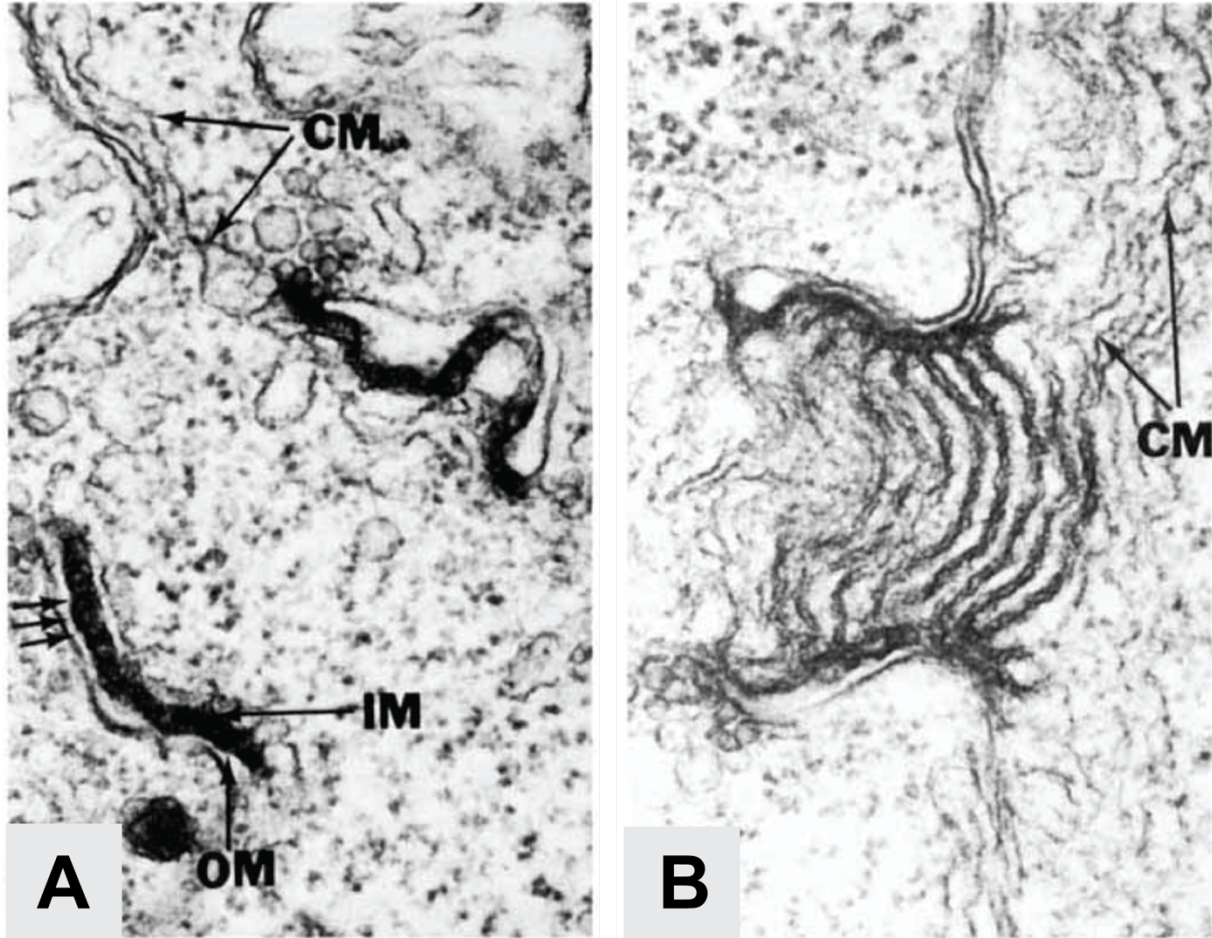


**Figure 1. 11: Electron micrographs of the intercellular bridges connecting blastoderm cells in the squid embryo**

(A) Open intercellular bridge (magnification X 56,000) and (B) fully occluded bridge (magnification X 63,000). IM, inner bridge membrane; OM, outer bridge membrane, CM, cytoplasmic membrane. Adapted from (Cartwright and Arnold, 1981).

### **1.3.2.1 Intercellular bridges in the epithelial follicle cells of *Drosophila***

During *Drosophila* oogenesis, the follicle cells originate in the germarium and stop proliferating during the maturation of the egg chamber at stage 6 in the vitellarium (Figure 1.4C). These follicle cells form a single epithelial layer around the germ cells at the surface of the egg chamber. Electron microscopy analysis of the *Drosophila* egg chamber revealed that the follicle cells are connected to one another through stable ICBs called ring canals in *Drosophila* (more about ring canal formation in section 1.3.3.1) that are about 250 nm in diameter (Giorgi, 1978). As opposed to other ICBs that sometimes vary in size, these were reported to be highly stable



(Airoidi et al., 2011). Further studies showed that these electron dense structures contain F-actin filaments and other regulators normally required for cytokinesis such as Pav-KLP (MLKP1 in mice), Anillin, Mucin-D and Cindr (de Cuevas and Spradling, 1998; Haglund et al., 2011; Kramerova and Kramerov, 1999; Minestrini et al., 2002; Woodruff and Tilney, 1998). It was later confirmed that these ring canals stabilize from cytokinetic furrows (Airoidi et al., 2011). All the regulators present in the epithelial follicle are also present in other tissues in which ring canals exist (germ cells and imaginal discs), suggesting that ring canals in *Drosophila* share structural similarities across different tissues. In addition to describing the structure of the ring canals, their functional properties were also investigated. As opposed to ring canals in the squid, the follicle cell ring canals are never occluded, and studies have shown that proteins and cytoplasm are able to transit through (Airoidi et al., 2011; McLean and Cooley, 2013).

### **1.3.3 Germline syncytia**

#### **1.3.3.1 The *Drosophila* egg chamber**

The female *Drosophila* germline is a well-established model for syncytium studies. Many groups have worked to describe the *Drosophila* germline development as well as the syncytial structure over the past 50 years, making it the most well understood germline syncytium (Greenbaum et al., 2011; Haglund et al., 2011; Pepling et al., 1999; Robinson and Cooley, 1996). As previously discussed (section 1.1.3.1), the female germline consists of two ovaries that comprise 16-20 ovarioles, each containing egg chambers at different developmental stages. At the tip of each ovariole, the germline stem cells differentiate into the cystoblast which then undergoes four incomplete rounds of division (Figure 1.6A). This gives rise to a cyst of 16 cells interconnected through stable cytoplasmic bridges called ring canals. One striking feature that is common to *Drosophila* and other insect germlines is the fusome. The fusome is a membranous organelle composed of  $\alpha$ -spectrin and hu-li tai shao (Hts) that bridges the germ cells along the ring canals (de Cuevas et al., 1997; Pepling et al., 1999; Robinson and Cooley, 1996). In the female germline, it emerges from the division of the cystoblast and elongates during each division and physically connects the cells in the cyst. The fusome breaks down upon selection of the oocyte and for maturation of the ring canals (de Cuevas and Spradling, 1998).

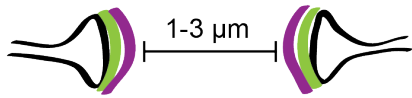
The composition and the dynamics of ring canal formation have been well studied and led to a better understanding of this multiple-step process (Figure 1.12A). The first step to ring canal formation is the cytokinetic furrow arrest at each round of germ cell division. At the third round of division, the apparition of phosphotyrosine (PY) epitopes at the arrested cytokinetic rings marks the initiation of ring canal formation (Cooley and Theurkauf, 1994; Robinson and Cooley, 1996). Although little is known about why proteins at the ring canal are tyrosine-phosphorylated, the tight regulation of this post-translational modification is essential to ring canal formation. The maturation of the ring canals is then specified by the departure and addition of several cytoskeletal components from and to the arrested cytokinetic furrow, some of which are not normally involved in cytokinesis. This protein transit results in the specification of an inner and an outer ring that composes the mature ring canal. The mature ring canal then enlarges from 1 to 10  $\mu\text{m}$  in diameter during late stages of oogenesis (Cooley, 1998).

### ***Formation of the ring canals***

In germline cysts of 2, 4 or 8 cells that have not finished their four rounds of division, the arrested furrows contain cytokinetic ring components such as actin from the contractile ring, Anillin, Pav-Klp, Mucin-D and Cindr. The apparition of PY epitopes at the arrested furrows after the third mitotic division results in the formation of rings of 0.5-1  $\mu\text{m}$  in diameter (Cooley and Theurkauf, 1994; Robinson et al., 1994). This accumulation of PY epitopes is in part dependent on the action of the Src64, Tec29 and Btk29A kinases (Guarnieri et al., 1998; Roulier et al., 1998). After the fourth division, F-actin and Cindr disappear from the ring canals in the 16-cell cyst and the fusome breaks down (de Cuevas and Spradling, 1998; Haglund et al., 2010; Haglund et al., 2011). At this point, the remaining proteins Anillin, Pav-Klp and the PY epitopes build up the outer rim of the nascent ring canals. Once the oocyte is specified, the inner ring of the ring canal is formed by recruitment of PY epitopes, Hts, and F-actin (Robinson et al., 1994; Tilney et al., 1996). The recruitment of F-actin is essential for proper ring canal formation and is solely mediated by Hts (Gerdes et al., 2020). Finally, Cheerio is recruited in the maturing inner ring to complete the formation of ring canals (Robinson et al., 1997; Sokol and Cooley, 1999).

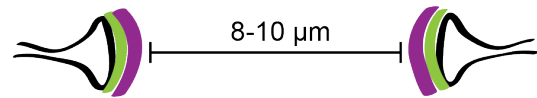
**A**

**Partly assembled ring canal**



Outer rim: PY  
Inner rim: Pav-klp, Mucin-D, F-actin, Hts

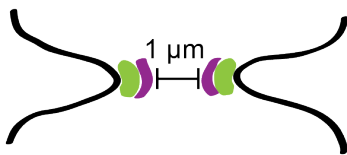
**Mature ring canal**



Outer rim: PY  
Inner rim: Pav-klp, Mucin-D, F-actin, Hts, PY, Kelch, Cherrio

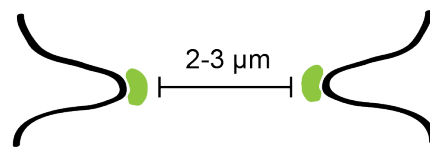
**B**

**Early spermatocyte ICB**



Outer rim: MKLP1, MgcRacGap, SEPT2, SEPT7, SEPT9  
Inner rim: TEX14

**Spermatid ICB**



MKLP1, mgcRacGap, TEX14

**Figure 1. 12: Formation of syncytial structure in the *Drosophila* egg chamber and in the mouse testis**

(A) The ring canals in the *Drosophila* egg chamber form from arrested cytokinetic furrows and are composed of an inner and an outer rim. (B) Intercellular bridges in the mouse testis are derived from midbodies and TEX14 forms an inner rim in the midbody. During maturation of the intercellular bridges, TEX14 extends until it merges with the outer rim. Figure inspired from (Greenbaum et al., 2011).

Overall, the events leading to the assembly of ring canals in the *Drosophila* egg chamber have been extensively described, but many mechanistic processes are yet to be discovered. For example, after furrow ingression, actomyosin is disassembled from the cytokinetic ring and only scaffolding regulators such as Anillin and Cindr are conserved. It is still unclear how this is achieved and what regulates the partial disassembly of the cytokinetic ring. In addition, transit of regulators in the ring canals is tightly time-regulated. It is unknown what regulates the precise timing in the departure and the addition of different regulators that constitute the ring canals and what blocks the completion of cytokinesis.

### ***Maturation of the ring canals***

When the egg chamber leaves the germarium and enters the vitellarium, the ring canals finish their maturation. Anillin disappears, and Kelch starts to localize at the inner edge of the ring canals (Robinson and Cooley, 1997). The incorporation of Kelch and F-actin at the ring canals is mainly dependant on Cheerio. At this point the bridge increases from 0.5-1  $\mu\text{m}$  to 3-4  $\mu\text{m}$  in diameter (Robinson and Cooley, 1997). During the process of ring canal maturation, Hts, Cheerio and Kelch are important to promote bundling of actin filaments in the inner rim of the ring canal and to ensure ring canal growth to 10  $\mu\text{m}$  in diameter (Cooley, 1998; Robinson and Cooley, 1997). The ability of Kelch to organize actin is regulated by Src64, which is required for the expansion of ring canal diameter (Dodson et al., 1998; Kelso et al., 2002). In addition, Kelch in complex with Cullin 3 also promotes the growth of the ring canal by regulating the levels of Hts at the ring canals through proteasome degradation (Hudson and Cooley, 2010; Hudson et al., 2015; Hudson et al., 2019). Other proteins that localize at the ring canals also have major roles in regulating the size of the ring canals. For example, the dissociation of the Beta-catenin Armadillo (Arm) from DE-cadherin through Btk29A phosphorylation is shown to be required for the normal growth of the ring canals. It is proposed that these signals enable the actin to reorganize for proper ring canal expansion (Hamada-Kawaguchi et al., 2015). In addition, the kinase Misshapen (Msn) was also shown to regulate ring canal size and stability by regulating the actin cytoskeleton (Kline et al., 2018). More recently, it was shown that the size of ring canals was further regulated by the balance between Arp2/3 complex promoting ring canal growth and the formin Diaphanous limiting ring canal growth (Hudson and Cooley, 2002; Thestrup et al., 2020).

In recent years, proximity labelling approaches have shed light on new proteins that regulate the stabilization of ring canals in the *Drosophila* egg chamber (Mannix et al., 2019). Previously known ring canal regulators mostly regulate actomyosin activity, but the discovery of new regulators with additional functions through proximity labeling opens new horizons on the study of ring canals. Some of these regulators are involved in post translational modifications such as SUMOylation, and others are involved in DNA and/or RNA binding and regulatory activities. Further work will need to address how these functions regulate ring canal formation and maintenance to better understand the biology of these syncytial structures.

### **1.3.3.2 The mouse testis**

The mouse testis is another well studied model of germline syncytium bearing ICBs. As previously discussed (in section 1.1.3.2), the seminiferous tubes in the mouse testis contain stem cells that give rise to spermatogonia that divide and form chains of cells containing from 2 to 16 cells (Figure 1.7) (Makela and Hobbs, 2019). These chains of cells are syncytial, and each cell is connected to one another through a stable ICB (Figure 1.12B). The ICBs are about 1  $\mu\text{m}$  in diameter and remain present when the spermatogonia differentiate into spermatocytes. When the spermatocytes differentiate into spermatids the ICBs expand from 1  $\mu\text{m}$  to 2-3  $\mu\text{m}$  in diameter and can form syncytia comprising up to 650 cells (Ren and Russell, 1991; Weber and Russell, 1987). The ICBs are finally broken down to release the mature spermatozoa in the lumen of seminiferous tube.

Although male germline ICBs were discovered during the second half of the 19<sup>th</sup> century, earlier than their counterpart in *Drosophila*, less is known today about the dynamic events and the components that lead to formation of ICBs in the mouse testis. This lack of dynamic information is probably inherent to the mouse model in which *in vivo* studies are more challenging. However, the mouse is the only model where a regulator was found to be specifically expressed in the germline ICBs (Greenbaum et al., 2009). This regulator, TEX14, is conserved in all chordates and is required for fertility and ICB formation in mice (both male and female) and its depletion leads to the loss of ICB and animal sterility (Greenbaum et al., 2009; Greenbaum et al., 2006; Ikami et al., 2021; Lei and Spradling, 2016). Furthermore, early in the investigation of

testis syncytium, several components of ICBs were discovered in the rat testis and are considered conserved in mice, such as F-actin, HSF2, Protocadherin- $\alpha$ , Cytokerin 5, Plectin and  $\delta$ -tubulin (Alastalo et al., 1998; Guttman et al., 1998; Johnson et al., 2004; Kato et al., 2004; Russell et al., 1987; Tres et al., 1996).

### ***Intercellular bridge formation***

In opposition to *Drosophila* ring canal, dividing germ cells in the mouse testis form midbodies containing microtubules, Anillin, the centralspindlin complex MLKP1 and MgcRacGAP, and Septins (SEPT7), similarly to cells that undergo complete cytokinesis (Greenbaum *et al.*, 2009; Greenbaum et al., 2007a). The only known difference in mouse germline is the presence of TEX14 during late cytokinetic furrow ingression (Figure 1.12B). In spermatogonia and spermatocytes, the first sign of ICB formation is when TEX14 forms an inner ring in the midbody which is surrounded by an outer ring composed of the centralspindlin complex (Greenbaum *et al.*, 2007a). The ability of TEX14 to form a ring at the midbody is probably facilitated by its capacity to interact with itself (Iwamori et al., 2010a; Iwamori et al., 2011). At the midbody TEX14 colocalizes with CEP55 (Chang et al., 2010). Meanwhile, Anillin and SEPT7 are relocated to the sides of the midbody (Greenbaum *et al.*, 2007a). Tubulin and Anillin are then removed from the forming ICB, SEPT7 returns to the outer rim, and other septins (SEPT2 and SEPT9) are recruited to the outer ring where the centralspindlin complex colocalizes (Greenbaum *et al.*, 2007a). Early ICBs in spermatogonia, spermatocytes, and spermatids are similar, suggesting that the mechanisms of ICB formation is conserved across these cell types.

### ***Intercellular bridge maturation***

During ICB maturation in spermatogonia, septins dissociate from the outer rim while TEX14, CEP55 and the centralspindlin complex will remain the core components of all mature germ cell ICBs (Chang et al., 2012; Greenbaum *et al.*, 2007a). As septins dissociate from the nascent ICB, the TEX14 ring grows in diameter and extends towards the outer ring until the TEX14 inner rim and the centralspindlin complex inner rim eventually merge (Greenbaum *et al.*, 2007a). Additional proteins are added to the ICBs of maturing spermatocytes and spermatids such as keratin 5, HSF2, protocadherin- $\alpha$  and plectin (Alastalo et al., 1998; Johnson et al., 2004; Tres et

al., 1996; Weber and Russell, 1987). The differences in protein recruitment during ICB maturation suggests different stability and roles between spermatogonia, spermatocytes and spermatids ICBs. Recent studies have identified additional proteins that localize in ICBs in the mouse testis (Iwamori et al., 2020). Investigating how these new players interact with the known ICB proteins will help better understand the regulation of ICB formation and maturation in the mouse testis.

## 1.4 How do syncytia form?

As described previously there is a myriad of syncytial organisations across living species. The significance of syncytial tissues is not well understood; however, it is known that they arise either from a tightly controlled development program, like it is the case for germline syncytia, or as a result of cellular malfunction or pathology. In either case, the formation of each is done in a specific manner depending on the tissue and organism. Although the mechanisms of syncytium formation are highly divergent, I will categorise them in four different groups. Developmentally-regulated syncytia are generally formed by **endoreplication**, **cytokinesis incompleteness**, **cell fusion**, or **cytokinesis failure** (Figure 1.13). In the following sections I will give examples for each of these four different mechanisms of syncytium formation.

### 1.4.1 Endoreplication (Bacteria, fungi, *Drosophila* embryo)

The definition of endoreplication differs in the scientific community as there is no consensus. Endoreplication broadly defines a cell that replicates its genome without completing cell division, leading to polyploidy. This could be considered the most trivial manner of forming syncytia, because it is the only case where cells do not go through cytokinesis. Syncytia emerging from endoreplication can be observed in many living organisms including bacteria, plants, and humans (de Almeida Engler and Gheysen, 2013; Gandarillas et al., 2018; Mendell et al., 2008). Here I will summarize two examples of endoreplication that have been well characterized in *Drosophila*.

#### 1.4.1.1 Endocycle in the *Drosophila* nurse cells

Endocycle (or endoreduplication) is a subcategory of endoreplication in which cells replicate their DNA without completing mitosis. This entails that there is neither nuclear or cytoplasmic division and that a single nucleus doubles in DNA content through the process. In addition to being syncytial because they communicate through ring canals, nurse cells in the *Drosophila* maturing egg chamber also endocycle. Instead of entering meiosis like the oocyte, the nurse cells alternate between G-phase (preparation for DNA synthesis) and S-phase (DNA replication) and become highly polyploid (Spradling, 1993). The nurse cell endocycle is controlled



by an oscillation in expression between the S-phase promoting cyclin (Cyclin E), and the CDK inhibitor Dacapo (de Nooij et al., 2000; Lilly and Spradling, 1996). How these two proteins are regulated during endocycle is not well understood. However, recent studies have shown that *dacapo* mRNA is enriched in the oocyte and that Dacapo protein can move from the oocyte to the nurse cells (de Nooij et al., 2000; Doherty et al., 2021; Shcherbata et al., 2004). Consistent with the fact that the oocyte is transcriptionally quiescent during maturation, Doherty and colleagues propose a model in which *dacapo* mRNA is synthesised in the nurse cells, then transported to the oocyte for translation. Dacapo protein then diffuses back into the nurse cells where it promotes endocycling and nurse cell growth. This diffusion model is supported by the finding that the closer the nurse cells are to the oocyte, the more copies of DNA they carry (Doherty et al., 2021).

#### **1.4.1.2 Karyokinesis**

Karyokinesis is a mitosis that is not coupled with cytokinesis, or in other words a nuclear division. There are multiple cases across multicellular species in which cells undergo nuclear division alone. In *Drosophila*, after fertilization, the embryo undergoes 13 synchronous nuclear division over the course of 2h, resulting in a multinucleated syncytium containing about 6000 nuclei (Blake-Hedges and Megraw, 2019; Foe and Alberts, 1983; Rabinowitz, 1941). Similarly to endocycles, these nuclear divisions are modified cell cycles, and are controlled by the activity of cyclin-dependant kinase 1 and the mitotic phosphatases PP1 and PP2A (Heim et al., 2017; Mochida et al., 2010; Wu et al., 2009). These synchronous divisions rely on a series of nuclear movements controlled by cytoskeletal dynamics that result in uniformly distributed nuclei (Foe and Alberts, 1983). Around the fourth division, the nuclei spread along the anterior-posterior axis, then between cycle 7 and 9 the majority of the nuclei progressively migrate to the embryo surface where they position evenly (Baker et al., 1993; Zalokar and Erk, 1976). Proper nuclear positioning is known to be generated by cortical gradient regulated by myosin II (Hatanaka and Okada, 1991). It is proposed that the local Cdk1 downregulation following mitotic exit enables PP1 activity, which is responsible for the recruitment of myosin II to the cortical region to generate contractility and properly position nuclei in the embryo (Deneke et al., 2019). Finally, the last cycles at the cortex before cellularization are marked by the formation of pseudo-cleavages, for which

furrowing is dependent on the polymerisation of two types of actin networks (di Pietro and Bellaiche, 2018; Stevenson et al., 2002).

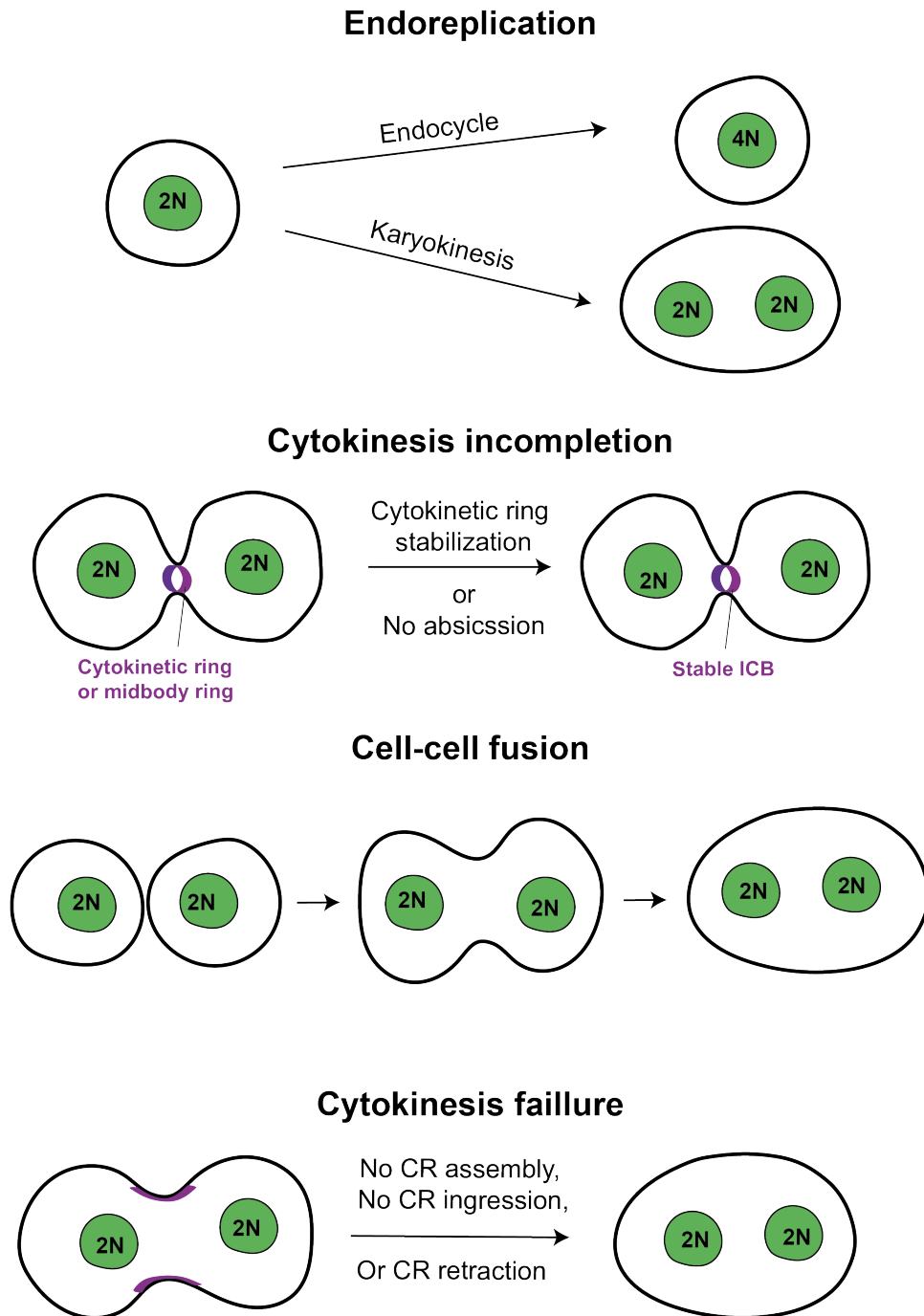


**Figure 1. 13: Different mechanisms of syncytium formation**

Figure inspired from Rana Amini's thesis, 2015.

### 1.4.2 Cell fusion

Cell fusion is another very common mechanism to give rise to a syncytial tissue. Cell fusion is a fundamental mechanism in multicellular organisms as it is required for essential developmental processes such as fertilization and organogenesis. It is a process conserved across phyla, including in filamentous fungi bearing multinucleated hyphae, multiple instances in plants, and in the formation of muscle fibers in most animals (Deng et al., 2017; Maruyama et al., 2016; Mela et al., 2020). Although regulated cell fusion is essential in many instances during normal development, it can also be the result of infection and disease like it is the case in HIV/AIDS (Compton and Schwartz, 2017). In *C. elegans* and other invertebrates, EFF-1 and AFF-1 were discovered to be essential for cell fusion (Hernandez and Podbilewicz, 2017; Mohler et al., 2002; Sapir et al., 2007). Here I will briefly describe the mechanism of myoblast cell fusion required for the formation muscle fibers in vertebrates.

The formation of syncytium through cell fusion is essential for muscle development and regeneration. Muscle cells originate from pluripotent stem cells that specify into myogenic precursors which later differentiate into fusion-competent myoblast. Myoblast differentiation is induced by the expression of two specific transcription factors, MyoD and Myogenin (Buckingham and Rigby, 2014; Comai and Tajbakhsh, 2014). One crucial step of myogenesis is myoblast fusion with another myoblast to generate a multinucleated myofiber. Myoblasts can also fuse with an existing myofiber to promote muscle growth. Cell fusion is a process in which the cells first recognize and adhere to each other, then bring their membranes together to finally create a pore between the two cells. During this process, the membranes undergo dramatic cytoskeletal reorganizations which involve F-actin remodeling and large quantities of membranes regulators such as integrins, cadherins, transmembrane lipids and adaptor proteins (Abmayr and Pavlath, 2012; Hindi et al., 2013; Pavlath, 2010). Although many proteins are involved in membrane fusion, Myomarker and Minion-Myomerger, two regulators essential and specific to membrane fusion have been recently discovered. The overexpression of these two regulators was sufficient to induce cell fusion of non-fusogenic cells (Bi et al., 2017; Quinn et al., 2017; Zhang et al., 2017). It is however not known how Myomarker and Minion-Myomerger regulate the cytoskeleton and

lipid bilayers to induce the changes necessary for membrane fusion. Further studies on how these two proteins function are needed to understand how they promote membrane fusion.

### **1.4.3 Cytokinesis failure**

Polyloid cells forming syncytia can be found in many tissues such as the liver (hepatocytes), the heart (cardiomyocytes), the trophoblast (Placenta) and in megakaryocytes (immune cells). In these tissues, a majority of cells undergo complete cell division and form two distinct daughter cells, whereas some of these cells undergo the same process but fail to fully divide and end up binucleated. All these cells can become polyloid through endoreplication or through cytokinesis incompleteness. Here I will only focus on cells that do not complete cytokinesis.

In these cells, the cytokinetic furrow regresses to give rise to the syncytium rather than stabilizing into an ICB so I will refer to this particular cytokinesis incompleteness as cytokinesis failure. Here I will briefly discuss what is known about the process by which cytokinesis fails in megakaryocytes and cardiomyocytes.

#### **1.4.3.1 Megakaryocytes**

Megakaryocytes are cells derived from multipotent hematopoietic cells and their fragmentation gives rise to platelets, an anucleate cell type. Because the number of platelets is dependent on megakaryocyte size, they become highly polyloid during their late differentiation (Ravid et al., 2002; Zimmet and Ravid, 2000). During megakaryocyte division, mitosis occurs similarly as in other cells and the events leading to polyloidization occur during the first steps of cytokinesis (Geddis et al., 2007). The cleavage furrow is properly formed and starts to ingress, but cytokinesis fails due to a regression of the furrow (Geddis and Kaushansky, 2006; Gentric and Desdouets, 2014). It was shown that cytokinesis failure in megakaryocytes is due to a reduced accumulation of RhoA and F-actin at the cytokinetic furrow (Lordier et al., 2008). In addition, myosin II fails to localize at these contractile rings which promotes cytokinetic failure and polyloidization (Lordier et al., 2012; Shin et al., 2011). This is most probably because ECT-2 (the Rho-activating GEF) is downregulated in megakaryocytes and therefore RhoA is not properly activated at the cytokinetic furrows (Gao et al., 2012; Roy et al., 2016).

### **1.4.3.2 Cardiomyocytes**

In rodents, soon after birth, cardiomyocytes divide but do not complete cytokinesis and this results in the formation of binucleated cells (Clubb and Bishop, 1984). Early on it was shown that cardiomyocytes formed contractile rings but binucleation resulted from improper furrow ingression (Clubb and Bishop, 1984; Li et al., 1997). Accordingly, midbodies are found to be formed in a non-canonical manner in binucleated cardiomyocytes. Instead of being positioned centrally between the two daughter cells, midbodies are found to be located asymmetrically towards one side of the cortex (Engel et al., 2006). In addition, several regulators required for cytokinesis are downregulated in cardiomyocytes (Ahuja et al., 2007). A more recent study that employed live imaging proposed that the defects observed in cytokinetic furrow ingression and in midbody positioning are due to early signalling inconsistencies during specification of the cytokinetic furrow. Authors observed that astral microtubules are not equally distributed during anaphase, and as a consequence, RhoA, myosin II and other regulators of cytokinesis are abnormally localized during cytokinesis (Leone et al., 2018).

### **1.4.4 Regulated cytokinesis incomplection**

Similarly to syncytia that arise from cytokinesis failure, syncytia that arise from regulated incomplete cytokinesis consists in modified cytokinesis. Where regulated incomplete cytokinesis diverges from cytokinesis failure is in its furrow stability. Instead of undergoing furrow regression leading to the loss of the membrane partition between the daughter cells, cells that divide through regulated incomplete cytokinesis are characterized by the stabilization of the cytokinetic ring and formation of a stable ICB. This is conserved in all known animal germlines and a few somatic tissues (as discussed previously in section 1.3). The assembly of regulators in the ICB and their requirement for its maintenance have been well described in most animal germlines. However, the molecular mechanisms that ensure the regulation of stable ICBs formation are not completely understood. There are two known time-points at which cytokinesis can be stopped to form stable ICBs. Cytokinesis can be stopped right after furrow ingression like in *Drosophila*, or cytokinesis can be stopped right before abscission, as is the case in the mouse testis. Here I will

describe the known molecular mechanisms that are known about regulated incomplete cytokinesis in the female *Drosophila* ring canals and in the mouse testis ICBs.

#### **1.4.4.1 Stopping the cytokinetic furrow ingression in the *Drosophila* ring canals**

In *Drosophila*, the ring canals directly arise from modified cytokinetic furrows. This suggests that the cytokinetic ring is never further processed into a midbody and that cytokinesis stops before abscission has initiated. The mechanisms by which the cytokinetic ring stops its ingression and stabilizes are not well understood. During mitotic germ cell division, cytokinesis and fusome formation are two events that happen simultaneously. Because the fusome forms at the center of the closing cytokinetic ring, one possibility is that the fusome physically blocks furrow ingression. Although specifically perturbing fusome integrity by  $\alpha$ -spectrin depletion has dramatic consequences on cell division and overall egg chamber maturation, it does not seem to affect the remaining ring canals (deCuevas et al., 1996). Even though the cytokinetic ring arrests at the fusome, there is no evidence correlating fusome formation with cytokinetic ring arrest. In addition, eliminating the fusome in the *Drosophila* testis has no effect on ring canal stability or fertility (Kaufman et al., 2020). To further understand what could stop the ingression of the cytokinetic furrow, proteins involved in furrow ingression have been studied. Non-muscle myosin II (myosin II) is the motor activity of cytokinetic ring ingression and disruption of the myosin light chain phosphatase (DMYPT) activity, which normally negatively regulates myosin II activity, leads to cytokinetic ring over-constriction and smaller ring canals (Ong et al., 2010; Tan et al., 2003). In addition, a recent genetic screen discovered *flapwing* (*flw*) which functions together with DMYPT to negatively regulate myosin activity during canal formation (Yamamoto et al., 2013). This finding suggests that the specific regulation of myosin II in the *Drosophila* egg chamber is a prerequisite for cytokinetic furrow arrest and ring canal formation. However, the signaling pathways that regulate myosin II specifically in the germline remain elusive.

#### **1.4.4.2 Blocking abscission in the mouse testis.**

In the mouse testis, it is well established that ICBs derived from midbodies, and the mechanism of syncytium formation is probably the most well understood. Except for the presence of TEX14 in the cytokinetic ring, cytokinesis is similar as in somatic cells until midbody formation.

In fact, the expression of TEX14 in the cytokinetic furrow is crucial because it has been shown that TEX14 is responsible for ICB formation (Greenbaum *et al.*, 2007a; Greenbaum *et al.*, 2006). It was further demonstrated that TEX14 interacts with CEP55 to specifically block cellular abscission (Iwamori *et al.*, 2010a). In somatic cells (as discussed section in 1.3.1.3) CEP55 is recruited to the midbody and interacts with ALIX and TSG101 to recruit ESCRT-III and thereby promoting abscission. In germ cells, the interaction of TEX14 with CEP55 inhibits the recruitment of ESCRT-III to the midbody and therefore blocks abscission (Figure 1.14) (Iwamori *et al.*, 2010a; Kim *et al.*, 2015). Further studies showed that TEX14 is the only regulator required to abrogate abscission in mouse testis germ cells. Indeed, the depletion of TEX14 in the germline leads to complete division of the germ cells whereas overexpression of TEX14 in somatic cells leads to the stabilization of ICBs between dividing cells (Greenbaum *et al.*, 2007a; Iwamori *et al.*, 2011; Kim *et al.*, 2015). These observations demonstrate that the germline-specific expression of TEX14 is necessary and sufficient for the formation of the germline syncytium in the mouse testis. TEX14 is conserved in chordates which suggests that ICB formation in germlines from this phylum arise by a mechanism similar to what is seen in mice. However, TEX14 and CEP55 have no homolog in invertebrates. This explains why ICB formation diverges in *Drosophila*, which mechanisms still remain largely unknown.

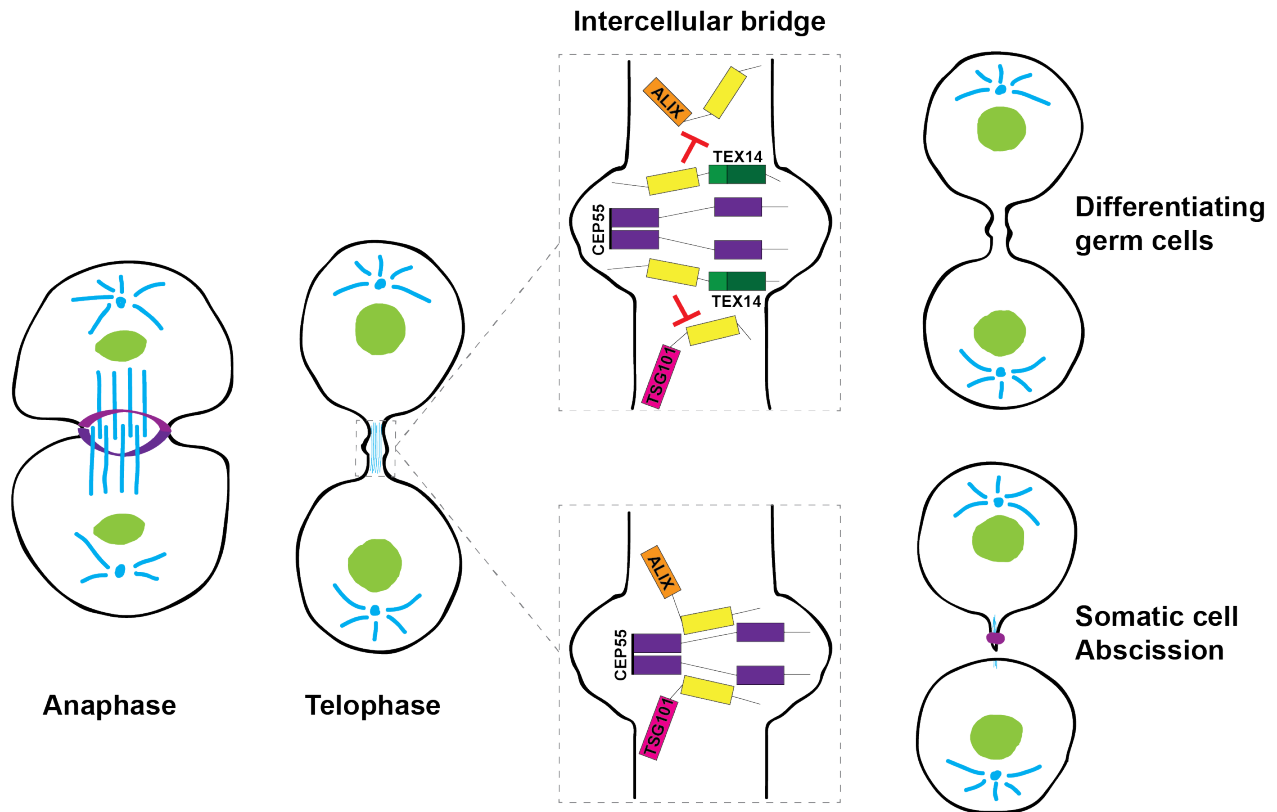


**Figure 1. 14: Intercellular bridge comparison between somatic cells and mouse testis differentiating germ cells**

Stable intercellular bridges in the male germline of mice form at the end of cytokinesis division. TEX14 is expressed exclusively in germ cells, preferentially interacts with CEP55 and competes with ALIX and TSG101 (yellow protein domains), which inhibits abscission and leads to intercellular bridge formation. In somatic cells, ALIX and TSG101 interact with CEP55 to promote cellular abscission. Figure inspired from (Greenbaum et al., 2011).



## 1.5 Function of syncytia in animal tissues

Syncytial tissues and their unique organization have intrigued scientists for decades. To better understand these structures, syncytia have been extensively described over the years and live imaging has provided important insight in how they form. The high occurrence of syncytia across multicellular species and their systematic presence in animal germlines suggest that they confer an evolutionary advantage in these tissues. In addition, the specificity of the mechanisms regulating syncytium formation in different tissues implies that this architecture is selected and has a specific function. In fact, the loss of the syncytial architecture is associated with sterility in all known animal germlines (Greenbaum et al., 2011; Haglund et al., 2011). This suggests that the syncytial architecture is essential to animal fertility. However, the functions of syncytia are not completely understood and seem to diverge from one tissue to another. In this section, I will summarize a few known functions for syncytia in the previously described animal tissues.

### 1.5.1 Synchronous cellular mechanisms

An obvious advantage that has been discussed early in the study of syncytial structure is behavioural synchrony within the syncytium. Indeed, it has been observed in many instances that cells that share a common cytoplasm are able to synchronize their cell cycles, their migration, and their differentiation (Fawcett, 1961; Robinson and Cooley, 1996).

This is the case in the *Drosophila* embryo, where nuclei undergo 13 rounds of synchronous karyokinesis (Blake-Hedges and Megraw, 2019; Rabinowitz, 1941). The reason why this has been selected in the *Drosophila* embryo remains unclear, but several advantages can be observed from this developmental mechanism. First, a cellular division undergoing cytokinesis requires more regulation and is more prone to segregation errors upon mis-regulation of the membrane partition process. Therefore, synchronous karyokinesis enables fast and efficient cell proliferation of the embryonic nuclei. Second, this syncytial organization is essential for the cortical flows that synchronously trigger the migration and the precise positioning of the nuclei (Foe and Alberts, 1983). Finally, this unique syncytial organization is characterized by the synchronous

cellularization of the nuclei at the cortex after the 13 nuclear division (di Pietro and Bellaiche, 2018; Stevenson et al., 2002).

Synchronous behavior is also observed in syncytial germlines, and it is proposed that the ICBs connecting the germ cells enables synchronous cell division. In the *Drosophila* germarium, to form the 16-cell germ line cyst, cells undergo synchronous division. It was shown that disruption of the fusome in the syncytium abrogates the synchronization of the cell cycle within the cyst, suggesting that the syncytial organization is required for synchronous cell division (Lilly et al., 2000; Mathieu et al., 2013; Ohlmeyer and Schupbach, 2003). In the mouse testis, spermatogonia, spermatocytes and spermatids are connected through stable ICBs, and loss of these structures leads to a loss of synchronous division in the germ cells (Rezende-Melo et al., 2020). In addition, these ICBs enable synchronous differentiation. Indeed, it was shown that in TEX14 mutant mice the germ cells remained largely undifferentiated (Rezende-Melo et al., 2020). Because mice lacking TEX14 are sterile, these results suggests that the synchronous differentiation of germ cells in the mouse testis is necessary to produce spermatozoa (Greenbaum et al., 2006).

### **1.5.2 Cytoplasmic exchange**

Cytoplasmic exchange is another function that is been largely proposed for syncytial tissues, especially in animal germlines. The connection between germ cells through stable ICBs enables efficient synchronicity in germ cell behaviour as described previously, and it also enables the transfer of cytoplasmic materiel.

In the *Drosophila* egg chamber, transport of organelles and other cellular components from the nurse cells to the oocyte through the ring canals have been shown to be essential for oocyte maturation. Indeed, proteins, mRNAs, centrosomes, and mitochondria are actively transported to the oocyte through the ring canals (Bolivar et al., 2001; Cox and Spradling, 2003; Huynh and St Johnston, 2004; Mische et al., 2007). In addition, this transport of cellular components through the ring canals has been recently proposed to be bilateral. During oocyte maturation, the nurse cells undergo endoreplication cycles which are regulated in part by *Dacapo* (as discussed 1.4.1.1). The *dacapo* mRNA is synthesised in the nurse cells and transported to the

oocyte where it is translated, then Dacapo diffuses back in the nurse cells to promote endocycling (Doherty *et al.*, 2021). This result suggests that the oocyte sustains its own maturation by regulating endocycle in the nurse cells through bilateral cytoplasmic exchange. Finally, not only is this accumulation of material to the oocyte through the ring canals important for its maturation, but it also prepares for embryo development. For example (and as discussed in 1.1.1.1), the transport of *oskar* mRNA from the nurse cells to the oocyte through a microtubule dependant mechanism is essential for the preformation of the germline because *oskar* mRNA enables the specification of the germ cells in the embryo (Lehmann, 2016; Trcek and Lehmann, 2019).

In the mouse testis syncytium, the exchange of cytoplasm through ICBs also seems to play an important role in the germline integrity. First, as mentioned previously the connection between the germ cells is necessary for their differentiation. In fact, germ cells that detach from the syncytial chain gain the potential to become GSCs rather than undergoing further differentiation (Griswold, 2016; Makela and Hobbs, 2019). This indicates that the signals that induce differentiation are shared through intercellular bridges. Another hypothesis suggests that after meiosis, intercellular exchange through ICBs in haploid spermatids is required for functioning as diploid cells through gene content sharing (Braun *et al.*, 1989). Genes that are required for further maturation in functional spermatozoa are located in sex specific chromosomes, so sharing these gene products through ICBs would be essential for this process.

### **1.5.3 Advantages of polyploidy**

Polyploid cells are conserved amongst many living organisms because they confer specific advantages necessary for development of the tissue in which they are found. However, several common advantages are foreseen in polyploidy. Polyploid cells bear multiple functional alleles, so they are proposed to be more resistant to genotoxicity. In addition, compared to diploid cells, polyploid cells would be less sensitive to haploinsufficiency upon mutations (Pandit *et al.*, 2013).

In megakaryocytes high ploidy is essential for efficient platelet formation. Platelets are formed by fragmentation of megakaryocytes, their number depends on the number and the volume of megakaryocytes. Because polyploidy is correlated with cytoplasmic volume, it serves to increase the number of platelets produced per megakaryocytes (Ravid et al., 2002; Zimmet and Ravid, 2000). It is estimated that a diploid megakaryocyte gives rise to one or two platelets in comparison to 16N megakaryocytes that can produce between 1000 and 5000 platelets (Winkelmann et al., 1987). In case of low platelet count, megakaryocytes can be synthesized in the bone marrow so polyploidization is not essential per se. However, polyploidization is more economic and efficient than classical mitosis and therefore provides an advantageous alternative process for platelet formation (Vainchenker and Raslova, 2020).

In the mammalian heart, during neonatal development, cardiomyocytes proliferation is essential for heart development (Mollova et al., 2013). Soon after the heart has completely formed, proliferation is highly reduced and less than 1% of cardiomyocytes undergo division. It was found that proliferative cardiomyocytes are diploid whereas non proliferative cardiomyocytes are polyploid (Bersell et al., 2009). It is proposed that polyploidy in cardiomyocytes specifically prevents proliferation in the adult heart. Cardiomyocytes exist as a network of long myofiber, and multiple cytokinesis may disrupt this organisation and lead to impairment in heart function. Indeed, during cytokinesis, a cell has to detach from its neighbours, which in cardiomyocytes could lead to a disassembly of sarcomere. Polyploidization is therefore proposed to restrain cell division in cardiomyocytes in order to ensure the integrity of the heart function (Gan et al., 2020). Another reason why polyploidization may be an advantage in cardiomyocyte is their bigger cell size (Gonzalez-Rosa et al., 2018). A fiber with long sarcomeres (containing few polyploid cardiomyocytes) may contract better than a fiber with short sarcomeres (containing multiple diploid cardiomyocytes), and this could be linked to the facilitation of contraction after myocardial infarction (Liu et al., 2010; Pandit et al., 2013).

## 1.6 The nematode *C. elegans* as a model to study syncytium formation

*Caenorhabditis elegans* is a species of nematode living in temperate soil environments. The free-living nematode was first introduced in the scientific community by Sydney Brenner in the 1960's to study neuronal development because of its simple organization (Brenner, 1974). *C. elegans* rapidly became an emerging model to answer a wide range of biological questions. The advantageous short and prolific life cycle, mode of reproduction and small size makes the worm an easy tool to maintain and study in laboratories. These characteristics encouraged multiple studies that put *C. elegans* at the center of historic scientific discoveries. For example, Sydney Brenner, Robert Horvitz and John E. Sulston discovered the genes regulating apoptosis (Brenner, 1974; Ellis and Horvitz, 1986; Sulston, 1976). Later in 1998, Andrew Fire and Craig C. Mello published their work related to the discovery of RNA interference (Fire et al., 1998); studying gene function by simple knockdown became then possible in *C. elegans* and other organisms. The same year, *C. elegans* was the first multicellular organism genome to be sequenced (Consortium, 1998). In addition, the nematode has no respiratory or circulatory system but shares a high proportion of conserved genes with humans, it is therefore an adequate tool to model and study human disease (Wilson, 1999). The growing interest around the round worm generated a great deal of knowledge which placed it as a powerful laboratory model currently at the focus of molecular biology and developmental biology studies. This is partly due to accessible genome editing facilitating mutation, knockout and insertion of reporters like GFP to study gene function. In addition, *C. elegans* is transparent and can therefore be easily imaged *in vivo* by microscopy to study its development, from the zygote to the adult. This allowed to easily map the worm's full cell lineage (Sulston, 1983), investigate the molecular mechanisms of embryonic asymmetric cell divisions (Pacquelet, 2017), and study the development of the gonad (Sulston and Horvitz, 1977).

*C. elegans* has both hermaphrodites that self-fertilize, and males that are more rare within growing populations. After fertilisation, the embryo starts developing in the gonad and is then expelled through the vulva. About 10-12 hours after it is laid, the embryo hatches into a larva. The nematode development is characterized by four different larval stages (L1, L2, L3 and L4) before animals reach adulthood (Figure 1.15). Every larval stage last approximatively 10 hours

and is terminated by a cuticle molt. When the worm reaches adulthood all the organs including the gonad are developed which enables to produce progeny.

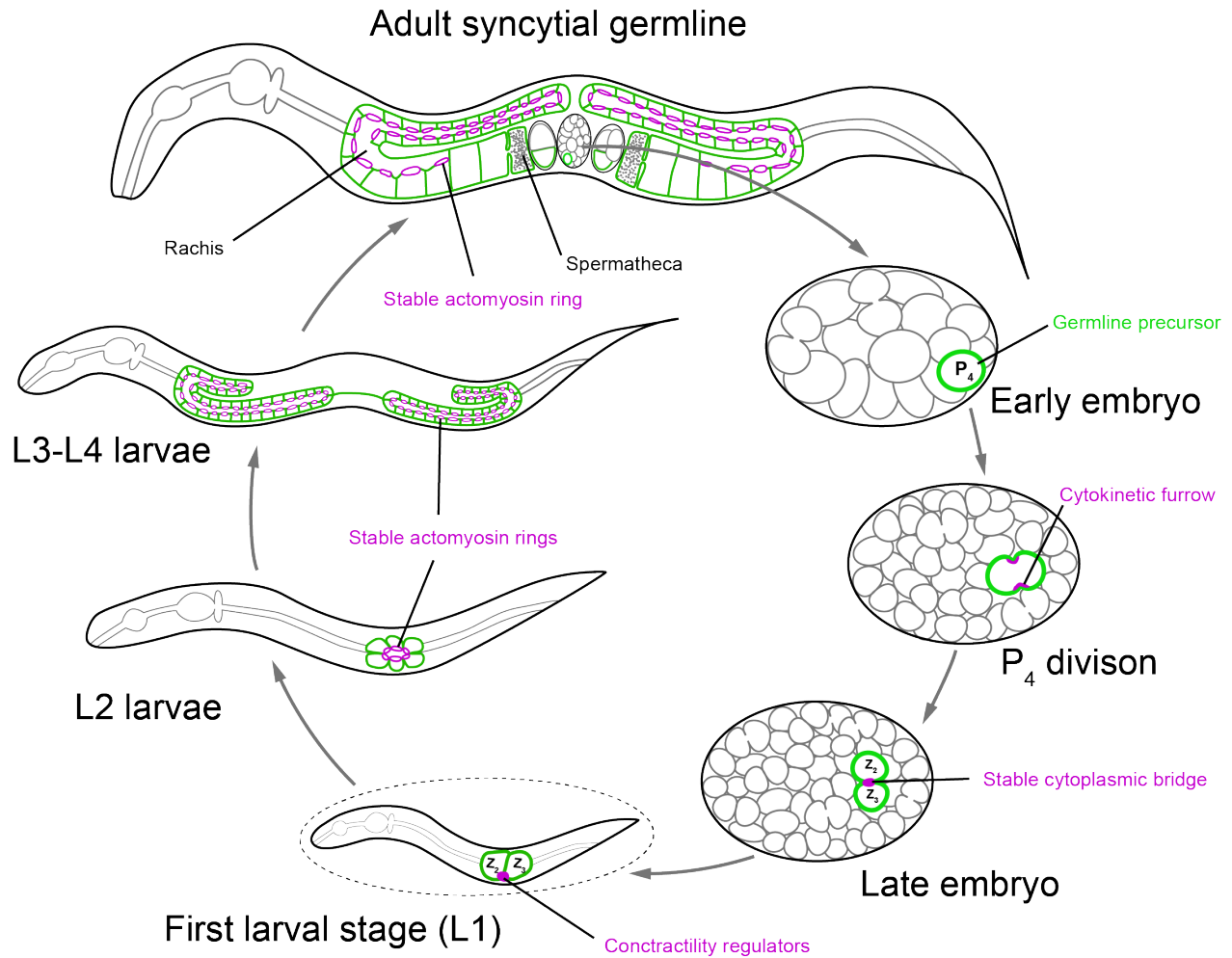


**Figure 1. 15: *C. elegans* life cycle and syncytial germline development**

The *C. elegans* germline specifies when the P<sub>4</sub> blastomere arise during early embryogenesis. P<sub>4</sub> then divides in an incomplete fashion leaving the two daughter cells Z<sub>2</sub> and Z<sub>3</sub> (the PGCs) connected through a stable intercellular bridge. After the embryo hatches, the PGCs start proliferating at the first larval stage (L1). The germ cells continue proliferating in subsequent larval stages and eventually form two gonad arms that produce embryos at the adult stage. The germline is a syncytium in the adult and in the larval stages, in which each germ cell is connected to a common cytoplasmic cavity called the rachis through stable intercellular bridges that form actomyosin rings.

### 1.6.1 The *C. elegans* germline

The *C. elegans* germline arises during early embryogenesis with the birth of the germline founder blastomere, termed P<sub>4</sub> (Figure 1.15) (Wang and Seydoux, 2013). P<sub>4</sub> then divides in the two primordial germ cells (PGCs), termed Z<sub>2</sub> and Z<sub>3</sub>, that remain mitotically quiescent until the worm hatches as a first instar larva. When the first-stage larva starts feeding, the PGCs initiate mitotic proliferation and expand the germline through the fourth larval stage (Hirsh et al., 1976; Sulston, 1983). The germline of adult hermaphrodites comprises a simple gonad organized in two U-shaped gonad arms that constitute symmetrical assembly lines for gamete production. In adults, mitotic germ cells are found within a niche at the distal end of each gonad arm. Germ cells enter meiosis when they exit the niche and progress towards the proximal end, where they mature into oocytes that are competent to be fertilized when they transit into the spermatheca (Kimble and Crittenden, 2007).

#### 1.6.1.1 Germline specification

The specification of the germline in *C. elegans* follows the preformation model, similarly to the *Drosophila* germline. The first events that leads to the specification of the germline in *C. elegans* occurs during the first zygotic division. The maternally inherited germ granules (called P-granules in *C. elegans*) and other germline specific factors are segregated to the posterior P<sub>1</sub> cell during the asymmetric division of the zygotic cell P<sub>0</sub> (Figure 1.1) (Strome et al., 2005; Strome et al., 1997). The asymmetric division is controlled by polarity regulators called the PAR proteins, which are positioned in the zygote as a the result of cortical flows induced from fertilization (Gubieda et al., 2020). PAR-1 and PAR-2 localize to the posterior together with the germ granules and segregate with the germ line for the three subsequent asymmetric P<sub>1</sub> divisions that give rise to the germline founder P<sub>4</sub>. This asymmetry in the cells from P-lineage is regulated by the activation of PAR-1 in the posterior which restricts the somatic factors MEX-5/6 to the anterior (Griffin et al., 2011). In turn, PAR-1 and MEX-5/6 promote the enrichment of germ granule proteins to the posterior such as PIE-1 and POS-1, which are essential to establish the germline identity (Schubert et al., 2000).

While the somatic cells initiate transcription, the P-lineage blastomeres remain transcriptionally quiescent through active transcriptional repression until after gastrulation, when the PGCs ( $Z_2$  and  $Z_3$ ) start showing first signs of transcription (Figure 1.2) (Seydoux and Dunn, 1997; Seydoux et al., 1996). This transcriptional repression is regulated at different levels by germline specific and maternally inherited regulators. In the  $P_0$  and  $P_1$  cells, OMA-1 and OMA-2 repress the initiation of transcription by sequestering a component necessary for the RNA Pol II initiation complex called TAF-4 (Guvén-Ozkan et al., 2008). In the  $P_2$  to  $P_4$  cell, transcriptional repression is mediated by PIE-1, a component of the germ granules (Seydoux and Dunn, 1997). Similarly to Pgc in flies (as discussed in 1.1.1.1), PIE-1 represses transcription by interacting with the P-TEFb kinase which prevents the phosphorylation of CTD of RNA Pol II at the Serine 2 position necessary for transcriptional elongation (Batchelder et al., 1999; Ghosh and Seydoux, 2008).

The maintenance of the P-lineage is in part ensured by the specific regulation of maternal mRNAs by germline specific regulators (Seydoux and Fire, 1994; Seydoux et al., 1996). Indeed, *nos-2* mRNA is tightly regulated over the course of germline specification by several germ granule components (Subramaniam and Seydoux, 1999). While OMA-1, OMA-2, MEX-3 and MEX-5 are required for the silencing of *nos-2* translation from  $P_0$  to  $P_3$ , PIE-1 and POS-1 are necessary to activate the translation of *nos-2* in  $P_4$  (D'Agostino et al., 2006; Jadhav et al., 2008; Tenenhaus et al., 2001). The translation of *nos-2* mRNA is required for specification of  $Z_2$  and  $Z_3$ , and it plays an important role in silencing somatic genes (Schaner et al., 2003). Soon after the PGCs arise, the SGPs  $Z_1$  and  $Z_4$  migrate towards the PGCs and wrap around  $Z_2$  and  $Z_3$  respectively forming the gonad primordium that will remain mitotically quiescent during the rest of embryogenesis (Rohrschneider and Nance, 2013; Sulston, 1983).

### **1.6.1.2 Germline development**

When the embryo hatches, the first larval stage (L1) PGCs are still flanked by the two SGPs (Kimble and Hirsh, 1979; Sulston, 1983). After hatching and 7 to 10 hours into the L1 stage, the PGCs divide for the first time and will continue to divide exponentially until the adult gonad is formed (Figure 1.16). The SGPs also start dividing during the L1 stage.



During the second larval stage (L2), the SGPs have generated 12 cells that are essential for the gonad development, meanwhile the germline consists of about 30 cells (Kimble and Hirsh, 1979). Two of the SGPs lie at each extremity of the gonad and are called the distal tip cells (DTCs). The DTCs promote germ cell proliferation and guide their migratory pathway and, as such, the DTCs are essential to the germline development (Kimble and White, 1981). By the end of the L2 stage, as opposed to the DTCs that localize at the opposing tip of the elongating gonad, the rest of the somatic cells move at the center of the gonad and separates the germ cells in two distinct gonad arms (Figure 1.16). These somatic cells are precursors for the sheath cells that form a single-cell layer to contain the germ cells, the spermathecae, and the uterus that localize around the dividing germ cells. Out of the uterine precursors, one cell is specified as the anchor cell through a stochastic Notch asymmetry while the other cell differentiates into uterine cell (Wilkinson et al., 1994).

During the third larval stage, the anchor cells invade the gonadal basement membrane to reach the epithelial vulval cells and induces vulval development (Kornfeld, 1997; Lattmann et al., 2020; Sundaram and Han, 1996). Meanwhile, as the gonad elongates, the germ cells start to enter meiosis at the proximal end of each gonad arm (Kimble and White, 1981). The cells that enter meiosis at this stage will differentiate as spermatocytes in later developmental stages. Finally, by the end of the L3 stage, each DTCs turn away from the ventral membrane and migrate towards the dorsal membrane (Figure 1.16).

During the early fourth larval stage (L4), the DTCs turn a second time along the dorsal membrane and towards the center of the worm and proliferate until they have formed two U-shaped gonads (Figure 1.16) (Hubbard and Greenstein, 2000). Because the proliferating germ cells follow the DTCs migratory pathway, these two turns determine the U-shaped pattern of the two *C. elegans* gonads. During the L4 stage, both the germline and the somatic gonad prepare to be ready for embryo formation. By the end of the L4 stage, the uterus and the vulva have finished their development, the spermatheca is formed and sperm production stops, and the proximal germ cells start to differentiate as oocyte.

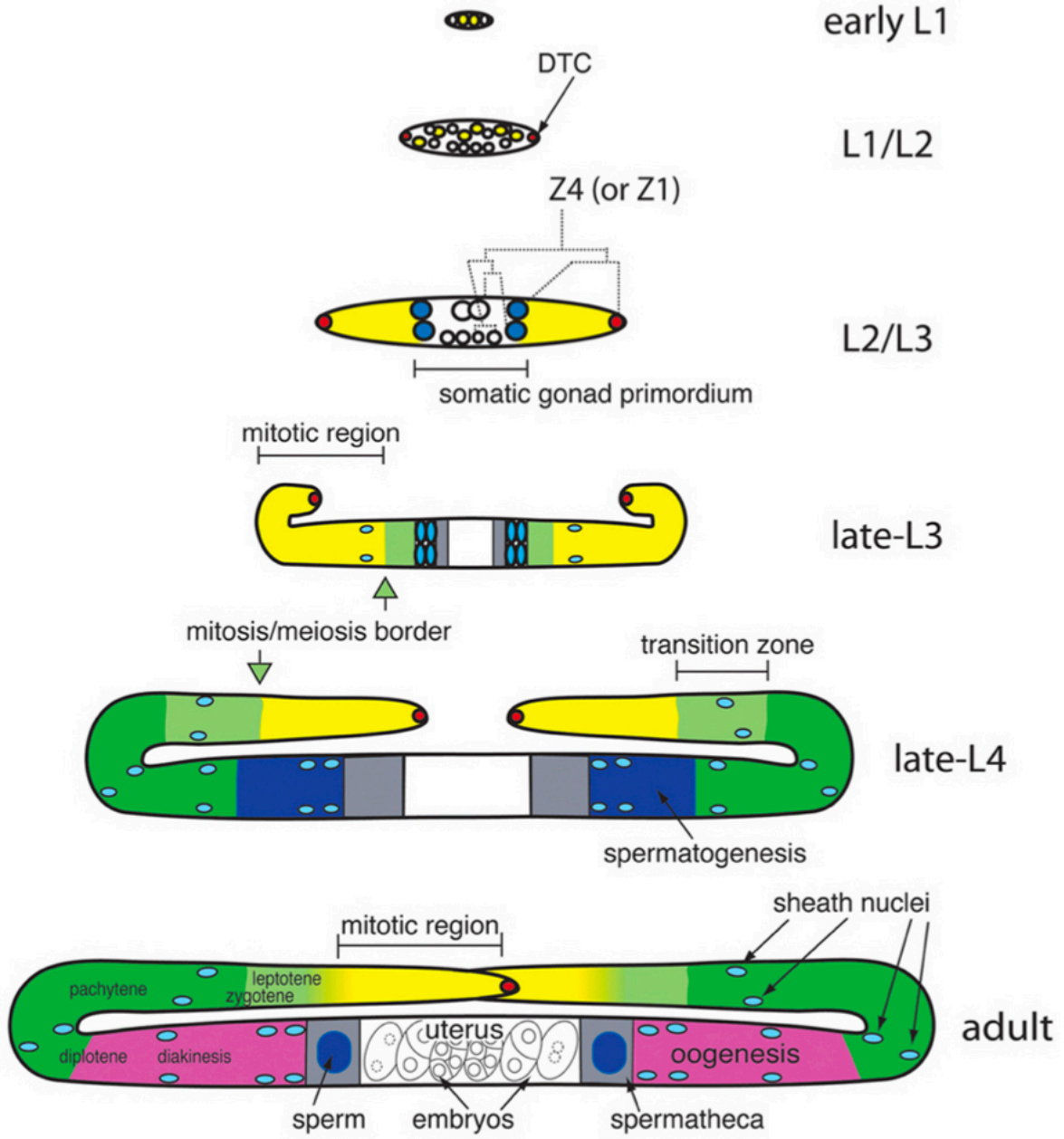


**Figure 1. 16: *C. elegans* hermaphrodite gonadogenesis**

Both somatic germ cells and germ cells start proliferating at the L1 stage, and the somatic gonad primordium develops separating two pools of germ cells during the L2 stage. By the late L3 stage, each gonad arm is U-shaped and germ cells start entering meiosis, and the spermatheca is formed during the L4 stage. The adult gonad organizes in different regions from distal to proximal when different events for embryo production occur: mitosis (in yellow), mitosis/meiosis transition (in light green), meiosis (dark green), oogenesis (pink), fertilization (grey), early embryogenesis (white). Image used with permission from (Hubbard and Greenstein, 2005).

### 1.6.1.3 Gamete production

The adult hermaphrodite gonad arms each contain approximately 1000 syncytial germ cells connected to a central cytoplasmic cavity called the rachis (Figure 1.15). The gonad organizes in different regions along the proximo-distal axis just as a supply chain for embryo production. At the distal end of the gonad, in the mitotic region, the germline stem cells (GSCs) form a niche to ensure continuous feeding in chain production. Proximally to the mitotic region, germ cells enter early phases of meiosis through the transition zone and then remain in pachytene region until the turn of the gonad where they initiate the process of oogenesis (Figure 1.16). At the proximal end, the oocytes transit through the spermatheca to be fertilized.

Similarly to other animal germlines, the somatic gonad in *C. elegans* plays an important role both in promoting GSCs maintenance and in the process of oocyte maturation (Hubbard and Schedl, 2019). At the distal end of each gonad arms, the DTC caps the gonad and directly contacts the GSCs through E-cadherin and L1CAM adhesion proteins (Gordon et al., 2019). The DTC promotes GSC proliferation and self-renewal by expressing the Notch signaling ligands LAG-2 and APX-1, which interact with the Notch receptor GLP-1 expressed at the surface of the germ cells (Crittenden et al., 1994; Henderson et al., 1994; Kimble and White, 1981; Tax et al., 1994). This interaction leads to the activation of transcription factors (LAG-1, LAG-3 and SEL-8) which promote the expression of *lst-1* and *sygl-1* (Doyle et al., 2000; Kershner et al., 2014; Petcherski and Kimble, 2000). LST-1 and SYGL-1 are thought to be necessary to promote self-renewal and proliferation of GSCs, in part by inhibiting GLD-1, a protein essential to promote meiotic entry (Brenner and Schedl, 2016). In addition, FBF-1 and FBF-2 are also required to promote GSC fate in the distal end (Kershner et al., 2013; Merritt and Seydoux, 2010). These two proteins post-transcriptionally repress the accumulation of several protein that are required for mitotic entry, including GLD-1 (Crittenden et al., 2002; Hansen et al., 2004). As opposed to the *Drosophila* germarium where the GSCs divide asymmetrically to maintain the stem cell niche, GSCs in *C. elegans* divide symmetrically and differentiate only when they advance proximally, away from the niche formed by the DTC.

As germ cells progress proximally in the gonad, the gradient of GLP-1 signaling they receive from the DTC diminishes and, eventually, reaches a threshold beyond which cells enter differentiation. GLP-1 can no longer inhibit the meiotic factor GLD-1 and germ cells enter meiosis. There are three main pathways that are redundant and promote the meiotic development of the germ cells: GLD-1, GLD-2 and SCF. GLD-1 represses the translation of *glp-1* mRNA, GLD-2 works with GLD-3 to promote *glp-1* mRNA translation, and SCF both downregulates mitotic cell cycle proteins and promotes the pairing of homologous chromosomes at the meiotic entry (Brenner and Schedl, 2016; MacQueen and Villeneuve, 2001; Mohammad et al., 2018; Suh et al., 2006). The balance between mitotic GSC renewal and meiotic transition entirely depends on mutual inhibition of the mitotic/meiotic programs. Indeed, while GLP-1 signaling from the DTC inhibits meiotic fate in distal GSCs, the meiotic pathways inhibit GLP-1 and mitotic proteins in cells that are no longer subject to DTC signaling.

### **1.6.2 The *C. elegans* germline is a syncytium**

In the past two decades, the nematode *C. elegans* has emerged as a powerful model to study germline syncytial architecture because the development of the germline can be readily studied *in vivo* (Rehain et al., 2017). The *C. elegans* germline is a syncytium in which the syncytial architecture is crucial for gamete production. A disorganization of the syncytial architecture leads to sterility of the worm (Green et al., 2011). Early morphological studies have shown evidence that the *C. elegans* gonad is a syncytium (Hirsh et al., 1976). With differential interference contrast and electron microscopy, Hirsh and colleagues had described that the gonad is organized in a central cytoplasmic core surrounded by peripheral nuclei encased in semi membrane partition. Subsequent work confirmed that all germ cell membranes harbor openings, forming stable intercellular bridges (termed rachis bridges) connecting germ cells to a central cavity named the rachis (Figure 1.15) (Hall et al., 1999; Hubbard and Greenstein, 2000; Zhou et al., 2013). The increasing performance of genome editing and fluorescence microscopy techniques, and the rising interest for the *C. elegans* gonad in the years 2000 led to the initiation of a multitude of studies to investigate the molecular mechanisms that regulate the syncytial architecture.

### **1.6.2.1 C. elegans syncytium maintenance**

Most proteins enriched at rachis bridges are contractility regulators usually found at cytokinetic rings (Figure 1.15) (D'Avino et al., 2015; Maddox et al., 2005). In addition, perturbation of these contractility regulators disorganizes the architecture of rachis bridges, results in germ cell multinucleation and can lead to defects in fertility (Green et al., 2011). To understand how the syncytium organizes, it is crucial to decipher the mechanisms by which the proteins enriched at rachis bridges regulate the stability of these membrane openings.

#### ***Rachis bridges are stable actomyosin rings***

The two cytoskeletal proteins F-actin and Non-muscle myosin II localize at rachis bridges in a ring-shaped structure, forming actomyosin rings similar to contractile rings in cytokinesis (D'Avino et al., 2015; Maddox et al., 2005; Strome, 1986). Two isoforms of anillin (ANI-1 and ANI-2) as well as other cytokinetic regulators, such as the septin UNC-59 and the formin CYK-1, also localize at rachis bridges (Amini et al., 2014; Priti et al., 2018). The related organization and molecular composition between actomyosin rings at rachis bridges and cytokinetic furrows lends credence to the notion that they share common characteristics. For example, during cytokinesis, anillin scaffolds F-actin and myosin and anchors the contractile ring to the membrane, suggesting that actomyosin rings are likewise anchored to the membrane at rachis bridges in *C. elegans* germ cells (Piekny and Maddox, 2010). Rings at rachis bridges bear similarity in organisation and composition to contractile rings but their function differ. Measurements of fluorescence recovery after photobleaching of Myosin in stable actomyosin rings shows lower turnover compared to cytokinetic rings in embryos, which is compatible with the notion that rachis bridges form more stable structures (Priti et al., 2018). Whereas contractile rings ingress during cytokinesis to physically separate daughter cells, the size of rachis bridges varies as germ cells transit through the gonad during their maturation into gametes (Rehain-Bell et al., 2017), and therefore the regulation of these two types of actomyosin rings must differ.

### ***Rachis bridges stability is regulated by cytokinetic regulators***

Functional analysis of several known cytokinetic regulators that are also found at rachis bridges, such as the Rho pathway components RGA-3/4, ECT-2, ROCK<sup>LET-502</sup>, Anillin, Formins<sup>CYK-1</sup> and Non-Muscle myosin II<sup>NMY-2</sup>, revealed that their depletion results in a loss of contractile rings at rachis bridges and adult syncytium disorganization (Amini *et al.*, 2014; Piekny and Mains, 2002; Priti *et al.*, 2018; Schmutz *et al.*, 2007; Zhou *et al.*, 2013). This suggests two possibilities for rachis bridge maintenance: the cytokinetic regulators at rachis bridges function just as in cytokinesis and an additional regulator or pathway blocks the contraction of actomyosin rings in the syncytium. Or, the cytokinetic regulators at rachis bridges function differently than in cytokinesis, leading to the stabilization of the actomyosin rings in the syncytium.

The centralspindlin complex is composed of MKPL1 and MgcRacGAP, respectively ZEN-4 and CYK-4 in *C. elegans*. During cytokinesis, centralspindlin functions to promote the recruitment of RhoA<sup>RHO-1</sup> and its activator ECT-2 at the equatorial region of the cortex, where RhoA subsequently coordinates the formation of the contractile ring (Pintard and Bowerman, 2019). While CYK-4 and ZEN-4 specifically localize at the central spindle microtubules during cytokinesis, they are enriched at germ cell rachis bridges where antiparallel microtubules are not readily detectable. Strikingly, partial depletion of CYK-4 or ZEN-4 results in rachis bridge instability and disorganizes the architecture of the adult germline (Zhou *et al.*, 2013). This suggests that the centralspindlin complex has a structural role at rachis bridges and is thus regulated differently in *C. elegans* syncytial germ cells. Zhou and colleagues took advantage of temperature sensitive alleles in the ZEN-4 kinesin motor domain and the CYK-4 GAP domain to functionally demonstrate that centralspindlin regulation at rachis bridges differs from cytokinesis in notable ways. First, localization of the centralspindlin complex at rachis bridges relies solely on CYK-4 (and not on ZEN-4) and is independent from microtubules. Second, while the GAP activity of CYK-4 acts upstream of RhoA during cytokinesis, RHO-1 or NMY-2 localization remain present at rachis bridges in mutants bearing loss-of-function alleles in the GAP domain of CYK-4 (Zhou *et al.*, 2013), and RNAi depletion of CYK-4 does not perturb germline syncytial architecture during larval development but results in a loss of expression of RGA-3, the RHO-1 GAP in adult animals, and thus germline disorganization (Lee *et al.*, 2018). This suggests that CYK-4 activity does not impinge

on the same set of effectors at rachis bridges compared to cytokinesis. Additional work is needed to unravel the function of the centralspindlin complex in the syncytium. Understanding how CYK-4 and ZEN-4 are targeted to rachis bridges and how they sustain syncytium integrity will help understanding how the syncytium architecture is regulated.

### ***Rachis bridges are stabilized by opposing forces***

To understand how actomyosin rings remain open at rachis bridges, researchers have asked what could antagonize the closure of actomyosin rings at rachis bridges. It is proposed that negative contractility regulators apply forces opposed to known contractility regulators to maintain rachis bridges opened.

Anillin is the first regulator which RNAi partial depletion has been found to destabilize actomyosin rings in the syncytium, resulting in collapses of the membrane partition between germ cells and multinucleation (Maddox et al., 2005). Out of the three predicted anillin encoding genes in *C. elegans*, ANI-1 and ANI-2 were shown to play an important role in the maintenance of rachis bridge stability. While ANI-1 possesses all the domains typically found in Anillin proteins of other species (and is thus considered the canonical *C. elegans* Anillin), ANI-2 lacks the predicted myosin- and actin-binding domains found in canonical Anillin proteins and was proposed to have dominant-negative function. Accordingly, ANI-1 is found at the cytokinetic ring in all cells whereas ANI-2 is only found in the germline. In *ani-2* mutants, rachis bridges are smaller in diameter compared to wild type whereas depletion of ANI-1 results in larger rachis bridges. In addition, depletion of ANI-1 in *ani-2* mutants partially restored the defects observed on rachis bridges in adult animals. This suggests that like in cytokinesis ANI-1 acts as a contractility regulator exerting forces to constrict the actomyosin rings, in opposition to ANI-2 which negatively regulates contractility by competing with ANI-1 at rachis bridges. It is therefore proposed that rachis bridges organization is maintained by a balance of activity between ANI-1 and ANI-2, which locally controls the engagement of contractility regulators (Amini et al., 2014). In support of this, ANI-1 depletion increases ANI-2::GFP fluorescence at rachis bridges (Rehain-Bell *et al.*, 2017). Interestingly, Anillin was recently proposed to regulate cytokinetic ring ingression by favouring the dissipation of tension resulting from actomyosin contraction (Carim et al., 2020). Whether

ANI-2 is a dominant-negative Anillin that locally impedes the activity of the canonical Anillin ANI-1 and thus impacts compressive force in stable actomyosin rings will require further cellular and/or biochemical validation.

### ***Activation levels of NMY-2 regulates tension at rachis bridges***

Non-muscle myosin II is a key component in most contractile networks, as both its motor and actin crosslinking activities are responsible for physical tension. NMY-1 and NMY-2 are the two Non-muscle myosin II heavy chains in *C. elegans*, but only NMY-2 is required for cytokinesis, and its motor activity is crucial for contractility during cytokinesis (D'Avino *et al.*, 2015; Osorio *et al.*, 2019; Piekny *et al.*, 2003). NMY-2 also localizes at rachis bridges actomyosin rings suggesting that it locally controls their contractility. Because it has previously been proposed that positive and negative contractility regulators control bridge stability, studies have looked into whether this regulation is done through NMY-2's activity.

The conserved serine-threonine kinase GCK-1 and its binding partner CCM-3 were recently identified as new ANI-1 interactors implicated in gonad organization and rachis bridges stability (Pal *et al.*, 2017; Rehai-Bell *et al.*, 2017). CCM-3 both localizes at rachis bridges and in cytokinetic rings in the embryo, suggesting that CCM-3 regulates contractility. RNAi depletion of GCK-1 and CCM-3 reduced the diameter of rachis bridges, a phenotype partially suppressed by co-depleting either protein with ANI-1. In addition, GCK-1 or CCM-3 depletion increased the density of ANI-1::mNeonGreen at rachis bridges. Together these results suggest that GCK-1 and CCM-3 regulate ANI-1 to promote rachis bridge stability (Rehai-Bell *et al.*, 2017). Rehai-Bell and colleagues have then looked into NMY-2 levels upon depletion of rachis bridges regulators to test whether this impacts NMY-2 function. In addition to reduce rachis perimeter, depletion of GCK-1, CCM-3 and ANI-2 increased the levels of NMY-2 in the rachis, suggesting that these three proteins control contractility at rachis bridges in part by limiting NMY-2 levels. This is consistent with the idea that an excess of NMY-2 at rachis bridges increases contractility, leading to a reduction of rachis perimeter. In opposition, the depletion of NMY-2's activator ROCK<sup>LET-502</sup> increased the size of rachis bridges, suggesting that a lack of NMY-2's activity decreases tension at rachis bridges.



The myosin-dependent tension exerted by the actomyosin network at the rachis was recently tested more directly. Puncturing the rachis surface with a laser under various conditions led to a rapid recoil of the surrounding actomyosin network and directly demonstrated that rachis bridges are under mechanical tension. Recoil was considerably reduced after partial depletion of NMY-2, suggesting that NMY-2 is responsible for most if not all the tension imparted at the rachis surface (Priti et al., 2018). To further study the role of actomyosin contraction in the rachis, Priti and colleagues used genetic and pharmacological perturbations of both actin and myosin regulators. Depletion of regulators promoting contractility such as the actin nucleation factor CYK-1, NMY-2's activator LET-502, and NMY-2 itself significantly decreased germ cells height and increased the perimeter of rachis bridges as well as the total diameter of the rachis, consistent with a loss of tension in the rachis (Figure 1.17). In addition, inhibition of actin polymerisation by latrunculin A treatment and inhibition of myosin light-chain kinase by ML-7 treatment led to similar but more severe phenotypes on the germline. This shows that perturbations of actin and myosin activity decreases contractility and diminishes tension in the syncytial structure. In opposition, RNAi depletion of regulator that limit NMY-2's activity such as the regulatory subunit of myosin phosphate MEL-11 and GCK-1 and CCM-3 led to an increase of germ cells height, a narrower rachis and smaller rachis bridges, compatible with an increase of the tension in the rachis (Figure 1.17).

Altogether, studies on *C. elegans* syncytium have shown that rachis bridges are stabilized by a balanced regulation of actomyosin tension. Except for ANI-2, all contractility proteins that regulate actomyosin tension at rachis bridges also generally regulate cytokinesis in embryonic cells. The specific mechanism by which negative and positive regulators of contractility balance actomyosin tension in the *C. elegans* germline remains unknown. This mechanism is most certainly inherent to germline identity and its specific regulation.

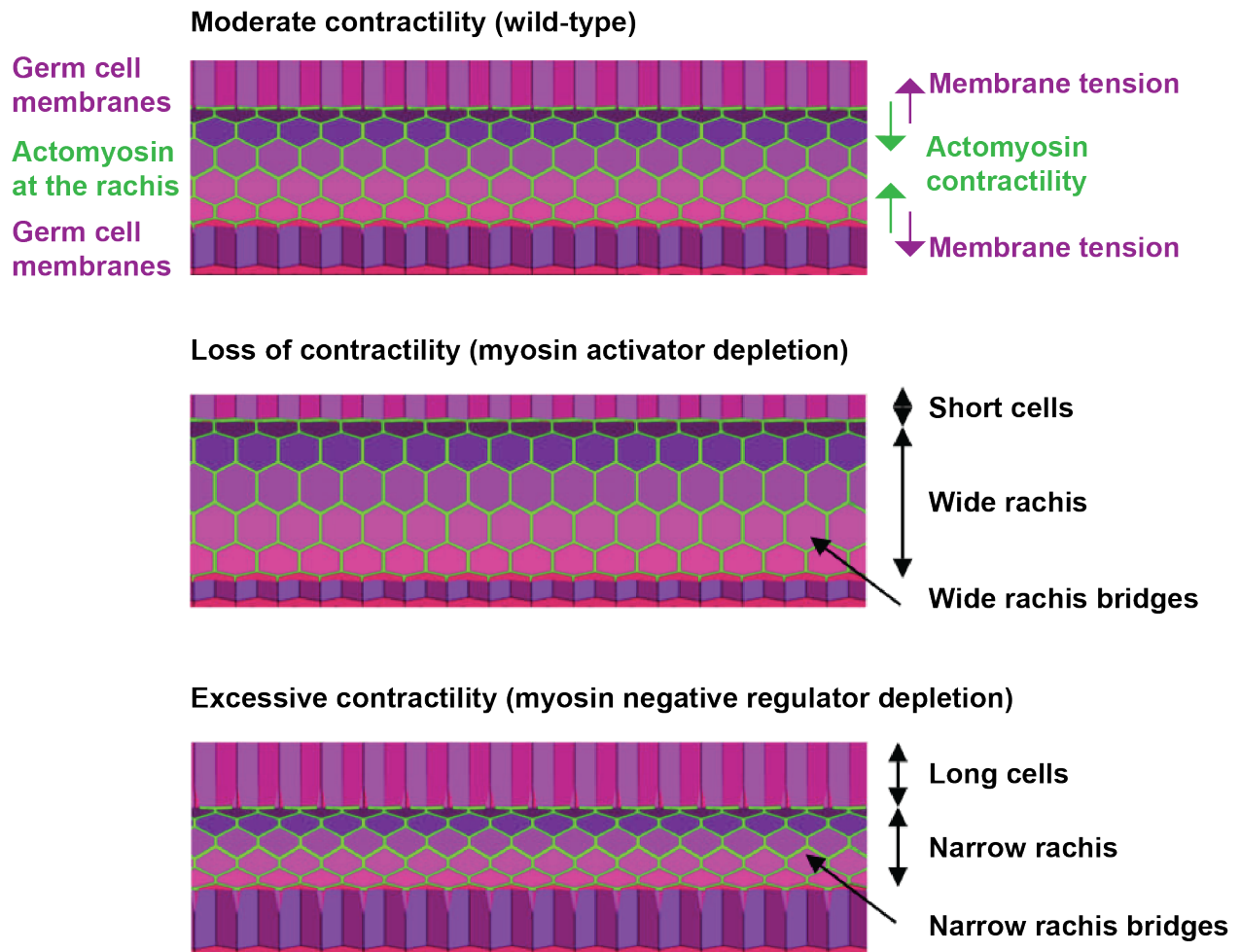


**Figure 1. 17: A model for the regulation of syncytial germline architecture in *C. elegans***

The syncytial architecture in the germline is regulated by mechanical tension from the germ cell membranes and from the actomyosin at the rachis bridges. The loss of myosin positive regulators causes a loss of contractility which widens the size of the rachis. In opposition, a loss of myosin negative regulators causes excessive contractility which narrows the size of the rachis. Figure adapted with permission from (Priti et al., 2018).

### 1.6.2.2 *C. elegans* syncytium genesis

#### ***How are rachis bridges formed?***

The appeal to understand the organization of *C. elegans* syncytium is in part due to the interest in studying contractile structures dynamics, but how the rachis bridges form and expand during development remains unknown. Indeed, the mechanisms by which a germ cell connected to the rachis by a stable actomyosin ring divides to give rise to two daughter cells with individual rachis bridges is undetermined. To elucidate how rachis bridges form and expand the syncytial structure, future work will have to focus on studying how mitotic germ cells organize during their division.

One study has reconstituted the steps of cells division in fixed tissues to attempt the study of how mitotic germ cells divide in *C. elegans'* syncytium (Seidel et al., 2018). Although F-actin is not a rachis specific marker, with F-actin and nuclei immuno-staining, Seidel and colleagues observed that rachis bridges narrow during cell division and that the cytokinetic ring ingresses towards the rachis. This is supported by an alpha tubulin staining that indicates that the mitotic spindle is parallel to the rachis bridges (Seidel et al., 2018). They proposed a model in which the cytokinetic ring enters in contact with the stable ring to eventually “pinch” the stable ring into two separate rings that will connect the daughter germ cells to the rachis (Seidel et al., 2018). This model emerges from electron microscopy data in *Drosophila* follicle cells and in the annelid germline where tripartite structures were observed at the syncytial bridges in cells undergoing division (Figure 1.18) (Airoldi et al., 2011; Swiatek et al., 2009; Tilney et al., 1996). This model remains speculative and remains to be validated by live imaging, ideally with markers enabling a discrimination between the dynamic cytokinetic ring and the stable rachis bridge ring.

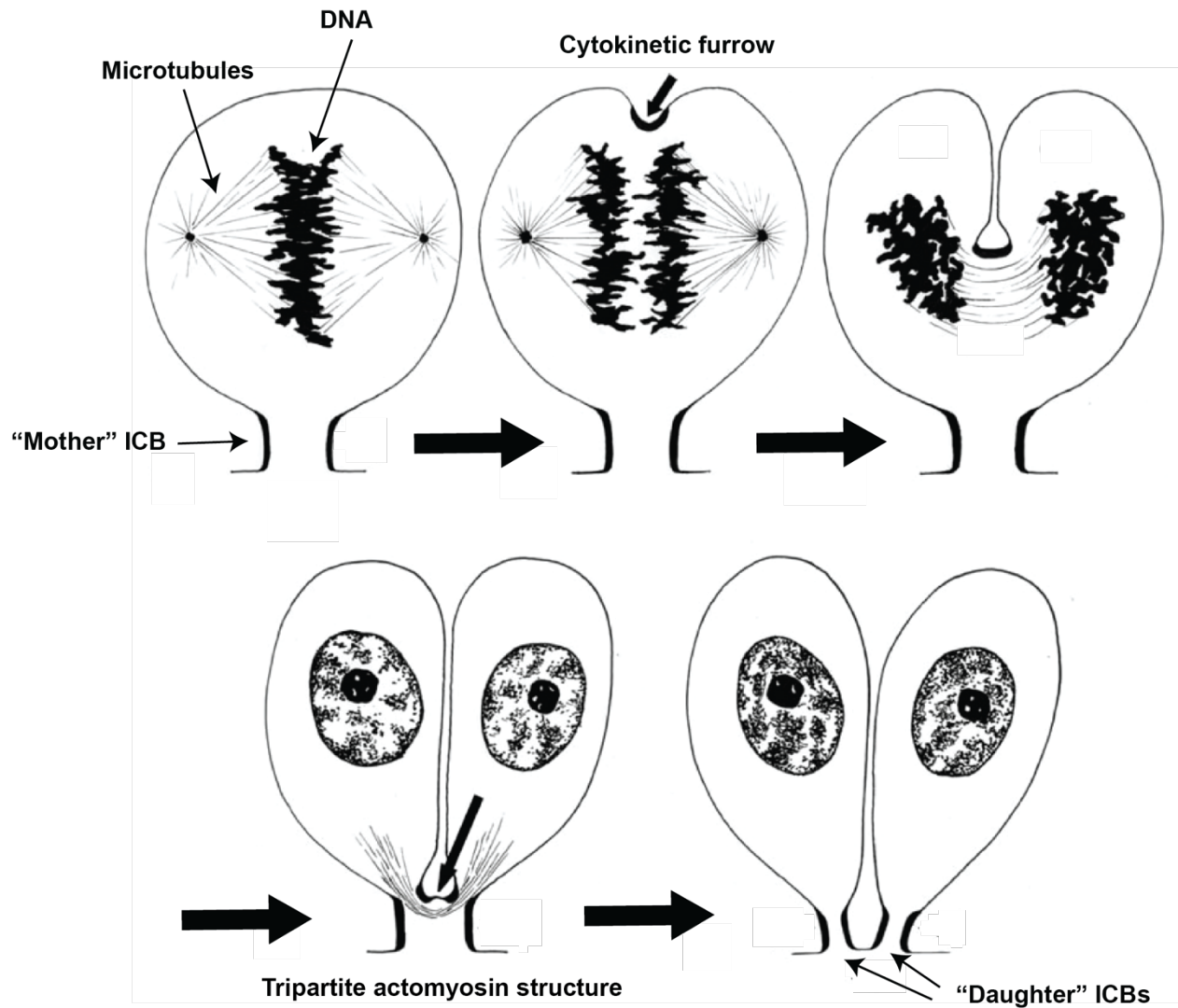


**Figure 1. 18: A model for syncytium expansion in annelids**

Model proposed by Swiatek and colleagues for the expansion of syncytia in annelids. The cytokinetic furrow is one sided and ingresses towards the "mother" ICB until it divides the "mother ICB" into two "daughter ICBs". Image adapted with permission from (Swiatek et al., 2009).

***How does the C. elegans syncytium nucleate?***

The syncytial architecture is inherent to the *C. elegans* germline identity but how it originates is unclear. While syncytial organizations are commonly found in animal germlines, what determines the *C. elegans* germline to be syncytial and how this mechanism is regulated is

unknown. To understand how the *C. elegans* syncytium nucleates research will need to focus on what differentiates the germ lineage from the somatic lineage.

To understand how the syncytium originates, recent work has retraced the first steps of syncytium formation in *C. elegans* germline. By tracking the division of the germline precursor P<sub>4</sub> into the two primordial germ cells Z<sub>2</sub> and Z<sub>3</sub> in the embryo, Goupil and colleagues have demonstrated that there is no abscission between Z<sub>2</sub> and Z<sub>3</sub>. This incomplete division leads to the stabilization of a contractility regulator-rich cytoplasmic bridge between Z<sub>2</sub> and Z<sub>3</sub> making the two cells syncytial (Goupil et al., 2017). Partial RNAi depletion of the contractility regulators at the bridge led to a regression of the membrane partition between Z<sub>2</sub> and Z<sub>3</sub>, suggesting that these regulators are locally active to stabilize the bridge (Goupil et al., 2017). Further epistatic analyses revealed that Rho regulators promote the accumulation of ANI-2 which promotes NMY-2 and CYK-7 at the cytoplasmic bridge, in part by limiting ANI-1 accumulation (Goupil et al., 2017). While the requirements for rachis bridge stabilization are similar in the embryo, when there are only two germ cells, and in adults, where thousands of cells are connected to the rachis, it remains unclear if and/or how the incompleteness of abscission that occurs in the early embryo relates to germline syncytial organization later in development.

The two *C. elegans* Anillin isoforms ANI-1 and ANI-2 are required for rachis bridge stability, although ANI-2 is specifically expressed in the germline (Maddox et al., 2005). ANI-2 is the only regulator found to be both germline specific and required for syncytium formation and maintenance (Amini et al., 2014; Goupil et al., 2017). This suggests that ANI-2 is the only regulator that differentiates cell divisions in the germline from somatic cells, making ANI-2 a potential master regulator for syncytium formation. Because of its specificity, one could imagine that eliminating ANI-2 in the germline would lead to complete cell divisions resulting in the formation of a non-syncytial germline. However previous studies have shown that depletion of ANI-2 leads to multinucleation, similarly to depletion of other contractility regulators (Amini et al., 2014; Goupil et al., 2017). Further work needs to investigate how ANI-2 interacts with other regulators during cell division to form the syncytial structure in the germline. In addition, screening for new

proteins associated with syncytium formation could lead to finding a regulator that orchestrate syncytium formation in *C. elegans*.

### **1.6.2.3 Advantages of *C. elegans* to understand syncytial structures**

The fruit fly and the mouse are pioneers in the study of syncytial germlines. Indeed, these models have considerably advanced the knowledge in defining syncytial structures. However, in the past decades, *C. elegans* has emerged as a valuable model to study syncytial germlines. This is due to its small size and transparency which gives direct access to the germline in living animals. These characteristics provide a unique opportunity to study *in vivo* the molecular mechanisms of syncytial germ cell division with live imaging, which is essential to better understand syncytium formation. In addition, the facility to partially deplete gene expression by RNAi in the worm, gives the possibility to easily carry out large screening for genes implicated in syncytium maintenance and formation. Such a study has been previously conducted on 5% of the *C. elegans* genome and found a large number of genes which depletion led to germline and rachis disorganization (Green et al., 2011). Some of these genes need further study to understand how they regulate the syncytial architecture in the *C. elegans* germline.

## 1. 7 Objectives

Although syncytia are prevalent amongst living species, there is still a lot to learn about what their function are and how they form. The mechanisms of syncytium formation are only beginning to become more understood in animal germlines where germ cells are directly connected with one another. However, these mechanisms remain completely unknown in germlines where germ cells are connected to a common structure but not directly to one another. The general objective of my thesis is to elucidate how the syncytium expands germlines organized around a central structure. We took advantage of the *C. elegans* germline model to better understand how the syncytium expands during germ cell division.

The study conducted in “Chapter 2” comprises two main objectives:

1. Examine whether the primordial germ cells are syncytial at the first larval stage.
2. Track the first division of the primordial germ cells to understand how the daughter cells connect to the syncytium

The single objective of “Chapter 3” is to investigate whether actomyosin regulators are required for the maintenance of the syncytial organization in the first larval stage primordial germ cells.

In “Chapter 4” I aim to immobilize first larval stage animals in conditions that simulate physiological settings to track several rounds of germ cell division.





## **2. Article 1 - The initial expansion of the *C. elegans* syncytial germ line is coupled to incomplete primordial germ cell cytokinesis**

**Jack Bauer**<sup>1</sup>, Vincent Poupart<sup>1</sup>, Eugénie Goupil<sup>1</sup>, Ken C. Q. Nguyen<sup>3</sup>, David H. Hall<sup>3</sup> and Jean-Claude Labbé<sup>1,2,\*</sup>

<sup>1</sup>Institute for Research in Immunology and Cancer (IRIC), Université de Montréal, C.P. 6128, Succ. Centre-ville, Montréal, QC H3C 3J7, Canada.

<sup>2</sup>Department of Pathology and Cell Biology, Université de Montréal, C.P. 6128, Succ. Centre-ville, Montréal, QC H3C 3J7, Canada.

<sup>3</sup>Department of Neuroscience, Albert Einstein College of Medicine, Bronx, NY 10461, USA.

\*Author for correspondence (jc.labbe@umontreal.ca)

Development, Volume 148, Issue 18, September 2021

## 2.1 Author contributions

**Jack Bauer** conceptualized, designed, and executed the experiments in (Figure 2.1; Figure 2.2; Figure 2.3; Figure 2.4, Figure S2.1; Figure S2.2; Figure S2.3; Figure S2.4; Figure S2.5; Movie 2.1; Movie 2.2; Movie 2.3; Movie 2.4; Movie 2.5; Movie 2.6), analysed the data, prepared the figures for the manuscript, wrote and edited the manuscript.

**Vincent Poupart** analysed the data in (Figure 2.1C,D and Figure S2.3) and designed the figures in (Figure 1.C,D; Figure S2.3; Movie 2.3).

**Eugénie Goupil** participated in the execution of experiments and analysed the data in (Figure 2.1G and Figure 2.4C)

**Ken C.Q. Nguyen** participated in the execution of the experiments in (Figure 2.1C,D and Figure S2.3)

**David H. Hall** supervised the experiments executed in (Figure 2.1C,D and Figure S2.3)

**Jean-Claude Labbé** supervised the experimental conceptualization and design, the data analysis, and wrote and edited the manuscript.

## 2.2 Abstract

The *C. elegans* germline is organized as a syncytium in which each germ cell possesses an intercellular bridge that is maintained by a stable actomyosin ring and connected to a common pool of cytoplasm, termed the rachis. How germ cells undergo cytokinesis while maintaining this syncytial architecture is not completely understood. Here, we use live imaging to characterize primordial germ cell (PGC) division in *C. elegans* first-stage larvae. We show that each PGC possesses a stable intercellular bridge that connects it to a common pool of cytoplasm, which we term the proto-rachis. We further show that the first PGC cytokinesis is incomplete and that the stabilized cytokinetic ring progressively moves towards the proto-rachis and eventually integrates with it. Our results support a model in which the initial expansion of the *C. elegans* syncytial germline occurs by incomplete cytokinesis, where one daughter germ cell inherits the actomyosin ring that was newly formed by stabilization of the cytokinetic ring, while the other inherits the pre-existing stable actomyosin ring. We propose that such a mechanism of iterative cytokinesis incompleteness underpins *C. elegans* germline expansion and maintenance.

**Keywords:** *C. elegans* germline development, Stable intercellular bridge, Incomplete cytokinesis, Syncytium expansion, Primordial germ cells, Actomyosin.

## 2.3 Introduction

The germ line is a specialized tissue that coordinates gamete production and thus ensures fertility in all animal species. Accordingly, primordial germ cell (PGC) specification typically occurs early during embryogenesis to ensure proper distinction from the soma and maintain totipotency (Marlow, 2015; Sybirna et al., 2019). Division of the PGCs will eventually lead to the formation of a pool of germline stem cells that have the capacity to self-renew and give rise to gamete progenitors. One striking feature of certain gamete progenitors, e.g. mammalian spermatocytes, *Drosophila* ovarian cystoblasts and zebrafish germ cells, is the presence of stable intercellular bridges that connect cells with one another, effectively forming a syncytial architecture (Bertho et al., 2021; Fawcett et al., 1959; Greenbaum et al., 2011; Robinson et al., 1994). This feature is common to the germ line of all animals studied to date (Swiatek and Urbisz, 2019), consistent with the notion that intercellular bridges play a fundamental role in fertility. Work in mouse and *Drosophila* demonstrates that stable germ cell intercellular bridges arise from incomplete cytokinesis at the end of mitosis (Greenbaum et al., 2011; Haglund et al., 2011). Although intercellular bridge stabilization was shown to rely on impaired recruitment of the abscission machinery by the protein TEX14 in mouse spermatocytes (Greenbaum et al., 2007b; Iwamori et al., 2010b) and differential actin regulation at the end of cytokinesis in *Drosophila* (Robinson et al., 1994; Tilney et al., 1996), our understanding of the molecular mechanism responsible for incomplete cytokinesis in animal germ cells is poor.

The adult *C. elegans* germline is contained within two U-shaped gonad arms, in which germ cells form a columnar monolayer around a central core of cytoplasm, termed the rachis (Hall et al., 1999; Hirsh et al., 1976). Except for the germ cells undergoing the last stages of gametogenesis, the entire architecture is syncytial and each cell possesses a stable actomyosin ring that maintains an intercellular bridge (also called ring channel) with the rachis (Amini et al., 2014; Maddox et al., 2005; Priti et al., 2018; Rehai-Bell et al., 2017; Wolke et al., 2007; Zhou et al., 2013). The entire adult germline originates from two PGCs that are born during early embryogenesis and remain mitotically quiescent until after hatching, when feeding of first-stage larvae (L1) promotes the initiation of their proliferation (Strome and Updike, 2015; Wang and

Seydoux, 2013). The cytokinesis leading to PGC formation is incomplete and leaves the two cells connected by a stable intercellular bridge (Goupil et al., 2017), a developmental feature that is common with the division of mouse and *Drosophila* gamete precursors. Yet how two PGCs that are directly connected to one another by a single intercellular bridge eventually give rise to thousands of germ cells that each possess a stable bridge connected to the rachis is not well understood.

Two previous studies, carried out in *C. elegans* and in several species of clitellate annelids, specifically focused on deciphering the mechanism by which germ cells divide within the syncytium (Seidel et al., 2018; Swiatek et al., 2009). Together, these studies suggested a model in which the diameter of the stable intercellular bridge shrinks below the level of optical resolution as a germ cell progresses through mitosis. During mitotic exit, the cytokinetic ring contacts the stable ring at the intercellular bridge, forming a tripartite actomyosin structure, and specific constriction of the cytokinetic ring effectively bisects the intercellular bridge (Seidel et al., 2018; Swiatek et al., 2009). However, the molecular mechanism that would enable the differential regulation of two contacting and intertwined actomyosin rings within the same cell, one dynamic and one stable, is not known. Importantly, neither study employed live imaging of germ cell cytokinesis, which may have masked mechanistically relevant dynamic events.

Here, we have used live imaging of the first PGC division to investigate how *C. elegans* germ cells undergo cytokinesis to form two daughter cells that each possess a stable intercellular bridge. We find that each PGC in L1 larvae has an intercellular bridge that opens to a common, adjoining cytoplasmic cavity, which we term the proto-rachis. This indicates that the primordial germ line undergoes a change during late embryogenesis, enabling the formation of at least one additional stable intercellular bridge. We also find that, upon PGC division, the cytokinetic ring persists and integrates into the proto-rachis. Our findings support a model in which PGC cytokinesis is incomplete and ends with an additional stable ring that is inherited by one of the daughter cells, while the other daughter inherits the pre-existing stable actomyosin ring. This mode of incomplete cytokinesis effectively enables expansion of the syncytial architecture when PGCs initiate proliferation, and iteration of this process with each germ cell division could further

provide a mechanism for expansion and maintenance of the syncytial architecture throughout development. Our results support the notion that, despite architectural differences between species, incomplete cytokinesis is a fundamental feature of germline development.

## 2.4 Results

### 2.4.1 Each *C. elegans* PGC possesses a stable intercellular bridge that opens to a common cytoplasmic compartment

The *C. elegans* germ line was previously proposed to be syncytial throughout development (Figure 2.1A); however, its architecture has not been thoroughly characterized at the L1 stage, where the two primordial germ cells are relatively small and difficult to resolve by light microscopy. To characterize germline organization at the L1 stage, we first performed enhanced-resolution confocal imaging of PGCs co-expressing fluorescent protein (FP)-labelled markers for the plasma membrane (mNeonGreen[mNG]::PH) and chromatin (mCherry[mCh]::HIS-58). As shown previously (Abdu et al., 2016; Lee et al., 2018), we found that the plasma membrane of the two L1-stage PGCs is mostly well resolved except for a region located between the two cells, where a membrane-dense structure, organized into lobes and lacking nuclear material, was present (Figure 2.1B). This membrane-dense structure could be observed in all L1 animals examined ( $n > 100$ ), although its overall size and shape and the number lobes of appeared variable. We used transmission electron microscopy (TEM) to validate these observations and gain further insight into this atypical, complex membrane organization. Analysis of serial TEM sections from an individual L1 larva revealed an architecture in which the plasma membrane of the two PGCs appears continuous, with a well-defined intercellular bridge formed between each germ cell and the common, adjoining membrane-dense structure (Figure 2.1C,D; Movie 2.1 can be found on *Development* website). Furthermore, although mitochondria could be observed within the cytoplasm of this adjoining membrane-dense structure, including through intercellular bridges (Figure 2.1C, inset), no electron-dense signal characteristic of chromatin was detected, consistent with optical microscopy images showing that this structure is devoid of chromatin. These results indicate that each PGC possesses its own distinct intercellular bridge at the L1 larval stage.

Previous findings monitoring the diffusion of photoactivatable rhodamine-dextran indicated that the cytoplasm of PGCs is isolated soon after they are born during embryogenesis but that the two PGCs exchange cytoplasm, and are thus effectively syncytial, after animals have hatched as L1 larvae (Abdu et al., 2016; Amini et al., 2014). To independently validate that PGCs share common cytoplasm at the L1 stage, we employed an approach that made use of animals expressing the photoconvertible fluorescent protein Dendra2 in germ cells (Griffin et al., 2011). To this end, we specifically photoconverted Dendra2 in one of the PGCs, and measured whether the photoconverted signal diffused to the other PGC (Figure 2.1E). Our photoconversion method was specific and precise, as the photoconverting laser illumination of one of the PGCs resulted in a rapid peak of fluorescence signal in this cell and no significant measured fluorescence change in the non-illuminated PGC (Figure 2.1F,G; Figure S2.1A). Monitoring bleach-corrected photoconverted fluorescence signal intensity over time revealed that it rapidly decreased in the illuminated cell while it concomitantly increased in the other, non-illuminated PGC (Figure 2.1F,G; Movie 2.2 can be found on *Development* website). No increase in photoconverted signal was observed in either cell when we imaged animals that had not been illuminated by the photoconverting laser (Figure S2.1B), indicating that the photoconverted signal in the non-illuminated PGC originates from the illuminated cell. Consistent with previous findings (Abdu et al., 2016), these results indicate that the intercellular bridges that we observed in the PGCs permit cytoplasmic exchange, and thus that the *C. elegans* primordial germ line is effectively syncytial when animals hatch as L1 larvae.



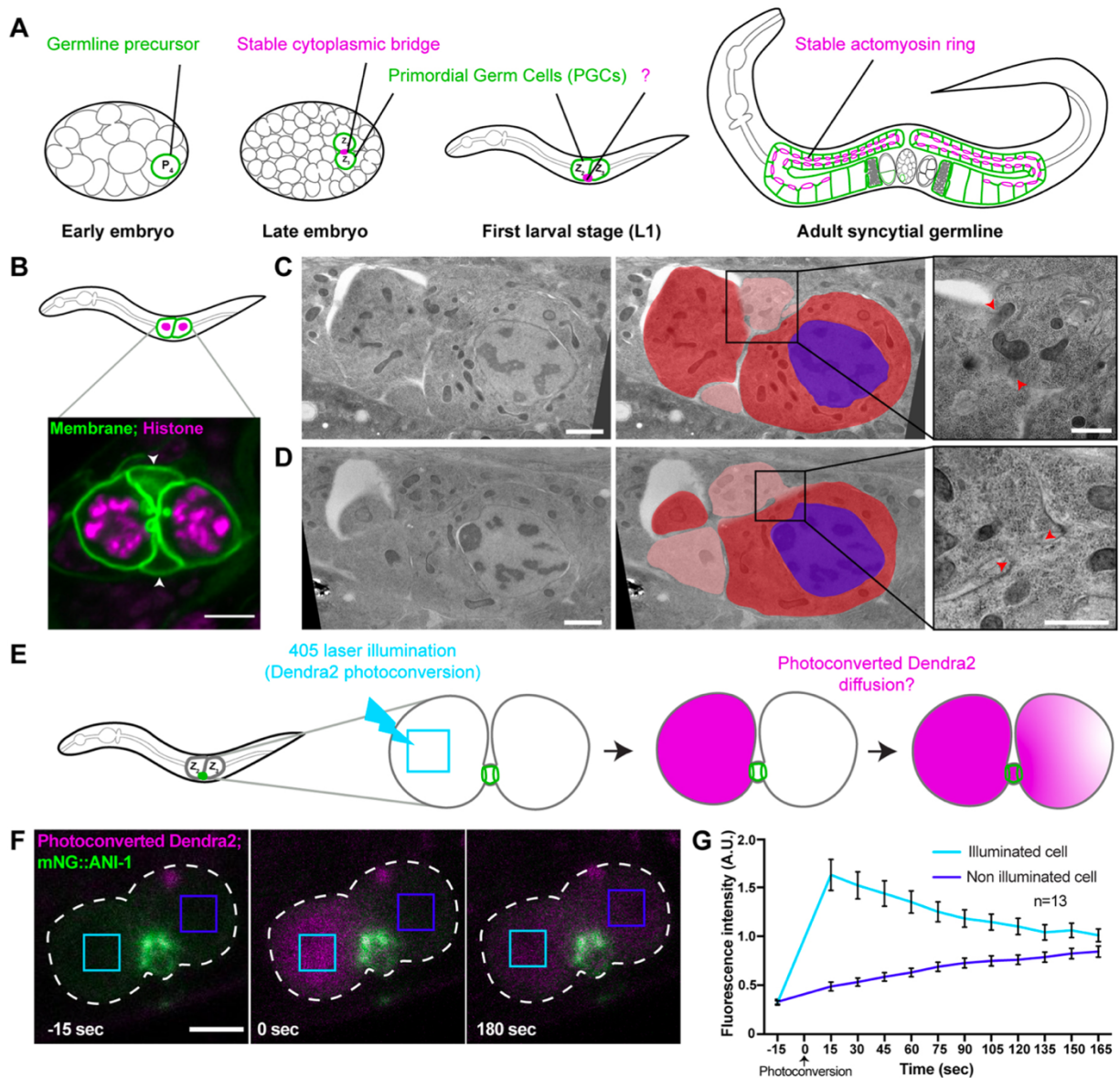


**Figure 2. 1: Both PGCs have an intercellular bridge in *C. elegans* first-stage larvae**

(A) Schematic representation of stages of *C. elegans* germline development, from the birth of two PGCs (Z2 and Z3) following division of the germ cell precursor P4 during embryogenesis to the adult architecture. Germ cell plasma membrane is in green and actomyosin rings stabilizing intercellular bridges are in magenta. (B) Confocal image (sum projection of three slices) of the PGCs in a first larval stage animal expressing markers for membrane (mNG-PH<sup>PLCδ</sup>, green) and chromatin (mCh-HIS-58, magenta). White arrowheads indicate the membrane-dense structure found between the two PGCs. Scale bar: 3 μm. (C,D) Selected transmission electron microscopy images from 90 nm sections of the primordial germ line from a first larval stage animal. The middle panel is a color-overlaid version of the left panel, depicting nuclei (blue), PGC cytoplasm (dark red) and cytoplasm within the membrane-dense structure between the PGCs (light red).

Scale bars: 1  $\mu\text{m}$ . Panels on the right are magnifications of the boxed regions in the middle panels, where intercellular bridges are visible (red arrowheads). Scale bars: 500 nm. (E) Schematic representation of the Dendra2 photoconversion and diffusion approach used to assess cytoplasmic exchange in first larval stage PGCs. (F) Confocal time-lapse images (sum projection of three slices) of PGCs in animals expressing mNG::ANI-1 (green) and Dendra2 before (left) and after (middle and right) Dendra2 photoconversion (magenta). The blue boxes indicate regions where fluorescence was measured over time, and the light blue box in the middle panel is where photoconverting laser illumination was carried out. Scale bar: 3  $\mu\text{m}$ . (G) Mean levels of photoconverted Dendra2 fluorescence intensity measured over time (in seconds) in the illuminated (light blue) and non-illuminated (dark blue) regions of the PGCs that are defined in F. Time 0 is the onset of photoconverting laser illumination. Data are mean $\pm$ s.e.m., n=13 animals.

In *C. elegans* late larvae and adults, each germ cell is connected to the central rachis via an intercellular bridge that is stabilized by an actomyosin ring (Hall et al., 1999; Hirsh et al., 1976; Maddox et al., 2005). In TEM sections, we observed electron-dense regions near the intercellular bridges connecting PGCs to the membrane-dense structure (Figure 2.1C,D; Movie 2.1 can be found on *Development* website), suggesting that these bridges may likewise be stabilized by actomyosin rings. To assess this, we used enhanced-resolution confocal microscopy to monitor the localization of several FP-labelled actomyosin regulators previously implicated in the regulation of stable rings at germ cell intercellular bridges in larvae and adults. Their localization was monitored in animals co-expressing fluorescent markers for the plasma membrane, facilitating germ cell identification and characterization. We found that all of the actomyosin regulators that we monitored were generally enriched at the membrane-dense structure located between the PGCs (Figure 2.2A; Figure S2.2A). Interestingly, several of these regulators, including Non-Muscle Myosin II (NMY-2::GFP) and its regulator CCM-3 (CCM-3::mNG), the Anillin protein ANI-1 (mNG::ANI-1), the *C. elegans*-specific cytokinetic regulator CYK-7 (CYK-7::GFP), and the two centralspindlin complex components CYK-4 (CYK-4::mNG) and ZEN-4 (GFP::ZEN-4), organized into ring-like patterns reminiscent of the actomyosin rings that stabilize the germ cell intercellular bridges in late larvae and adult animals (Figure 2.2A; Figure S2.2A). To assess this, we measured the fluorescence distribution of membrane and actomyosin markers across PGC intercellular bridges. As reported previously (Amini et al., 2014), stable germ cell intercellular bridges show a distinct pattern of fluorescence distribution for both of these markers in confocal sections: a

fluorescence intensity minimum bordered by peaks of fluorescence intensity. We observed this characteristic fluorescence distribution pattern in most (136/154) PGCs of animals expressing FP-tagged ANI-1, NMY-2, CYK-7, CYK-4 and ZEN-4, consistent with the presence of intercellular bridges stabilized by actomyosin rings, as in animals of later developmental stages (Figure 2.2B,C; Figure S2.2B-E). The measured distance between fluorescence intensity peaks, corresponding to the diameter of the intercellular bridge, varied from 0.3 to 2 $\mu$ m (mean $\pm$ s.d.=1.0  $\pm$ 0.4  $\mu$ m, n=136 cells; Figure 2.2D). This intercellular bridge diameter is smaller than that reported for late (L4) larvae and adults (~2-4  $\mu$ m) but comparable with that measured in L2 and L3 larvae (~1.5  $\mu$ m; (Amini et al., 2014; Rehai-Bell et al., 2017). Well-defined intercellular bridges could not be measured in a small fraction of PGCs analyzed (18/154), which may indicate that some bridges bear a diameter below the limit of optical resolution and/or that their position within the optical plane does not permit proper visualization. These results indicate that, as in other developmental stages, each *C. elegans* PGC intercellular bridge is stabilized by an actomyosin ring.

In addition to accumulating at PGC intercellular bridges, actomyosin regulators could often be observed to form ring-like patterns in other regions of the membrane-dense structure found between the PGCs, specifically near the base of defined membrane lobes (Figure 2.2B,C; Figure S2.2B-E). Together with points of membrane constriction bordered by electron-dense regions that could be observed by TEM within the membrane-dense structure (Figure S2.3A-C), this suggested that membrane lobes are likewise stabilized by actomyosin rings. To assess this, we measured the fluorescence distribution of membrane and actomyosin markers at the base of lobes. Interestingly, we found a fluorescence distribution pattern characteristic of germ cell intercellular bridges (peaks of fluorescence intensities bordering minima), with a bridge diameter comparable with that measured in PGCs and varying between 0.3 and 1.8  $\mu$ m (mean $\pm$ s.d.=0.7 $\pm$ 0.3, n=114 membrane lobes; Figure 2.2D). Together, these results indicate that the membrane-dense structure found between the two PGCs at the L1 stage is enriched in contractility regulators that form stable actomyosin rings. These rings stabilize intercellular bridges between the two PGCs, a varying number of membrane lobes and a common central cavity (Figure 2.2E; Movie 2.3 can be found on *Development* website), forming a proto-rachis that bears the same fundamental organization principles as the rachis in adult animals (Figure 2.1A).

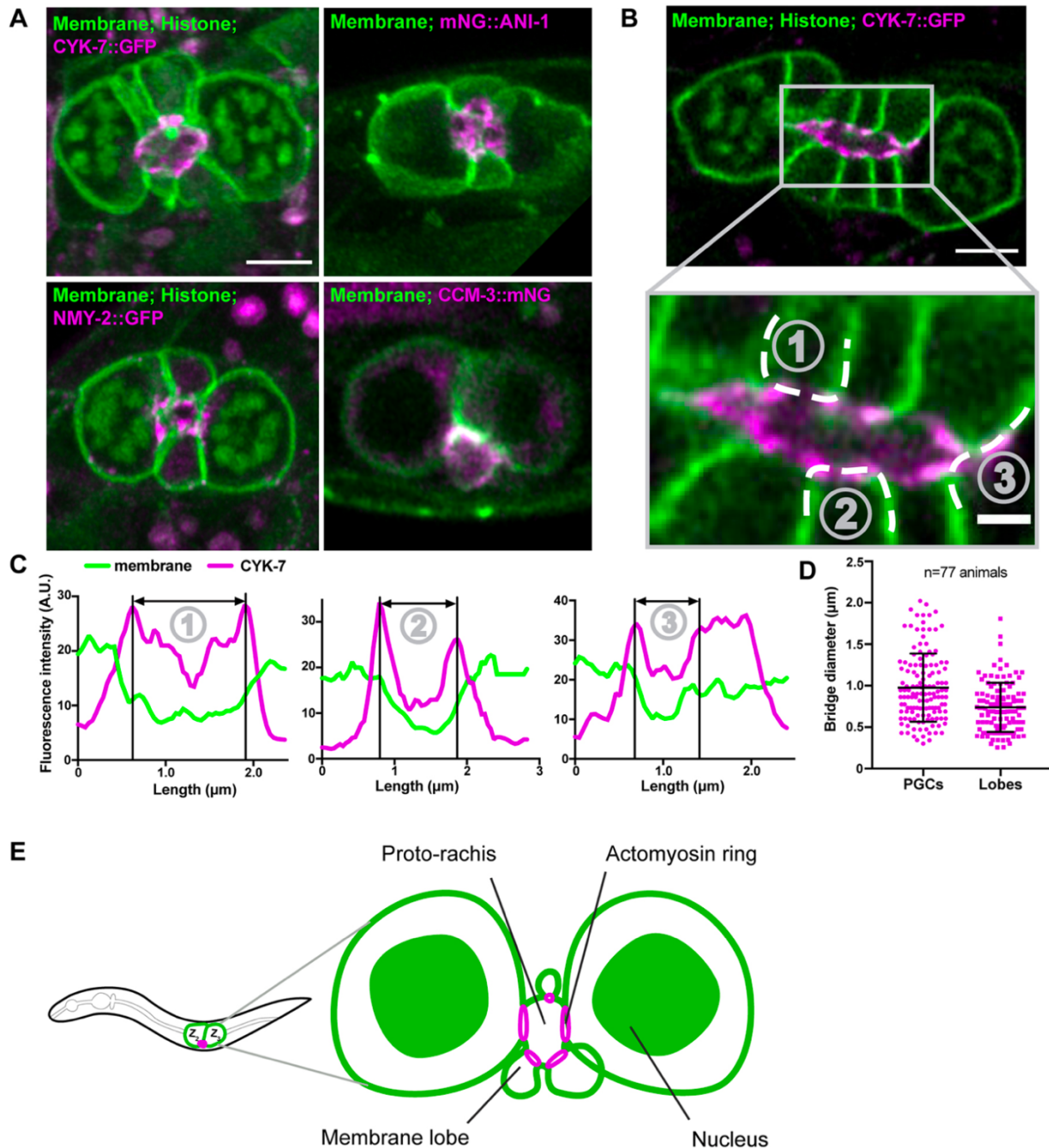


**Figure 2. 2: Actomyosin rings organize a functional proto-rachis in the *C. elegans* primordial germ line**

(A) Confocal images (maximum projection of three slices) of the PGCs in first larval stage animals expressing FP-tagged markers for membrane and chromatin (TagRFP-PH<sup>PLC $\delta$</sup>  and mCh-HIS-58, green) and specified actomyosin contractility regulators (magenta). Scale bar: 3  $\mu\text{m}$ . (B) As in A but for a single confocal slice instead of a maximum projection. The lower panel is a higher

magnification depicting cortical regions in lobes (1 and 2) and a PGC (3) where fluorescence intensity was measured. Scale bars: 3  $\mu\text{m}$  (top) and 1  $\mu\text{m}$  (bottom). (C) Fluorescence intensity of membrane (TagRFP-PH<sup>PLC $\delta$</sup> , green) or CYK-7::GFP (magenta) signal measured along each line (1-3) drawn in B. Intensity peaks of CYK-7::GFP define bridge diameter (black lines and arrows). (D) Intercellular bridge diameters (in  $\mu\text{m}$ ) measured in PGCs (n=136) or lobes (n=114) of animals co-expressing a membrane marker and either CYK-7::GFP, mNG::ANI-1, NMY-2::GFP, CYK-4::mNG or GFP::ZEN-4 (n=77 animals in total). Data are mean $\pm$ s.d. with individual data points indicated. (E) Schematic representation of the *C. elegans* primordial germ line at the first larval stage. Each PGC has an actomyosin ring that stabilizes an intercellular bridge open to a central proto-rachis. The proto-rachis bears a varying number of membrane lobes (three are depicted here) that are also defined by actomyosin rings.

#### **2.4.2 The PGC cytokinetic ring is stabilized and integrates into the proto-rachis at the end of mitosis**

We next sought to exploit the relative simplicity of the germline in L1 larvae to study the mechanism by which germ cell division is coupled to expansion of the syncytial architecture. As each germ cell is connected to the rachis by a stable actomyosin ring from the onset of germline expansion (Figure 2.2E), germ cell division must occur through a mechanism that systematically enables the duplication of the stable actomyosin ring. As a first step, we imaged populations of developing L1 animals expressing FP-tagged reporters for the plasma membrane and actomyosin contractility regulators, to characterize the changes in germline architecture that occur when PGCs have undergone their first division. PGCs were previously reported to divide asynchronously (Butuči et al., 2015) and, accordingly, L1 populations contained a significant number of animals with three germ cells, along with those having two (undivided PGCs) and four (both PGCs divided) germ cells (Figure 2.3A). We measured the total fluorescence intensity of FP-tagged ANI-1, NMY-2, CYK-7 and CCM-3 at the proto-rachis in gonads comprising two, three and four cells. Except for NMY-2, we found that the fluorescence levels of these actomyosin regulators increased in a unitary step-wise manner as germ cell number increased (Figure 2.3A,B). The levels of NMY-2 at the proto-rachis increased significantly between the 2- and 3-germ cell stages but remained stable in 4-germ cell stage larvae (Figure 2.3B). These results show that expansion of the proto-rachis during PGC division is tightly coupled to a local increase in actomyosin contractility regulators. As

each germ cell possesses an intercellular bridge, this is consistent with the notion that a stable actomyosin ring is added to the proto-rachis with each germ cell division.

To gain further insight into syncytial expansion during germ cell division, we employed live confocal imaging of animals co-expressing FP-tagged ANI-1 and a membrane marker to monitor actomyosin dynamics during PGC division. Because live imaging of PGCs requires that animals are removed from food, a condition that causes germ cells to rapidly exit mitotic proliferation (Zellag et al., 2021), we tracked PGC cytokinesis in cells that had already entered mitosis and formed a metaphase plate (Figure 2.3C; Movie 2.4 can be found on *Development* website). Analysis of ANI-1 dynamics during PGC cytokinesis revealed two noticeable features. The first one is that the pool of ANI-1 fluorescence in the PGC cytokinetic ring persisted in late cytokinesis and remained visually distinct for at least 20 min after the apparent completion of cytokinetic ring ingression (Figure 2.3C,D). This contrasts with previous measurements in embryonic blastomeres showing that contractility regulators disappear within ~10 min after the completion of cytokinetic furrow ingression, but is similar to the measured persistence of contractility regulators at the intercellular bridge formed between the two PGCs when they are born (Goupil et al., 2017; Green et al., 2013). The second feature is that the cytokinetic ring ingressed toward the center of the cell and a gap in fluorescence signal could be observed between the pool of ANI-1 at the cytokinetic ring and that at the proto-rachis (Figure 2.3C). The presence of such a gap cannot be reconciled with the current model for germ cell division within the syncytium, which proposes that the cytokinetic ring physically contacts the stable actomyosin ring (Seidel et al., 2018; Swiatek et al., 2009). Tracking the gap formed between the pools of ANI-1 at the persistent cytokinetic ring and at the proto-rachis revealed that it progressively decreases (Figure 2.3C,E), eventually resulting in a situation where the two actomyosin pools can no longer be distinguished, suggesting that they have merged. Accordingly, measurements of FP-tagged ANI-1 fluorescence levels at the proto-rachis revealed that they remain relatively stable until late in mitosis, when they increase by an amount that is comparable to that measured in the cytokinetic ring at the end of furrow ingression (Figure 2.3F). Similar results were obtained when monitoring NMY-2::GFP dynamics during PGC cytokinesis (Figure S2.4; Movie 2.5 can be found on *Development* website). Together with our measured increase in FP-tagged contractility regulators at the proto-rachis with each

germ cell division (Figure 2.3B), this suggests a model in which abscission is impaired at the end of PGC cytokinesis, resulting in the stabilization of the cytokinetic ring remnant and its integration into the proto-rachis, rather than its transition into a midbody ring and subsequent abscission.

To test this model, we devised an approach enabling us to track more directly the fate of contractility regulators in the cytokinetic ring during PGC division. This was carried out by specifically photobleaching the mNG::ANI-1 signal present at the proto-rachis in late cytokinesis without impacting the pool of ANI-1 fluorescence in the cytokinetic ring (Figure 2.3G,H). We found that the levels of ANI-1 in the cytokinetic ring are relatively stable as mitosis progresses and when this pool progressively integrates with that of the proto-rachis (Figure 2.3H; Figure S2.5C,D). To correct for fluorescence recovery after photobleaching (FRAP) at subsequent timepoints, and thus better assess the contribution of the cytokinetic ring ANI-1 pool to the proto-rachis, we measured the average FRAP of mNG::ANI-1 at the proto-rachis of L1 larvae in which PGCs were not dividing (Figure S2.5A,B) and subtracted this amount from the measured mNG::ANI-1 levels at the proto-rachis of larvae undergoing PGC cytokinesis (Figure S2.5C,D; see Materials and Methods). After FRAP correction, we found that the levels of mNG::ANI-1 fluorescence measured at the cytokinetic ring in late mitosis were indistinguishable from those that were measured at the proto-rachis following the integration of the cytokinetic ring signal (Figure 2.3H; Figure S2.5D). Similar results were obtained when using NMY-2::GFP as actomyosin marker (Figure S2.5E,F). These results demonstrate that the pool of actomyosin contractility regulators in the cytokinetic ring directly contributes to the proto-rachis following PGC division. They strongly support a model in which the cytokinetic ring does not undergo its typical maturation prior to abscission, but rather integrates into the proto-rachis as a stable actomyosin ring at the end of cytokinesis, effectively adding one stable ring to the syncytial architecture.

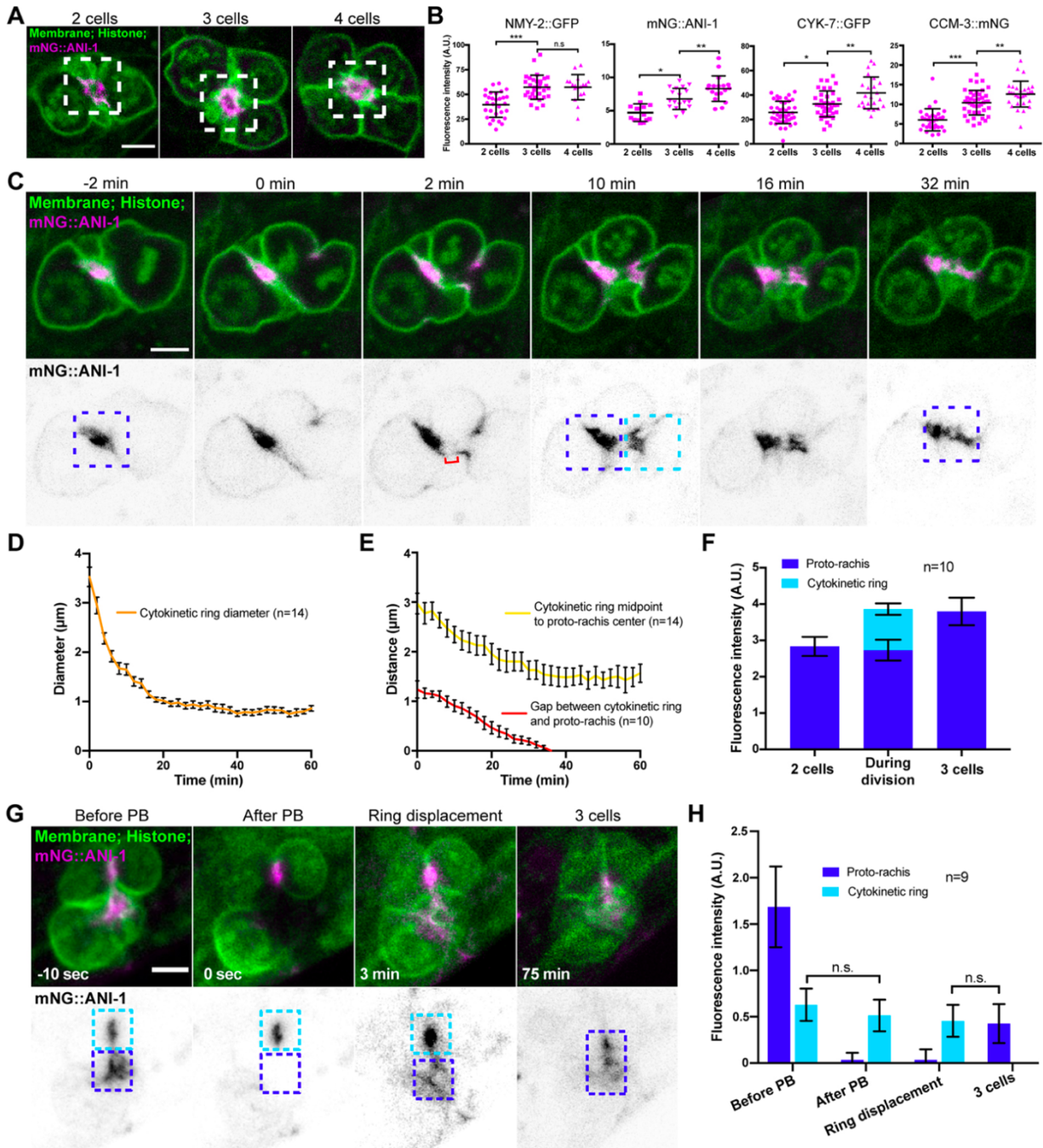


**Figure 2. 3: The cytokinetic ring integrates and expands the proto-rachis at the end of PGC division**

(A) Confocal images (maximum projection of three slices) of the primordial germ line containing 2 (left), 3 (middle) and 4 (right) germ cells in first larval stage animals co-expressing markers for membrane and chromatin (TagRFP-PH $\text{PLC}\delta$  and mCh-HIS-58, green) and mNG::ANI-1 (magenta). Dashed boxes indicate regions where fluorescence intensity was measured. (B) Measured sum fluorescence intensity of the specified markers of actomyosin contractility at the proto-rachis of



first larval stage animals possessing two, three and four germ cells. Data are median $\pm$ s.d. with individual data points indicated. Statistical analyses were carried out using one-way ANOVA with Tukey's post-hoc test (n.s., not significant; \* $P < 0.03$ ; \*\* $P < 0.01$ ; \*\*\*\* $P < 0.0001$ ). (C) Confocal time-lapse images (sum projection of three slices) of PGCs undergoing first division in animals co-expressing markers for membrane and chromatin (TagRFP-PH<sup>PLC $\delta$</sup>  and mCh-HIS-58, green), and mNG::ANI-1 (magenta and bottom panels). The boxes indicate regions where fluorescence intensity was measured at the cytokinetic ring (light blue) and proto-rachis (dark blue) at the specified stages of cytokinesis. The bracket (red) indicates the gap between the cytokinetic ring and the proto-rachis. Time 0 is the onset of cytokinetic ring ingression. (D,E) Measures of cytokinetic ring diameter (D; n=14) and distance between the cytokinetic ring midpoint and the center of the proto-rachis (yellow line; n=14) or the gap between the cytokinetic ring and the proto-rachis (red line; n=10; E) over time in animals imaged as in C. Data are mean $\pm$ s.e.m. (F) Mean levels of mNG::ANI-1 sum fluorescence intensity measured at the proto-rachis (dark blue) and cytokinetic ring (light blue, as depicted in C) before (two cells), during and after (three cells) PGC division. Data are mean $\pm$ s.e.m., n=10. (G) Confocal time-lapse images (sum projection of three slices) of PGCs undergoing first division in animals co-expressing markers for membrane and chromatin (TagRFP-PH<sup>PLC $\delta$</sup>  and mCh-HIS-58, green) and mNG::ANI-1 (magenta and bottom panels), taken before and after photobleaching (PB) of the signal at the proto-rachis (time 0). The boxes indicate regions where fluorescence intensity was measured at the cytokinetic ring (light blue) and proto-rachis (dark blue) over time. (H) Mean bleach-corrected levels of mNG::ANI-1 sum fluorescence intensity measured at the proto-rachis (dark blue) and cytokinetic ring (light blue, as depicted in G) before and after photobleaching (PB) of the signal at the proto-rachis. Data are mean $\pm$ s.e.m., n=9 animals. Statistical analyses were carried out using one-way ANOVA with Tukey's post-hoc test (n.s., not significant;  $P > 0.92$ ). Scale bar: 3  $\mu$ m.

### **2.4.3 The stable intercellular bridge permits cytoplasmic exchange during PGC cytokinesis**

Previous work carried out in adult *C. elegans* animals revealed that the stable actomyosin ring connecting germ cells to the rachis decreases in diameter during germ cell mitosis (Seidel et al., 2018). As PGCs possess a stable actomyosin ring prior to their entry into mitosis, we hypothesized that this stable ring remains open and functional during PGC division and transiently co-exists with the dynamic cytokinetic ring until late cytokinesis, when the two stable rings are each inherited by a daughter cell to maintain their intercellular bridge with the proto-rachis. To test this, we photoconverted Dendra2 in PGCs undergoing cytokinesis (n=12) and measured the dynamics of photoconverted fluorescence levels distribution in illuminated (dividing) and non-

illuminated (non- dividing) PGCs (Figure 2.4A). As was observed in mitotically quiescent PGCs (Figure 2.1E-G), we found that the photoconverted signal measured in PGCs undergoing cytokinesis progressively decreased and this was concomitant with an increase in photoconverted signal in the other, non-dividing PGCs (Figure 2.4B,C; Movie 2.6 can be found on *Development* website). Notably, in all dividing PGCs, fluorescence loss was apparent from the first timepoint after photoconverting illumination and, on average, decreased by  $6.6\pm 4.5\%$  within the first 15 s. This is comparable with the decrease of  $5.9\pm 4.3\%$  that we measured within the first 15 s of photoconversion in mitotically quiescent PGCs (see Figure 2.1F,G). This indicates that dividing PGCs possess an intercellular bridge that allows cytoplasmic exchange with the rest of the primordial germ line and further supports the notion that the pre-existing, stable actomyosin ring present in PGCs prior to their division is maintained as cells progress through mitosis.

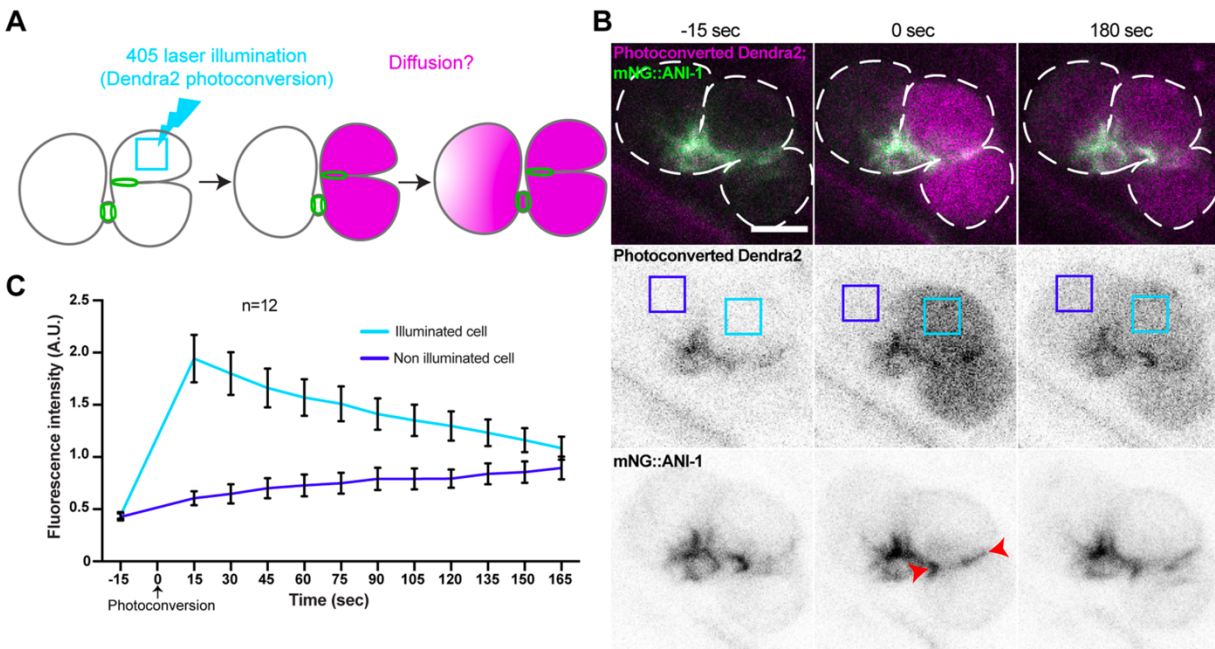


**Figure 2. 4: PGCs maintain their intercellular bridge to the proto-rachis during division**

(A) Schematic representation of the Dendra2 photoconversion and diffusion approach to assess cytoplasmic exchange in a dividing PGC. (B) Confocal time-lapse images (sum projection of three slices) of PGCs in animals expressing mNG::ANI-1 (green) and Dendra2 before (left) and after (middle and right) Dendra2 photoconversion (magenta). The blue boxes in the middle panel

indicate regions where fluorescence was measured over time, and the light-blue box in the center panel is where photoconverting laser illumination was carried out. Red arrowheads in the bottom panel delineate the cytokinetic ring. Scale bar: 3  $\mu\text{m}$ . (C) Mean levels of photoconverted Dendra2 fluorescence intensity measured over time (in seconds) in the illuminated (light blue) and non-illuminated (dark blue) regions of the PGCs that are defined in B. Time 0 is the onset of photoconverting laser illumination. Data are mean $\pm$ s.e.m., n=12 animals.

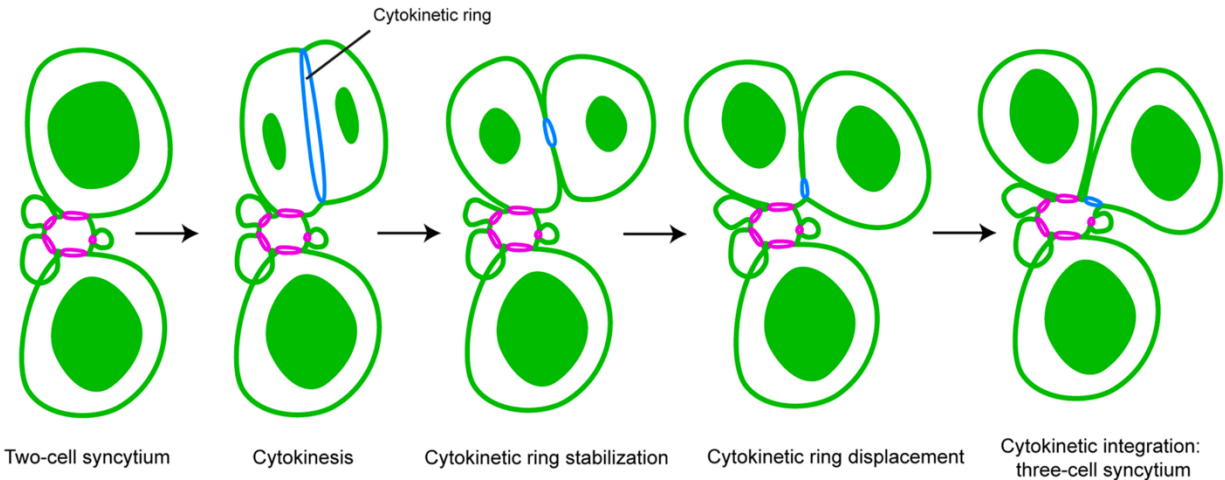


**Figure 2. 5: Proposed model for initial expansion of the primordial *C. elegans* germ line by incomplete PGC cytokinesis**

The model depicts plasma membrane and chromatin in green, stable intercellular bridges in magenta and the cytokinetic ring in blue at various mitotic stages. See main text for details.

## 2.5 Discussion

Together, our work demonstrates that *C. elegans* PGCs are organized as a functional syncytium at the first larval stage and share common cytoplasm through intercellular bridges that are stabilized by actomyosin rings, in an architecture fundamentally similar to that reported for late larvae and adult animals (Figure 2.2E; Movie 2.3 can be found on *Development* website). It further shows that the pool of actomyosin contractility regulators in the cytokinetic ring integrates the proto-rachis at the end of mitosis and that the stable intercellular bridge present in PGCs remains open during mitosis. We propose a model in which the initial syncytial expansion of the *C. elegans* germline in L1 larvae occurs by incomplete cytokinesis. In this model, the PGC cytokinetic ring initially forms and ingresses normally but fails to mature into a midbody ring, effectively resulting in a stable actomyosin ring that is specifically inherited by one of the daughter cells, with the other germ cell inheriting the pre-existing stable actomyosin ring (Figure 5). The molecular mechanism promoting incomplete cytokinesis is not yet known but may be an integral feature of the *C. elegans* germ line, as birth of the PGCs during embryogenesis has been shown to occur by incomplete cytokinesis (Goupil et al., 2017). We thus posit that the incomplete

cytokinesis program that is engaged in PGCs during embryogenesis remains active as the germ line expands, enabling the formation of one stable intercellular bridge with each germ cell division. Iterative incomplete cytokinesis has previously been demonstrated to sustain germline development in other organisms (Swiatek et al., 2009), most clearly in *Drosophila* and mouse (Greenbaum et al., 2011; Haglund et al., 2011), suggesting that this mechanism is a conserved feature of germline development in all animals, despite differences in tissue architecture. Furthermore, the notion that daughter germ cells each inherits an 'old' (pre-existing) and 'new' (cytokinetic) actomyosin ring to maintain intercellular bridges suggests that stable rings are bona fide organelles that, like centrioles, undergo controlled duplication during germ cell division.

Our results demonstrate that each PGC in L1 animals possesses an intercellular bridge, an architecture that is strikingly different from that found shortly after PGC birth during embryogenesis, where the two cells are directly connected to one another by a single stable intercellular bridge (Goupil et al., 2017). This indicates that the syncytial organization of the primordial germ line undergoes significant changes as embryogenesis progresses, enabling the formation of one additional PGC intercellular bridge. One change in primordial germ line organization that was previously documented to take place during embryogenesis is the formation of PGC lobes, which was shown to rely on the formation of actomyosin rings without concomitant mitoses (Abdu et al., 2016; Maniscalco et al., 2020). These extra membranes and actomyosin rings could conceivably be precursors to the proto-rachis that we document here. However, PGC lobe formation during embryogenesis was demonstrated to occur independently of the centralspindlin components CYK-4 and ZEN-4 (Maniscalco et al., 2020), and we find that both regulators are present at all intercellular bridges of the proto-rachis, whether at a PGC or a membrane lobe. While this raises an apparent discrepancy between PGC lobes formed during embryogenesis and those observed in L1 larvae, we rather favor a hypothesis in which the actomyosin rings that enable PGC lobe formation during embryogenesis eventually mature into bona fide intercellular bridges and acquire additional components through this process, such as centralspindlin regulators. They perhaps then serve as a source for the additional PGC bridge that arises in the process.

Finally, our work demonstrates that the two PGCs share cytoplasm during both interphase and cytokinesis, indicating that the stable intercellular bridges remain open throughout cell cycle progression. This is an apparent discrepancy with observations made in adult animals, in which intercellular bridges have been shown to drastically decrease in diameter during germ cell mitosis (Seidel et al., 2018). Intercellular bridges were previously shown to be under tension and to demonstrate some degree of lability (Amini et al., 2014; Priti et al., 2018; Rehai-Bell et al., 2017), suggesting that they respond to various forces imparted on the germ line. The closure of stable bridges upon germ cell cytokinesis in adult animals could perhaps be afforded by the capacity to better redistribute forces in this larger rachis, a response that may not be as efficient in a structure as small as the proto-rachis of L1 larvae. Perhaps more puzzling is the notion that the first mitotic entry and division of the two PGCs is asynchronous, despite the fact that they share cytoplasm and presumably receive comparable amounts of growth factors. Although photoactivatable rhodamine-dextran and Dendra2 can rapidly exchange between cells, diffusion may be more limited for some cellular components, such as cell cycle and mitotic regulators. In support of this view, the protein DAO-5 was reported to show limited diffusion upon germ cell division in adult animals (Seidel et al., 2018). Whether this is the case for other cellular components will require further investigation.

## 2.6 Materiel and methods

### 2.6.1 Strains and alleles

The strains and alleles used in this study are listed in Table S2.1. All strains were maintained at 20°C, except for UM785 (25°C), and were grown on nematode growth medium agar plates containing *E. coli* strain OP50, as described previously (Brenner, 1974). First-stage (L1) larvae were obtained by dissolving gravid hermaphrodites in sodium hypochlorite solution (1.2% NaOCl, 250 mM NaOH) and hatching recovered embryos for 24 h at room temperature in M9 buffer (22.04 mM KH<sub>2</sub>PO<sub>4</sub>, 42.27 mM Na<sub>2</sub>HPO<sub>4</sub>, 85.55 mM NaCl, 1 mM MgSO<sub>4</sub>). Animals were either processed and imaged as unfed L1 larvae or were imaged after transfer to plates with food and grown for 5-7 h at 25°C, to allow PGC division.

### 2.6.2 Confocal microscopy

L1 animals were immobilized in M9 buffer supplemented with 0.2% tetramisole, mounted on a 5% agarose pad and a coverslip was applied and sealed with VaLaP (1:1:1 Vaseline, lanolin, and paraffin). Images were acquired at 16-bit depth with a Zeiss LSM880 laser-scanning confocal microscope, controlled by ZEN black 2.1 SP3 software and using a Plan- Apochromat 63x/1.4 oil DIC M27 objective.

To acquire enhanced resolution images, a series of 0.2 µm confocal slices comprising the entire primordial germ line were sequentially acquired with 488 nm (argon) and 561 nm (solid state) laser lines and signal was collected by the Zeiss Airyscan detector operated in its super-resolution mode, with a zoom factor of 6 and an optimal frame size of 488×488 (except for UM463: 1024×1024). Post-acquisition image processing was carried out using with the 2D Airyscan processing tool provided in ZEN black 2.1 SP3.

For time-lapse acquisitions of dividing PGCs, a series of 0.5 µm confocal slices comprising the entire primordial germ line were simultaneously acquired at 2 min intervals with 488 nm and 561 nm laser lines. Signals were, respectively, collected with a GaAsP and a PMT detector, with a

zoom factor of 4, a frame size of 512×512 and a frame averaging of 4. All images were further processed and analyzed using ImageJ software (National Institutes of Health).

### **2.6.3 Bridge diameter and fluorescence intensity measurements**

The diameter of cytoplasmic bridges was determined on single enhanced resolution confocal slices by measuring the fluorescence intensity of FP- tagged membrane and contractility regulators along a 3-pixel-thick line drawn along the membrane of either a PGC or a membrane lobe that faces the proto-rachis (as illustrated in Figure 2.2B and Figure S2.2B-E). Bridge diameter was determined by measuring the distance between the two maximal peaks of fluorescence for FP-tagged contractility regulators. The fluorescence profile of 18/154 PGCs showed a distance between the two peaks that was less than 0.2  $\mu\text{m}$  or no concomitant decrease in FP-tagged membrane fluorescence, so these were excluded from the analysis.

The fluorescence intensity of contractility regulators at the proto-rachis and cytokinetic ring were determined by measuring the raw integrated density of a selected region (as depicted in each figure) in sum projections of z-slices comprising the entire primordial germ line. Fluorescence background was measured in the same sum projections, in regions located in the cytoplasm of the PGCs (when possible, otherwise next to the PGCs) and subtracted from measurements made at the proto-rachis or cytokinetic ring. The cytokinetic ring diameter and the position of the cytokinetic ring midpoint were obtained by measuring the distribution and length of FP- tagged contractility regulator signal along a 1-pixel-wide line drawn along the cytokinetic furrow at each timepoint on sum projections, from furrow initiation until the signal could no more be distinguished from that at the proto-rachis. The center of the proto-rachis was approximated as the center of a circle comprising the entire FP-tagged contractility regulator fluorescence signal at the proto-rachis and was used to measure its distance from the cytokinetic midpoint.

Statistical analyses were made using GraphPad – Prism software.



### **2.6.4 Fluorescence photobleaching**

Samples were mounted as described above, and photobleaching was performed by simultaneously illuminating fluorescence signal at the proto-rachis with 405 nm (solid state) and 454 nm (argon) lasers, both at 100% power and with 100 iterations. Time-lapse images were acquired as described above, at 10 s intervals for the time points immediately before and after photobleaching, and then at 3 min intervals for the rest of the acquisition.

Contractility regulator fluorescence intensity at the proto-rachis and cytokinetic ring were measured as described above. The rate of fluorescence recovery after photobleaching (FRAP) for FP-tagged contractility regulators was obtained by measuring changes in fluorescence intensity over time at the proto-rachis of L1 larvae in which PGCs were not dividing (Figure S2.5A,B). To correct for FRAP, this rate was subtracted at each timepoint from the measured fluorescence intensity at the proto-rachis (Figure S2.5C,D).

### **2.6.5 Dendra2 photoconversion**

Samples were mounted as described above, and photoconversion was performed by simultaneously illuminating a selected region in the cytoplasm of a PGC with both 405nm and 454nm lasers, at, respectively, 80% and 20% power and with 500 iterations. For time-lapse acquisitions, a series of 0.8  $\mu\text{m}$ -thick confocal slices comprising the entire primordial germ line were simultaneously acquired at 15 s intervals with 488 nm and 561 nm laser lines. Signals were respectively collected with a PMT and a GaAsP detector, with a zoom factor of 4, a frame size of 512 $\times$ 512 and a frame averaging of 4.

Photoconverted Dendra2 fluorescence intensity was determined by measuring the raw integrated density of a selected region (as depicted in each figure) in sum projections of z-slices comprising the entire primordial germ line, and correcting for photoconverted Dendra2 photobleaching. The rate of photoconverted Dendra2 photobleaching was determined by measuring changes in fluorescence intensity over time in primordial germ lines that had been entirely illuminated by 405 nm and 454 nm laser light (Figure S2.1B).

### **2.6.6 Transmission electron microscopy**

Samples were prepared as described previously (Hall et al., 2012). Briefly, L1 larvae were fed on bacterial plates for 6 h and fixed by high pressure freezing in a Bal-Tec HPM 010 instrument. Samples were then transferred into a primary fix solution of 2% osmium tetroxide and 0.2% uranyl acetate in 98% acetone and 2% deionized H<sub>2</sub>O, and freeze substitution was performed in a Leica EM AFS2 system as follows: -90°C for 72 h, ramped up to -60°C for 6 h (5°C change per hour), held at -60°C for 12 h, ramped up to -30°C (5°C change per hour), held at -30°C for 12 h, ramped up to 0°C for 6 h (5°C change per hour) and held at 0°C for another 6 h. After three washes (20 min each) in pure acetone at 0°C, samples were washed twice (30 min each) in acetone at room temperature, and transferred to microporous capsules (type C) for embedding. Samples were embedded into Hardplus Embed 812 resin for 2 h each in a mix of 1:3 resin/acetone and 1:1 resin/acetone, then held for 18 h in 3:1 resin/acetone, followed by six changes in pure resin over 2 days, before curing in a mold at 60°C for 2 days in an oven. All preparations were then sectioned at 90 nm using a diamond knife, and serial sections collected on Formvar-coated slot grids. Images were acquired using a FEI Tecnai G2 Spirit BioTwin electron microscope. Images were aligned with the ImageJ TrakEM2 plug-in, then nuclei, cells and membrane lobes were colored by manually tracing membranes.

## 2.7 Supplemental material

### 2.7.1 Online supplemental material

**Movie 2.1.** Serial transmission electron microscopy images from 90 nm-thick sections of the primordial germ line from a first larval stage animal. The bottom panel is a color-overlaid version of the top panel, depicting nuclei (blue), PGC cytoplasm (dark red) and cytoplasm within the membrane-dense structure between the PGCs (i.e. the proto-rachis, light red). The nuclei of the somatic primordial gonad (Z1 and Z4) are depicted in green. Images were aligned manually.

**Movie 2.2.** Time-lapse movie of the primordial germ line with two mitotically quiescent PGCs before and after Dendra2 fluorescence photoconversion (same images as shown in figure 2.1F), in animals co-expressing mNG::ANI-1 and cytoplasmic Dendra2. Images were acquired every 15 sec and are played at 1 frame per sec.

**Movie 2.3.** Tridimensional rendering of the primordial germ line displaying the proto-rachis (white compartment), to which both PGCs (red, with nuclei in blue) and membrane lobes (magenta) are connected via intercellular bridges (yellow spheres). This rendering was made from reconstructed EM images. Each image was imported into Inkscape software (v1.1) and the membrane defining each compartment was manually traced. To make intercellular bridges more visible, each was defined as a yellow sphere with a diameter equal to that of the bridge. Each compartment was then filled with colour in separate channels (1 channel per colour) and saved as a tif file. The file was imported into Imaris software (v9.2.1, Bitplane) and the "surface" tool was used to generate a 3D rendering of each defined compartment in each slice. The "clipping plane" tool was used to generate a composite image of each slice and these composite images were assembled with ImageJ software into a movie that sequentially goes from the bottom to the top of the primordial germ line. The "animation" tool from Imaris software was used to rotate the entire reconstructed 3D image.

**Movie 2.4.** Time-lapse movie of the first division of the PGCs (same images as shown in figure 2.3C), in animals co-expressing mNG::ANI-1, a membrane (TagRFP::PH) and a histone (mCherry::HIS-58) marker. Images were acquired every 2 min and are played at 3 frames per sec.

**Movie 2.5.** Time-lapse movie of the first division of the PGCs (same images as shown in figure S2.4A), in animals co-expressing NMY-2::GFP, a membrane (TagRFP::PH) and a histone (mCherry::HIS-58) marker. Images were acquired every 2 min and are played 3 frames per sec.

**Movie 2.6.** Time-lapse movie of the primordial germ line with one PGC undergoing cytokinesis before and after Dendra2 fluorescence photoconversion (same images as shown in figure 2.4B), in animals co-expressing mNG::ANI-1 and cytoplasmic Dendra2. Images were acquired every 15 sec and are played at 1 frame per sec.

## 2.7.2 Tables and figures

**Table S2. 1: Strains used in this study**

Strain	Genotype	Allele Reference
N2	Wild type	(Brenner, 1974)
UM208	<i>nc-119(ed3) III; ItIs81[Ppie-1::gfp-tev-Stag::ani-2; unc-119(+)]; ItIs44[Ppie- 1::mCherry::PH(PLC1delta1); unc-119(+)]</i>	(Amini et al., 2014), (Kachur et al., 2008)
UM463	<i>cpIs42[Pmex-5::mNeonGreen::PLCδ-PH::tbb-2 3'UTR; unc-119(+)] II; ItIs37[pAA64; Ppie-1::mCherry::HIS-58; unc-119(+)] IV</i>	(Heppert et al., 2016), (McNally et al., 2006)
UM639	<i>cpSi20[Pmex-5::TAGRFPT::PH::tbb-2 3'UTR; unc-119(+)] II; zuls45[Pnmy- 2::nmy-2::GFP; unc-119(+)]; ItIs37 [pAA64; Ppie-1::mCherry::HIS-58; unc- 119(+)] IV</i>	(Heppert et al., 2016), (McNally et al., 2006), (Nance et al., 2003)
UM641	<i>cpSi20[Pmex-5::TAGRFPT::PH::tbb-2 3'UTR; unc-119 (+)] II; ani- 1(mon7[mNeonGreen^3xFlag::ani-1]) III; unc-119 (ed3) III</i>	(Heppert et al., 2016), (Strome et al., 2001)
UM655	<i>cpSi20[Pmex-5::TAGRFPT::PH::tbb-2 3'UTR; unc-119 (+)] II; ani- 1(mon7[mNeonGreen^3xFlag::ani-1]) III; unc-119 (ed3) III(?); ItIs37 [pAA64; Ppie-1::mCherry::HIS-58; unc-119(+)] IV</i>	(Heppert et al., 2016), (McNally et al., 2006), (Strome et al., 2001)
UM717	<i>cp52[nmy-2::mkate2 + LoxP unc-119(+ LoxP) I; ccm-3(mon9[ccm- 3::mNeonGreen^3xFlag]) II; unc-119(ed3) III; ItIs44[pAA173, Ppie- 1::mCherry::PH(PLC1delta1); unc-119(+)]</i>	(Dickinson et al., 2017), (Lee et al., 2018), (Strome et al., 2001)
UM735	<i>xnSi1[Pmex-5::GFP::PH(PLC1delta1)::nos-2 3'UTR] II; estSi71[pAC257;Pmex-5::lifeAct::mKate2::tbb-2 3'UTR; cb-unc-119(+)] IV</i>	(Chihara and Nance, 2012), (Mangal et al., 2018)

UM740	<i>cpSi20</i> [ <i>Pmex-5::TAGRFPT::PH::tbb-2 3'UTR; unc-119 (+) II; ItIs37 [pAA64; Ppie-1::mCherry::HIS-58; unc-119(+)] IV; ItIs154 [pOD539(pBG3); Ppie-1::cyk- 7::GFP; unc-119 (+)]</i>	(Green et al., 2011), (Heppert et al., 2016), (McNally et al., 2006)
UM785	<i>axIs1959</i> [ <i>Ppie-1::Dendra2::TEV::S-peptide::pie-1 3'UTR; unc-119(+); ani- 1(mon7[mNeonGreen^3xFlag::ani-1]) III; unc-119 (ed3) III; ojIs1[Ppie- 1::GFP::tbb-2; unc-119(+)] V</i>	(Griffin et al., 2011), (Rehain-Bell et al., 2017), (Strome et al., 2001)
OD3840	<i>ItSi849</i> [ <i>pKL120; Pmex-5::mCherry::PH(PLC1delta1)::tbb-2 3'UTR; cb-unc- 119(+)] I; unc-119(ed3) III(?) ; zen-4(It30[GFP::loxP::zen-4]) IV</i>	(Lee et al., 2018)
OD3686	<i>ItSi849</i> [ <i>pKL120; Pmex-5::mCherry::PH(PLC1delta1)::tbb-2 3'UTR; cb-unc- 119(+)] I; ItSi1124</i> [ <i>pSG092; Pcyk-4::CYK-4reencoded::mNeonGreen::cyk-4 3'-UTR; cb- unc-119(+)] II; unc- 119(ed3) III</i>	(Lee et al., 2018)

---

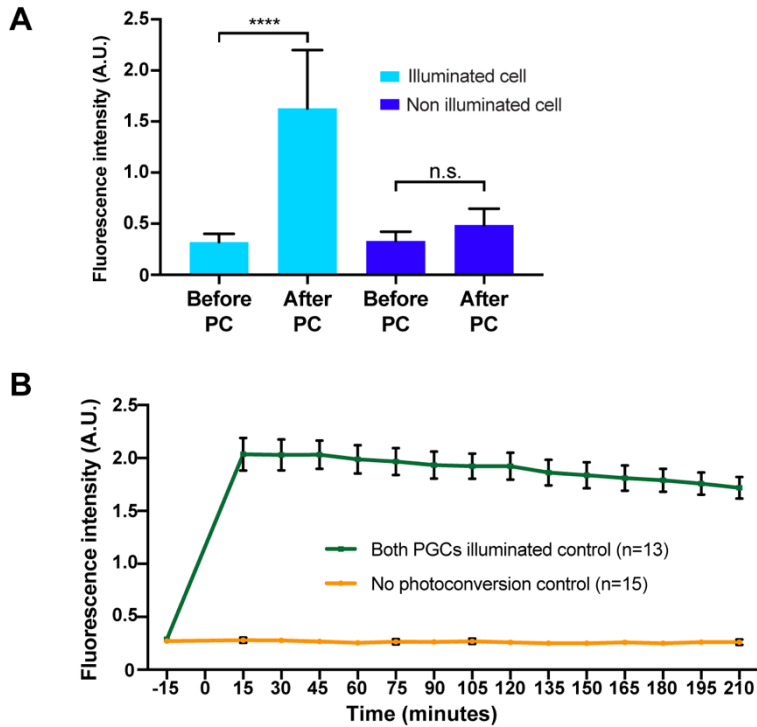


**Figure S2. 1:**

(A) Mean levels of photoconverted Dendra2 fluorescence intensity measured before and immediately after photoconversion (PC) in the illuminated (light blue) and non-illuminated (dark blue) regions of the PGCs that are defined in Figure 2.1F. Dendra2 photoconversion in one cell (light blue) does not significantly impact fluorescence levels in the other cell (dark blue). Error bars are standard error of the mean,  $n = 13$  animals. Statistical analyses were done using a one-way ANOVA test with a Tukey *post hoc* test (ns = not significant,  $p = 0.55$ , \*\*\*\* =  $p < 0.0001$ ). (B) Mean levels of photoconverted Dendra2 fluorescence intensity measured over time (in seconds) when the entire primordial germ line is illuminated by the photoconverting laser at time 0 (green line,  $n = 15$ ) or when no photoconverting laser illumination is performed (orange line,  $n = 13$ ). Error bars are standard error of the mean.

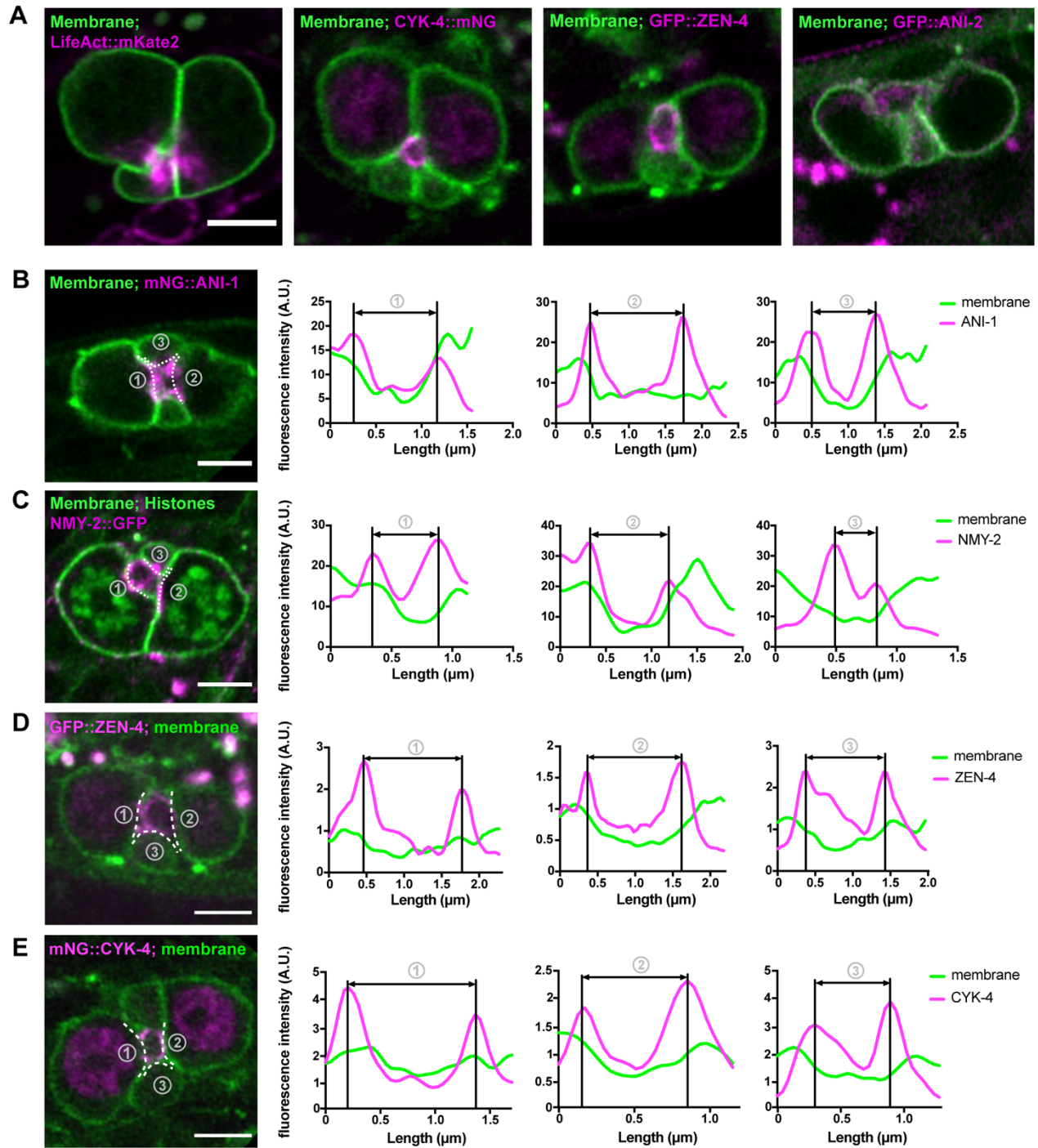


**Figure S2. 2 :**

(A) Confocal images (sum projection of 3 slices) of the PGCs in first larval stage animals expressing FP-tagged markers for membrane (mCh- $\text{PHPLC}\delta$  or GFP- $\text{PHPLC}\delta$ , green) and specified actomyosin contractility regulators (magenta). (B-E) Same as in (C) but for a single confocal slice instead of a sum projection for animals expressing mNG::ANI-1 (B), NMY-2::GFP (C), GFP::ZEN-4 (D) and mNG::CYK-4 (E). The three graphs on the right report the fluorescence intensity of

membrane (green) or contractility regulator (magenta) signal measured along each dotted line (1-3) drawn in the image on the left. Intensity peaks of contractility regulators define bridge diameter (black lines and arrows). In all panels, scale bar = 3 $\mu$ m.

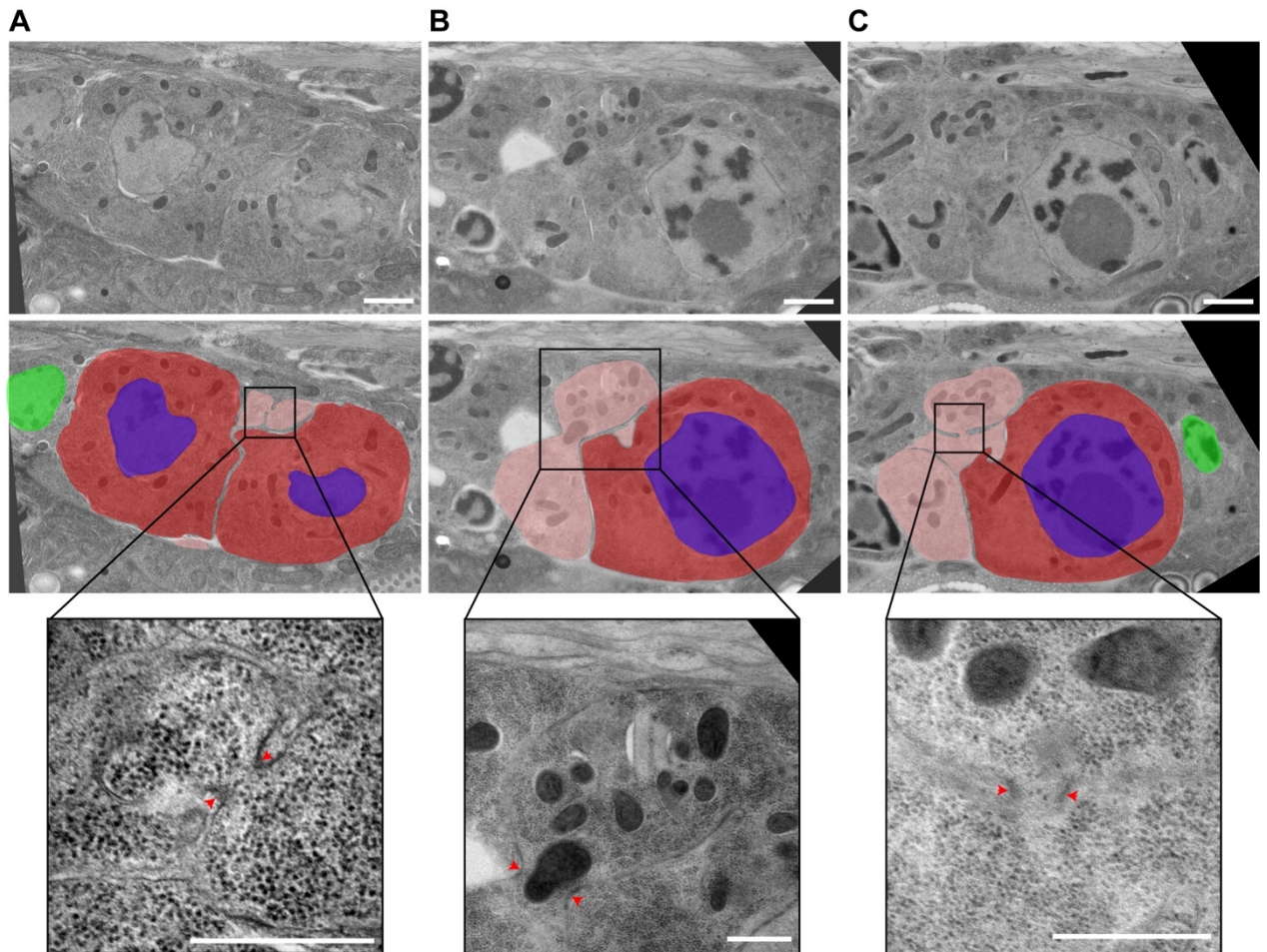


**Figure S2. 3:**

(A-C) Selected TEM images from 90 nm-thick sections of the primordial germ line from a first larval stage animal. The middle panel is a color-overlaid version of the top panel, depicting nuclei (blue), PGC cytoplasm (dark red) and cytoplasm within the membrane-dense structure between the PGCs (light red). Scale bar = 1  $\mu$ m. Insets at the bottom are magnifications of the boxed regions in the middle panels, where cytoplasmic bridges are visible within the membrane-dense structure (red arrowheads), possibly at the base of membrane lobes. The nuclei of the somatic primordial gonad (Z1 and Z4) are depicted in green. Scale bar = 500 nm.



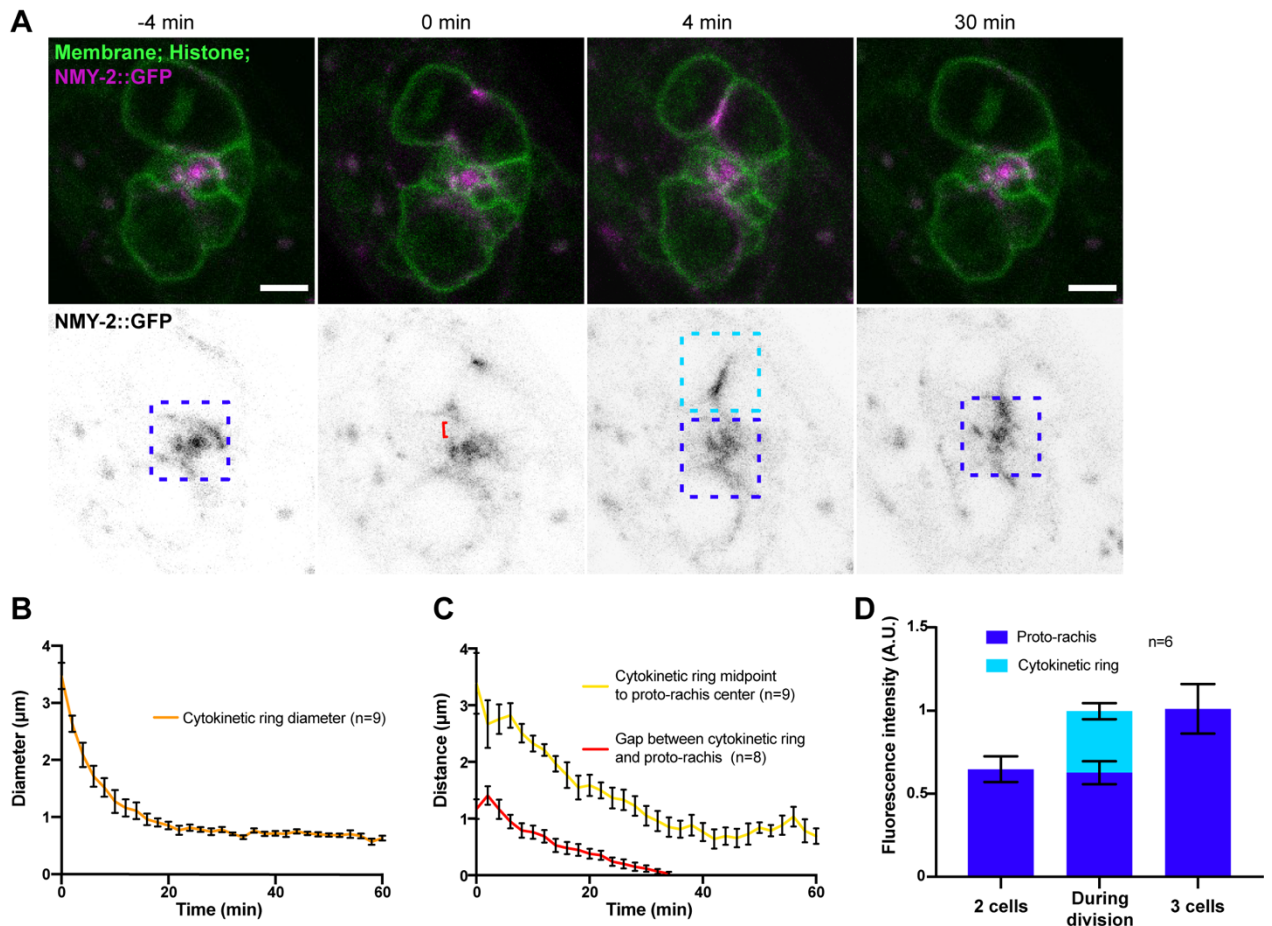


**Figure S2. 4:**

(A) Confocal time-lapse images (sum projection of 3 slices) of PGCs undergoing first division in animals co-expressing markers for membrane and chromatin (TagRFP-PHPLC $\delta$  & mCh-HIS-58, green) and NMY-2::GFP (magenta & bottom panels). The boxes indicate regions where fluorescence intensity was measured at the cytokinetic ring (light blue) and proto-rachis (dark blue) at the specified stages of cytokinesis. The bracket (red) indicates the gap between the cytokinetic ring and the proto-rachis. Time 0 is the onset of cytokinetic ring ingression. Scale bar = 3  $\mu\text{m}$ . (B-C) Measures of cytokinetic ring diameter (B; n = 9) and distance between the cytokinetic ring midpoint and the center of the proto-rachis (yellow line; n = 9) or the gap between the cytokinetic ring and the proto-rachis (red line; n = 8; C) over time in animals imaged as in (A). Error bars represent standard error of the mean. (D) Mean levels of NMY-2::GFP sum fluorescence intensity measured at the proto-rachis (dark blue) and cytokinetic ring (light blue, as depicted in A) before (2 cells), during and after (3 cells) PGC division. Error bars represent standard error of the mean, n = 6.

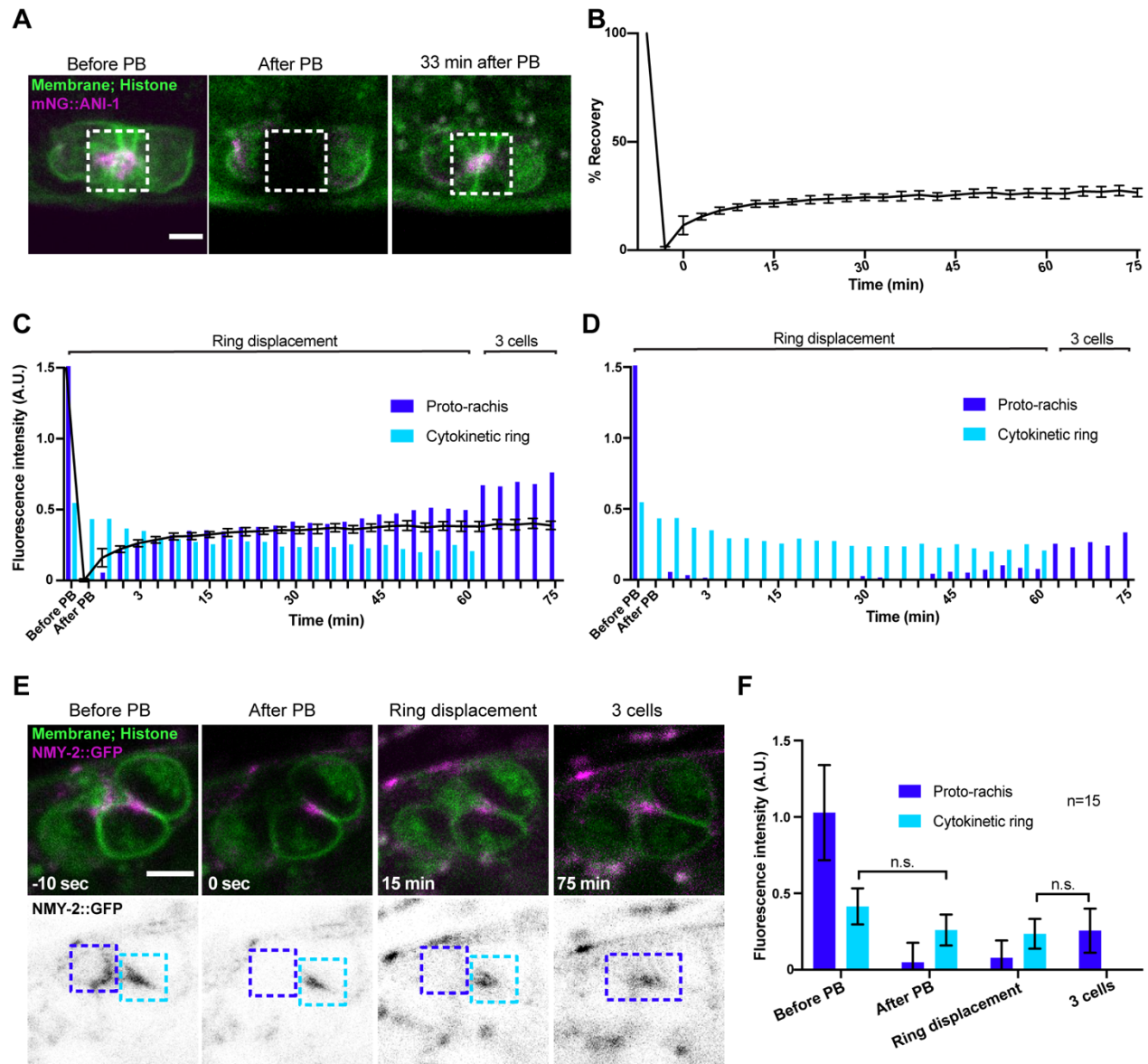


**Figure S2. 5:**

(A) Confocal time-lapse images (sum projection of 3 slices) of non-dividing (mitotically quiescent) PGCs in animals co-expressing markers for membrane and chromatin (TagRFP-PH<sup>PLCδ</sup> & mCh-HIS-58, green) and mNG::ANI-1 (magenta), taken before and after photobleaching (PB) of the signal at the proto-rachis (time 0). The boxes indicate regions where fluorescence intensity was measured at the proto-rachis over time. (B) Mean percentage of mNG::ANI-1 fluorescence recovery after photobleaching (FRAP) measured at the proto-rachis (as depicted in A). Error bars are standard error of the mean,  $n = 8$  animals. (C-D) Mean levels of mNG::ANI-1 sum fluorescence intensity measured at the proto-rachis (dark blue) and cytokinetic ring (light blue, as depicted in Figure 2.3G) before and after photobleaching (PB) of the signal at the proto-rachis. The percent mNG::ANI-1 FRAP measured in B is overlaid in panel C and panel D represents the values at each timepoint after subtraction of these relative FRAP levels are subtracted from the measured

fluorescence levels at the proto-rachis, thus effectively correcting for FRAP. (E) Confocal time-lapse images (sum projection of 3 slices) of PGCs undergoing first division in animals co-expressing markers for membrane and chromatin (TagRFP-PH<sup>PLCδ</sup> & mCh-HIS-58, green) and NMY-2::GFP (magenta & bottom panels), taken before and after photobleaching (PB) of the signal at the proto-rachis (time 0). The boxes indicate regions where fluorescence intensity was measured at the cytokinetic ring (light blue) and proto-rachis (dark blue) over time. (F) Mean bleach-corrected levels of GFP::NMY-2 sum fluorescence intensity measured at the proto-rachis (dark blue) and cytokinetic ring (light blue, as depicted in E) before and after photobleaching (PB) of the signal at the proto-rachis. Error bars are standard error of the mean, n = 15 animals. Statistical analyses were done using an ordinary one-way ANOVA test with a Tukey post hoc test (ns = not significant, p > 0.12). In all panels, scale bar = 3μm.

## 2.8 Acknowledgements

We thank Bob Goldstein (UNC Chapel Hill), Erik Griffin (Dartmouth), Amy Maddox (UNC Chapel Hill), Karen Oegema (UC San Diego) and Esther Zanin (LMU München) for strains and reagents, and Vincent Archambault, Abigail Gerhold and Greg FitzHarris for comments on the manuscript. We are also grateful to Christian Charbonneau of IRIC's Bio-imaging Facility for technical assistance, to Kelly Sears and Jeannie Mui at the McGill University Facility for Electron Microscopy Research for help with microscope operation, and to all members of the FitzHarris, Gerhold, Hickson and Labbé laboratories for helpful discussions. Some strains were provided by the CGC, which is funded by NIH Office of Research Infrastructure Programs (P40 OD010440).

# **3. Article 2 - The primordial germ line is refractory to perturbations of actomyosin regulator function in *C. elegans* L1 larvae**

**Jack Bauer**<sup>1</sup>, Léa Lacroix<sup>1</sup> and Jean-Claude Labbé<sup>1,2,\*</sup>

<sup>1</sup>Institute for Research in Immunology and Cancer (IRIC), Université de Montréal, C.P. 6128, Succ. Centre-ville, Montréal, QC H3C 3J7, Canada.

<sup>2</sup>Department of Pathology and Cell Biology, Université de Montréal, C.P. 6128, Succ. Centre-ville, Montréal, QC H3C 3J7, Canada.

\*Author for correspondence ([jc.labbe@umontreal.ca](mailto:jc.labbe@umontreal.ca))

microPublication Biology, August 2021

### **3.1 Author contributions**

**Jack Bauer** conceptualized, designed, and executed the experiments in (Figure 3.1A,B,C,D,G,H), analysed the data, prepared the figures for the manuscript, wrote and edited the manuscript.

**Léa Lacroix** conceptualized, designed and executed the experiments in (Figure 3.1E,F)

**Jean-Claude Labbé** supervised the experimental conceptualization and design, the data analysis, and wrote and edited the manuscript.

## 3.2 Abstract

Cytokinesis, the separation of daughter cells at the end of mitosis, relies on the coordinated activity of several regulators of actomyosin assembly and contractility (Green et al., 2012). These include the small GTPase RhoA (RHO-1) and its guanine-nucleotide exchange factor Ect2 (ECT-2), the scaffold protein Anillin (ANI-1), the non-muscle myosin II (NMY-2), the formin CYK-1 and the centralspindlin complex components ZEN-4 and CYK-4. These regulators were also shown to be required for maintenance of *C. elegans* germline syncytial organization by stabilizing intercellular bridges in embryos and adults (Amini et al., 2014; Goupil et al., 2017; Green et al., 2011; Priti et al., 2018; Zhou et al., 2013). We recently demonstrated that many of these regulators are enriched at intercellular bridges in the small rachis (proto-rachis) of L1-stage larvae (Bauer et al., 2021). We sought to assess whether these contractility regulators are functionally required for stability of intercellular bridges and maintenance of the primordial germ line syncytial architecture in L1-stage *C. elegans* animals. Here we report that temperature-sensitive alleles, RNAi-mediated depletion and latrunculin A treatment are largely ineffective to perturb actomyosin function in the L1-stage primordial germ line.

### 3.3 Description

To perturb actomyosin function in the primordial germ line, we first monitored germ line organization in L1-stage animals bearing temperature-sensitive (ts) alleles in genes encoding actomyosin regulators and that were reported to interfere with cytokinesis during embryogenesis (Davies et al., 2014). Previous work demonstrated that the initial stages of germline expansion occur normally in *cyk-4(ts)* and *zen-4(ts)* animals raised at restrictive temperature from the L1 stage (Lee et al., 2018). We found that primordial germ line organization in *cyk-1(ts)*, *nmy-2(ts)*, *cyk-4(ts)* or *zen-4(ts)* L1 larvae maintained at restrictive temperature for 12h was no different than control (Figure 3.1A-B). Furthermore, the first primordial germ cell (PGC) division occurred normally upon feeding these animals at restrictive temperature with typical bacterial food (*E. coli* OP50). As noted previously (Lee et al., 2018), germ line disorganization and sterility were observed in all cases when animals reached adulthood (Figure 3.1B).

We then used RNAi to deplete actomyosin regulators in L1 larvae expressing NMY-2::GFP or mNG::ANI-1, as well as fluorescent markers for membrane and histone. We found that soaking L1 animals for 24h in a dsRNA solution against *nmy-2* or *ani-1* did not significantly perturb primordial germ line organization nor decreased fluorescence levels of these proteins compared to control L1-stage larvae (Figure 3.1C-D). Feeding of these soaked animals with OP50 revealed that the first PGC division occurred normally, and germ line disorganization was observed when these animals reached adulthood (Figure 3.1C). This demonstrates that the RISC complex had effectively been engaged by dsRNA treatment at the L1 stage but that the phenotype only manifested itself later in development. Similar results (lack of phenotype in L1 larvae, potent phenotype in adults) were obtained when we soaked RNAi-hypersensitive *rff-3(pk1426)* mutants in dsRNA against *ani-1*, *rho-1* or *ect-2* for 24h (Figure 3.1E-F).

Finally, we treated L1 larvae expressing mNG::ANI-1 or LifeAct::mKate2 (marking F-actin) with the actin depolymerizing drug latrunculin A and scored primordial germ line organization. We found that incubating L1 larvae for 3-5 hours in a solution of 100  $\mu$ M latrunculin A did not result in significant primordial germ line disorganization and the fluorescence levels of either marker at the proto-rachis remained unchanged compared to control (Figure 3.1G-H). As shown



previously (Priti et al., 2018), latrunculin A treatment of L4 larvae (even with a lower dose of 25  $\mu$ M) resulted in an extensive collapse of the germ cell intercellular bridges (Figure 3.1G), demonstrating that the drug is effective.

Together with previous work (Lee et al., 2018), our results demonstrate that perturbing the function of actomyosin contractility regulators in the *C. elegans* primordial germ line is difficult to achieve at the L1 stage by means of ts alleles, RNAi or latrunculin A treatment. The reasons for this are unclear and could vary depending on the treatment, yet we consider it unlikely that these gene products are dispensable for germline development. Notably, RNAi depletion in PGCs was previously achieved for regulators of the spindle assembly checkpoint (Lara-Gonzalez et al., 2019), and our finding that RNAi treatment at the L1 stage results in phenotypes later in development indicates that the RNAi machinery can be engaged in L1 animals. One possibility is that actomyosin regulators within the primordial germ line are organized in a very compact and/or stable manner that makes perturbation difficult, a situation perhaps analogous to microtubule organization at the midbody prior to abscission (Hu et al., 2012; Salmon et al., 1976). While other approaches for gene depletion could be more effective (e.g. degron-based), this phenomenon will require further investigation.

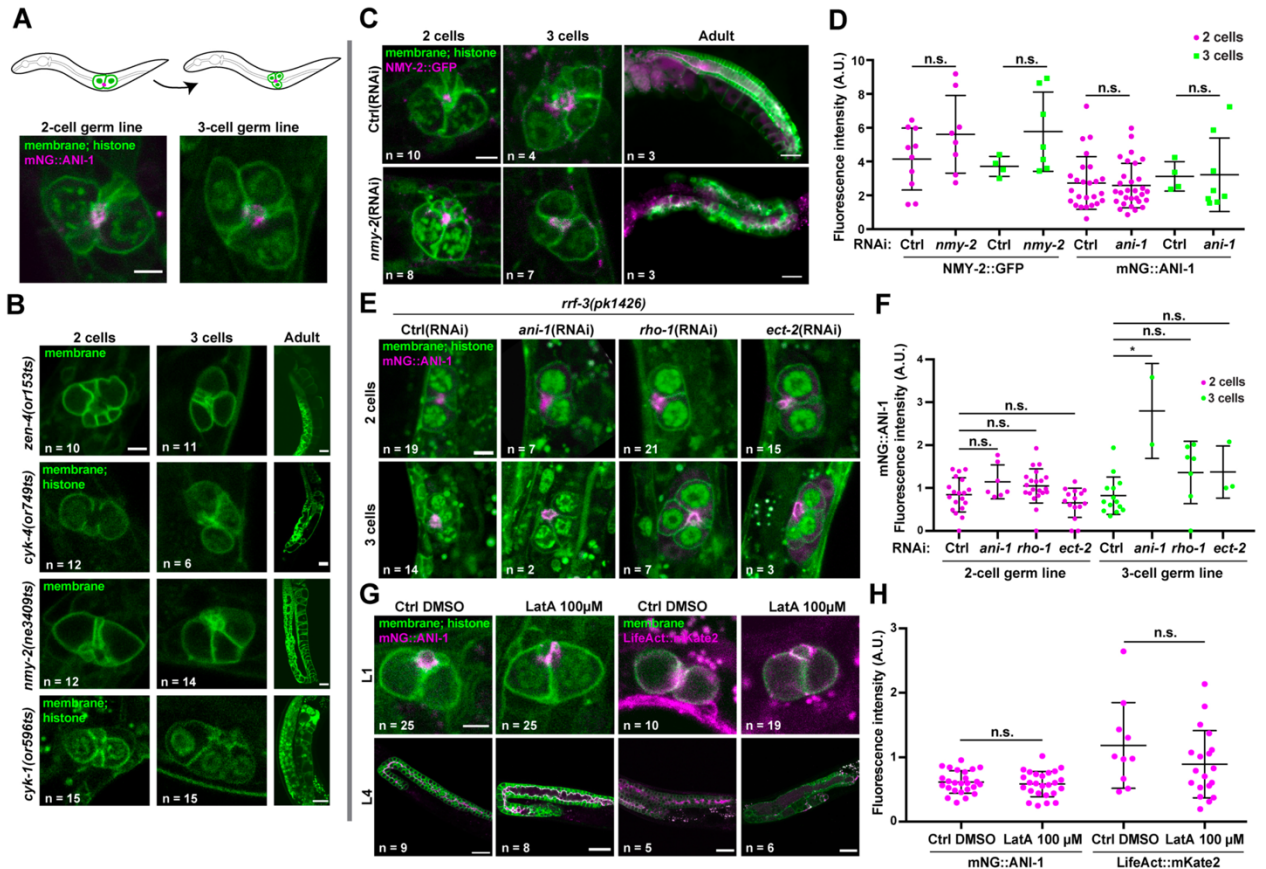


**Figure 3. 1: Perturbation of actomyosin function in the *C. elegans* primordial germ line**

(A) Schematic representation (top) and confocal images (bottom) of the 2-cell (left) and 3-cell (right) primordial germ line in control L1-stage animals. (B) Confocal images of the primordial germ line containing 2 (left) or 3 (middle) germ cells in L1-stage animals bearing temperature-sensitive alleles for *cyk-4(or749ts)*, *zen-4(or153ts)*, *nmy-2(ne3409ts)* or *cyk-1(or596ts)* that were upshifted at 26°C for 12h. The panels on the right show the adult germ line after animals of each genotype were grown at 26°C. (C) Images of the 2-cell (left), 3-cell (middle) and adult (right) germ line in animals co-expressing NMY-2::GFP (magenta) and markers for membranes and histones (green) that were soaked at the L1 stage in control (top) or *nmy-2* (bottom) dsRNA. (D) Measured fluorescence intensity of NMY-2::GFP and mNG::ANI-1 at the proto-rachis of L1-stage animals soaked respectively in control, *nmy-2* or *ani-1* dsRNA (RNAi). (E) Confocal images of the 2-cell (top) and 3-cell (bottom) germ line in *rrf-3(pk1426)* mutant animals co-expressing mNG::ANI-1 (magenta) and markers for membranes and histones (green) that were soaked at the L1 stage in control (far left), *ani-1* (middle left), *rho-1* (middle right) or *ect-2* (far right) dsRNA. (F) Measured fluorescence intensity of mNG::ANI-1 at the proto-rachis of L1-stage animals soaked respectively in control, *ani-1*, *rho-1*, or *ect-2* dsRNA (RNAi). (G) Confocal images of the germ line in L1 (top) and L4 (bottom) animals co-expressing mNG::ANI-1 (left) or LifeAct::mKate2 (right; magenta) and markers for membranes and histones (green) after treatment with 100 μM latrunculin A or solvent alone (control DMSO). (H) Measured fluorescence intensity of mNG::ANI-1 and LifeAct::mKate2 at the proto-rachis of L1-stage animals treated with 100 μM of latrunculin A

(LatA) or solvent alone (DMSO control). In all panels, images shown are sum projections of 3 confocal slices, membranes are marked with TagRFP-, GFP- or mNG-tagged PH<sup>PLCδ</sup> and histones are marked with mCh-HIS-58 (see Table S3.1 for details). For all images of L1 animals, scale bar = 3 μm. For all images of L4 and adult animals, scale bar = 30 μm. For all graphs, black lines represent mean ± standard deviation, and statistical analyses were done using a one-way ANOVA test with a Tukey *post hoc* test (n.s. =  $p > 0.05$ ; \* =  $p < 0.001$ ).

## 3.4 Methods

### 3.4.1 *C. elegans* strain maintenance

The strains and alleles used in this study are listed in Table S3.1. Animals were grown on NGM plates seeded with *E. coli* strain OP50 and maintained at 20°C as described (Brenner 1974), with the exception of temperature-sensitive strains and *rrf-3(pk1426)* mutants that were maintained at 15°C. First stage (L1) larvae were obtained by dissolving gravid hermaphrodites in sodium hypochlorite solution (1.2% NaOCl, 250 mM NaOH) and hatching recovered embryos for 24h at room temperature (or at 15°C for ts strains) in M9 buffer (22.04 mM KH<sub>2</sub>PO<sub>4</sub>, 42.27 mM Na<sub>2</sub>HPO<sub>4</sub>, 85.55 mM NaCl, 1 mM MgSO<sub>4</sub>).

### 3.4.2 Imaging

Animals were immobilized in M9 buffer supplemented with 0.2% tetramisole, mounted on an agarose pad (3% for L4s/adults and 5% L1s), and a coverslip was applied and sealed with VaLaP (1:1:1 Vaseline, lanolin, and paraffin). With one exception, images were acquired with a GaAsP detector at 16-bit depth mounted on a Zeiss LSM880 laser-scanning confocal microscope, controlled by ZEN black 2.1 SP3 software, and using a Plan-Apochromat 63x/1.4 oil DIC M27 objective; images of adult animals in Figure 3.1B were acquired with an HRM camera mounted on a Zeiss AxioImager Z1 microscope and using a Plan-Apochromat 10x/1.4 NA objective. All images were further processed and analyzed using ImageJ software (National Institutes of Health). The fluorescence intensity of contractility regulators was determined by measuring the raw integrated density of the proto-rachis region in sum projections of z-slices comprising the entire primordial germ line. Fluorescence background was measured in the same sum projections, in regions located in the germ cell cytoplasm (when possible, otherwise next to the PGCs) and subtracted from measurements made at the proto-rachis.

### 3.4.4 Temperature-sensitive strain upshifts

Newly hatched and unfed L1 animals were upshifted at 26°C for 12h in M9 buffer, then transferred to NGM plates seeded with *E. coli* OP50 at 26°C, for 2-3h to image 2-cell germ lines

and 5-6h to image 3-cell germ lines. For controls, unfed L1 animals were left at 15°C for 12h, then plated on NGM plates seeded with *E. coli* OP50 at 15°C for 4-5h to image 2-cell germ lines and 9-10h to image 3-cell germ lines.

### **3.4.5 dsRNA production**

Bacterial clones targeting the genes *nmy-2* (sjj\_F20G4.3), *ani-1* (sjj\_Y49E10.19), *rho-1* (cenix:169-h12) and *ect-2* (sjj\_T19E10.1a) as well as the L4440 empty vector we used as template in PCR reactions and individual inserts flanked by T7 promoters were amplified using T7 promoter-specific primers. PCR products were purified on columns (Qiagen) and used as template for in vitro transcription reactions using the T7 Ribomax Express RNAi System (Promega).

### **3.4.6 RNA Interference**

First larval stage (L1) animals were soaked for 24h at 15°C in 2-4 µl of buffer (10.9 mM Na<sub>2</sub>HPO<sub>4</sub>, 5.5 mM KH<sub>2</sub>PO<sub>4</sub>, 2.1 mM NaCl, 4.7 mM NH<sub>4</sub>Cl, 6.3 mM spermidine, 0.11% gelatin) supplemented with 8-20 µg of dsRNA targeting *nmy-2*, *ani-1*, *rho-1* or *ect-2*, as described (Green et al. 2011). Animals were then washed 3 times with M9 buffer and allowed to recover in M9 buffer for 24h at 15°C. Animals were either imaged immediately or grown at 15°C on NGM plates seeded with *E. coli* OP50 and imaged after first PGC division or after having reached the adult stage.

### **3.4.7 Latrunculin A treatments**

L1- or L4-stage animals were individually picked and incubated for 3-5h in M9 buffer supplemented with either 25 µM or 100 µM of latrunculin A (from a 50 mM stock solution in DMSO). For controls, animals were incubated in M9 buffer supplemented with solvent alone (0.5% or 2% DMSO, respectively).

### 3.5 Supplementary material

**Table S3. 1 : Strains used in this study**

Strain	Genotype	Available from
JCC146	<i>cyk-1(or596ts) unc-119(ed3)* ItIs38[pAA1; pie-1/GFP::(PLC1delta1); unc-119 (+)] III; ItIs37 [pAA64; pie-1/mCherry::his-58; unc-119 (+)] IV</i>	Canman lab
OD239	<i>cyk-4(or749ts) unc-119(ed3) ItIs38[pAA1; pie-1/GFP::(PLC1delta1); unc-119 (+)] III; ItIs37 [pAA64; pie-1/mCherry::his-58; unc-119 (+)] IV</i>	Oegema
UM639	<i>cpSi20[Pmex-5::TAGRFPT::PH::tbb-2 3'UTR + unc-119(+)] II; zuls45[nmy-2::NMY-2::GFP + This unc-119(+)]; ItIs37 [pAA64; pie-1::mCherry::HIS-58; unc-119(+)] IV</i>	This study
UM646	<i>cpls42[Pmex-5::mNeonGreen::PLCδ-PH::tbb-23'UTR+unc-119(+)]II;zen-4(or153)IV</i>	This study
UM655	<i>cpSi20[Pmex-5::TAGRFPT::PH::tbb-2 3'UTR + unc-119 (+)] II; ani-1(mon7[mNeonGreen^3xFlag::ani-1]) unc-119 (ed3)* III; ItIs37 [pAA64; pie-1::mCherry::HIS-58; unc-119(+)] IV</i>	This study
UM657	<i>nmy-2(ne3409ts) I; cpSi20[Pmex-5::TAGRFPT::PH::tbb-2 3'UTR + unc-119 (+)] II; ani-1(mon7[mNeonGreen^3xFlag::ani-1]) unc-119 (ed3)* III</i>	This study
UM735	<i>xnSi1[Pmex-5::GFP::PH(PLC1delta1)::nos-23'UTR] II; estSi71[pAC257;Pmex-5::lifeAct::mKate2::tbb-2 3'UTR; cb-unc-119(+)] IV</i>	This study
UM761	<i>rrf-3(pk1426) II; ani-1(mon7[mNeonGreen^3xFlag::ani-1]) unc-119 (ed3)* III; ItIs37 [pAA64; pie-1::mCherry::HIS-58;unc-119(+)]IV;ItIs44[pAA173,pie-1p mCherry::PH(PLC1delta1)+unc-119(+)]</i>	This study

### **3.6 Acknowledgements**

We thank Bob Goldstein (UNC Chapel Hill), Julie Canman (Columbia University) Amy Maddox (UNC Chapel Hill), Karen Oegema (UC San Diego) and Esther Zanin (LMU München) for strains. We are also grateful to Christian Charbonneau of IRIC's Bio-imaging Facility for technical assistance, Eugénie Goupil for experimental advice, and all members of the FitzHarris, Gerhold, Hickson and Labbé laboratories for helpful discussions. Some strains were provided by the CGC, which is funded by NIH Office of Research Infrastructure Programs (P40 OD010440).





## **4. Article 3 - Following *C. elegans* first larval stage germline development**

**Jack Bauer**, Christophe Clément, Delphine Bouilly, Michael Hendricks, and Jean-Claude Labbé

This manuscript is in preparation

## 4.1 Author contributions

**Jack Bauer** conceptualized, designed, and executed all the experiments, analysed the data, prepared the figures for the manuscript, wrote and edited the manuscript.

**Christophe Clément** participated in the design and the execution of experiments in (Figure 4.4A,C)

**Delphine Bouilly** participated in the conceptualization and the design of experiments in (Figure 4.2A,B,C; Figure 4.3; Figure 4.4B)

**Michael Hendricks** participated in the design and the execution of experiments in (Figure 4.4D,E)

**Jean-Claude Labbé** supervised the experimental conceptualization and design, the data analysis, and wrote and edited the manuscript.

## 4.2 Introduction

The nematode *C. elegans* is a powerful model to study developmental mechanisms *in vivo*, as its small size and transparency enable easy immobilization and imaging (Corsi et al., 2015). Over the years, these unique features have been used to characterize germline development and monitor germ cell division (Gerhold et al., 2018; Goupil et al., 2017). The *C. elegans* germline is organized as a syncytium in which each the germ cell is connected through a stable actomyosin ring to a central core of cytoplasm termed the rachis. However, the mechanisms of syncytium expansion remain partially uncovered. To better understand how the syncytium expands, we study the divisions of the Primordial Germ Cells (PGCs) at the first larval stage (L1). The PGCs remain quiescent through the end of embryogenesis and start proliferating during the L1 stage when animals start feeding. If L1 animals hatch in an environment deprived of food, they enter diapause: their development is arrested and the PGCs remain quiescent (Fukuyama et al., 2006). We previously showed that during the first division of the PGCs cytokinesis is incomplete, and we propose incomplete cytokinesis as a mechanism for the initial syncytium expansion (Bauer et al., 2021). To test whether this mechanism is specific to the first PGC division or conserved during larval development, we seek to image animals throughout their first larval stage and track the subsequent PGC divisions.

*C. elegans* imaging usually requires physical immobilization between an agarose pad and a coverslip coupled with chemical anesthesia (Fang-Yen et al., 2012). These standard methods were optimized multiple times to attempt the complete immobilization of the nematode and achieve high-resolution imaging (Kim et al., 2013; Rehain et al., 2017). However, these immobilization techniques prevent the animals to feed, which disturbs physiological functions such as germ cell division and eventually leads to developmental arrest (Zellag et al., 2021). To overcome food deprivation and study long-term developmental mechanisms, a multitude of microfluidic devices have been created in the last decade (Kamili and Lu, 2018; Midkiff and San-Miguel, 2019). These devices are conceived to immobilize the nematodes without altering their development and have been shown to be highly effective for long-term imaging in adult animals (Levine and Lee, 2020; San-Miguel and Lu, 2013). However, only a few of these methods can

immobilize *C. elegans* in their first larval stage (L1), all of which function as a catch and release mechanism where worms are immobilized solely during imaging but can otherwise move freely (Keil et al., 2017; Krajniak and Lu, 2010). These tools are useful to study development over long periods of time, but do not allow the continuous immobilization necessary to resolve molecular events like cytokinesis.

Here we test two different techniques to track PGC division throughout the first larval stage. The first one relies on a genetic mutation that enables PGC proliferation in absence of food and the second one is adapted from Dong et al 2018 which proposed the use of a biocompatible hydrogel enabling immobilization in presence of growth medium. Because we were not able to visualize PGC divisions with these methods we designed and created a microfluidic device that in principle should specifically enable long-term imaging of L1 animals to visualize germ cell division.

## 4.3 Results and Discussion

### 4.3.1 A genetic approach to track PGC divisions

In a first attempt to track PGC division using live imaging we took advantage of a mutant for *daf-18(ok480)*. *daf-18* codes for the PTEN ortholog in *C. elegans*, which antagonizes insulin signaling and is required to prevent germline proliferation during diapause. Accordingly, in *daf-18* mutants, PGCs start proliferating during L1 diapause (Fukuyama et al., 2006; Kipreos and van den Heuvel, 2019). We generated a strain bearing the *daf-18(ok480)* mutation and co-expressing fluorescent protein markers for membranes (TagRFP-PH<sup>PLCδ</sup>, green) and anillin (mNG::ANI-1, magenta) that enable us to follow the dynamics of the cytokinetic ring during PGC division. To test whether PGCs would divide in absence of food in the *daf-18(ok480)* mutant strain, we imaged L1 animals every hour for 10 hours alongside wild-type controls. As expected, in control animals the PGCs remained quiescent throughout the imaging period (n=20). Surprisingly however, all *daf-18(ok480)* mutant animals died during imaging, typically after 2-3 hours (n=24) (Figure 4.1A). The reason why *daf-18(ok480)* mutants did not survive is unclear.

Previous studies that imaged *daf-18(ok480)* mutants at the L1 stage did not use live imaging but rather immunofluorescence (Fukuyama et al., 2006). One possibility is that animals bearing the *daf-18(ok480)* mutation are hyper-sensitive to one or several conditions in our imaging method: compression, tetramisole or laser intensity. Regardless, using *daf-18(ok480)* mutants in which PGCs are insensitive to dietary restrictions did not enable us to track PGC divisions in L1 animals.

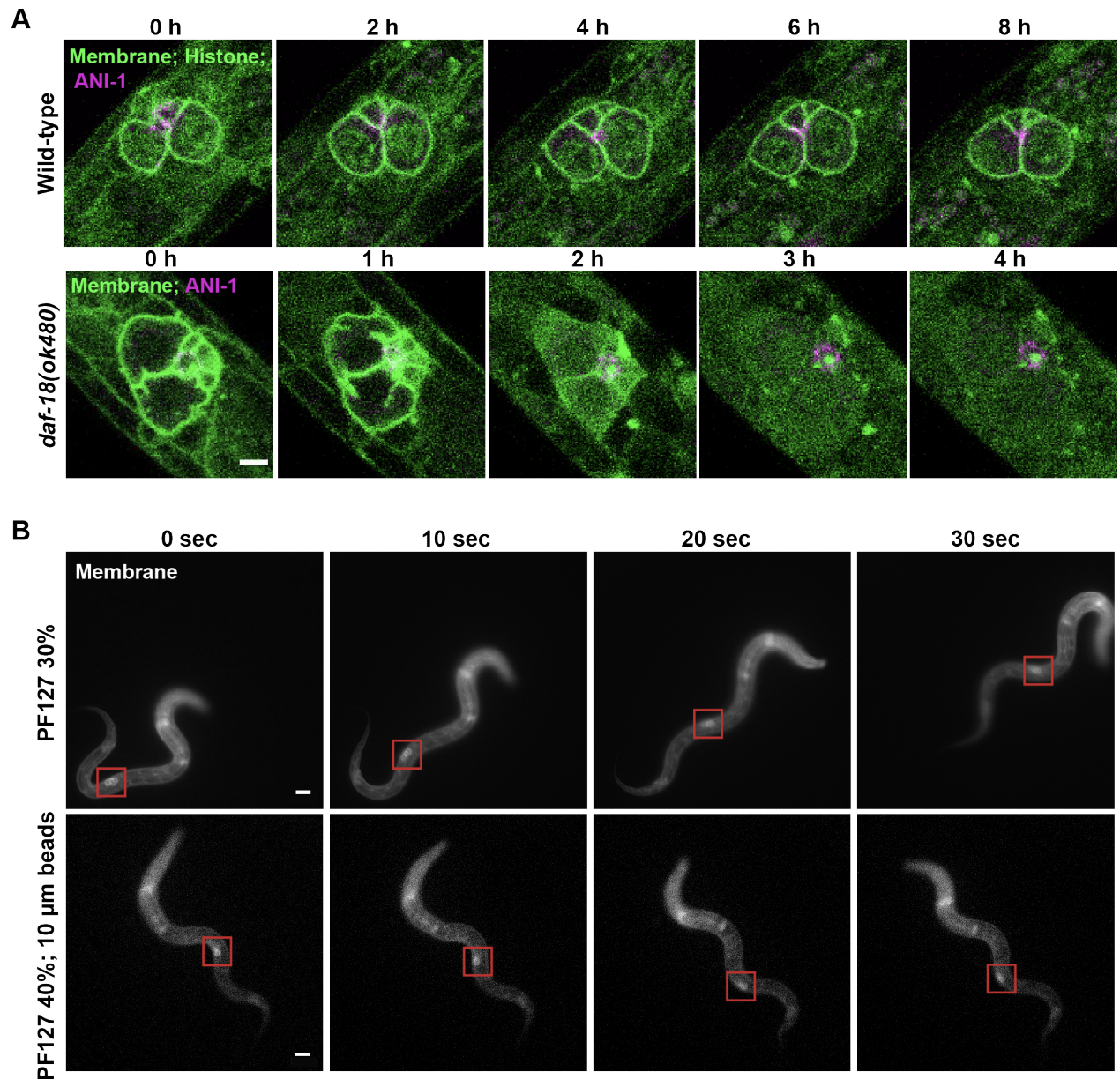


**Figure 4. 1: Tracking PGC division with a genetic approach or hydrogel immobilization**

(A) Confocal time-lapse images (maximum projection of three slices) of the PGCs in first larval stage wild-type or *daf-18(ok480)* mutant animals expressing FP-tagged markers for membrane and chromatin (TagRFP-PH<sup>PLC $\delta$</sup>  and mCh-HIS-58, green) and mNeonGreen::ANI-1 (magenta). Scale bar: 3  $\mu$ m. (B) Fluorescence microscopy images (single plane) of first larval stage animals expressing membrane TagRFP-PH<sup>PLC $\delta$</sup>  (white) in solutions of 30% PF127 or 40%PF127 with 10  $\mu$ m beads. Scale bar: 10  $\mu$ m

### 4.3.2 Trapping worms in a viscous hydrogel for long-term imaging

Our genetic approach to image PGC divisions with *daf-18* mutants was not successful, so we sought to modify our immobilization method to overcome dietary restrictions. There are several techniques that enable *C. elegans* long-term imaging, but they often require specific chip designs coupled with a complex microfluidic montage. A promising alternative that can be easily implemented in any laboratory was proposed by Dong et al. 2018, which enables the immobilization of all *C. elegans* larval stages in liquid growth medium with a bio-compatible and temperature-responsive hydrogel matrix (Dong et al., 2018). The Pluronic F127 (PF127) hydrogel transitions from solution to gel in a small temperature range—compatible with *C. elegans* development—depending on its concentration. At 12°C with PF127 concentration ranging from 19% to 30%, the solution viscosity is minimal; at 25°C the gel viscosity increases with concentration within the same range. Dong and colleagues took advantage of these properties to mount animals in 30% PF127 at 12°C which, once raised at room temperature, successfully immobilized worms in all larval stages.

We repeated these experimental procedures to immobilize L1 animals in 30% PF127 and took images every 10 seconds. In our hands, L1 animals mounted in 30% PF127 were highly mobile, and exited the field of view after 1 minute of acquisition, n=10 (Figure 4.1B). Mounting L1 animals in 30% PF127 is not suitable for PGC division imaging parameters, since this requires the acquisition of high-resolution images magnified in a region of interest (red square in Fig. 1B) every 2 to 4 minutes. We further tried to immobilize L1 animals with PF127 and challenged Dong and colleagues technique by increasing the hydrogel concentration to 40%. In addition, we complemented PF127 with 10 µm-diameter polystyrene beads to serve as a spacer between the microscopy slide and coverslip, to slightly compress L1 animals (which are about 10-15 µm in diameter (Dong et al., 2016)). These microbeads were used in different sizes for optimal PF127 immobilization of adult animals but were not recommended for larval stages (Dong et al., 2018). Mounting L1 animals in 40% PF127 coupled with 10 µm diameter microbeads drastically reduced movement compared to what we observed in 30% PF127, n=20 (Figure 4.1B). However, the

worms were still able to move and the region comprising the PGCs was not immobilized well enough for our high-resolution imaging requirements (Figure 4.1B).

Dong and colleagues created a hydrogel-microbead matrix for long-term *C. elegans* imaging and have shared strong evidence that their method is efficient for the immobilization of adult animals. The study further offers a additional protocol for the immobilization of all other larval stages. However, authors do not provide experimental evidence that their method enables the immobilization of animals in the different larval stages. Additional optimization of this method is required to efficiently immobilize L1 animals. We tried to increase the concentration of PF127 over 40%, but we were not able to efficiently dissolve PF127 even by varying temperature. It is also possible that small size of these animals may also challenge the viscosity of the PF127 hydrogel to its physical limits.



### 4.3.3 Microfluidic chip design and creation for long-term immobilization of L1 animals

In a last effort to immobilize L1 worms without impacting their development we sought to design and create a microfluidic chip that allowed for continuous immobilization for long-term live imaging. This device was designed to immobilize the posterior of the animals—where the PGCs are localized—while the anterior remains free of movement and exposed to food (Berger et al., 2018). To achieve this, we designed a worm chamber opened to microfluidic circuits which are connected to four valves that are used in an orderly manner as inlets/outlets and for pressurizing the device (Figure 4.2A,B). First, the specimen is loaded in the chip using the “worm inlet”, then it is positioned in the chamber by alternatively applying negative and positive pressure on the “positioning vacuum” and “worm inlet”. Once the specimen is properly localized in the chamber, it is maintained in place throughout the whole imaging session by applying lateral negative pressure on the worm with the “stabilization vacuum”. Finally, after immobilization, a solution of bacteria is loaded in the “food inlet” and collected from the “food outlet” to create bacterial flow to which the worm is exposed (Figure 4.2A,B).

To design such a device with a chamber that specifically fits their size, we first measured the diameter and the length of L1 animals. We virtually reconstituted a worm model based on the measurements made using the ImageJ measuring tool on DIC images of L1 animals. Similarly to what has been reported (Dong et al., 2016), we found that L1 animal length varied from 227 to 252  $\mu\text{m}$  (average  $\pm$  SD =  $238 \pm 12 \mu\text{m}$ ,  $n=4$ ) and their maximum width varied from 12.6 to 17.6  $\mu\text{m}$  (average  $\pm$  SD =  $15.4 \pm 2 \mu\text{m}$ ,  $n=4$ ) (Figure 4.2C). To maximize our chances of immobilizing L1 animals with success, we design different devices with two constants and three variables (Figure 4.2D). The first constant is the length of the chamber which is 120  $\mu\text{m}$  long, which leaves about 120  $\mu\text{m}$  of the anterior portion of the worm free to feed. The second constant is the 10  $\mu\text{m}$  width of the chamber which slightly compresses the worms. The three variables in the chamber design are: the opening to the “positioning vacuum” is either 2, 3, 4, 5 or 6  $\mu\text{m}$  wide; the lateral openings to the “stabilizing vacuum” are either 5, 6 or 10  $\mu\text{m}$  wide; and the neck of the chamber either progressively enlarged to 13  $\mu\text{m}$  or not, to potentially allow for better head mobility (Figure

4.3A,B). All the 25 design variations were created in the chip fabrication process (Figure 4.3C, Table 4.1).

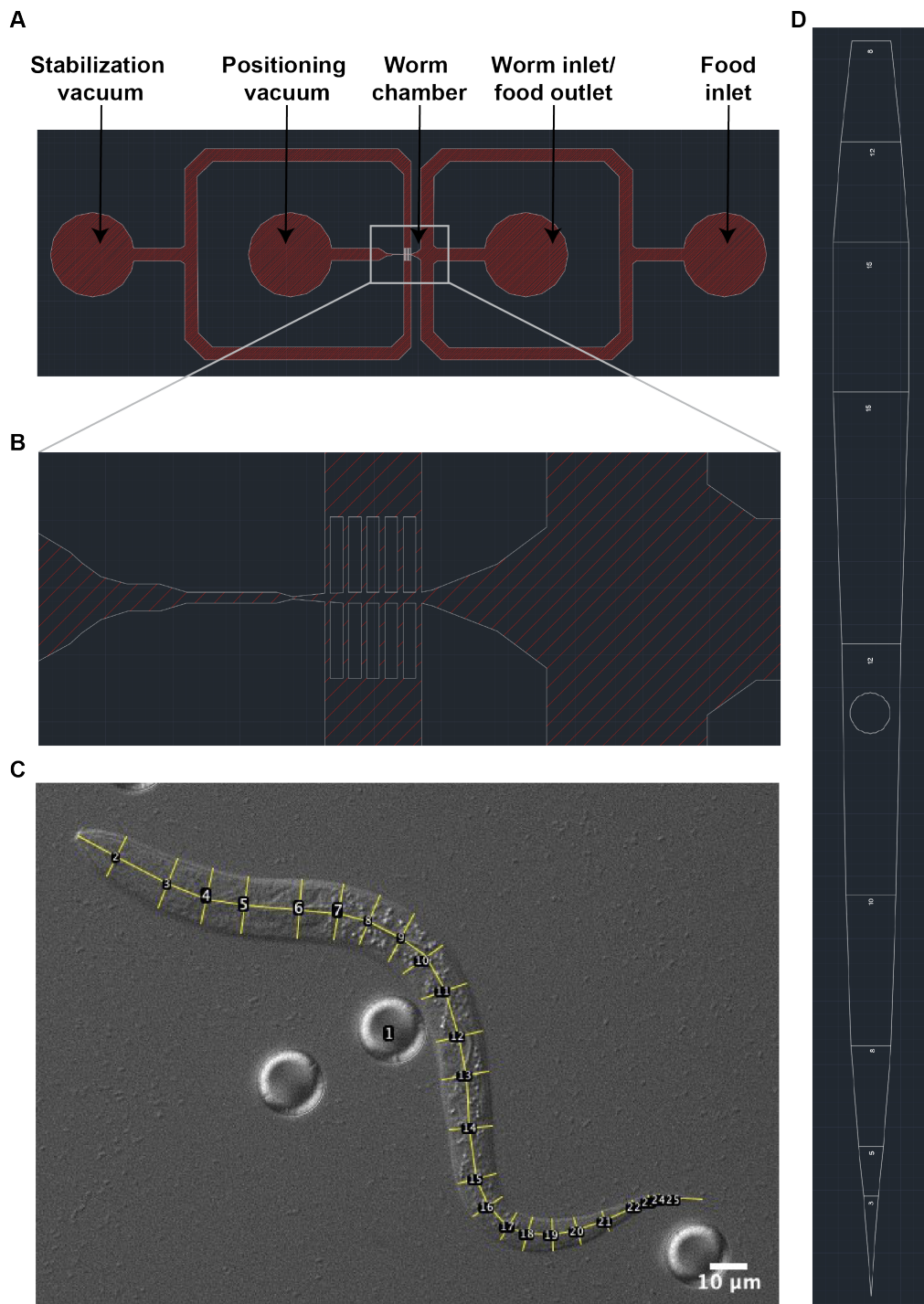
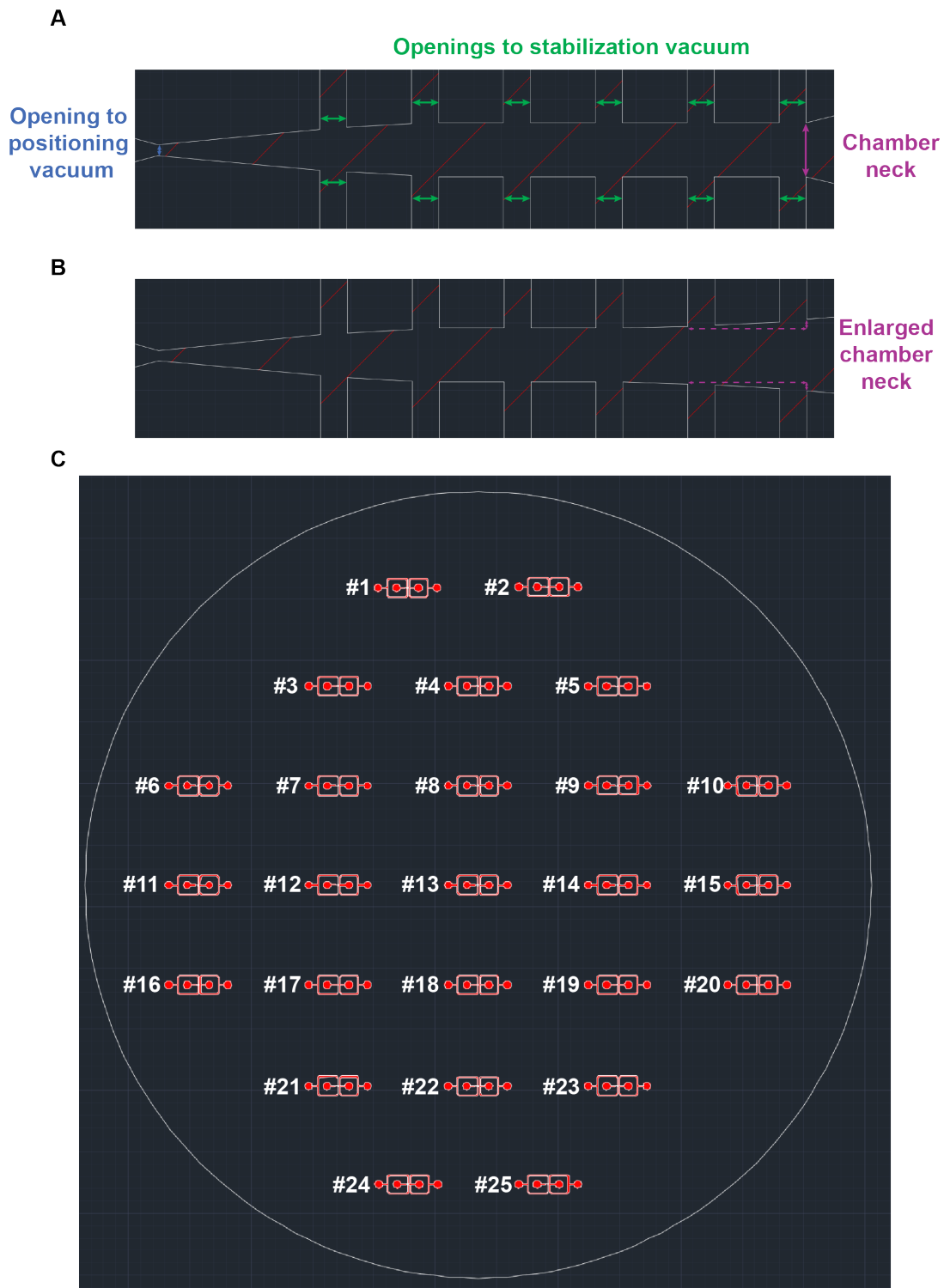


Figure 4. 2 : Design of a microfluidic device to immobilize L1 stage animals

(A) Design of the microfluidic device to immobilize L1 stage animals. (B) Inset on the worm chamber. (C) Differential interference contrast image of an animal at the first larval stage mounted 40% PF127 hydrogel and 10  $\mu\text{m}$  microbeads. Numbers corresponds to yellow lines drawn for measurement.  $n=4$ . (D) Average representation of the length and the width of an animal at the L1 stage based on measurements made in (C).

Once we had designed our device, we engineered the material necessary to create the microfluidic chips. Bio-compatible microfluidic chips are usually made of polydimethylsiloxane (PDMS) and require the engineering of a “master mold” which has the features of the chip and serves as a cast to imprint the microfluidic pattern into the PDMS (Duffy et al., 1998; McDonald et al., 2000). The high resolution of our design (smallest feature = 2  $\mu\text{m}$ ) specifically required the creation of a master mold with photolithography coupled to Deep Reactive Ion Etching (DRIE) (Laermer et al., 1999; Xia and Whitesides, 1998). First, we used photolithography to pattern our design with a resin coat on a silicon wafer (which would become the future master mold) (Figure 4.4A,B). Then, DRIE carved out the silicon that had not been covered in resin, creating a three-dimensional template, with a depth determined by the duration of DRIE (Figure 4.4C,D), see methods for more details. We aimed to etch 10  $\mu\text{m}$  of the silicon to give a 10  $\mu\text{m}$  depth to our microfluidic chip channels. The depth of the channels on the master mold were then verified with a profilometer and varied from 9.7 to 11.4  $\mu\text{m}$  across the wafer (Table 1). We then cast and cured a PDMS mixture over the master mold which contained all our designs, peeled off the PDMS, created the microfluidic inlets and outlets in our chip, and bound each chip to a glass coverslip (Figure 4.4E), see methods for more details.



**Figure 4. 3 : Different variations of the microfluidic chamber design**

Immobilization chambers with an invariable chamber neck (A) and with an enlarged chamber neck (B). (C) 25 variations of the microfluidic devices were designed (see Table S4.1). The number at the left of each design corresponds to the characteristics of the devices in Table S4.1.

We then proceeded with a preliminary loading of L1 animal into our microfluidic chip by connecting polyethene tubing to our chip and adjusting the pressure with syringes (Figure 4.4E). We were unable to successfully load and immobilize L1 in the worm chambers because our microfluidic montage clogged nearly immediately after loading buffer into the chip. In addition, manually pressing on syringes to control the pressure in the device was challenging. It resulted in damaging the animals and/or them going right through the immobilization chamber.

We have successfully created microfluidic devices that in theory could work to immobilize L1 animals for extended imaging periods. However, our preliminary tests to immobilize L1 animals in the chip chambers were unsuccessful. There are many factors that could have limited our ability to load the chambers. First, our experimental environment may not have been suitable for our microfluidic system. We worked in a standard laboratory environment whereby any air contaminants may have entered the microfluidic system and clogged our microfluidic chip. Setting up our fluidic system in a clean room environment may have prevented the clogging of the smallest features of our chips (2 to 6  $\mu\text{m}$  wide) from air contaminants such as dust (which vary from 1 to 100  $\mu\text{m}$  in diameter) (Calvert, 1990). In addition, the animal's medium may have been a source of contamination. We thoroughly washed L1 animals with filtered buffer, but debris may have remained attached to the nematodes. One solution for this could be to filter the worms through a 10  $\mu\text{m}$  cell strainer in a clean room environment to remove as much contaminants as possible from the animals (Berger et al., 2021). Finally, our material was not optimal to control our microfluidic system. We pressurized our chips by manually pressing on syringes, which has been shown to be suitable for devices bearing larger channels for advanced larval stages animals but not for earlier stages (McCormick et al., 2011). Perhaps the small size of both the channels and the animals requires a more controlled system to properly regulate the flow in our microfluidic chips.

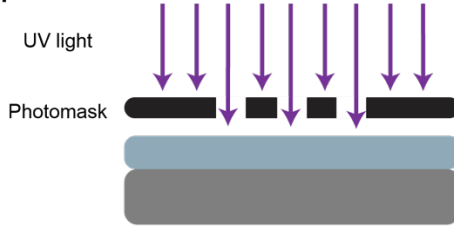
Further optimization is required to ensure the functionality of our microfluidic device. By improving both the laboratory environment and the materials to control the fluidics in our chip, we may be able to achieve long-term immobilization of L1 animals to track several rounds of PGC division. Recently Berger et al. 2021 reported a microfluidic device that enables long-term imaging

of L1 animals and across *C. elegans* larval stages while maintaining worm orientation over time (Berger et al., 2021). This promising technique could be tested as an alternative for our device to try to track PGC division over the *C. elegans* first larval stage.

**A 1. Spin-coat photoresist on a silicon wafer**



**2. Expose photoresist to UV light through a photomask**



**2. Develop exposed wafer with photoresist**



**C 1. Passivation: coating**



**3. Isotropic plasma etching**



**3. Repeat until desired depth is reached**

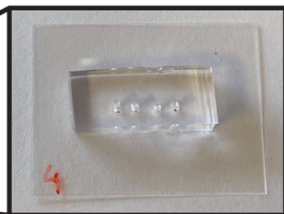
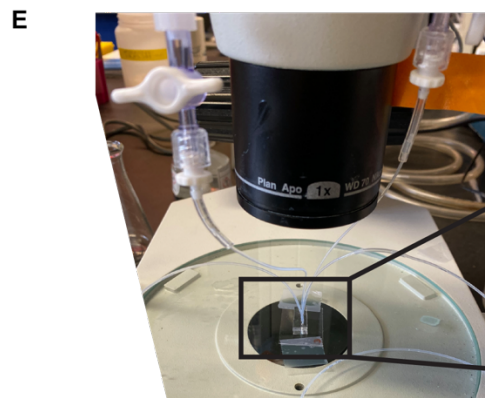
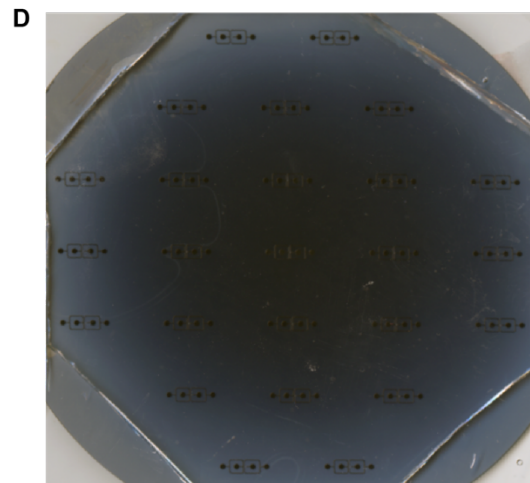
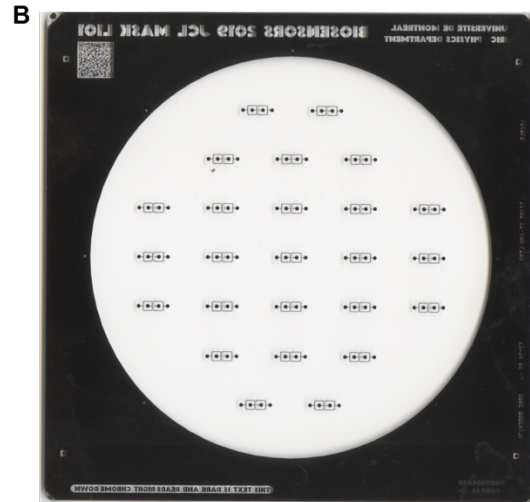


**Figure 4. 4 : Fabrication of the master mold and microfluidic setup**

(A) Illustration explaining the different steps of photolithography. (B) Image of the photomask. (C) Illustration explaining the different steps of deep reactive ion etching (DRIE). Image of the master mold. (E) Microfluidic setup. Inset is the microfluidic chip bound to a glass coverslip.

## 4.4 Material and methods

### 4.4.1 *C. elegans* strains and maintenance

The two *C. elegans* strains used for this study are UM711 (*cpSi20[Pmex-5::TAGRFPT::PH::tbb-2 3'UTR + unc-119 (+)] II; ani-1(mon7[mNeonGreen<sup>3</sup>xFlag::ani-1]) unc-119 (ed3) III; daf-18(ok480) IV*) and UM655 (*cpSi20[Pmex-5::TAGRFPT::PH::tbb-2 3'UTR + unc-119 (+)] II; ani-1(mon7[mNeonGreen<sup>3</sup>xFlag::ani-1]) unc-119 (ed3) III; ItIs37 [pAA64; pie-1::mCherry::HIS-58; unc-119(+)] IV*). Animals were grown on NGM plates seeded with *E. coli* strain OP50 and maintained at 20°C as described (Brenner, 1974). First stage (L1) larvae were obtained by dissolving gravid hermaphrodites in sodium hypochlorite solution (1.2% NaOCl, 250 mM NaOH) and hatching recovered embryos for 24h at room temperature in M9 buffer (22.04 mM KH<sub>2</sub>PO<sub>4</sub>, 42.27 mM Na<sub>2</sub>HPO<sub>4</sub>, 85.55 mM NaCl, 1 mM MgSO<sub>4</sub>).

### 4.4.2 Imaging and worm measurement

*daf-18(ok480)* animals were immobilized in M9 buffer supplemented with 0.2% tetramisole, mounted on a 3-5% agarose and a coverslip was applied and sealed with VaLaP (1:1:1 Vaseline, lanolin, and paraffin). Images were acquired every hour with a GaAsP detector at 16-bit depth mounted on a Zeiss LSM880 laser-scanning confocal microscope, controlled by ZEN black 2.1 SP3 software, and using a Plan-Apochromat 63x/1.4 oil DIC M27 objective. Animals immobilized with the PF127 hydrogel were imaged every 10 seconds with an HRM camera mounted on a Zeiss AxioImager Z1 microscope and using a Plan-Apochromat Objective 20x/0.8 M27 objective. All images were further processed and analyzed using ImageJ software (National Institutes of Health). L1 animal measurements were done by manually tracing lines on images of nematodes immobilized with 40% PF127 hydrogel and 10 μm microbeads. Length was determined by tracing a lane that symmetrically divided the animals along the anterior-posterior axis. Width was measured by tracing 24 separate lanes perpendicularly to the anterior-posterior axis.



### **4.4.3 Hydrogel immobilization**

Immobilisation of animals in PF127 hydrogel was done as described in Dong et al., 2018. 40% PF127 was mixed at 4°C to obtain a homogenous hydrogel. For 40% PF127 immobilization, the hydrogel was mixed with 2,5% of 10 µm polystyrene microbeads.

### **4.4.4 Microfluidic device design**

The design of our microfluidic chips was done with AutoCAD 2018.2. This design was used to create a chromed photomask at Photomask Portal (Richardson TX).

### **4.4.5 Master mold engineering**

Photolithography (Figure 4.4A,B): A 4-inch silicon wafer with a 1 µm thick layer of OiR674-11 photoresist by spinning 1 minute at 4000 RPM, followed by soft bake (1 min at 90°C). The photomask was aligned to the coated wafer using low vacuum contact and exposed the wafer to UV light (8.3 intensity) for 4.8 sec with a Karl Suss MA6 mask aligner. Finally, AZ 726 MIF was used to develop our coated wafer and remove the photoresist that was exposed to UV light.

Deep Reactive Ion Etching (Figure 4.4C,D): The coated wafer was then etched by repeating 50 cycles of C<sub>4</sub>F<sub>8</sub> coating then SF<sub>6</sub> etching using an Oxford Instruments Plasmalab System 100 with the parameters in Table 4.2. The depth of the etching was then measured with a Veeco Dektak 3030st profilometer.

### **4.4.6 Chip fabrication**

Two-component PDMS was mixed at 10:1 w/w, degassed under vacuum, poured over the master mold, degassed again, then cured over night at 50°C. Cured PDMS was cut out, removed from the master mold, then inlet holes were made with a Milltex 1mm biopsy puncher. Finally, the PDMS was cut into chips and were bonded to microscopy glass coverslip using an air plasma generated by a corona surface treater (Haubert et al., 2006).

## 4.5 Supplementary material

**Table S4. 1: Dimensions of the different microfluidic chips**

Device number (As specified in fig. 3C)	Opening to positioning vacuum Width ( $\mu\text{m}$ )	Openings to stabilization vacuum Width ( $\mu\text{m}$ )	Enlarged neck chamber	Depth measured in the worm chamber ( $\mu\text{m}$ )
#1	2	5	No	10.8
#2	2	5	Yes	11
#3	2	6	No	10.3
#4	2	6	Yes	10
#5	2	10	No	10.5
#6	3	5	Yes	10.5
#7	3	5	No	9.9
#8	3	6	Yes	9.8
#9	3	6	No	10.1
#10	3	10	Yes	11.4
#11	4	5	No	10.3
#12	4	5	Yes	9.8
#13	4	6	No	9.6
#14	4	6	Yes	9.9
#15	4	10	No	11.2
#16	5	5	Yes	10.6
#17	5	5	No	9.9
#18	5	6	Yes	9.7
#19	5	6	No	9.9
#20	5	10	Yes	11.3
#21	6	5	No	10.6
#22	6	5	Yes	10
#23	6	6	No	10.2
#24	6	6	Yes	10.9
#25	6	10	No	11

**Table S4. 2: Parameters for deep reactive ion etching**

<b>RECIPE LMF BOSCH4s6s</b>									
STEPS	Time (seconds)	Pressure (mTorr)	Temperature (Celcius)	Helium pressure (Torr)	SF6 (sccm)	C4F8 (sccm)	O2 (sccm)	ICP Power (W)	CCP Power (W)
Stab Temp	120	N.A	20	11	0	0	0	0	0
Stab Gaz	10	20	20	11	1	65	0	0	0
Strike	2	20	20	11	1	65	0	450	50
Repeat	REPEAT STEP (dep-etch)								
Deposition	4	20	20	11	1	65	0	450	10
Transition buffer	2	20	20	11	65	15	0	0	0
Etching	6	20	20	11	65	15	0	450	25
Loop	Go back to dep step								



## 5. Discussion

Syncytial tissues have been puzzling researchers for nearly two hundred years and the mechanisms by which these tissues form and their biological significance remain partly undetermined. All animal germlines are syncytia in which germ cells share a common cytoplasm through intercellular bridges (ICBs), and these ICBs have been extensively studied primarily in the *Drosophila* ovary and the mouse testis. These investigations have provided a clear description of the molecular composition in *Drosophila* ICBs and insight on how they form in the mouse. However, these molecular mechanisms are not conserved across all animal germlines and studying syncytial structures in different species will help to better understand what is common to all animal ICBs and what is specific to each germline. This is why the development of the *C. elegans* germline syncytium is the focus of my PhD thesis. To better understand how the syncytium forms in the *C. elegans* germline, we first studied the organization of the germline before the syncytium expands. We found that the germline at the first larval stage (L1) was organized similarly to the adult gonad where the primordial germ cells (PGCs) individually connect to a central cytoplasm through stable ICBs (Chapter 2). Because these ICBs are maintained by actomyosin rings in the adult gonad, we verified whether this was the case at the L1 stage. As opposed to adult gonads, any perturbation of actomyosin regulator protein function at the L1 did not affect the syncytial organization of the PGCs (Chapter 3). Once the L1 stage germline was characterized I tracked the first division of the PGCs to better understand how the syncytium expands in *C. elegans*. I found that the cytokinetic ring stabilizes into an ICB to connect one of the daughter cells to the syncytium, while the other cell inherits the ICB from the mother cell (Chapter 2). Finally, to test if the mechanisms of syncytium expansion I discovered are conserved in subsequent germ cell divisions, I designed and engineered a tool that could theoretically enable long-term imaging of L1 stage animals (Chapter 4). In the next sections I will take a few steps back to discuss my results, their limitations, and the significance of my discoveries. I will also mention new questions raised by my research and what remains understood in the germline syncytium field.

## 5.1 Preparing for syncytium expansion

The syncytial structure in animal germlines usually arises once the gonad is fully formed. In *Drosophila* females, the syncytium forms during larval stages, after the establishment of the stem cell niche in the germarium, when the cystoblast (that arises from GSC divisions) divides to form the 16-cell interconnected germline-cyst (Greenbaum et al., 2011; Haglund et al., 2011; Robinson and Cooley, 1996; Spradling, 1993). Although the mechanisms of germline formation are very different in the mouse testis, it is also only after the germ cells have found their place in the gonad that the spermatogonia proliferate and form syncytial chains of 2, 4, 8 or 16 cells during postnatal development. As opposed to the mouse and *Drosophila*, the events that lead to syncytium formation in *C. elegans* occur during early embryogenesis, right after the germline is specified. Previous work in our laboratory has shown that the syncytium arises from the incomplete division of P<sub>4</sub>, that leads to the formation of an ICB between the two PGCs (Goupil et al., 2017). However, this direct connection between the embryonic PGCs is very different from the adult syncytium organization where each germ cell is connected to the rachis. This suggests that there is a reorganization of the syncytial architecture that results in the apparition of the rachis. My work indicates that this reorganization occurs after the establishment of the ICB between the PGCs during late embryogenesis, that leads to the formation of a rachis primordium at the L1 stage.

### 5.1.1 The first larval stage PGCs: precursors to the adult syncytium

The first events that lead to syncytium formation in *C. elegans* occur during the division of P<sub>4</sub>, but the rachis has been previously proposed to only become apparent at the L2 stage. Both electron microscopy and confocal microscopy have shown that the germ cells connect to a rachis through intercellular bridges at the L2 stage similarly to the adult syncytium (Amini et al., 2014; Hirsh et al., 1976). More recently, with electron microscopy sections of the PGCs, a study has proposed that the rachis was nascent at the L1 stage, but the authors did not further characterize the organization of the syncytium at this stage (Lee et al., 2018). Our work confirmed the presence of a rachis primordium between the two PGCs both with electron and enhanced resolution confocal microscopy. Indeed, we demonstrated that each PGC is independently connected

through ICBs to a common central cytoplasmic cavity that we termed the proto-rachis (Chapter 2). This indicates that the organization of the PGCs at the L1 is comparable to the adult gonad in which all germ cells are connected through the rachis through stable ICBs. This suggests that the organization of the syncytium is set at the onset of germline expansion at the L1 stage, and that the gonad will not undergo any major syncytial reorganization during the rest of its development. The organization of the gonad at the L1 stage would therefore be the starting point for syncytial expansion. From the L1 stage, the rachis would enlarge as new intercellular bridges are incorporated into the rachis during germ cell division until the gonad is fully formed.

The ICBs that connect cells in germline syncytia generally derive from cytokinetic furrows. They can be modified midbodies like it appears to be the case in the mouse testis and in the embryonic *C. elegans* PGCs, or they can be arrested cytokinetic rings like in the *Drosophila* egg chamber and in the *C. elegans* developing gonad. Despite differences in the timing of ICB formation during cytokinesis, in all instances ICBs form ring like structures that contain at least some actomyosin regulators found in the cytokinetic furrows. In *C. elegans*, it is known that from the L2 stage to the adult the ICBs form stable actomyosin rings in which components identified to date are also found in cytokinetic rings (Amini et al., 2014; Lee et al., 2018; Zhou et al., 2013). I demonstrated that this is also true for the PGCs at the L1 stage, where each ICB that connects the PGCs to the proto-rachis form actomyosin rings that share similar regulators with cytokinetic furrows, such as CYK-4 and ZEN-4, ANI-1, NMY-2 and CYK-7. These stable actomyosin rings are about 1  $\mu\text{m}$  in diameter at the L1 stage whereas they are about 2 to 4  $\mu\text{m}$  in L4 stage gonads. Although they vary in size, ICBs share similar characteristics over gonad development.

In all studied germline syncytia, germ cells share a common cytoplasm. One example is the germ cells in the mouse testis in which cytoplasmic sharing through ICBs enables synchronous germ cell division and differentiation (Braun et al., 1989; Caldwell and Handel, 1991). Another example is the *Drosophila* egg chamber where multiple organelles, proteins and mRNAs are transported from the nurse cells to the oocyte through the ring canals (Bolivar et al., 2001; Cox and Spradling, 2003; Huynh and St Johnston, 2004; Mische et al., 2007). This characteristic is also common to the adult *C. elegans* germline where the germ cell ICBs enable common cytoplasm

between the germ cells and the rachis. In fact, a cytoplasmic streaming originates from the pachytene cells in the distal end and moves towards the proximal end of the gonad (Amini et al., 2014; Wolke et al., 2007). This cytoplasmic streaming ends into the enlarging oocytes, and this has been proposed to be required for proper oocyte formation (Wolke et al., 2007). Similarly to the adult gonad, my results indicate that the PGCs share a common cytoplasm in the L1 stage gonad as it was also shown previously (Abdu et al., 2016). There is no evidence of active cytoplasmic streaming in the developing gonad that compares to the actin-contraction-mediated streaming in the adult, but our results support that the ICBs connecting the PGCs to the proto-rachis enables cytoplasmic exchange between the L1 stage germ cells. This reinforces our model in which the syncytial structure of the PGCs at the L1 stage is a direct precursor to the adult gonad.

Altogether our results show that not only the organization of the syncytium at the L1 stage is fundamentally identical to that in the adult, but that the structures in both developmental stages share similar characteristics. The *C. elegans* germline is therefore a fully formed and functional syncytium right after embryogenesis at the L1 stage. This is in opposition to other syncytial germlines (the mouse testis and the *Drosophila* ovary) that arise only with the initiation of the gamete formation process. The early formation of the syncytium in *C. elegans* suggests that the property of the syncytium is required for proper gonad development from the L1 stage.

### **5.1.2 A robust syncytial organization**

In syncytial germlines the ICBs are maintained by stable actomyosin rings. In the *C. elegans* adult gonad, perturbation of the function of any regulator localized at the stable actomyosin rings leads to the collapse of ICBs, binucleation of germ cells, and a disorganization of the germline (Amini et al., 2014; Priti et al., 2018; Zhou et al., 2013). This is also the case in the embryo where perturbation of the same regulators leads to a collapse in the membrane partition between the two PGCs (Goupil et al., 2017). Surprisingly, we were not able to perturb actomyosin regulator function in the PGCs at the L1 stage (Chapter 3).



One possibility that could explain why the RNAi treatment did not deplete actomyosin regulators in the PGCs is the sensitivity of L1 stage animals to RNAi. In the adult *C. elegans* RNAi is systemic, and this property is ensured by several transmembrane cell receptors. SID-2 is present at the surface of the intestinal lumen and enables dsRNA uptake from the lumen into the intestinal cells (McEwan et al., 2012; Winston et al., 2007). The transport from the intestinal cells to the rest of the body is ensured by SID-1 which is expressed systemically in the animal (McEwan et al., 2012; Winston et al., 2007). The lack of sensitivity to RNAi in L1 stage PGCs may be the result of SID-2 not being expressed in the early L1 intestine, or the absence of SID-1 transporters in the PGCs. Because the effect of RNAi depletion for regulators of spindle assembly checkpoint in the L1 stage gonad has previously been observed in L2, it is unlikely that L1 animals lack SID-2 receptors (Lara-Gonzalez et al., 2019). In addition, the low or null expression of SID-1 in the PGCs is a more probable possibility as this is the case in neurons which are highly refractory to RNAi treatment (Calixto et al., 2010; Feinberg and Hunter, 2003). To test this hypothesis, we could overexpress SID-1 under a germline promoter to sensitise the PGCs to RNAi like it was previously done for neurons (Calixto et al., 2010). Although a specific deficiency in the pathway that enables systemic RNAi is possible, it is hard to conceive why this would be specifically the case at the L1 stage.

The organization of the PGCs at the L1 stage was also unaffected when direct perturbation of the protein function of different actomyosin regulators was mediated by temperature upshift of animals bearing temperature sensible alleles. My results are consistent with a study demonstrating that the use of temperature sensitive alleles for central spindle complex components (CYK-4 and ZEN-4) did not disrupt the germline organization during its larval development, from L1 to L4 (Lee et al., 2018). This suggests that the function of the actomyosin regulators might not be required to stabilize the ICBs during the germline development. This is surprising considering that regulators like CYK-4, ZEN-4 and NMY-2 are essential for cell division (D'Avino *et al.*, 2015; Guse et al., 2005; Jantsch-Plunger et al., 2000). Another possibility is that these temperature sensitive alleles are inefficient specifically during the early development of the gonad.

Finally, the PGCs at L1 stage remained syncytial upon Latrunculin A treatment. The overall structure of the PGCs was unchanged but I was able to detect some qualitative changes in the organization of the actomyosin rings. It is possible that in the L1 stage, actin is required for the formation of the ICBs, but not essential to the maintenance of the stable actomyosin rings. The changes observed in the organization of these rings may reflect a relaxation of the stable rings in the proto-rachis upon actin depolymerization. This could be verified by measuring the diameter of the actomyosin rings that connect the PGCs to the rachis with augmented resolution confocal microscopy (like it was done in Chapter 2). The hypothesis that actin is not required for ring stabilization in the early *C. elegans* germline would be consistent with what is found in *Drosophila* ring canals. In the female germline there is a reorganization of actin during the formation of the ring canals, while in the male germline, actin is not part of the mature ring canals (Greenbaum et al., 2011). However, there is no evidence for reorganization of stable actomyosin rings or changes in the composition in the stable actomyosin rings during their formation and their maintenance in *C. elegans*.

Overall, the reasons why I was not able to disrupt the syncytial organization of the PGCs at the L1 stage remain unclear. I have used three different techniques (RNAi, temperature sensitive alleles, and Latrunculin A treatment) to disrupt the protein function of regulators which normally destabilize any actomyosin ring, that fail to perturb the stable actomyosin rings in the L1 stage PGCs. It is unlikely that the individual hypotheses formulated above converge specifically in the L1 stage to explain why the PGCs are refractory to the different perturbations in actomyosin regulators. I think that the refractory property of the PGCs at the L1 stage is rather inherent to the germline identity. The effects of both RNAi depletion and upshift of animals bearing temperature sensitive alleles becomes only highly penetrant in the adult gonad. Indeed, no perturbation in the syncytium organization has ever been reported during the germline development upon perturbation of actomyosin regulator function. A possibility is that there is a developmental program that actively protects the syncytial architecture from any perturbation during the expansion of the germline between the L1 and the L4 stage.

### 5.1.3 What about the membrane lobes?

During the characterization of the organization of the PGCs at the L1 stage, we discovered the presence of membrane lobes, that similarly to the PGCs were connected to the proto-rachis through ICBs that formed actomyosin rings. These membrane lobes persist after PGC division and in further larval stages, at least until the L2 stage (data not shown). In addition, similar structures have been previously observed in the embryonic PGCs, suggesting that the membrane lobes that arise during embryogenesis are the same that the ones that persist during larval development (Abdu et al., 2016; Maniscalco et al., 2020). In the embryo, these membrane lobes have been proposed to arise from the formation and the ingression of an actomyosin ring, similar to an incomplete cytokinesis without concomitant mitosis (Maniscalco et al., 2020). However, why these membrane lobes form remains completely unclear. Abdu and colleagues have found that these lobes in the embryo function as a receptacle for the PGCs to discard organelles and cytoplasmic components that are internalised and digested by endodermal cells.

Nonetheless, these results do not explain why these membrane lobes persist in subsequent larval stages. The fact that these membrane lobes are variable in number, in size and position in the proto-rachis suggests that their function is not important as a unit but rather as an entity. Because they connect to the proto-rachis with stable actomyosin rings, these lobes may be required for the organization of the proto-rachis. Indeed, it is possible that the connection of the lobes to the proto-rachis balances tensile stress upon the proto-rachis that is necessary for the maintenance of the central cytoplasmic cavity. It is hard to conceive how a central cytoplasmic cavity could be physically maintained between the two PGCs with only the two stable actomyosin rings that would connect the PGCs. The extra actomyosin rings from the membrane lobes would therefore be an adequate physical support to sustain the architecture of the proto-rachis. In fact, this would be consistent with the organization of the adult syncytium in which the rachis is maintained by the contraction of a continuous actomyosin corset (Priti et al., 2018). The membrane lobes at the L1 stage bring continuity to the actomyosin meshwork that could be necessary for the maintenance of the proto-rachis, as is the case in the adult syncytium.

#### **5.1.4 Rewiring connections: formation of the rachis primordium**

In the embryo, after the division of P<sub>4</sub> the PGCs are directly connected with one another through a single ICB, while at the L1 stage the PGCs are both connected to a central proto-rachis through individual ICBs. This suggests that the syncytial structure reorganizes during late embryogenesis and that another stable ICB is formed to individually connect the PGCs to the proto-rachis at the L1. How the single ICB that connects the PGCs in the embryo reorganizes to individually connect the L1 PGCs to the proto-rachis is not completely understood. One promising lead relies on the formation of the membrane lobes in the embryonic PGCs discussed in the previous section. Maniscalco and colleagues have reported that there is initially only one lobe that forms with the contraction of an actomyosin ring, effectively forming a second ICB in the gonad. In addition, they observed the presence of a “division ring” which corresponds to the ICB between the PGCs that is adjacent to the membrane lobe stable actomyosin ring (Maniscalco et al., 2020). Because our laboratory has previously shown that there is no cytoplasmic exchange between the PGCs right after the division of P<sub>4</sub>, Maniscalco’s results suggest that the ICB between the two PGCs has reopened into a stable actomyosin ring. The presence of these two stable actomyosin rings in the gonad may be the onset of the formation of the proto-rachis. However, if one stable ring is associated to one PGC, and another to the membrane lobe, the other PGC is devoid of a stable ring. For the proto-rachis to form, both PGCs need to bear a connection to it. One possibility is that a third actomyosin ring would arise with neither cell division or membrane lobe formation to connect the PGC and form the proto-rachis. Another possibility relies on the findings that the endoderm endocytoses the membrane lobe during embryogenesis (Abdu et al., 2016). After endocytosis of the membrane lobe, the stable ring that connected the lobe to the gonad may remain in the gonad and be transferred to one of the PGCs to form the proto-rachis. However, it is not clear how such events would be regulated in the embryonic PGCs. These two hypotheses need further investigation by tracking dynamics of both membrane and actomyosin rings during morphogenesis to better understand what happens to the initial ICB that directly connects the PGCs and how new ICBs arise to individually connect each PGC to the proto-rachis.

## 5.2 A model for syncytium expansion in *C. elegans*

### 5.2.1 It is just another incomplete cytokinesis

In most animal germlines the syncytium arises and expands by the stabilization of cytokinetic furrows. As discussed previously, in *C. elegans* the syncytium arises also with the stabilization of the cytokinetic furrow between the PGCs, which later reorganizes to give rise to the rachis. However, no clear mechanism explains how cells within the rachis divide to give rise to two cells that will also connect to the rachis. One model has previously proposed that the cytokinetic ring bisects the stable ring to connect the two daughter cells to the rachis in the adult *C. elegans* germline (Figure 5.1; Figure 5.2) (Seidel et al., 2018; Swiatek et al., 2009). In this model, the cytokinetic ring enters in contact with the stable ring that connects the germ cell to the rachis. The cytokinetic ring then ingresses towards the stable ring until it partitions the stable ring into two distinct stable rings (Swiatek and Urbisz, 2019). My findings in the L1 stage PGCs are somewhat different from the model proposed in the adult syncytium. They indicate that during germ cell division, the cytokinetic ring stabilizes then displaces towards the proto-rachis to integrate into the syncytium and connect one the daughter cell to the proto-rachis (Figure 2.5). My results also show that the connection between the PGCs is maintained during germ cell division and support a model where the daughter germ cell that has not inherited the stabilized cytokinetic ring, inherits the stable ring from the mother cell.

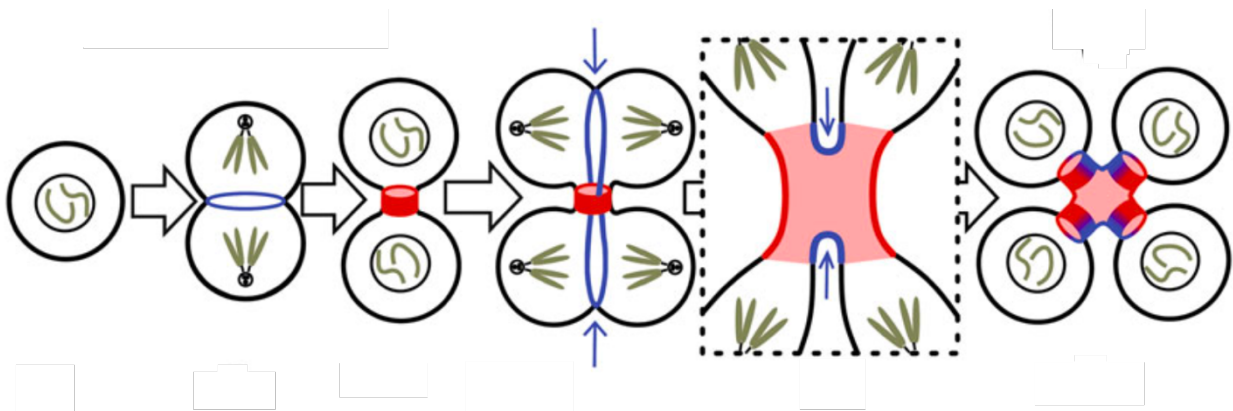


**Figure 5. 1: Cyst formation.**

Model for formation of the germline cyst in annelids proposed by Swiatek and colleagues. The first division leads to the stabilization of an ICB between the two cells (red). During the second

division, the furrow anchors into the membrane opposed to the ICB and ingresses towards the ICB (blue). Finally the furrow partitions the ICB into two new ICB (blue-red). Figure adapted with permission from (Swiatek and Urbisz, 2019).

#### **5.2.1.1 Different mechanisms for syncytium expansion in *C. elegans*?**

There are many possible reasons why my findings diverge from the model proposed by Seidel and colleagues. One explanation is that germ cell division is differentially regulated over germline development and as a consequence the mechanisms of syncytium expansion are not the same at the L1 stage and in the adult gonad. That would be consistent with the fact that the germline undergoes dramatic physiological and regulatory changes over the course of development. Indeed, the proliferation of germ cells in the adult gonad relies on GLP-1/Notch signalling from the DTC, whereas the PGCs can proliferate in absence of these signals (Austin and Kimble, 1987; Korta and Hubbard, 2010). In addition, the proliferation of PGCs at the L1 stage is correlated to chromatin changes that release the cells from transcriptional silencing. These regulatory differences in germ cell division may trigger different mechanisms for syncytium expansion that would explain the discrepancies observed between the L1 PGCs and the adult germ cells. However, my results strongly point out that the organization and the characteristics of the syncytium in L1 animals are identical in the adult. This suggests that the mechanism of syncytium expansion is consistent throughout germline development. As a parallel consideration, the mechanisms of cell division usually remain the same across tissues, although the signals that trigger division may vary. It is therefore unlikely that the mechanisms of syncytium expansion differ over germline development.

#### **5.2.1.2 The rationale behind the incomplete cytokinesis model**

We favor our model because incomplete cytokinesis as the mechanism for syncytial expansion in *C. elegans* because it is conserved in most animal germlines. This suggest that syncytium formation and expansion is similar in all animal germlines despite differences in germline organization. This would show that there is developmental consistency across all animal germline and would reinforce the idea that germline syncytia arose from a common ancestor in evolution. In addition, a structure like the one described by Swiatek et al. where two actomyosin rings contact each other has not been reported in living organisms before. There are no

mechanisms known by which a cytokinetic ring could specify within another actomyosin ring. Finally, how such a cytokinetic ring can ingress towards the stable actomyosin ring is very hard to conceive. Indeed, the forces that would be applied during constriction of the cytokinetic ring would deform the stable actomyosin ring and the adjacent membrane leading to a disorganization of the syncytium.

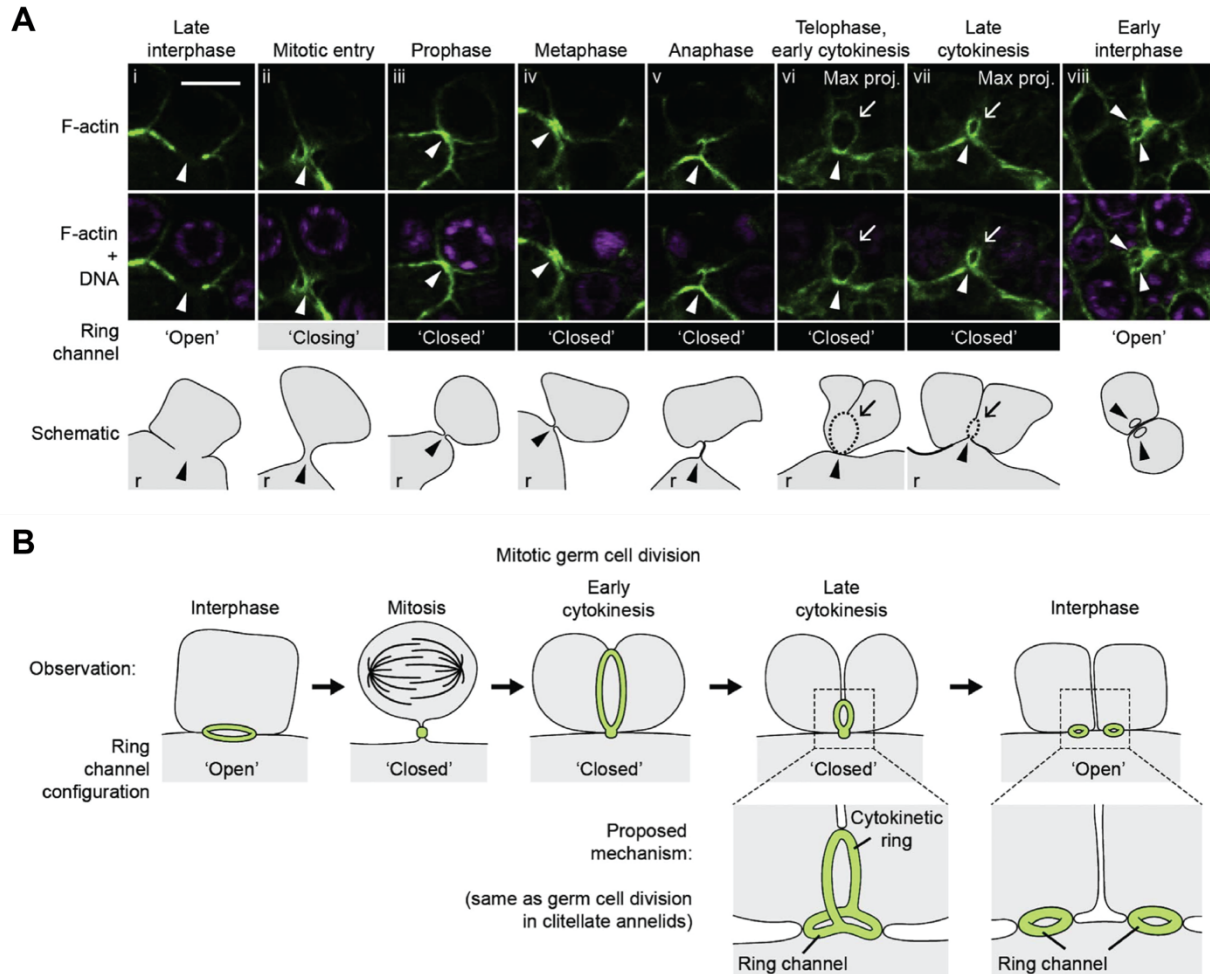


**Figure 5. 2: Dividing germ cells in the adult germline and model for syncytium expansion**

(A) Germ cells stained for F-actin and DNA. Arrowhead, ring channel. Arrow, cytokinetic ring. Maximum projection, maximum-intensity z- projection through a z-range of 1.8  $\mu\text{m}$ . r, rachis. (B) Schematic of mitotic germ cell division. The proposed mechanism is the same as germ cell division in clitellate annelids. Figure adapted with permission from (Seidel et al., 2018).

### **5.2.1.3 More information is needed to complete the stable actomyosin ring bisection model**

The differences in the models proposed for syncytium expansion could also arise from the divergence in experimental approaches. First, the model proposed by Seidel et al. relies on the electron microscopy observation of Swiatek et al. that the cytokinetic furrow in dividing germ cells is positioned perpendicularly to the stable actomyosin ring that connects the germ cells to the cytophore—the rachis equivalent in the annelids. The interpretation that the cytokinetic ring is anchored to the stable actomyosin ring might be biased by the fact that these observations were made on single section in the annelid gonad. A three-dimensional reconstruction of serial sections of the dividing cells that delimits the membranes and that enable the positioning of both the stable actomyosin ring and the cytokinetic ring is necessary to verify where the cytokinetic ring anchors.

Second, Seidel et al. have not shown that the cytokinetic ring enters in contact with the stable actomyosin ring in their study. In fact, their microscopy approach does not allow for the specific visualization of either the stable actomyosin rings or the cytokinetic ring, and the marking of actin used only displays germ cell membranes (Figure 5.2A). With this approach, they cannot visualize the stable actomyosin ring and that the ingression of a cytokinetic ring is oriented towards the rachis. It is therefore impossible to assess whether the cytokinetic ring is anchored to the stable actomyosin ring. However, my approach enabled the visualization of both actomyosin rings and membranes in the dividing PGCs. We found that there is a gap of fluorescence between the cytokinetic ring and the proto-rachis, indicating that the cytokinetic ring anchors in the membrane, beside the proto-rachis. It is only after the cytokinetic ring has finished its ingression that its fluorescence merges with that of the proto-rachis.

In addition, the ring bisection model proposes that during germ cell division, the stable actomyosin ring that connects the germ cell to the rachis adopts a “closed conformation” (Figure 5.2B). Because it was not possible to detect the presence of a whole in the membrane during cell division, the authors concluded that stable actomyosin rings reduce in size in a way that the germ cell is no longer connected to the rachis. To confirm these results, Seidel et al. have taken



advantage of DAO-5—which is nuclear during interphase and becomes cytoplasmic during interphase—to assess cytoplasmic exchange between the dividing germ cells and the rest of the gonad. No DAO-5 staining was found in the rachis or the cytoplasm of non-dividing cells, suggesting that the stable actomyosin ring is closed because there is no cytoplasmic exchange during germ cell division. However, DAO-5 is a large protein of about 100 kD that may not be able to transit through the stable actomyosin ring that reduces in size during germ cell division. In addition, DAO-5 is associated with RNA polymerase I activity. Whether it is cytoplasmic or nuclear, DAO-5 may remain in close contact with RNA polymerase I and it may therefore never be free in the cytoplasm, preventing it from transiting through stable actomyosin rings. Finally, although there is no evidence for this in *C. elegans*, transit through stable actomyosin rings may be regulated and selective. If this were the case, DAO-5 may be restricted within the germ cells. In contrast to Seidel and colleagues' findings, I show that the 25 kD fluorescent protein Dendra2 can transit from the dividing PGC to the rest of the syncytium, suggesting that there is cytoplasmic exchange and that the stable actomyosin rings remain open during germ cell division. In accordance to Seidel et al., I observe that the diameter of the stable actomyosin ring decreases during germ cell division (data not shown). The high temporal resolution that I needed to track the division of the germ cell impacted the pixel resolution of the images which also prevents me from visualizing the stable actomyosin ring of the dividing cell. Further work is needed to detect and confirm the presence of an open stable actomyosin ring during germ cell division. This could be achieved by an electron microscopy or an enhanced resolution confocal microscopy approach.

Finally, Seidel et al. did not use live imaging to track the division of the germ cells. Their technique relies on an arbitrary sequential alignment of germ cells dividing in different animals (Figure 5.2A). This approach is helpful to have an overview of how germ cells divide but it may mask one or multiple dynamic events that occur over the course of division. To understand the different events that lead to syncytium expansion it is essential to use both high time resolute and high resolute fluorescence detection techniques like live imaging and super resolution, respectively.

### 5.2.1 An oriented furrow ingression

Similarly to Seidel et al., I found that during germ cell division, the cytokinetic ring assembles perpendicularly to the rachis. This suggests that the division is oriented and that the germ cells are polarized. It is unknown what polarizes germ cell division in the *C. elegans* gonad, but many different players can act as polarizing cues in living tissues. For example, polarizing proteins such as PAR proteins are responsible for the positioning of the mitotic spindle in the first zygotic division in *C. elegans* as well as polarized epithelia (Goldstein and Macara, 2007; Pacquelet, 2017). Similar cues may also be implicated in the orientation of germ cell division in *C. elegans*, however no evidence has yet found the enrichment of polarity proteins within the germline. In addition, my preliminary results suggest that PAR proteins are not enriched within the L1 stage gonad (data not shown). Another known polarizing cue is the midbody. It has been previously proposed that during tissue luminogenesis and during the second embryonic *C. elegans* division, the midbody orients cell division (Pohl, 2017). This is consistent with the finding that the posterior polarity protein PAR-2 is specifically enriched in the midbody during the first *C. elegans* embryonic division (Pittman and Skop, 2012). Together these findings may suggest that the midbody contains polarity cues that would enable the orientation of mitotic spindle and subsequent cytokinetic ring assembly. Because actomyosin rings and midbodies are related structures, the stable actomyosin rings in the *C. elegans* syncytium may contain such polarity cues that orient germ cell division perpendicularly to the rachis. The stable actomyosin rings may restrict spindle assembly regulators away from the rachis and therefore promote a cell division that is perpendicular to the rachis.

Another striking feature that I observed in accordance with Seidel et al. is that furrow ingression is asymmetric during germ cell division both in adults and in L1 stage gonads. In germ cells, the cytokinetic furrow specifies in an apicobasal manner, then as cytokinesis proceeds, the cytokinetic ring forms a leading edge that closes the membrane from basal to apical and towards the rachis ((Seidel et al., 2018);Chapter 2). This phenomenon has been observed multiple times across metazoan cell division including in the *C. elegans* embryo (Maddox et al., 2007). During the first zygotic division, the asymmetry in furrow ingression is linked to an

accumulation of Anillin and septins at the leading edge (Maddox et al., 2007). The accumulation of Anillin and septins would promote localized contractility that would cause the asymmetry in the furrow ingression (Dorn et al., 2016; Maddox et al., 2007). Asymmetric division in fact mostly occurs in polarized tissues such as the vulval precursor cells, and epithelial gut cells in the embryo (Bai et al., 2020; Bourdages et al., 2014). As opposed to the first zygotic division, Anillin is not required for asymmetric cytokinesis in the vulval precursor cells and it is proposed that asymmetry is caused by the mechanical resistance by apical junction (Bourdages et al., 2014). This explanation is consistent with other studies that have found that in polarized tissues where tension is not uniformly distributed, mechanical forces will pull the cytokinetic ring in one direction (Guillot and Lecuit, 2013; Morais-de-Sa and Sunkel, 2013). A recent study has shown that Aurora B is enriched in midbodies that localize apically after asymmetric cytokinesis. Authors show that Aurora B is required for the formation and the maintenance of polarity in epithelial gut cells, which suggests an eventual role in asymmetric cytokinesis (Bai et al., 2020). Overall, asymmetric cytokinesis arises in different tissues and appears to be regulated in different manners. In the *C. elegans* dividing germ cells, there is no evidence of a specific spatial enrichment of actomyosin regulators (such as Anillin or septins) in the cytokinetic ring, suggesting that the asymmetry is regulated differently from the first zygotic division. In addition, Aurora B does not appear to be enriched in the *C. elegans* germline, and it is therefore unlikely to play a role in polarizing germ cells. However, every cell in the germline is polarized because they are apically connected to the rachis with a stable actomyosin ring. The stable actomyosin rings could potentially be the source of tension that promote cytokinesis asymmetry. Indeed, during division, the cytokinetic ring anchors on the membrane next to the rachis where the stable actomyosin ring already exerts tension on the membrane. The forces applied on the membrane by the constriction of the cytokinetic ring may deform more easily the membrane that is opposed to the rachis rather than the membrane that is already under tension next to the stable actomyosin ring.

### **5.2.2 Stabilizing the furrow**

How the ICBs stabilize from cytokinetic furrows during syncytium expansion in *C. elegans* remains unclear. One possibility is that the cytokinetic furrows are processed into a

midbody, and that abscission is blocked similarly to that in the mouse testis ICBs and in the *C. elegans* P<sub>4</sub> blastomere. The formation of midbodies is normally characterized by the departure and the localization of regulators at the cytokinetic furrows, like it is observed in the mouse testis ICBs where Anillin is absent in mature stable ICBs (Greenbaum *et al.*, 2007b). This hypothesis is unlikely because I do not observe any actomyosin regulator rearrangements at the cytokinetic furrow during the first division of the PGCs, or upon the formation of a new stable ring at the L1 stage. Indeed, the actomyosin regulators that are present in cytokinetic rings are the same that localize in stable actomyosin rings in the *C. elegans* germline.

A second possibility for syncytium expansion is that the cytokinetic furrows arrest before the formation of midbodies, as it is proposed to be the case in *Drosophila* ring canals. In the forming ring canals of the *Drosophila* egg chamber, the cytokinetic furrows arrest at the fusome, which suggest that the fusome may physically constrain the cytokinetic ring from further ingression. In *C. elegans*, there is no evidence of such a structure throughout the development of the germline, therefore physical constrains do not appear to be responsible for the arrest of the cytokinetic furrows. In addition, it was also proposed in *Drosophila* that the fusome was not responsible for the arrest of cytokinetic furrows in forming ring canals (deCuevas *et al.*, 1996). It was rather proposed that a negative regulation of the myosin activity was responsible for cytokinetic furrow arrest in the ring canals ((Ong *et al.*, 2010; Tan *et al.*, 2003); discussed in 1.4.4.1). This is consistent with the finding that myosin is tightly regulated by a balance of positive and negative myosin regulators that enables the stabilization of stable actomyosin rings forming the syncytium in the adult *C. elegans* germline ((Priti *et al.*, 2018); discussed in 1.6.2.1). The negative regulation of myosin during furrow ingression could also be responsible for the arrest of cytokinetic furrows in the *C. elegans* germline. This could be tested by verifying the presence of positive and negative regulators of myosin in dividing germ cells. A specific accumulation of myosin negative regulators at the cytokinetic furrows that coincides with the timing of the cytokinetic ring stabilization would suggest that the downregulation of the myosin activity is responsible for the formation of stable actomyosin rings in the *C. elegans* germline.

Finally, the stabilization of actomyosin ring in the *C. elegans* syncytium could also depend on the action of a specific germline regulator. This regulator would be responsible for the arrest of furrow ingression specifically in germ cells, like TEX14 is responsible for abscission blockage in the mouse testis. To date, only the non-conical Anillin ANI-2 has been found to be specifically localize to stable actomyosin ring in the *C. elegans* germline, but its depletion leads to the collapse of the stable actomyosin rings rather than complete cytokinesis (Amini et al., 2014; Goupil et al., 2017). This suggests that ANI-2 is one of the regulators required for the stability of the syncytial rings, but it is not specifically required to stop the ingression of the cytokinetic ring. Further work needs to address whether there is a specific regulator mediating the cytokinetic furrow arrest in the *C. elegans* germline. This could be done using a proximity labeling technique that could uncover all the interactors of an actomyosin regulator in the stable actomyosin rings.

### 5.3 Why be syncytial?

Syncytia are unique tissues that have the common characteristic of being polyploid. These structures arise in different biological contexts, but their function remains poorly understood. Indeed, our current knowledge does not provide a global understanding on the biological significance of syncytia, but we are beginning to uncover functions that are specific for each syncytial tissue. During normal development, one advantage I envision is polyploidy being a sort of shortcut to be more efficient at achieving a specific biological process. One example is the *Drosophila* embryo, where the nuclear division enables the rapid multiplication of nuclei (Blake-Hedges and Megraw, 2019; Foe and Alberts, 1983; Rabinowitz, 1941). Undergoing a whole cellular cycle with cytokinesis is more energy-consuming and slower than karyokinesis. Another example is megakaryocytes in which multinucleation enables the specific production of large quantities of proteins required for platelet production (Vainchenker and Raslova, 2020). These examples could be extended to other syncytial tissues like muscle fibers and osteoclasts, where multinucleation most likely confers an advantage for the function of these tissues.

In germlines, several advantages have also been proposed for the syncytial organization which appear to be common to most animals: synchronous cell division, and cytoplasmic exchange. Indeed, cytoplasmic exchange has been shown to enable synchronous cell division and to be essential for oocyte maturation in the *Drosophila* egg chamber, as well as for spermatocyte maturation in the mouse testis (Greenbaum et al., 2011; Haglund et al., 2011; Lu et al., 2017). A similar role has been proposed in the *C. elegans* adult germline where cytoplasmic exchange from the germ cells in the pachytene region would enable the transport of cytoplasmic components to the oocyte that are essential for its maturation, similarly to what is observed in the *Drosophila* egg chamber (Wolke et al., 2007). In addition, the finding that a consequent proportion of germ cells in the pachytene region undergo apoptosis strengthen the argument that these are used as nurse cells for the maturation of the oocyte (Andux and Ellis, 2008). However, in opposition with other syncytial germlines, the *C. elegans* germ cells do not appear to display any synchronous behaviours. Indeed, in the adult germline, the mitotic GSCs at the distal end do not undergo simultaneous cell division. This is also the case in L1 stage where the PGCs divide asynchronously

(Butuci 2015). It is surprising that germ cells in the *C. elegans* germline do not divide synchronously as we found that they remain connected to the rachis during their division (chapter 2). One explanation is that there is a regulation of the cytoplasmic components that go through the actomyosin rings and that cell cycle mitotic regulators are restricted within the germ cells. How the transit of cellular components through the stable actomyosin rings is regulated and controlled remains ambiguous and needs further investigation.

As discussed previously, the syncytial organization in the *C. elegans* germline arises during the end of embryogenesis, which is early in development compared to other animal germlines. Although there are a few clear explanations for the function of the syncytium in the adult germline, the reason why the organization of the syncytium is already set at the L1 stage is unclear. One possibility is that the syncytium carries out an important function for the germline during early development. Maybe the proliferative signals from the DTC would not be received efficiently by the germ cells if these were not syncytial. Therefore, in the absence of a syncytial architecture the germline would only proliferate at the very distal end where the cells are in direct contact with the DTC. Similarly, in absence of a syncytium, the signals that enable sex determination may not diffuse properly in the germline to differentiate the spermatozoa from the oocyte fate. Another possibility to explain why the syncytium arises soon after germ cell specification is developmental constraint. Indeed, it might be developmentally easier to form a syncytial structure when the germline contains only two germ cells rather than about a thousand. Indeed, it is hard to conceive how the rachis would be built in a gonad where the germ cells are not syncytial. The possibilities that the syncytium has a determined function or that it arises because of physical constraints during early development are not mutually exclusive. Further work is needed to understand why the syncytium in *C. elegans* arises at during late embryogenesis.

## 5.4 Concluding remarks

Syncytial cells are fascinating structures to me because they constitute an exception amongst the classical definition of eukaryotic cells and cell division. Initially, we most certainly were all taught that a cell contains a single nucleus and is delimited by its membrane, and that during cell division the cell duplicates its material and physically separates to give rise to two distinct cells. However, a syncytium is defined by several nuclei contained in a single pool of cytoplasm which is delimited by a continuous membrane. In addition, cell division within the syncytium does not lead to two physically separated daughter cells. Although syncytial tissues are still composed of cells that divide, the classical definitions for cell and cell division are not suitable to any syncytial tissue.

The work that I have achieved during my thesis is a grain of sand in the desert of understanding what syncytial tissues are. Although we are beginning to understand how syncytial germlines are formed, the mechanism of syncytium expansion in the *C. elegans* germline was unclear before my arrival in the Labbé laboratory. My work has provided a detailed characterisation of the syncytium primordium organization in the *C. elegans* first larval stage. We discovered that the fundamental organization of the syncytium in the first larval stage is identical to the adult gonad. In addition, my results uncovered the different events that underlie the initial expansion of the germline primordium during PGC division. Our findings support a model in which the cytokinetic ring stabilizes and integrates into the rachis to connect one of the daughter cells, while the other daughter cell is connected by the stabilized ring that connected the mother cell. Overall, my research points out that despite functional and organizational differences between germline syncytium, regulated incomplete cytokinesis is conserved in *C. elegans* like in all animal germlines. Further studies are necessary to characterize the regulatory network that leads to the formation of syncytia in animal germlines. This will eventually lead to a better understanding of why syncytia are conserved throughout all animal germlines.



## References

- Abdu, Y., Maniscalco, C., Heddleston, J.M., Chew, T.L., and Nance, J. (2016). Developmentally programmed germ cell remodelling by endodermal cell cannibalism. *Nat Cell Biol* *18*, 1302-1310. 10.1038/ncb3439.
- Abmayr, S.M., and Pavlath, G.K. (2012). Myoblast fusion: lessons from flies and mice. *Development* *139*, 641-656. 10.1242/dev.068353.
- Addi, C., Presle, A., Fremont, S., Cuvelier, F., Rocancourt, M., Milin, F., Schmutz, S., Chamot-Rooke, J., Douche, T., Duchateau, M., et al. (2020). The Flemmingsome reveals an ESCRT-to-membrane coupling via ALIX/syntenin/syndecan-4 required for completion of cytokinesis. *Nat Commun* *11*, 1941. 10.1038/s41467-020-15205-z.
- Ahuja, P., Perriard, E., Pedrazzini, T., Satoh, S., Perriard, J.C., and Ehler, E. (2007). Re-expression of proteins involved in cytokinesis during cardiac hypertrophy. *Exp Cell Res* *313*, 1270-1283. 10.1016/j.yexcr.2007.01.009.
- Airoldi, S.J., McLean, P.F., Shimada, Y., and Cooley, L. (2011). Intercellular protein movement in syncytial *Drosophila* follicle cells. *J Cell Sci* *124*, 4077-4086. 10.1242/jcs.090456.
- Alastalo, T.P., Lonnstrom, M., Leppa, S., Kaarniranta, K., Pelto-Huikko, M., Sistonen, L., and Parvinen, M. (1998). Stage-specific expression and cellular localization of the heat shock factor 2 isoforms in the rat seminiferous epithelium. *Exp Cell Res* *240*, 16-27. DOI 10.1006/excr.1997.3926.
- Amini, R., Goupil, E., Labella, S., Zetka, M., Maddox, A.S., Labbe, J.C., and Chartier, N.T. (2014). *C. elegans* Anillin proteins regulate intercellular bridge stability and germline syncytial organization. *J Cell Biol* *206*, 129-143. 10.1083/jcb.201310117.
- Anderson, E., and Huebner, E. (1968). Development of Oocyte and Its Accessory Cells of Polychaete *Diopatra Cuprea* (Bosc). *J Morphol* *126*, 163-&. DOI 10.1002/jmor.1051260203.
- Anderson, R., Copeland, T.K., Scholer, H., Heasman, J., and Wylie, C. (2000). The onset of germ cell migration in the mouse embryo. *Mech Dev* *91*, 61-68. 10.1016/s0925-4773(99)00271-3.
- Andux, S., and Ellis, R.E. (2008). Apoptosis maintains oocyte quality in aging *Caenorhabditis elegans* females. *PLoS Genet* *4*, e1000295. 10.1371/journal.pgen.1000295.
- Ara, T., Nakamura, Y., Egawa, T., Sugiyama, T., Abe, K., Kishimoto, T., Matsui, Y., and Nagasawa, T. (2003). Impaired colonization of the gonads by primordial germ cells in mice lacking a chemokine, stromal cell-derived factor-1 (SDF-1). *Proc Natl Acad Sci U S A* *100*, 5319-5323. 10.1073/pnas.0730719100.
- Aramaki, S., Hayashi, K., Kurimoto, K., Ohta, H., Yabuta, Y., Iwanari, H., Mochizuki, Y., Hamakubo, T., Kato, Y., Shirahige, K., and Saitou, M. (2013). A mesodermal factor, T, specifies mouse

- germ cell fate by directly activating germline determinants. *Dev Cell* 27, 516-529. 10.1016/j.devcel.2013.11.001.
- Arnold, J.M. (1974). Intercellular bridges in somatic cells: cytoplasmic continuity of blastoderm cells of *Loligo pealei*. *Differentiation* 2, 335-341. 10.1111/j.1432-0436.1974.tb00368.x.
- Asaoka, M., and Lin, H. (2004). Germline stem cells in the *Drosophila* ovary descend from pole cells in the anterior region of the embryonic gonad. *Development* 131, 5079-5089. 10.1242/dev.01391.
- Austin, J., and Kimble, J. (1987). *glp-1* is required in the germ line for regulation of the decision between mitosis and meiosis in *C. elegans*. *Cell* 51, 589-599. 10.1016/0092-8674(87)90128-0.
- Bai, X., Melesse, M., Sorensen Turpin, C.G., Sloan, D.E., Chen, C.Y., Wang, W.C., Lee, P.Y., Simmons, J.R., Nebenfuehr, B., Mitchell, D., et al. (2020). Aurora B functions at the apical surface after specialized cytokinesis during morphogenesis in *C. elegans*. *Development* 147. 10.1242/dev.181099.
- Baker, J., Theurkauf, W.E., and Schubiger, G. (1993). Dynamic Changes in Microtubule Configuration Correlate with Nuclear Migration in the Preblastoderm *Drosophila* Embryo. *Journal of Cell Biology* 122, 113-121. DOI 10.1083/jcb.122.1.113.
- Basant, A., and Glotzer, M. (2018). Spatiotemporal Regulation of RhoA during Cytokinesis. *Curr Biol* 28, R570-R580. 10.1016/j.cub.2018.03.045.
- Batchelder, C., Dunn, M.A., Choy, B., Suh, Y., Cassie, C., Shim, E.Y., Shin, T.H., Mello, C., Seydoux, G., and Blackwell, T.K. (1999). Transcriptional repression by the *Caenorhabditis elegans* germ-line protein PIE-1. *Gene Dev* 13, 202-212. DOI 10.1101/gad.13.2.202.
- Bauer, J., Poupart, V., Goupil, E., Nguyen, K.C.Q., Hall, D.H., and Labbe, J.C. (2021). The initial expansion of the *C. elegans* syncytial germ line is coupled to primordial germ cell cytokinesis incompleteness. *Development*. 10.1242/dev.199633.
- Bement, W.M., Benink, H.A., and von Dassow, G. (2005). A microtubule-dependent zone of active RhoA during cleavage plane specification. *J Cell Biol* 170, 91-101. 10.1083/jcb.200501131.
- Berger, S., Lattmann, E., Aegerter-Wilmsen, T., Hengartner, M., Hajnal, A., deMello, A., and Casadevall i Solvas, X. (2018). Long-term *C. elegans* immobilization enables high resolution developmental studies in vivo. *Lab Chip* 18, 1359-1368. 10.1039/c7lc01185g.
- Berger, S., Spiri, S., deMello, A., and Hajnal, A. (2021). Microfluidic-based imaging of complete *C. elegans* larval development. *Development*. 10.1242/dev.199674.
- Bersell, K., Arab, S., Haring, B., and Kuhn, B. (2009). Neuregulin1/ErbB4 signaling induces cardiomyocyte proliferation and repair of heart injury. *Cell* 138, 257-270. 10.1016/j.cell.2009.04.060.
- Bertho, S., Clapp, M., Banisch, T.U., Bandemer, J., Raz, E., and Marlow, F.L. (2021). Zebrafish *dazl* regulates cystogenesis and germline stem cell specification during the primordial germ cell to germline stem cell transition. *Development* 148. 10.1242/dev.187773.

- Bi, P., Ramirez-Martinez, A., Li, H., Cannavino, J., McAnally, J.R., Shelton, J.M., Sanchez-Ortiz, E., Bassel-Duby, R., and Olson, E.N. (2017). Control of muscle formation by the fusogenic micropeptide myomixer. *Science* 356, 323-327. 10.1126/science.aam9361.
- Blake-Hedges, C., and Megraw, T.L. (2019). Coordination of Embryogenesis by the Centrosome in *Drosophila melanogaster*. *Results Probl Cell Differ* 67, 277-321. 10.1007/978-3-030-23173-6\_12.
- Bolivar, J., Huynh, J.R., Lopez-Schier, H., Gonzalez, C., St Johnston, D., and Gonzalez-Reyes, A. (2001). Centrosome migration into the *Drosophila* oocyte is independent of BicD and egl, and of the organisation of the microtubule cytoskeleton. *Development* 128, 1889-1897.
- Bourdages, K.G., Lacroix, B., Dorn, J.F., Descovich, C.P., and Maddox, A.S. (2014). Quantitative analysis of cytokinesis in situ during *C. elegans* postembryonic development. *PLoS One* 9, e110689. 10.1371/journal.pone.0110689.
- Boyle, M., and Dinardo, S. (1995). Specification, Migration and Assembly of the Somatic-Cells of the *Drosophila* Gonad. *Development* 121, 1815-1825.
- Braun, R.E., Behringer, R.R., Peschon, J.J., Brinster, R.L., and Palmiter, R.D. (1989). Genetically haploid spermatids are phenotypically diploid. *Nature* 337, 373-376. 10.1038/337373a0.
- Brenner, J.L., and Schedl, T. (2016). Germline Stem Cell Differentiation Entails Regional Control of Cell Fate Regulator GLD-1 in *Caenorhabditis elegans*. *Genetics* 202, 1085-1103. 10.1534/genetics.115.185678.
- Brenner, S. (1974). The genetics of *Caenorhabditis elegans*. *Genetics* 77, 71-94.
- Bringmann, H., and Hyman, A.A. (2005). A cytokinesis furrow is positioned by two consecutive signals. *Nature* 436, 731-734. 10.1038/nature03823.
- Brown, E.H., and King, R.C. (1964). Studies on Events Resulting in Formation of Egg Chamber in *Drosophila Melanogaster*. *Growth* 28, 41-+.
- Buckingham, M., and Rigby, P.W. (2014). Gene regulatory networks and transcriptional mechanisms that control myogenesis. *Dev Cell* 28, 225-238. 10.1016/j.devcel.2013.12.020.
- Burgos, M.H., and Fawcett, D.W. (1955). Some Observations on Spermatogenesis in *Bufo-Arenarum Hensel* with the Electron Microscope. *Anatomical Record* 122, 468-469.
- Caldwell, K.A., and Handel, M.A. (1991). Protamine transcript sharing among postmeiotic spermatids. *Proc Natl Acad Sci U S A* 88, 2407-2411. 10.1073/pnas.88.6.2407.
- Calixto, A., Chelur, D., Topalidou, I., Chen, X., and Chalfie, M. (2010). Enhanced neuronal RNAi in *C. elegans* using SID-1. *Nat Methods* 7, 554-559. 10.1038/nmeth.1463.
- Calvert, J.G. (1990). Glossary of Atmospheric Chemistry Terms - (Recommendations 1990). *Pure Appl Chem* 62, 2167-2219. DOI 10.1351/pac199062112167.
- Campolo, F., Gori, M., Favaro, R., Nicolis, S., Pellegrini, M., Botti, F., Rossi, P., Jannini, E.A., and Dolci, S. (2013). Essential role of Sox2 for the establishment and maintenance of the germ cell line. *Stem Cells* 31, 1408-1421. 10.1002/stem.1392.

- Cao, L.G., and Wang, Y.L. (1996). Signals from the spindle midzone are required for the stimulation of cytokinesis in cultured epithelial cells. *Mol Biol Cell* 7, 225-232. 10.1091/mbc.7.2.225.
- Capalbo, L., Montembault, E., Takeda, T., Bassi, Z.I., Glover, D.M., and D'Avino, P.P. (2012). The chromosomal passenger complex controls the function of endosomal sorting complex required for transport-III Snf7 proteins during cytokinesis. *Open Biol* 2, 120070. 10.1098/rsob.120070.
- Carim, S.C., Kechad, A., and Hickson, G.R.X. (2020). Animal Cell Cytokinesis: The Rho-Dependent Actomyosin-Anilloseptin Contractile Ring as a Membrane Microdomain Gathering, Compressing, and Sorting Machine. *Front Cell Dev Biol* 8, 575226. 10.3389/fcell.2020.575226.
- Carlton, J.G., Agromayor, M., and Martin-Serrano, J. (2008). Differential requirements for Alix and ESCRT-III in cytokinesis and HIV-1 release. *Proc Natl Acad Sci U S A* 105, 10541-10546. 10.1073/pnas.0802008105.
- Carmena, M., Wheelock, M., Funabiki, H., and Earnshaw, W.C. (2012). The chromosomal passenger complex (CPC): from easy rider to the godfather of mitosis. *Nat Rev Mol Cell Biol* 13, 789-803. 10.1038/nrm3474.
- Cartwright, J., Jr., and Arnold, J.M. (1980). Intercellular bridges in the embryo of the Atlantic squid, *Loligo pealei*. I. Cytoplasmic continuity and tissue differentiation. *J Embryol Exp Morphol* 57, 3-24.
- Cartwright, J., Jr., and Arnold, J.M. (1981). Intercellular bridges in the embryo of the Atlantic squid, *Loligo pealei*. II: Formation of the bridge. *Cell Motil* 1, 455-468. 10.1002/cm.970010406.
- Casanueva, M.O., and Ferguson, E.L. (2004). Germline stem cell number in the *Drosophila* ovary is regulated by redundant mechanisms that control Dpp signaling. *Development* 131, 1881-1890. 10.1242/dev.01076.
- Chambers, I., Silva, J., Colby, D., Nichols, J., Nijmeijer, B., Robertson, M., Vrana, J., Jones, K., Grotewold, L., and Smith, A. (2007). Nanog safeguards pluripotency and mediates germline development. *Nature* 450, 1230-1234. 10.1038/nature06403.
- Chang, Y.C., Chen, Y.J., Wu, C.H., Wu, Y.C., Yen, T.C., and Ouyang, P. (2010). Characterization of centrosomal proteins Cep55 and pericentrin in intercellular bridges of mouse testes. *J Cell Biochem* 109, 1274-1285. 10.1002/jcb.22517.
- Chang, Y.C., Wu, C.H., Yen, T.C., and Ouyang, P. (2012). Centrosomal protein 55 (Cep55) stability is negatively regulated by p53 protein through Polo-like kinase 1 (Plk1). *J Biol Chem* 287, 4376-4385. 10.1074/jbc.M111.289108.
- Chen, L.Y., Willis, W.D., and Eddy, E.M. (2016). Targeting the Gdnf Gene in peritubular myoid cells disrupts undifferentiated spermatogonial cell development. *Proc Natl Acad Sci U S A* 113, 1829-1834. 10.1073/pnas.1517994113.
- Chihara, D., and Nance, J. (2012). An E-cadherin-mediated hitchhiking mechanism for *C. elegans* germ cell internalization during gastrulation. *Development* 139, 2547-2556. 10.1242/dev.079863.

- Cinalli, R.M., and Lehmann, R. (2013). A spindle-independent cleavage pathway controls germ cell formation in *Drosophila*. *Nat Cell Biol* *15*, 839-845. 10.1038/ncb2761.
- Clubb, F.J., Jr., and Bishop, S.P. (1984). Formation of binucleated myocardial cells in the neonatal rat. An index for growth hypertrophy. *Lab Invest* *50*, 571-577.
- Comai, G., and Tajbakhsh, S. (2014). Molecular and cellular regulation of skeletal myogenesis. *Curr Top Dev Biol* *110*, 1-73. 10.1016/B978-0-12-405943-6.00001-4.
- Compton, A.A., and Schwartz, O. (2017). They Might Be Giants: Does Syncytium Formation Sink or Spread HIV Infection? *PLoS Pathog* *13*, e1006099. 10.1371/journal.ppat.1006099.
- Connell, J.W., Lindon, C., Luzio, J.P., and Reid, E. (2009). Spastin couples microtubule severing to membrane traffic in completion of cytokinesis and secretion. *Traffic* *10*, 42-56. 10.1111/j.1600-0854.2008.00847.x.
- Consortium, C.e.S. (1998). Genome sequence of the nematode *C. elegans*: a platform for investigating biology. *Science* *282*, 2012-2018. 10.1126/science.282.5396.2012.
- Cooley, L. (1998). *Drosophila* ring canal growth requires Src and Tec kinases. *Cell* *93*, 913-915. 10.1016/s0092-8674(00)81196-4.
- Cooley, L., and Theurkauf, W.E. (1994). Cytoskeletal Functions during *Drosophila* Oogenesis. *Science* *266*, 590-596. DOI 10.1126/science.7939713.
- Corsi, A.K., Wightman, B., and Chalfie, M. (2015). A Transparent Window into Biology: A Primer on *Caenorhabditis elegans*. *Genetics* *200*, 387-407. 10.1534/genetics.115.176099.
- Cox, R.T., and Spradling, A.C. (2003). A Balbiani body and the fusome mediate mitochondrial inheritance during *Drosophila* oogenesis. *Development* *130*, 1579-1590. 10.1242/dev.00365.
- Crittenden, S.L., Bernstein, D.S., Bachorik, J.L., Thompson, B.E., Gallegos, M., Petcherski, A.G., Moulder, G., Barstead, R., Wickens, M., and Kimble, J. (2002). A conserved RNA-binding protein controls germline stem cells in *Caenorhabditis elegans*. *Nature* *417*, 660-663. 10.1038/nature754.
- Crittenden, S.L., Troemel, E.R., Evans, T.C., and Kimble, J. (1994). GLP-1 is localized to the mitotic region of the *C. elegans* germ line. *Development* *120*, 2901-2911.
- D'Agostino, I., Merritt, C., Chen, P.L., Seydoux, G., and Subramaniam, K. (2006). Translational repression restricts expression of the *C-elegans* Nanos homolog NOS-2 to the embryonic germline. *Developmental Biology* *292*, 244-252. 10.1016/j.ydbio.2005.11.046.
- D'Avino, P.P., Giansanti, M.G., and Petronczki, M. (2015). Cytokinesis in animal cells. *Cold Spring Harb Perspect Biol* *7*, a015834. 10.1101/cshperspect.a015834.
- D'Avino, P.P., Savoian, M.S., and Glover, D.M. (2005). Cleavage furrow formation and ingression during animal cytokinesis: a microtubule legacy. *J Cell Sci* *118*, 1549-1558. 10.1242/jcs.02335.
- Davies, T., Jordan, S.N., Chand, V., Sees, J.A., Laband, K., Carvalho, A.X., Shirasu-Hiza, M., Kovar, D.R., Dumont, J., and Canman, J.C. (2014). High-resolution temporal analysis reveals a

- functional timeline for the molecular regulation of cytokinesis. *Dev Cell* 30, 209-223. 10.1016/j.devcel.2014.05.009.
- Davis, J.C., Snyder, E.M., Hogarth, C.A., Small, C., and Griswold, M.D. (2013). Induction of spermatogenic synchrony by retinoic acid in neonatal mice. *Spermatogenesis* 3, e23180. 10.4161/spmg.23180.
- de Almeida Engler, J., and Gheysen, G. (2013). Nematode-induced endoreduplication in plant host cells: why and how? *Mol Plant Microbe Interact* 26, 17-24. 10.1094/MPMI-05-12-0128-CR.
- de Cuevas, M., Lilly, M.A., and Spradling, A.C. (1997). Germline cyst formation in *Drosophila*. *Annu Rev Genet* 31, 405-428. 10.1146/annurev.genet.31.1.405.
- de Cuevas, M., and Spradling, A.C. (1998). Morphogenesis of the *Drosophila* fusome and its implications for oocyte specification. *Development* 125, 2781-2789.
- de Nooij, J.C., Graber, K.H., and Hariharan, I.K. (2000). Expression of the cyclin-dependent kinase inhibitor Dacapo is regulated by cyclin E. *Mech Dev* 97, 73-83. 10.1016/S0925-4773(00)00435-4.
- de Rooij, D.G., and Griswold, M.D. (2012). Questions about spermatogonia posed and answered since 2000. *J Androl* 33, 1085-1095. 10.2164/jandrol.112.016832.
- Dechant, R., and Glotzer, M. (2003). Centrosome separation and central spindle assembly act in redundant pathways that regulate microtubule density and trigger cleavage furrow formation. *Dev Cell* 4, 333-344. 10.1016/S1534-5807(03)00057-1.
- deCuevas, M., Lee, J.K., and Spradling, A.C. (1996). alpha-spectrin is required for germline cell division and differentiation in the *Drosophila* ovary. *Development* 122, 3959-3968.
- Deneke, V.E., Puliafito, A., Krueger, D., Narla, A.V., De Simone, A., Primo, L., Vergassola, M., De Renzis, S., and Di Talia, S. (2019). Self-Organized Nuclear Positioning Synchronizes the Cell Cycle in *Drosophila* Embryos. *Cell* 177, 925-941 e917. 10.1016/j.cell.2019.03.007.
- Deng, S., Azevedo, M., and Baylies, M. (2017). Acting on identity: Myoblast fusion and the formation of the syncytial muscle fiber. *Semin Cell Dev Biol* 72, 45-55. 10.1016/j.semcdb.2017.10.033.
- di Pietro, F., and Bellaiche, Y. (2018). Actin Network Discussion during Mitotic Pseudo-Furrowing. *Developmental Cell* 45, 539-541. 10.1016/j.devcel.2018.05.018.
- Dickinson, D.J., Schwager, F., Pintard, L., Gotta, M., and Goldstein, B. (2017). A Single-Cell Biochemistry Approach Reveals PAR Complex Dynamics during Cell Polarization. *Dev Cell* 42, 416-434 e411. 10.1016/j.devcel.2017.07.024.
- Dodson, A.E., and Kennedy, S. (2020). Phase Separation in Germ Cells and Development. *Dev Cell* 55, 4-17. 10.1016/j.devcel.2020.09.004.
- Dodson, G.S., Guarnieri, D.J., and Simon, M.A. (1998). Src64 is required for ovarian ring canal morphogenesis during *Drosophila* oogenesis. *Development* 125, 2883-2892.

- Doherty, C.A., Diegmiller, R., Kapasiawala, M., Gavis, E.R., and Shvartsman, S.Y. (2021). Coupled oscillators coordinate collective germline growth. *Dev Cell* 56, 860-870 e868. 10.1016/j.devcel.2021.02.015.
- Dong, L., Cornaglia, M., Krishnamani, G., Zhang, J., Mouchiroud, L., Lehnert, T., Auwerx, J., and Gijs, M.A.M. (2018). Reversible and long-term immobilization in a hydrogel-microbead matrix for high-resolution imaging of *Caenorhabditis elegans* and other small organisms. *PLoS One* 13, e0193989. 10.1371/journal.pone.0193989.
- Dong, L., Cornaglia, M., Lehnert, T., and Gijs, M.A. (2016). Versatile size-dependent sorting of *C. elegans* nematodes and embryos using a tunable microfluidic filter structure. *Lab Chip* 16, 574-585. 10.1039/c5lc01328c.
- Dorn, J.F., Zhang, L., Phi, T.T., Lacroix, B., Maddox, P.S., Liu, J., and Maddox, A.S. (2016). A theoretical model of cytokinesis implicates feedback between membrane curvature and cytoskeletal organization in asymmetric cytokinetic furrowing. *Mol Biol Cell* 27, 1286-1299. 10.1091/mbc.E15-06-0374.
- Doyle, T.G., Wen, C., and Greenwald, I. (2000). SEL-8, a nuclear protein required for LIN-12 and GLP-1 signaling in *Caenorhabditis elegans*. *Proc Natl Acad Sci U S A* 97, 7877-7881. 10.1073/pnas.97.14.7877.
- Duffy, D.C., McDonald, J.C., Schueller, O.J., and Whitesides, G.M. (1998). Rapid Prototyping of Microfluidic Systems in Poly(dimethylsiloxane). *Anal Chem* 70, 4974-4984. 10.1021/ac980656z.
- Dym, M., and Fawcett, D.W. (1971). Further Observations on Numbers of Spermatogonia, Spermatocytes, and Spermatids Connected by Intercellular Bridges in Mammalian Testis. *Biology of Reproduction* 4, 195-&. DOI 10.1093/biolreprod/4.2.195.
- Eddy, E.M. (1975). Germ plasm and the differentiation of the germ cell line. *Int Rev Cytol* 43, 229-280. 10.1016/s0074-7696(08)60070-4.
- El Amine, N., Kechad, A., Jananji, S., and Hickson, G.R. (2013). Opposing actions of septins and Sticky on Anillin promote the transition from contractile to midbody ring. *J Cell Biol* 203, 487-504. 10.1083/jcb.201305053.
- El-Amine, N., Carim, S.C., Wernike, D., and Hickson, G.R.X. (2019). Rho-dependent control of the Citron kinase, Sticky, drives midbody ring maturation. *Mol Biol Cell* 30, 2185-2204. 10.1091/mbc.E19-04-0194.
- Ellis, H.M., and Horvitz, H.R. (1986). Genetic control of programmed cell death in the nematode *C. elegans*. *Cell* 44, 817-829. 10.1016/0092-8674(86)90004-8.
- Engel, F.B., Schebesta, M., and Keating, M.T. (2006). Anillin localization defect in cardiomyocyte binucleation. *J Mol Cell Cardiol* 41, 601-612. 10.1016/j.yjmcc.2006.06.012.
- Ernst, C., Eling, N., Martinez-Jimenez, C.P., Marioni, J.C., and Odom, D.T. (2019). Staged developmental mapping and X chromosome transcriptional dynamics during mouse spermatogenesis. *Nat Commun* 10, 1251. 10.1038/s41467-019-09182-1.

- Extavour, C.G., and Akam, M. (2003). Mechanisms of germ cell specification across the metazoans: epigenesis and preformation. *Development* 130, 5869-5884. 10.1242/dev.00804.
- Fang-Yen, C., Gabel, C.V., Samuel, A.D., Bargmann, C.I., and Avery, L. (2012). Laser microsurgery in *Caenorhabditis elegans*. *Methods Cell Biol* 107, 177-206. 10.1016/B978-0-12-394620-1.00006-0.
- Fawcett, D.W. (1950). Bilateral ovarian teratomas in a mouse. *Cancer Res* 10, 705-707.
- Fawcett, D.W. (1961). Intercellular bridges. *Exp Cell Res Suppl* 8, 174-187. 10.1016/0014-4827(61)90347-0.
- Fawcett, D.W. (1970). A comparative view of sperm ultrastructure. *Biol Reprod* 2, Suppl 2:90-127.
- Fawcett, D.W. (1973). Observations on the organization of the interstitial tissue of the testis and on the occluding cell junctions in the seminiferous epithelium. *Adv Biosci* 10, 83-99.
- Fawcett, D.W., Ito, S., and Slautterback, D. (1959). The occurrence of intercellular bridges in groups of cells exhibiting synchronous differentiation. *J Biophys Biochem Cytol* 5, 453-460. 10.1083/jcb.5.3.453.
- Feinberg, E.H., and Hunter, C.P. (2003). Transport of dsRNA into cells by the transmembrane protein SID-1. *Science* 301, 1545-1547. 10.1126/science.1087117.
- Fire, A., Xu, S., Montgomery, M.K., Kostas, S.A., Driver, S.E., and Mello, C.C. (1998). Potent and specific genetic interference by double-stranded RNA in *Caenorhabditis elegans*. *Nature* 391, 806-811. 10.1038/35888.
- Flora, P., McCarthy, A., Upadhyay, M., and Rangan, P. (2017). Role of Chromatin Modifications in *Drosophila* Germline Stem Cell Differentiation. *Results Probl Cell Differ* 59, 1-30. 10.1007/978-3-319-44820-6\_1.
- Foe, V.E., and Alberts, B.M. (1983). Studies of nuclear and cytoplasmic behaviour during the five mitotic cycles that precede gastrulation in *Drosophila* embryogenesis. *J Cell Sci* 61, 31-70.
- Foor, W.E. (1967). Ultrastructural Aspects of Oocyte Development and Shell Formation in *Ascaris Lumbricoides*. *J Parasitol* 53, 1245-+. Doi 10.2307/3276689.
- Fremont, S., and Echard, A. (2018). Membrane Traffic in the Late Steps of Cytokinesis. *Curr Biol* 28, R458-R470. 10.1016/j.cub.2018.01.019.
- Fukuyama, M., Rougvie, A.E., and Rothman, J.H. (2006). *C. elegans* DAF-18/PTEN mediates nutrient-dependent arrest of cell cycle and growth in the germline. *Curr Biol* 16, 773-779. 10.1016/j.cub.2006.02.073.
- Gan, P., Patterson, M., and Sucov, H.M. (2020). Cardiomyocyte Polyploidy and Implications for Heart Regeneration. *Annu Rev Physiol* 82, 45-61. 10.1146/annurev-physiol-021119-034618.
- Gandarillas, A., Molinuevo, R., and Sanz-Gomez, N. (2018). Mammalian endoreplication emerges to reveal a potential developmental timer. *Cell Death Differ* 25, 471-476. 10.1038/s41418-017-0040-0.



- Gao, Y., Mao, Y., Xu, R.G., Zhu, R., Zhang, M., Sun, J., Shen, D., Peng, P., Xie, T., and Ni, J.Q. (2019). Defining gene networks controlling the maintenance and function of the differentiation niche by an in vivo systematic RNAi screen. *J Genet Genomics* 46, 19-30. 10.1016/j.jgg.2018.10.008.
- Gao, Y., Smith, E., Ker, E., Campbell, P., Cheng, E.C., Zou, S., Lin, S., Wang, L., Halene, S., and Krause, D.S. (2012). Role of RhoA-specific guanine exchange factors in regulation of endomitosis in megakaryocytes. *Dev Cell* 22, 573-584. 10.1016/j.devcel.2011.12.019.
- Geddis, A.E., Fox, N.E., Tkachenko, E., and Kaushansky, K. (2007). Endomitotic megakaryocytes that form a bipolar spindle exhibit cleavage furrow ingression followed by furrow regression. *Cell Cycle* 6, 455-460. 10.4161/cc.6.4.3836.
- Geddis, A.E., and Kaushansky, K. (2006). Endomitotic megakaryocytes form a midzone in anaphase but have a deficiency in cleavage furrow formation. *Cell Cycle* 5, 538-545. 10.4161/cc.5.5.2537.
- Gentric, G., and Desdouets, C. (2014). Polyploidization in liver tissue. *Am J Pathol* 184, 322-331. 10.1016/j.ajpath.2013.06.035.
- Gerdes, J.A., Mannix, K.M., Hudson, A.M., and Cooley, L. (2020). HtsRC-Mediated Accumulation of F-Actin Regulates Ring Canal Size During *Drosophila melanogaster* Oogenesis. *Genetics* 216, 717-734. 10.1534/genetics.120.303629.
- Gerhold, A.R., Poupart, V., Labbe, J.C., and Maddox, P.S. (2018). Spindle assembly checkpoint strength is linked to cell fate in the *Caenorhabditis elegans* embryo. *Mol Biol Cell* 29, 1435-1448. 10.1091/mbc.E18-04-0215.
- Ghosh, D., and Seydoux, G. (2008). Inhibition of transcription by the *Caenorhabditis elegans* germline protein PIE-1: Genetic evidence for distinct mechanisms targeting initiation and elongation. *Genetics* 178, 235-243. 10.1534/genetics.107.083212.
- Gilboa, L. (2015). Organizing stem cell units in the *Drosophila* ovary. *Curr Opin Genet Dev* 32, 31-36. 10.1016/j.gde.2015.01.005.
- Giorgi, F. (1978). Intercellular bridges in ovarian follicle cells of *Drosophila melanogaster*. *Cell Tissue Res* 186, 413-422. 10.1007/BF00224931.
- Glotzer, M. (2004). Cleavage furrow positioning. *J Cell Biol* 164, 347-351. 10.1083/jcb.200310112.
- Glotzer, M. (2017). Cytokinesis in Metazoa and Fungi. *Cold Spring Harb Perspect Biol* 9. 10.1101/cshperspect.a022343.
- Goldstein, B., and Macara, I.G. (2007). The PAR proteins: fundamental players in animal cell polarization. *Dev Cell* 13, 609-622. 10.1016/j.devcel.2007.10.007.
- Gomperts, M., Garcia-Castro, M., Wylie, C., and Heasman, J. (1994). Interactions between primordial germ cells play a role in their migration in mouse embryos. *Development* 120, 135-141.
- Gondos, B., and Conner, L.A. (1973). Ultrastructure of Developing Germ-Cells in Fetal Rabbit Testis. *Am J Anat* 136, 23-41. DOI 10.1002/aja.1001360104.

- Gonzalez-Rosa, J.M., Sharpe, M., Field, D., Soonpaa, M.H., Field, L.J., Burns, C.E., and Burns, C.G. (2018). Myocardial Polyploidization Creates a Barrier to Heart Regeneration in Zebrafish. *Dev Cell* 44, 433-446 e437. 10.1016/j.devcel.2018.01.021.
- Gordon, K.L., Payne, S.G., Linden-High, L.M., Pani, A.M., Goldstein, B., Hubbard, E.J.A., and Sherwood, D.R. (2019). Ectopic Germ Cells Can Induce Niche-like Enwrapment by Neighboring Body Wall Muscle. *Curr Biol* 29, 823-833 e825. 10.1016/j.cub.2019.01.056.
- Goupil, E., Amini, R., Hall, D.H., and Labbe, J.C. (2017). Actomyosin contractility regulators stabilize the cytoplasmic bridge between the two primordial germ cells during *Caenorhabditis elegans* embryogenesis. *Mol Biol Cell* 28, 3789-3800. 10.1091/mbc.E17-08-0502.
- Green, R.A., Kao, H.L., Audhya, A., Arur, S., Mayers, J.R., Fridolfsson, H.N., Schulman, M., Schloissnig, S., Niessen, S., Laband, K., et al. (2011). A high-resolution *C. elegans* essential gene network based on phenotypic profiling of a complex tissue. *Cell* 145, 470-482. 10.1016/j.cell.2011.03.037.
- Green, R.A., Mayers, J.R., Wang, S., Lewellyn, L., Desai, A., Audhya, A., and Oegema, K. (2013). The midbody ring scaffolds the abscission machinery in the absence of midbody microtubules. *J Cell Biol* 203, 505-520. 10.1083/jcb.201306036.
- Green, R.A., Paluch, E., and Oegema, K. (2012). Cytokinesis in animal cells. *Annu Rev Cell Dev Biol* 28, 29-58. 10.1146/annurev-cellbio-101011-155718.
- Greenbaum, M.P., Iwamori, N., Agno, J.E., and Matzuk, M.M. (2009). Mouse TEX14 Is Required for Embryonic Germ Cell Intercellular Bridges but Not Female Fertility. *Biology of Reproduction* 80, 449-457. 10.1095/biolreprod.108.070649.
- Greenbaum, M.P., Iwamori, T., Buchold, G.M., and Matzuk, M.M. (2011). Germ cell intercellular bridges. *Cold Spring Harb Perspect Biol* 3, a005850. 10.1101/cshperspect.a005850.
- Greenbaum, M.P., Ma, L., and Matzuk, M.M. (2007a). Conversion of midbodies into germ cell intercellular bridges. *Developmental Biology* 305, 389-396. 10.1016/j.ydbio.2007.02.025.
- Greenbaum, M.P., Ma, L., and Matzuk, M.M. (2007b). Conversion of midbodies into germ cell intercellular bridges. *Dev Biol* 305, 389-396. 10.1016/j.ydbio.2007.02.025.
- Greenbaum, M.P., Yan, W., Wu, M.H., Lin, Y.N., Agno, J.E., Sharma, M., Braun, R.E., Rajkovic, A., and Matzuk, M.M. (2006). TEX14 is essential for intercellular bridges and fertility in male mice. *P Natl Acad Sci USA* 103, 4982-4987. 10.1073/pnas.0505123103.
- Griffin, E.E., Odde, D.J., and Seydoux, G. (2011). Regulation of the MEX-5 gradient by a spatially segregated kinase/phosphatase cycle. *Cell* 146, 955-968. 10.1016/j.cell.2011.08.012.
- Griswold, M.D. (2016). Spermatogenesis: The Commitment to Meiosis. *Physiol Rev* 96, 1-17. 10.1152/physrev.00013.2015.
- Guarnieri, D.J., Dodson, G.S., and Simon, M.A. (1998). SRC64 regulates the localization of a Tec-family kinase required for *Drosophila* ring canal growth. *Mol Cell* 1, 831-840. 10.1016/s1097-2765(00)80082-9.

- Gubieda, A.G., Packer, J.R., Squires, I., Martin, J., and Rodriguez, J. (2020). Going with the flow: insights from *Caenorhabditis elegans* zygote polarization. *Philos T R Soc B* 375. ARTN 20190555  
10.1098/rstb.2019.0555.
- Guillot, C., and Lecuit, T. (2013). Adhesion disengagement uncouples intrinsic and extrinsic forces to drive cytokinesis in epithelial tissues. *Dev Cell* 24, 227-241. 10.1016/j.devcel.2013.01.010.
- Guizetti, J., Schermelleh, L., Mantler, J., Maar, S., Poser, I., Leonhardt, H., Muller-Reichert, T., and Gerlich, D.W. (2011). Cortical constriction during abscission involves helices of ESCRT-III-dependent filaments. *Science* 331, 1616-1620. 10.1126/science.1201847.
- Guse, A., Mishima, M., and Glotzer, M. (2005). Phosphorylation of ZEN-4/MKLP1 by aurora B regulates completion of cytokinesis. *Curr Biol* 15, 778-786. 10.1016/j.cub.2005.03.041.
- Guttman, J.A., Mulholland, D.J., and Vogl, A.W. (1998). Plectin is concentrated at intercellular junctions and at the nuclear surface in morphologically differentiated rat Sertoli cells. *Molecular Biology of the Cell* 9, 67a-67a.
- Guyen-Ozkan, T., Nishi, Y., Robertson, S.M., and Lin, R.L. (2008). Global transcriptional repression in *C.elegans* germline precursors by regulated sequestration of TAF-4. *Cell* 135, 149-160. 10.1016/j.cell.2008.07.040.
- Haglund, K., Nezis, I.P., Lemus, D., Grabbe, C., Wesche, J., Liestol, K., Dikic, I., Palmer, R., and Stenmark, H. (2010). Cindr interacts with anillin to control cytokinesis in *Drosophila melanogaster*. *Curr Biol* 20, 944-950. 10.1016/j.cub.2010.03.068.
- Haglund, K., Nezis, I.P., and Stenmark, H. (2011). Structure and functions of stable intercellular bridges formed by incomplete cytokinesis during development. *Commun Integr Biol* 4, 1-9. 10.4161/cib.4.1.13550.
- Hall, C.R. (1855). On the Mode of Development of Tubercle in the Lungs in Chronic Phthisis: Its Connexion with Fatty Degeneration of the Epithelium of the Air-Vesicles, and Its Early Manifestation by Fatty Epithelial Cells in the Sputa. *Br Foreign Med Chir Rev* 15, 477-501.
- Hall, D.H., Winfrey, V.P., Blaeuer, G., Hoffman, L.H., Furuta, T., Rose, K.L., Hobert, O., and Greenstein, D. (1999). Ultrastructural features of the adult hermaphrodite gonad of *Caenorhabditis elegans*: relations between the germ line and soma. *Dev Biol* 212, 101-123. 10.1006/dbio.1999.9356.
- Hamada-Kawaguchi, N., Nishida, Y., and Yamamoto, D. (2015). Btk29A-mediated tyrosine phosphorylation of armadillo/beta-catenin promotes ring canal growth in *Drosophila* oogenesis. *PLoS One* 10, e0121484. 10.1371/journal.pone.0121484.
- Hanley, N.A., Hagan, D.M., Clement-Jones, M., Ball, S.G., Strachan, T., Salas-Cortes, L., McElreavey, K., Lindsay, S., Robson, S., Bullen, P., et al. (2000). SRY, SOX9, and DAX1 expression patterns during human sex determination and gonadal development. *Mech Dev* 91, 403-407. 10.1016/s0925-4773(99)00307-x.

- Hansen, D., Wilson-Berry, L., Dang, T., and Schedl, T. (2004). Control of the proliferation versus meiotic development decision in the *C. elegans* germline through regulation of GLD-1 protein accumulation. *Development* *131*, 93-104. 10.1242/dev.00916.
- Hara, K., Nakagawa, T., Enomoto, H., Suzuki, M., Yamamoto, M., Simons, B.D., and Yoshida, S. (2014). Mouse spermatogenic stem cells continually interconvert between equipotent singly isolated and syncytial states. *Cell Stem Cell* *14*, 658-672. 10.1016/j.stem.2014.01.019.
- Hatanaka, K., and Okada, M. (1991). Mutations Affecting Embryonic F-Actin Reorganization Also Affect Separation of Nuclei from Their Sisters and from the Cortex in *Drosophila* Cleavage Embryos. *Dev Growth Differ* *33*, 535-542.
- Haubert, K., Drier, T., and Beebe, D. (2006). PDMS bonding by means of a portable, low-cost corona system. *Lab Chip* *6*, 1548-1549. 10.1039/b610567j.
- Heim, A., Rymarczyk, B., and Mayer, T.U. (2017). Regulation of Cell Division. *Adv Exp Med Biol* *953*, 83-116. 10.1007/978-3-319-46095-6\_3.
- Hektoen, L. (1898). The Fate of the Giant Cells in Healing Tuberculous Tissue, as Observed in a Case of Healing Tuberculous Meningitis. *J Exp Med* *3*, 21-52.
- Henderson, S.T., Gao, D., Lambie, E.J., and Kimble, J. (1994). lag-2 may encode a signaling ligand for the GLP-1 and LIN-12 receptors of *C. elegans*. *Development* *120*, 2913-2924.
- Heppert, J.K., Dickinson, D.J., Pani, A.M., Higgins, C.D., Steward, A., Ahringer, J., Kuhn, J.R., and Goldstein, B. (2016). Comparative assessment of fluorescent proteins for in vivo imaging in an animal model system. *Mol Biol Cell* *27*, 3385-3394. 10.1091/mbc.E16-01-0063.
- Hernandez, J.M., and Podbilewicz, B. (2017). The hallmarks of cell-cell fusion. *Development* *144*, 4481-4495. 10.1242/dev.155523.
- Hindi, S.M., Tajrishi, M.M., and Kumar, A. (2013). Signaling mechanisms in mammalian myoblast fusion. *Sci Signal* *6*, re2. 10.1126/scisignal.2003832.
- Hinnant, T.D., Merkle, J.A., and Ables, E.T. (2020). Coordinating Proliferation, Polarity, and Cell Fate in the *Drosophila* Female Germline. *Front Cell Dev Biol* *8*, 19. 10.3389/fcell.2020.00019.
- Hirsh, D., Oppenheim, D., and Klass, M. (1976). Development of the reproductive system of *Caenorhabditis elegans*. *Dev Biol* *49*, 200-219. 10.1016/0012-1606(76)90267-0.
- Hu, C.K., Coughlin, M., and Mitchison, T.J. (2012). Midbody assembly and its regulation during cytokinesis. *Mol Biol Cell* *23*, 1024-1034. 10.1091/mbc.E11-08-0721.
- Hubbard, E.J., and Greenstein, D. (2000). The *Caenorhabditis elegans* gonad: a test tube for cell and developmental biology. *Dev Dyn* *218*, 2-22. 10.1002/(SICI)1097-0177(200005)218:1<2::AID-DVDY2>3.0.CO;2-W.
- Hubbard, E.J., and Greenstein, D. (2005). Introduction to the germ line. *WormBook*, 1-4. 10.1895/wormbook.1.18.1.

- Hubbard, E.J.A., and Schedl, T. (2019). Biology of the *Caenorhabditis elegans* Germline Stem Cell System. *Genetics* *213*, 1145-1188. 10.1534/genetics.119.300238.
- Hudson, A.M., and Cooley, L. (2002). A subset of dynamic actin rearrangements in *Drosophila* requires the Arp2/3 complex. *J Cell Biol* *156*, 677-687. 10.1083/jcb.200109065.
- Hudson, A.M., and Cooley, L. (2010). *Drosophila* Kelch functions with Cullin-3 to organize the ring canal actin cytoskeleton. *J Cell Biol* *188*, 29-37. 10.1083/jcb.200909017.
- Hudson, A.M., Mannix, K.M., and Cooley, L. (2015). Actin Cytoskeletal Organization in *Drosophila* Germline Ring Canals Depends on Kelch Function in a Cullin-RING E3 Ligase. *Genetics* *201*, 1117-1131. 10.1534/genetics.115.181289.
- Hudson, A.M., Mannix, K.M., Gerdes, J.A., Kottemann, M.C., and Cooley, L. (2019). Targeted substrate degradation by Kelch controls the actin cytoskeleton during ring canal expansion. *Development* *146*. 10.1242/dev.169219.
- Hughes, S.E., Miller, D.E., Miller, A.L., and Hawley, R.S. (2018). Female Meiosis: Synapsis, Recombination, and Segregation in *Drosophila melanogaster*. *Genetics* *208*, 875-908. 10.1534/genetics.117.300081.
- Hutterer, A., Glotzer, M., and Mishima, M. (2009). Clustering of centralspindlin is essential for its accumulation to the central spindle and the midbody. *Curr Biol* *19*, 2043-2049. 10.1016/j.cub.2009.10.050.
- Huynh, J.R., and St Johnston, D. (2004). The origin of asymmetry: early polarisation of the *Drosophila* germline cyst and oocyte. *Curr Biol* *14*, R438-449. 10.1016/j.cub.2004.05.040.
- Ikami, K., Nuzhat, N., Abbott, H., Pandoy, R., Haky, L., Spradling, A.C., Tanner, H., and Lei, L. (2021). Altered germline cyst formation and oogenesis in *Tex14* mutant mice. *Biol Open* *10*. 10.1242/bio.058807.
- Illmensee, K., and Mahowald, A.P. (1974). Transplantation of posterior polar plasm in *Drosophila*. Induction of germ cells at the anterior pole of the egg. *Proc Natl Acad Sci U S A* *71*, 1016-1020. 10.1073/pnas.71.4.1016.
- Iwamori, T., Iwamori, N., Ma, L., Edson, M., Greenbaum, M., and Matzuk, M. (2010a). Analysis of Intercellular Bridge Proteins. *Journal of Andrology*, 52-52.
- Iwamori, T., Iwamori, N., Ma, L., Edson, M.A., Greenbaum, M.P., and Matzuk, M.M. (2010b). *TEX14* interacts with *CEP55* to block cell abscission. *Mol Cell Biol* *30*, 2280-2292. 10.1128/MCB.01392-09.
- Iwamori, T., Iwamori, N., Matsumoto, M., Imai, H., and Ono, E. (2020). Novel localizations and interactions of intercellular bridge proteins revealed by proteomic profiling dagger. *Biol Reprod* *102*, 1134-1144. 10.1093/biolre/iaaa017.
- Iwamori, T., Lin, Y.N., Ma, L., Iwamori, N., and Matzuk, M.M. (2011). Identification and Characterization of *RBM44* as a Novel Intercellular Bridge Protein. *Plos One* *6*. ARTN e17066  
10.1371/journal.pone.0017066.

- Jadhav, S., Rana, M., and Subramaniam, K. (2008). Multiple maternal proteins coordinate to restrict the translation of *C. elegans* nanos-2 to primordial germ cells. *Development* *135*, 1803-1812. 10.1242/dev.013656.
- Jantsch-Plunger, V., Gonczy, P., Romano, A., Schnabel, H., Hamill, D., Schnabel, R., Hyman, A.A., and Glotzer, M. (2000). CYK-4: A Rho family gtpase activating protein (GAP) required for central spindle formation and cytokinesis. *J Cell Biol* *149*, 1391-1404. 10.1083/jcb.149.7.1391.
- Johnson, K.J., Zecevic, A., and Kwon, E.J. (2004). Protocadherin alpha 3 acts at sites distinct from classic cadherins in rat testis and sperm. *Biology of Reproduction* *70*, 303-312. 10.1095/biolreprod.103.021758.
- Jordan, S.N., and Canman, J.C. (2012). Rho GTPases in animal cell cytokinesis: an occupation by the one percent. *Cytoskeleton (Hoboken)* *69*, 919-930. 10.1002/cm.21071.
- Kachur, T.M., Audhya, A., and Pilgrim, D.B. (2008). UNC-45 is required for NMY-2 contractile function in early embryonic polarity establishment and germline cellularization in *C. elegans*. *Dev Biol* *314*, 287-299. 10.1016/j.ydbio.2007.11.028.
- Kalkan, T., Bornelov, S., Mulas, C., Diamanti, E., Lohoff, T., Ralser, M., Middelkamp, S., Lombard, P., Nichols, J., and Smith, A. (2019). Complementary Activity of ETV5, RBPJ, and TCF3 Drives Formative Transition from Naive Pluripotency. *Cell Stem Cell* *24*, 785-801 e787. 10.1016/j.stem.2019.03.017.
- Kamili, F., and Lu, H. (2018). Recent Advances and Trends in Microfluidic Platforms for *C. elegans* Biological Assays. *Annu Rev Anal Chem (Palo Alto Calif)* *11*, 245-264. 10.1146/annurev-anchem-061417-125604.
- Karasmanis, E.P., Hwang, D., Nakos, K., Bowen, J.R., Angelis, D., and Spiliotis, E.T. (2019). A Septin Double Ring Controls the Spatiotemporal Organization of the ESCRT Machinery in Cytokinetic Abscission. *Curr Biol* *29*, 2174-2182 e2177. 10.1016/j.cub.2019.05.050.
- Kato, A., Nagata, Y., and Todokoro, K. (2004). delta-Tubulin is a component of intercellular bridges and both the early and mature perinuclear rings during spermatogenesis. *Developmental Biology* *269*, 196-205. 10.1016/j.ydbio.2004.01.026.
- Kaufman, R.S., Price, K.L., Mannix, K.M., Ayers, K.M., Hudson, A.M., and Cooley, L. (2020). *Drosophila* sperm development and intercellular cytoplasm sharing through ring canals do not require an intact fusome. *Development* *147*. 10.1242/dev.190140.
- Kechad, A., Jananji, S., Ruella, Y., and Hickson, G.R. (2012). Anillin acts as a bifunctional linker coordinating midbody ring biogenesis during cytokinesis. *Curr Biol* *22*, 197-203. 10.1016/j.cub.2011.11.062.
- Kehler, J., Tolkunova, E., Koschorz, B., Pesce, M., Gentile, L., Boiani, M., Lomeli, H., Nagy, A., McLaughlin, K.J., Scholer, H.R., and Tomilin, A. (2004). Oct4 is required for primordial germ cell survival. *EMBO Rep* *5*, 1078-1083. 10.1038/sj.embor.7400279.

- Keil, W., Kutscher, L.M., Shaham, S., and Siggia, E.D. (2017). Long-Term High-Resolution Imaging of Developing *C. elegans* Larvae with Microfluidics. *Dev Cell* *40*, 202-214. 10.1016/j.devcel.2016.11.022.
- Kelso, R.J., Hudson, A.M., and Cooley, L. (2002). *Drosophila* Kelch regulates actin organization via Src64-dependent tyrosine phosphorylation. *J Cell Biol* *156*, 703-713. 10.1083/jcb.200110063.
- Kershner, A., Crittenden, S.L., Friend, K., Sorensen, E.B., Porter, D.F., and Kimble, J. (2013). Germline stem cells and their regulation in the nematode *Caenorhabditis elegans*. *Adv Exp Med Biol* *786*, 29-46. 10.1007/978-94-007-6621-1\_3.
- Kershner, A.M., Shin, H., Hansen, T.J., and Kimble, J. (2014). Discovery of two GLP-1/Notch target genes that account for the role of GLP-1/Notch signaling in stem cell maintenance. *Proc Natl Acad Sci U S A* *111*, 3739-3744. 10.1073/pnas.1401861111.
- Kim, E., Sun, L., Gabel, C.V., and Fang-Yen, C. (2013). Long-term imaging of *Caenorhabditis elegans* using nanoparticle-mediated immobilization. *PLoS One* *8*, e53419. 10.1371/journal.pone.0053419.
- Kim, H., Johnson, J.M., Lera, R.F., Brahma, S., and Burkard, M.E. (2017). Anillin Phosphorylation Controls Timely Membrane Association and Successful Cytokinesis. *PLoS Genet* *13*, e1006511. 10.1371/journal.pgen.1006511.
- Kim, H.J., Yoon, J., Matsuura, A., Na, J.H., Lee, W.K., Kim, H., Choi, J.W., Park, J.E., Park, S.J., Kim, K.T., et al. (2015). Structural and biochemical insights into the role of testis-expressed gene 14 (TEX14) in forming the stable intercellular bridges of germ cells. *Proc Natl Acad Sci U S A* *112*, 12372-12377. 10.1073/pnas.1418606112.
- Kimble, J., and Crittenden, S.L. (2007). Controls of germline stem cells, entry into meiosis, and the sperm/oocyte decision in *Caenorhabditis elegans*. *Annu Rev Cell Dev Biol* *23*, 405-433. 10.1146/annurev.cellbio.23.090506.123326.
- Kimble, J., and Hirsh, D. (1979). Post-Embryonic Cell Lineages of the Hermaphrodite and Male Gonads in *Caenorhabditis-Elegans*. *Developmental Biology* *70*, 396-417. Doi 10.1016/0012-1606(79)90035-6.
- Kimble, J.E., and White, J.G. (1981). On the Control of Germ-Cell Development in *Caenorhabditis-Elegans*. *Developmental Biology* *81*, 208-219. Doi 10.1016/0012-1606(81)90284-0.
- Kipreos, E.T., and van den Heuvel, S. (2019). Developmental Control of the Cell Cycle: Insights from *Caenorhabditis elegans*. *Genetics* *211*, 797-829. 10.1534/genetics.118.301643.
- Kitadate, Y., Jorg, D.J., Tokue, M., Maruyama, A., Ichikawa, R., Tsuchiya, S., Segi-Nishida, E., Nakagawa, T., Uchida, A., Kimura-Yoshida, C., et al. (2019). Competition for Mitogens Regulates Spermatogenic Stem Cell Homeostasis in an Open Niche. *Cell Stem Cell* *24*, 79-92 e76. 10.1016/j.stem.2018.11.013.
- Kline, A., Curry, T., and Lewellyn, L. (2018). The Misshapen kinase regulates the size and stability of the germline ring canals in the *Drosophila* egg chamber. *Dev Biol* *440*, 99-112. 10.1016/j.ydbio.2018.05.006.

- Kornfeld, K. (1997). Vulval development in *Caenorhabditis elegans*. *Trends Genet* 13, 55-61. 10.1016/s0168-9525(97)01005-6.
- Korta, D.Z., and Hubbard, E.J. (2010). Soma-germline interactions that influence germline proliferation in *Caenorhabditis elegans*. *Dev Dyn* 239, 1449-1459. 10.1002/dvdy.22268.
- Krajniak, J., and Lu, H. (2010). Long-term high-resolution imaging and culture of *C. elegans* in chip-gel hybrid microfluidic device for developmental studies. *Lab Chip* 10, 1862-1868. 10.1039/c001986k.
- Kramerova, I.A., and Kramerov, A.A. (1999). Mucinoprotein is a universal constituent of stable intercellular bridges in *Drosophila melanogaster* germ line and somatic cells. *Dev Dyn* 216, 349-360. 10.1002/(SICI)1097-0177(199912)216:4/5<349::AID-DVDY4>3.0.CO;2-X.
- Kunwar, P.S., Sano, H., Renault, A.D., Barbosa, V., Fuse, N., and Lehmann, R. (2008). Tre1 GPCR initiates germ cell transepithelial migration by regulating *Drosophila melanogaster* E-cadherin. *J Cell Biol* 183, 157-168. 10.1083/jcb.200807049.
- Kunwar, P.S., Siekhaus, D.E., and Lehmann, R. (2006). In vivo migration: a germ cell perspective. *Annu Rev Cell Dev Biol* 22, 237-265. 10.1146/annurev.cellbio.22.010305.103337.
- Lacroix, B., and Maddox, A.S. (2012). Cytokinesis, ploidy and aneuploidy. *J Pathol* 226, 338-351. 10.1002/path.3013.
- Laermer, F., Schilp, A., Funk, K., and Offenberg, M. (1999). Bosch deep silicon etching: Improving uniformity and etch rate for advanced MEMS applications. *Proc IEEE Micr Elect*, 211-216. Doi 10.1109/Memsys.1999.746812.
- Lara-Gonzalez, P., Moyle, M.W., Budrewicz, J., Mendoza-Lopez, J., Oegema, K., and Desai, A. (2019). The G2-to-M Transition Is Ensured by a Dual Mechanism that Protects Cyclin B from Degradation by Cdc20-Activated APC/C. *Dev Cell* 51, 313-325 e310. 10.1016/j.devcel.2019.09.005.
- Lattmann, E., Deng, T., and Hajnal, A. (2020). To Divide or Invade: A Look Behind the Scenes of the Proliferation-Invasion Interplay in the *Caenorhabditis elegans* Anchor Cell. *Front Cell Dev Biol* 8, 616051. 10.3389/fcell.2020.616051.
- Lee, H.H., Elia, N., Ghirlando, R., Lippincott-Schwartz, J., and Hurley, J.H. (2008). Midbody targeting of the ESCRT machinery by a noncanonical coiled coil in CEP55. *Science* 322, 576-580. 10.1126/science.1162042.
- Lee, K.Y., Green, R.A., Gutierrez, E., Gomez-Cavazos, J.S., Kolotuev, I., Wang, S., Desai, A., Groisman, A., and Oegema, K. (2018). CYK-4 functions independently of its centralspindlin partner ZEN-4 to cellularize oocytes in germline syncytia. *Elife* 7. 10.7554/eLife.36919.
- Lehmann, R. (2016). Germ Plasm Biogenesis--An Oskar-Centric Perspective. *Curr Top Dev Biol* 116, 679-707. 10.1016/bs.ctdb.2015.11.024.
- Lehmann, R., and Nusslein-Volhard, C. (1986). Abdominal segmentation, pole cell formation, and embryonic polarity require the localized activity of oskar, a maternal gene in *Drosophila*. *Cell* 47, 141-152. 10.1016/0092-8674(86)90375-2.



- Lei, L., and Spradling, A.C. (2016). Mouse oocytes differentiate through organelle enrichment from sister cyst germ cells. *Science* 352, 95-99. 10.1126/science.aad2156.
- Lengil, T., Gancz, D., and Gilboa, L. (2015). Activin signaling balances proliferation and differentiation of ovarian niche precursors and enables adjustment of niche numbers. *Development* 142, 883-892. 10.1242/dev.113902.
- Leone, M., Musa, G., and Engel, F.B. (2018). Cardiomyocyte binucleation is associated with aberrant mitotic microtubule distribution, mislocalization of RhoA and IQGAP3, as well as defective actomyosin ring anchorage and cleavage furrow ingression. *Cardiovasc Res* 114, 1115-1131. 10.1093/cvr/cvy056.
- Levine, E., and Lee, K.S. (2020). Microfluidic approaches for *Caenorhabditis elegans* research. *Anim Cells Syst (Seoul)* 24, 311-320. 10.1080/19768354.2020.1837951.
- Lewellyn, L., Dumont, J., Desai, A., and Oegema, K. (2010). Analyzing the effects of delaying aster separation on furrow formation during cytokinesis in the *Caenorhabditis elegans* embryo. *Mol Biol Cell* 21, 50-62. 10.1091/mbc.E09-01-0089.
- Li, F., Wang, X., Bungler, P.C., and Gerdes, A.M. (1997). Formation of binucleated cardiac myocytes in rat heart: I. Role of actin-myosin contractile ring. *J Mol Cell Cardiol* 29, 1541-1551. 10.1006/jmcc.1997.0381.
- Lilly, M.A., de Cuevas, M., and Spradling, A.C. (2000). Cyclin A associates with the fusome during germline cyst formation in the *Drosophila* ovary. *Dev Biol* 218, 53-63. 10.1006/dbio.1999.9570.
- Lilly, M.A., and Spradling, A.C. (1996). The *Drosophila* endocycle is controlled by Cyclin E and lacks a checkpoint ensuring S-phase completion. *Genes Dev* 10, 2514-2526. 10.1101/gad.10.19.2514.
- Lin, Y., Gill, M.E., Koubova, J., and Page, D.C. (2008). Germ cell-intrinsic and -extrinsic factors govern meiotic initiation in mouse embryos. *Science* 322, 1685-1687. 10.1126/science.1166340.
- Liu, Z., Yue, S., Chen, X., Kubin, T., and Braun, T. (2010). Regulation of cardiomyocyte polyploidy and multinucleation by CyclinG1. *Circ Res* 106, 1498-1506. 10.1161/CIRCRESAHA.109.211888.
- Lord, T., and Oatley, J.M. (2017). A revised Asingle model to explain stem cell dynamics in the mouse male germline. *Reproduction* 154, R55-R64. 10.1530/REP-17-0034.
- Lordier, L., Bluteau, D., Jalil, A., Legrand, C., Pan, J., Rameau, P., Jouni, D., Bluteau, O., Mercher, T., Leon, C., et al. (2012). RUNX1-induced silencing of non-muscle myosin heavy chain IIB contributes to megakaryocyte polyploidization. *Nat Commun* 3, 717. 10.1038/ncomms1704.
- Lordier, L., Jalil, A., Aurade, F., Larbret, F., Larghero, J., Debili, N., Vainchenker, W., and Chang, Y. (2008). Megakaryocyte endomitosis is a failure of late cytokinesis related to defects in the contractile ring and Rho/Rock signaling. *Blood* 112, 3164-3174. 10.1182/blood-2008-03-144956.

- Lu, K., Jensen, L., Lei, L., and Yamashita, Y.M. (2017). Stay Connected: A Germ Cell Strategy. *Trends Genet* *33*, 971-978. 10.1016/j.tig.2017.09.001.
- Lu, T., Wang, S., Gao, Y., Mao, Y., Yang, Z., Liu, L., Song, X., Ni, J., and Xie, T. (2015). COP9-Hedgehog axis regulates the function of the germline stem cell progeny differentiation niche in the *Drosophila* ovary. *Development* *142*, 4242-4252. 10.1242/dev.124768.
- Lu, W., Casanueva, M.O., Mahowald, A.P., Kato, M., Lauterbach, D., and Ferguson, E.L. (2012). Niche-Associated Activation of Rac Promotes the Asymmetric Division of *Drosophila* Female Germline Stem Cells. *Plos Biol* *10*. ARTN e1001357  
10.1371/journal.pbio.1001357.
- MacQueen, A.J., and Villeneuve, A.M. (2001). Nuclear reorganization and homologous chromosome pairing during meiotic prophase require *C. elegans* chk-2. *Genes Dev* *15*, 1674-1687. 10.1101/gad.902601.
- Maddox, A.S., Habermann, B., Desai, A., and Oegema, K. (2005). Distinct roles for two *C. elegans* anillins in the gonad and early embryo. *Development* *132*, 2837-2848. 10.1242/dev.01828.
- Maddox, A.S., Lewellyn, L., Desai, A., and Oegema, K. (2007). Anillin and the septins promote asymmetric ingression of the cytokinetic furrow. *Dev Cell* *12*, 827-835. 10.1016/j.devcel.2007.02.018.
- Mahajan-Miklos, S., and Cooley, L. (1994). Intercellular cytoplasm transport during *Drosophila* oogenesis. *Dev Biol* *165*, 336-351. 10.1006/dbio.1994.1257.
- Makela, J.A., and Hobbs, R.M. (2019). Molecular regulation of spermatogonial stem cell renewal and differentiation. *Reproduction* *158*, R169-R187. 10.1530/REP-18-0476.
- Makela, J.A., Koskenniemi, J.J., Virtanen, H.E., and Toppari, J. (2019). Testis Development. *Endocr Rev* *40*, 857-905. 10.1210/er.2018-00140.
- Makela, J.A., and Toppari, J. (2018). Spermatogenic Cell Syncytium. *Encyclopedia of Reproduction* *1*, 124-133. 10.1016/B978-0-12-801238-3.64569-5.
- Mangal, S., Sacher, J., Kim, T., Osorio, D.S., Motegi, F., Carvalho, A.X., Oegema, K., and Zanin, E. (2018). TPXL-1 activates Aurora A to clear contractile ring components from the polar cortex during cytokinesis. *J Cell Biol* *217*, 837-848. 10.1083/jcb.201706021.
- Maniscalco, C., Hall, A.E., and Nance, J. (2020). An interphase contractile ring reshapes primordial germ cells to allow bulk cytoplasmic remodeling. *J Cell Biol* *219*. 10.1083/jcb.201906185.
- Mannix, K.M., Starble, R.M., Kaufman, R.S., and Cooley, L. (2019). Proximity labeling reveals novel interactomes in live *Drosophila* tissue. *Development* *146*. 10.1242/dev.176644.
- Marlow, F. (2015). Primordial Germ Cell Specification and Migration. *F1000Res* *4*. 10.12688/f1000research.6995.1.
- Martinho, R.G., Kunwar, P.S., Casanova, J., and Lehmann, R. (2004). A noncoding RNA is required for the repression of RNApolIII-dependent transcription in primordial germ cells. *Curr Biol* *14*, 159-165. 10.1016/j.cub.2003.12.036.

- Maruyama, D., Ohtsu, M., and Higashiyama, T. (2016). Cell fusion and nuclear fusion in plants. *Semin Cell Dev Biol* 60, 127-135. 10.1016/j.semcdb.2016.07.024.
- Mathieu, J., Cauvin, C., Moch, C., Radford, S.J., Sampaio, P., Perdigoto, C.N., Schweisguth, F., Bardin, A.J., Sunkel, C.E., McKim, K., et al. (2013). Aurora B and cyclin B have opposite effects on the timing of cytokinesis abscission in *Drosophila* germ cells and in vertebrate somatic cells. *Dev Cell* 26, 250-265. 10.1016/j.devcel.2013.07.005.
- Matson, C.K., Murphy, M.W., Griswold, M.D., Yoshida, S., Bardwell, V.J., and Zarkower, D. (2010). The mammalian doublesex homolog DMRT1 is a transcriptional gatekeeper that controls the mitosis versus meiosis decision in male germ cells. *Dev Cell* 19, 612-624. 10.1016/j.devcel.2010.09.010.
- Matsuda, K., Sugawa, M., Yamagishi, M., Kodera, N., and Yajima, J. (2020). Visualizing dynamic actin cross-linking processes driven by the actin-binding protein anillin. *FEBS Lett* 594, 1237-1247. 10.1002/1873-3468.13720.
- McCormick, K.E., Gaertner, B.E., Sottile, M., Phillips, P.C., and Lockery, S.R. (2011). Microfluidic devices for analysis of spatial orientation behaviors in semi-restrained *Caenorhabditis elegans*. *PLoS One* 6, e25710. 10.1371/journal.pone.0025710.
- McDonald, J.C., Duffy, D.C., Anderson, J.R., Chiu, D.T., Wu, H., Schueller, O.J., and Whitesides, G.M. (2000). Fabrication of microfluidic systems in poly(dimethylsiloxane). *Electrophoresis* 21, 27-40. 10.1002/(SICI)1522-2683(20000101)21:1<27::AID-ELPS27>3.0.CO;2-C.
- McEwan, D.L., Weisman, A.S., and Hunter, C.P. (2012). Uptake of extracellular double-stranded RNA by SID-2. *Mol Cell* 47, 746-754. 10.1016/j.molcel.2012.07.014.
- McLean, P.F., and Cooley, L. (2013). Protein equilibration through somatic ring canals in *Drosophila*. *Science* 340, 1445-1447. 10.1126/science.1234887.
- McNally, K., Audhya, A., Oegema, K., and McNally, F.J. (2006). Katanin controls mitotic and meiotic spindle length. *J Cell Biol* 175, 881-891. 10.1083/jcb.200608117.
- Mela, A.P., Rico-Ramirez, A.M., and Glass, N.L. (2020). Syncytia in Fungi. *Cells-Basel* 9. ARTN 2255 10.3390/cells9102255.
- Mendell, J.E., Clements, K.D., Choat, J.H., and Angert, E.R. (2008). Extreme polyploidy in a large bacterium. *P Natl Acad Sci USA* 105, 6730-6734. 10.1073/pnas.0707522105.
- Meola, S.M., Mollenhauer, H.H., and Thompson, J.M. (1977). Cytoplasmic bridges within the follicular epithelium of the ovarioles of two diptera, *Aedes aegypti* and *Stomoxys calcitrans*. *J Morphol* 153, 81-85. 10.1002/jmor.1051530105.
- Merritt, C., and Seydoux, G. (2010). Transgenic solutions for the germline. *WormBook*, 1-21. 10.1895/wormbook.1.148.1.
- Midkiff, D., and San-Miguel, A. (2019). Microfluidic Technologies for High Throughput Screening Through Sorting and On-Chip Culture of *C. elegans*. *Molecules* 24. 10.3390/molecules24234292.

- Mierzwa, B., and Gerlich, D.W. (2014). Cytokinetic abscission: molecular mechanisms and temporal control. *Dev Cell* *31*, 525-538. 10.1016/j.devcel.2014.11.006.
- Mierzwa, B.E., Chiaruttini, N., Redondo-Morata, L., von Filseck, J.M., Konig, J., Larios, J., Poser, I., Muller-Reichert, T., Scheuring, S., Roux, A., and Gerlich, D.W. (2017). Dynamic subunit turnover in ESCRT-III assemblies is regulated by Vps4 to mediate membrane remodelling during cytokinesis. *Nat Cell Biol* *19*, 787-798. 10.1038/ncb3559.
- Minestrini, G., Mathe, E., and Glover, D.M. (2002). Domains of the Pavarotti kinesin-like protein that direct its subcellular distribution: effects of mislocalisation on the tubulin and actin cytoskeleton during *Drosophila* oogenesis. *J Cell Sci* *115*, 725-736.
- Mische, S., Li, M., Serr, M., and Hays, T.S. (2007). Direct observation of regulated ribonucleoprotein transport across the nurse cell/oocyte boundary. *Mol Biol Cell* *18*, 2254-2263. 10.1091/mbc.e06-10-0959.
- Mishima, M., Kaitna, S., and Glotzer, M. (2002). Central spindle assembly and cytokinesis require a kinesin-like protein/RhoGAP complex with microtubule bundling activity. *Dev Cell* *2*, 41-54. 10.1016/s1534-5807(01)00110-1.
- Mochida, S., Maslen, S.L., Skehel, M., and Hunt, T. (2010). Greatwall phosphorylates an inhibitor of protein phosphatase 2A that is essential for mitosis. *Science* *330*, 1670-1673. 10.1126/science.1195689.
- Mohammad, A., Vanden Broek, K., Wang, C., Daryabeigi, A., Jantsch, V., Hansen, D., and Schedl, T. (2018). Initiation of Meiotic Development Is Controlled by Three Post-transcriptional Pathways in *Caenorhabditis elegans*. *Genetics* *209*, 1197-1224. 10.1534/genetics.118.300985.
- Mohler, W.A., Shemer, G., del Campo, J.J., Valansi, C., Opoku-Serebuoh, E., Scranton, V., Assaf, N., White, J.G., and Podbilewicz, B. (2002). The type I membrane protein EFF-1 is essential for developmental cell fusion. *Dev Cell* *2*, 355-362. 10.1016/s1534-5807(02)00129-6.
- Mollova, M., Bersell, K., Walsh, S., Savla, J., Das, L.T., Park, S.Y., Silberstein, L.E., Dos Remedios, C.G., Graham, D., Colan, S., and Kuhn, B. (2013). Cardiomyocyte proliferation contributes to heart growth in young humans. *Proc Natl Acad Sci U S A* *110*, 1446-1451. 10.1073/pnas.1214608110.
- Molyneaux, K., and Wylie, C. (2004). Primordial germ cell migration. *Int J Dev Biol* *48*, 537-544. 10.1387/ijdb.041833km.
- Molyneaux, K.A., Stallock, J., Schaible, K., and Wylie, C. (2001). Time-lapse analysis of living mouse germ cell migration. *Dev Biol* *240*, 488-498. 10.1006/dbio.2001.0436.
- Molyneaux, K.A., Zinszner, H., Kunwar, P.S., Schaible, K., Stebler, J., Sunshine, M.J., O'Brien, W., Raz, E., Littman, D., Wylie, C., and Lehmann, R. (2003). The chemokine SDF1/CXCL12 and its receptor CXCR4 regulate mouse germ cell migration and survival. *Development* *130*, 4279-4286. 10.1242/dev.00640.

- Morais-de-Sa, E., and Sunkel, C. (2013). Adherens junctions determine the apical position of the midbody during follicular epithelial cell division. *EMBO Rep* 14, 696-703. 10.1038/embor.2013.85.
- Morison, A. (1873). Bone Absorption by Means of Giant Cells. *Edinb Med J* 19, 305-311.
- Morita, E., Sandrin, V., Chung, H.Y., Morham, S.G., Gygi, S.P., Rodesch, C.K., and Sundquist, W.I. (2007). Human ESCRT and ALIX proteins interact with proteins of the midbody and function in cytokinesis. *EMBO J* 26, 4215-4227. 10.1038/sj.emboj.7601850.
- Morris, L.X., and Spradling, A.C. (2011). Long-term live imaging provides new insight into stem cell regulation and germline-soma coordination in the *Drosophila* ovary. *Development* 138, 2207-2215. 10.1242/dev.065508.
- Mottier-Pavie, V.I., Palacios, V., Eliazer, S., Scoggin, S., and Buszczak, M. (2016). The Wnt pathway limits BMP signaling outside of the germline stem cell niche in *Drosophila* ovaries. *Dev Biol* 417, 50-62. 10.1016/j.ydbio.2016.06.038.
- Mulas, C., Kalkan, T., and Smith, A. (2017). NODAL Secures Pluripotency upon Embryonic Stem Cell Progression from the Ground State. *Stem Cell Rep* 9, 77-91. 10.1016/j.stemcr.2017.05.033.
- Munger, S.C., Natarajan, A., Looger, L.L., Ohler, U., and Capel, B. (2013). Fine time course expression analysis identifies cascades of activation and repression and maps a putative regulator of mammalian sex determination. *PLoS Genet* 9, e1003630. 10.1371/journal.pgen.1003630.
- Nagano, R., Tabata, S., Nakanishi, Y., Ohsako, S., Kurohmaru, M., and Hayashi, Y. (2000). Reproliferation and relocation of mouse male germ cells (gonocytes) during prespermatogenesis. *Anat Rec* 258, 210-220. 10.1002/(SICI)1097-0185(20000201)258:2<210::AID-AR10>3.0.CO;2-X.
- Nakagawa, T., Sharma, M., Nabeshima, Y., Braun, R.E., and Yoshida, S. (2010). Functional hierarchy and reversibility within the murine spermatogenic stem cell compartment. *Science* 328, 62-67. 10.1126/science.1182868.
- Nakamura, A., and Seydoux, G. (2008). Less is more: specification of the germline by transcriptional repression. *Development* 135, 3817-3827. 10.1242/dev.022434.
- Nance, J., Munro, E.M., and Priess, J.R. (2003). *C. elegans* PAR-3 and PAR-6 are required for apicobasal asymmetries associated with cell adhesion and gastrulation. *Development* 130, 5339-5350. 10.1242/dev.00735.
- Nguyen, P.A., Groen, A.C., Loose, M., Ishihara, K., Wuhr, M., Field, C.M., and Mitchison, T.J. (2014). Spatial organization of cytokinesis signaling reconstituted in a cell-free system. *Science* 346, 244-247. 10.1126/science.1256773.
- Niiya, F., Xie, X., Lee, K.S., Inoue, H., and Miki, T. (2005). Inhibition of cyclin-dependent kinase 1 induces cytokinesis without chromosome segregation in an ECT2 and MgcRacGAP-dependent manner. *J Biol Chem* 280, 36502-36509. 10.1074/jbc.M508007200.

- Nishimura, Y., and Yonemura, S. (2006). Centralspindlin regulates ECT2 and RhoA accumulation at the equatorial cortex during cytokinesis. *J Cell Sci* 119, 104-114. 10.1242/jcs.02737.
- Ohinata, Y., Payer, B., O'Carroll, D., Ancelin, K., Ono, Y., Sano, M., Barton, S.C., Obukhanych, T., Nussenzweig, M., Tarakhovsky, A., et al. (2005). Blimp1 is a critical determinant of the germ cell lineage in mice. *Nature* 436, 207-213. 10.1038/nature03813.
- Ohlmeyer, J.T., and Schupbach, T. (2003). Encore facilitates SCF-Ubiquitin-proteasome-dependent proteolysis during *Drosophila* oogenesis. *Development* 130, 6339-6349. 10.1242/dev.00855.
- Ong, S., Foote, C., and Tan, C. (2010). Mutations of DMYP1 cause over constriction of contractile rings and ring canals during *Drosophila* germline cyst formation. *Dev Biol* 346, 161-169. 10.1016/j.ydbio.2010.06.008.
- Osorio, D.S., Chan, F.Y., Saramago, J., Leite, J., Silva, A.M., Sobral, A.F., Gassmann, R., and Carvalho, A.X. (2019). Crosslinking activity of non-muscle myosin II is not sufficient for embryonic cytokinesis in *C. elegans*. *Development* 146. 10.1242/dev.179150.
- Pacquelet, A. (2017). Asymmetric Cell Division in the One-Cell *C. elegans* Embryo: Multiple Steps to Generate Cell Size Asymmetry. *Results Probl Cell Differ* 61, 115-140. 10.1007/978-3-319-53150-2\_5.
- Pal, S., Lant, B., Yu, B., Tian, R., Tong, J., Krieger, J.R., Moran, M.F., Gingras, A.C., and Derry, W.B. (2017). CCM-3 Promotes *C. elegans* Germline Development by Regulating Vesicle Trafficking Cytokinesis and Polarity. *Curr Biol* 27, 868-876. 10.1016/j.cub.2017.02.028.
- Pandit, S.K., Westendorp, B., and de Bruin, A. (2013). Physiological significance of polyploidization in mammalian cells. *Trends Cell Biol* 23, 556-566. 10.1016/j.tcb.2013.06.002.
- Pavlat, G.K. (2010). Spatial and functional restriction of regulatory molecules during mammalian myoblast fusion. *Exp Cell Res* 316, 3067-3072. 10.1016/j.yexcr.2010.05.025.
- Pepling, M.E., de Cuevas, M., and Spradling, A.C. (1999). Germline cysts: a conserved phase of germ cell development? *Trends Cell Biol* 9, 257-262. 10.1016/s0962-8924(99)01594-9.
- Petcherski, A.G., and Kimble, J. (2000). LAG-3 is a putative transcriptional activator in the *C. elegans* Notch pathway. *Nature* 405, 364-368. 10.1038/35012645.
- Piekny, A., Werner, M., and Glotzer, M. (2005). Cytokinesis: welcome to the Rho zone. *Trends Cell Biol* 15, 651-658. 10.1016/j.tcb.2005.10.006.
- Piekny, A.J., Johnson, J.L., Cham, G.D., and Mains, P.E. (2003). The *Caenorhabditis elegans* nonmuscle myosin genes *nmy-1* and *nmy-2* function as redundant components of the *let-502*/Rho-binding kinase and *mel-11*/myosin phosphatase pathway during embryonic morphogenesis. *Development* 130, 5695-5704. 10.1242/dev.00807.
- Piekny, A.J., and Maddox, A.S. (2010). The myriad roles of Anillin during cytokinesis. *Semin Cell Dev Biol* 21, 881-891. 10.1016/j.semcdb.2010.08.002.

- Piekny, A.J., and Mains, P.E. (2002). Rho-binding kinase (LET-502) and myosin phosphatase (MEL-11) regulate cytokinesis in the early *Caenorhabditis elegans* embryo. *J Cell Sci* *115*, 2271-2282.
- Pintard, L., and Bowerman, B. (2019). Mitotic Cell Division in *Caenorhabditis elegans*. *Genetics* *211*, 35-73. 10.1534/genetics.118.301367.
- Pittman, K.J., and Skop, A.R. (2012). Anterior PAR proteins function during cytokinesis and maintain DYN-1 at the cleavage furrow in *Caenorhabditis elegans*. *Cytoskeleton (Hoboken)* *69*, 826-839. 10.1002/cm.21053.
- Plachno, B.J., and Swiatek, P. (2011). Syncytia in plants: cell fusion in endosperm-placental syncytium formation in *Utricularia* (Lentibulariaceae). *Protoplasma* *248*, 425-435. 10.1007/s00709-010-0173-1.
- Pohl, C. (2017). The Midbody and its Remnant in Cell Polarization and Asymmetric Cell Division. *Results Probl Cell Differ* *61*, 165-182. 10.1007/978-3-319-53150-2\_7.
- Pollard, T.D., and O'Shaughnessy, B. (2019). Molecular Mechanism of Cytokinesis. *Annu Rev Biochem* *88*, 661-689. 10.1146/annurev-biochem-062917-012530.
- Potapova, T.A., Daum, J.R., Pittman, B.D., Hudson, J.R., Jones, T.N., Satinover, D.L., Stukenberg, P.T., and Gorbsky, G.J. (2006). The reversibility of mitotic exit in vertebrate cells. *Nature* *440*, 954-958. 10.1038/nature04652.
- Potter, D.D., Furshpan, E.J., and Lennox, E.S. (1966). Connections between cells of the developing squid as revealed by electrophysiological methods. *Proc Natl Acad Sci U S A* *55*, 328-336. 10.1073/pnas.55.2.328.
- Priti, A., Ong, H.T., Toyama, Y., Padmanabhan, A., Dasgupta, S., Krajnc, M., and Zaidel-Bar, R. (2018). Syncytial germline architecture is actively maintained by contraction of an internal actomyosin corset. *Nat Commun* *9*, 4694. 10.1038/s41467-018-07149-2.
- Prokopenko, S.N., Brumby, A., O'Keefe, L., Prior, L., He, Y., Saint, R., and Bellen, H.J. (1999). A putative exchange factor for Rho1 GTPase is required for initiation of cytokinesis in *Drosophila*. *Genes Dev* *13*, 2301-2314. 10.1101/gad.13.17.2301.
- Pui, H.P., and Saga, Y. (2017). Gonocytes-to-spermatogonia transition initiates prior to birth in murine testes and it requires FGF signaling. *Mech Dev* *144*, 125-139. 10.1016/j.mod.2017.03.002.
- Quinn, M.E., Goh, Q., Kurosaka, M., Gamage, D.G., Petrany, M.J., Prasad, V., and Millay, D.P. (2017). Myomerger induces fusion of non-fusogenic cells and is required for skeletal muscle development. *Nat Commun* *8*, 15665. 10.1038/ncomms15665.
- Rabinowitz, M. (1941). *Studies on the cytology and early embryology of the egg of Drosophila melanogaster* (Press of the Wistar institute of anatomy and biology).
- Ramamurty, P.S., and Engels, W. (1977). Occurrence of intercellular bridges between follicle epithelial cells in the ovary of *Apis mellifica* queens. *J Cell Sci* *24*, 195-202.

- Rappaport, R. (1961). Experiments concerning the cleavage stimulus in sand dollar eggs. *J Exp Zool* *148*, 81-89. 10.1002/jez.1401480107.
- Rappaport, R. (1996). *Cytokinesis in animal cells* (Cambridge University Press).
- Ravid, K., Lu, J., Zimmet, J.M., and Jones, M.R. (2002). Roads to polyploidy: the megakaryocyte example. *J Cell Physiol* *190*, 7-20. 10.1002/jcp.10035.
- Rehain, K., Green, R.A., Bourdages, K.G., and Maddox, A.S. (2017). Variations on a theme: Imaging cytokinetic and stable rings in situ using *Caenorhabditis elegans*. *Methods Cell Biol* *137*, 267-281. 10.1016/bs.mcb.2016.03.039.
- Rehain-Bell, K., Love, A., Werner, M.E., MacLeod, I., Yates, J.R., 3rd, and Maddox, A.S. (2017). A Sterile 20 Family Kinase and Its Co-factor CCM-3 Regulate Contractile Ring Proteins on Germline Intercellular Bridges. *Curr Biol* *27*, 860-867. 10.1016/j.cub.2017.01.058.
- Ren, H.P., and Russell, L.D. (1991). Clonal development of interconnected germ cells in the rat and its relationship to the segmental and subsegmental organization of spermatogenesis. *Am J Anat* *192*, 121-128. 10.1002/aja.1001920203.
- Renshaw, M.J., Liu, J., Lavoie, B.D., and Wilde, A. (2014). Anillin-dependent organization of septin filaments promotes intercellular bridge elongation and Chmp4B targeting to the abscission site. *Open Biol* *4*, 130190. 10.1098/rsob.130190.
- Respuela, P., Nikolic, M., Tan, M., Frommolt, P., Zhao, Y., Wysocka, J., and Rada-Iglesias, A. (2016). Foxd3 Promotes Exit from Naive Pluripotency through Enhancer Decommissioning and Inhibits Germline Specification. *Cell Stem Cell* *18*, 118-133. 10.1016/j.stem.2015.09.010.
- Rezende-Melo, C.A., Caldeira-Brant, A.L., Drumond-Bock, A.L., Buchold, G.M., Shetty, G., Almeida, F., Matzuk, M.M., Hara, K., Yoshida, S., Meistrich, M.L., and Chiarini-Garcia, H. (2020). Spermatogonial asynchrony in Tex14 mutant mice lacking intercellular bridges. *Reproduction* *160*, 205-215. 10.1530/REP-20-0118.
- Robert, V.J., Garvis, S., and Palladino, F. (2015). Repression of somatic cell fate in the germline. *Cell Mol Life Sci* *72*, 3599-3620. 10.1007/s00018-015-1942-y.
- Robinson, D.N., Cant, K., and Cooley, L. (1994). Morphogenesis of *Drosophila* ovarian ring canals. *Development* *120*, 2015-2025.
- Robinson, D.N., and Cooley, L. (1996). Stable intercellular bridges in development: the cytoskeleton lining the tunnel. *Trends Cell Biol* *6*, 474-479. 10.1016/0962-8924(96)84945-2.
- Robinson, D.N., and Cooley, L. (1997). Genetic analysis of the actin cytoskeleton in the *Drosophila* ovary. *Annu Rev Cell Dev Biol* *13*, 147-170. 10.1146/annurev.cellbio.13.1.147.
- Robinson, D.N., Smith-Leiker, T.A., Sokol, N.S., Hudson, A.M., and Cooley, L. (1997). Formation of the *Drosophila* ovarian ring canal inner rim depends on cheerio. *Genetics* *145*, 1063-1072.
- Rohrschneider, M.R., and Nance, J. (2013). The union of somatic gonad precursors and primordial germ cells during *Caenorhabditis elegans* embryogenesis. *Developmental Biology* *379*, 139-151. 10.1016/j.ydbio.2013.03.019.



- Roulier, E.M., Panzer, S., and Beckendorf, S.K. (1998). The Tec29 tyrosine kinase is required during *Drosophila* embryogenesis and interacts with Src64 in ring canal development. *Mol Cell* *1*, 819-829. 10.1016/s1097-2765(00)80081-7.
- Roy, A., Lordier, L., Pioche-Durieu, C., Souquere, S., Roy, L., Rameau, P., Lapierre, V., Le Cam, E., Plo, I., Debili, N., et al. (2016). Uncoupling of the Hippo and Rho pathways allows megakaryocytes to escape the tetraploid checkpoint. *Haematologica* *101*, 1469-1478. 10.3324/haematol.2016.149914.
- Rubin, T., Christophorou, N., and Huynh, J.R. (2016). How to pre-pair chromosomes for meiosis. *Cell Cycle* *15*, 609-610. 10.1080/15384101.2015.1131524.
- Russell, L.D., Vogl, A.W., and Weber, J.E. (1987). Actin Localization in Male Germ-Cell Intercellular Bridges in the Rat and Ground-Squirrel and Disruption of Bridges by Cytochalasin-D. *Am J Anat* *180*, 25-40. DOI 10.1002/aja.1001800103.
- Saffman, E.E., and Lasko, P. (1999). Germline development in vertebrates and invertebrates. *Cell Mol Life Sci* *55*, 1141-1163. 10.1007/s000180050363.
- Sahut-Barnola, I., Dastugue, B., and Couderc, J.L. (1996). Terminal filament cell organization in the larval ovary of *Drosophila melanogaster*: ultrastructural observations and pattern of divisions. *Roux Arch Dev Biol* *205*, 356-363. 10.1007/BF00377215.
- Saitou, M., Barton, S.C., and Surani, M.A. (2002). A molecular programme for the specification of germ cell fate in mice. *Nature* *418*, 293-300. 10.1038/nature00927.
- Saitou, M., Payer, B., O'Carroll, D., Ohinata, Y., and Surani, M.A. (2005). Blimp1 and the emergence of the germ line during development in the mouse. *Cell Cycle* *4*, 1736-1740. 10.4161/cc.4.12.2209.
- Salmon, E.D., Goode, D., Mangel, T.K., and Bonar, D.B. (1976). Pressure-induced depolymerization of spindle microtubules. III. Differential stability in HeLa cells. *J Cell Biol* *69*, 443-454. 10.1083/jcb.69.2.443.
- San-Miguel, A., and Lu, H. (2013). Microfluidics as a tool for *C. elegans* research. *WormBook*, 1-19. 10.1895/wormbook.1.162.1.
- Sano, H., Renault, A.D., and Lehmann, R. (2005). Control of lateral migration and germ cell elimination by the *Drosophila melanogaster* lipid phosphate phosphatases Wunen and Wunen 2. *J Cell Biol* *171*, 675-683. 10.1083/jcb.200506038.
- Santos, A.C., and Lehmann, R. (2004). Germ cell specification and migration in *Drosophila* and beyond. *Curr Biol* *14*, R578-589. 10.1016/j.cub.2004.07.018.
- Sapir, A., Choi, J., Leikina, E., Avinoam, O., Valansi, C., Chernomordik, L.V., Newman, A.P., and Podbilewicz, B. (2007). AFF-1, a FOS-1-regulated fusogen, mediates fusion of the anchor cell in *C. elegans*. *Dev Cell* *12*, 683-698. 10.1016/j.devcel.2007.03.003.
- Sarikaya, D.P., Belay, A.A., Ahuja, A., Dorta, A., Green, D.A., and Extavour, C.G. (2012). The roles of cell size and cell number in determining ovariole number in *Drosophila*. *Developmental Biology* *363*, 279-289. 10.1016/j.ydbio.2011.12.017.

- Schaner, C.E., Deshpande, G., Schedl, P.D., and Kelly, W.G. (2003). A conserved chromatin architecture marks and maintains the restricted germ cell lineage in worms and flies. *Dev Cell* 5, 747-757. 10.1016/s1534-5807(03)00327-7.
- Schmutz, C., Stevens, J., and Spang, A. (2007). Functions of the novel RhoGAP proteins RGA-3 and RGA-4 in the germ line and in the early embryo of *C. elegans*. *Development* 134, 3495-3505. 10.1242/dev.000802.
- Schubert, C.M., Lin, R.L., de Vries, C.J., Plasterk, R.H.A., and Priess, J.R. (2000). MEX-5 and MEX-6 function to establish soma/germline asymmetry in early *C. elegans* embryos. *Molecular Cell* 5, 671-682. Doi 10.1016/S1097-2765(00)80246-4.
- Seidel, H.S., Smith, T.A., Evans, J.K., Stamper, J.Q., Mast, T.G., and Kimble, J. (2018). *C. elegans* germ cells divide and differentiate in a folded tissue. *Dev Biol* 442, 173-187. 10.1016/j.ydbio.2018.07.013.
- Seifert, J.R., and Lehmann, R. (2012). *Drosophila* primordial germ cell migration requires epithelial remodeling of the endoderm. *Development* 139, 2101-2106. 10.1242/dev.078949.
- Sekido, R., and Lovell-Badge, R. (2008). Sex determination involves synergistic action of SRY and SF1 on a specific Sox9 enhancer. *Nature* 453, 930-934. 10.1038/nature06944.
- Senft, A.D., Bikoff, E.K., Robertson, E.J., and Costello, I. (2019). Genetic dissection of Nodal and Bmp signalling requirements during primordial germ cell development in mouse. *Nat Commun* 10, 1089. 10.1038/s41467-019-09052-w.
- Seydoux, G., and Braun, R.E. (2006). Pathway to totipotency: lessons from germ cells. *Cell* 127, 891-904. 10.1016/j.cell.2006.11.016.
- Seydoux, G., and Dunn, M.A. (1997). Transcriptionally repressed germ cells lack a subpopulation of phosphorylated RNA polymerase II in early embryos of *Caenorhabditis elegans* and *Drosophila melanogaster*. *Development* 124, 2191-2201.
- Seydoux, G., and Fire, A. (1994). Soma-Germline Asymmetry in the Distributions of Embryonic Rnas in *Caenorhabditis-Elegans*. *Development* 120, 2823-2834.
- Seydoux, G., Mello, C.C., Pettitt, J., Wood, W.B., Priess, J.R., and Fire, A. (1996). Repression of gene expression in the embryonic germ lineage of *C. elegans*. *Nature* 382, 713-716. DOI 10.1038/382713a0.
- Shcherbata, H.R., Althausen, C., Findley, S.D., and Ruohola-Baker, H. (2004). The mitotic-to-endocycle switch in *Drosophila* follicle cells is executed by Notch-dependent regulation of G1/S, G2/M and M/G1 cell-cycle transitions. *Development* 131, 3169-3181. 10.1242/dev.01172.
- Shin, J.W., Swift, J., Spinler, K.R., and Discher, D.E. (2011). Myosin-II inhibition and soft 2D matrix maximize multinucleation and cellular projections typical of platelet-producing megakaryocytes. *Proc Natl Acad Sci U S A* 108, 11458-11463. 10.1073/pnas.1017474108.
- Slautterback, D.B., and Fawcett, D.W. (1959). The development of the cnidoblasts of *Hydra*; an electron microscope study of cell differentiation. *J Biophys Biochem Cytol* 5, 441-452. 10.1083/jcb.5.3.441.

- Sokol, N.S., and Cooley, L. (1999). Drosophila filamin encoded by the cheerio locus is a component of ovarian ring canals. *Curr Biol* 9, 1221-1230. 10.1016/S0960-9822(99)80502-8.
- Song, X., Call, G.B., Kirilly, D., and Xie, T. (2007). Notch signaling controls germline stem cell niche formation in the Drosophila ovary. *Development* 134, 1071-1080. 10.1242/dev.003392.
- Song, X., and Xie, T. (2002). DE-cadherin-mediated cell adhesion is essential for maintaining somatic stem cells in the Drosophila ovary. *Proc Natl Acad Sci U S A* 99, 14813-14818. 10.1073/pnas.232389399.
- Spiller, C., Koopman, P., and Bowles, J. (2017). Sex Determination in the Mammalian Germline. *Annu Rev Genet* 51, 265-285. 10.1146/annurev-genet-120215-035449.
- Spradling, A.C. (1993). Germline Cysts - Communes That Work. *Cell* 72, 649-651. Doi 10.1016/0092-8674(93)90393-5.
- Stevant, I., and Nef, S. (2019). Genetic Control of Gonadal Sex Determination and Development. *Trends Genet* 35, 346-358. 10.1016/j.tig.2019.02.004.
- Stevant, I., Neirijnck, Y., Borel, C., Escoffier, J., Smith, L.B., Antonarakis, S.E., Dermitzakis, E.T., and Nef, S. (2018). Deciphering Cell Lineage Specification during Male Sex Determination with Single-Cell RNA Sequencing. *Cell Rep* 22, 1589-1599. 10.1016/j.celrep.2018.01.043.
- Stevenson, V., Hudson, A., Cooley, L., and Theurkauf, W.E. (2002). Arp2/3-dependent pseudocleavage furrow assembly in syncytial Drosophila embryos. *Current Biology* 12, 705-711. Pii S0960-9822(02)00807-2  
Doi 10.1016/S0960-9822(02)00807-2.
- Strome, S. (1986). Fluorescence visualization of the distribution of microfilaments in gonads and early embryos of the nematode *Caenorhabditis elegans*. *J Cell Biol* 103, 2241-2252. 10.1083/jcb.103.6.2241.
- Strome, S., Bender, L., Suh, J., Carroll, C., Wang, W.C., Phippen, T., Cao, R., and Zhang, Y. (2005). Epigenetic control of the X chromosomes by the C-elegans MES proteins methylation of histone tails. *Developmental Biology* 283, 575-575.
- Strome, S., Kawasaki, I., Garvin, C., Holdeman, R., and Korf, I. (1997). Maternal control of early germline development in C-elegans. *Developmental Biology* 186, S61-S61.
- Strome, S., Powers, J., Dunn, M., Reese, K., Malone, C.J., White, J., Seydoux, G., and Saxton, W. (2001). Spindle dynamics and the role of gamma-tubulin in early *Caenorhabditis elegans* embryos. *Mol Biol Cell* 12, 1751-1764. 10.1091/mbc.12.6.1751.
- Strome, S., and Updike, D. (2015). Specifying and protecting germ cell fate. *Nat Rev Mol Cell Biol* 16, 406-416. 10.1038/nrm4009.
- Subramaniam, K., and Seydoux, G. (1999). nos-1 and nos-2, two genes related to Drosophila nanos, regulate primordial germ cell development and survival in *Caenorhabditis elegans*. *Development* 126, 4861-4871.

- Suh, N., Jedamzik, B., Eckmann, C.R., Wickens, M., and Kimble, J. (2006). The GLD-2 poly(A) polymerase activates *gld-1* mRNA in the *Caenorhabditis elegans* germ line. *Proc Natl Acad Sci U S A* *103*, 15108-15112. 10.1073/pnas.0607050103.
- Sulston, J.E. (1976). Post-embryonic development in the ventral cord of *Caenorhabditis elegans*. *Philos Trans R Soc Lond B Biol Sci* *275*, 287-297. 10.1098/rstb.1976.0084.
- Sulston, J.E. (1983). Neuronal cell lineages in the nematode *Caenorhabditis elegans*. *Cold Spring Harb Symp Quant Biol* *48 Pt 2*, 443-452. 10.1101/sqb.1983.048.01.049.
- Sulston, J.E., and Horvitz, H.R. (1977). Post-embryonic cell lineages of the nematode, *Caenorhabditis elegans*. *Dev Biol* *56*, 110-156. 10.1016/0012-1606(77)90158-0.
- Sumi, T., Oki, S., Kitajima, K., and Meno, C. (2013). Epiblast ground state is controlled by canonical Wnt/beta-catenin signaling in the postimplantation mouse embryo and epiblast stem cells. *PLoS One* *8*, e63378. 10.1371/journal.pone.0063378.
- Sundaram, M., and Han, M. (1996). Control and integration of cell signaling pathways during *C. elegans* vulval development. *Bioessays* *18*, 473-480. 10.1002/bies.950180609.
- Suzuki, H., Ahn, H.W., Chu, T., Bowden, W., Gassei, K., Orwig, K., and Rajkovic, A. (2012). SOHLH1 and SOHLH2 coordinate spermatogonial differentiation. *Dev Biol* *361*, 301-312. 10.1016/j.ydbio.2011.10.027.
- Swiatek, P., Kubrakiewicz, J., and Klag, J. (2009). Formation of germ-line cysts with a central cytoplasmic core is accompanied by specific orientation of mitotic spindles and partitioning of existing intercellular bridges. *Cell Tissue Res* *337*, 137-148. 10.1007/s00441-009-0788-8.
- Swiatek, P., and Urbisz, A.Z. (2019). Architecture and Life History of Female Germ-Line Cysts in Clitellate Annelids. *Results Probl Cell Differ* *68*, 515-551. 10.1007/978-3-030-23459-1\_21.
- Sybirna, A., Wong, F.C.K., and Surani, M.A. (2019). Genetic basis for primordial germ cells specification in mouse and human: Conserved and divergent roles of PRDM and SOX transcription factors. *Curr Top Dev Biol* *135*, 35-89. 10.1016/bs.ctdb.2019.04.004.
- Takeuchi, Y., Molyneaux, K., Runyan, C., Schaible, K., and Wylie, C. (2005). The roles of FGF signaling in germ cell migration in the mouse. *Development* *132*, 5399-5409. 10.1242/dev.02080.
- Tan, C., Stronach, B., and Perrimon, N. (2003). Roles of myosin phosphatase during *Drosophila* development. *Development* *130*, 671-681. 10.1242/dev.00298.
- Tanaka, S.S., Yamaguchi, Y.L., Tsoi, B., Lickert, H., and Tam, P.P. (2005). IFITM/Mil/fragilis family proteins IFITM1 and IFITM3 play distinct roles in mouse primordial germ cell homing and repulsion. *Dev Cell* *9*, 745-756. 10.1016/j.devcel.2005.10.010.
- Tatsumoto, T., Xie, X., Blumenthal, R., Okamoto, I., and Miki, T. (1999). Human ECT2 is an exchange factor for Rho GTPases, phosphorylated in G2/M phases, and involved in cytokinesis. *J Cell Biol* *147*, 921-928. 10.1083/jcb.147.5.921.

- Tax, F.E., Yeagers, J.J., and Thomas, J.H. (1994). Sequence of *C. elegans* lag-2 reveals a cell-signalling domain shared with Delta and Serrate of *Drosophila*. *Nature* 368, 150-154. 10.1038/368150a0.
- Tenenhaus, C., Subramaniam, K., Dunn, M.A., and Seydoux, G. (2001). PIE-1 is a bifunctional protein that regulates maternal and zygotic gene expression in the embryonic germ line of *Caenorhabditis elegans*. *Gene Dev* 15, 1031-1040. DOI 10.1101/gad.876201.
- Thestrup, J., Tipold, M., Kindred, A., Stark, K., Curry, T., and Lewellyn, L. (2020). The Arp2/3 complex and the formin, Diaphanous, are both required to regulate the size of germline ring canals in the developing egg chamber. *Dev Biol* 461, 75-85. 10.1016/j.ydbio.2020.01.007.
- Tilney, L.G., Tilney, M.S., and Guild, G.M. (1996). Formation of actin filament bundles in the ring canals of developing *Drosophila* follicles. *J Cell Biol* 133, 61-74. 10.1083/jcb.133.1.61.
- Trcek, T., and Lehmann, R. (2019). Germ granules in *Drosophila*. *Traffic* 20, 650-660. 10.1111/tra.12674.
- Tres, L.L., Rivkin, E., and Kierszenbaum, A.L. (1996). Sak 57, an intermediate filament keratin present in intercellular bridges of rat primary spermatocytes. *Mol Reprod Dev* 45, 93-105. Doi 10.1002/(Sici)1098-2795(199609)45:1<93::Aid-Mrd13>3.0.Co;2-Y.
- Tse, Y.C., Piekny, A., and Glotzer, M. (2011). Anillin promotes astral microtubule-directed cortical myosin polarization. *Mol Biol Cell* 22, 3165-3175. 10.1091/mbc.E11-05-0399.
- Vainchenker, W., and Raslova, H. (2020). Megakaryocyte polyploidization: role in platelet production. *Platelets* 31, 707-716. 10.1080/09537104.2019.1667497.
- Van Doren, M., Broihier, H.T., Moore, L.A., and Lehmann, R. (1998). HMG-CoA reductase guides migrating primordial germ cells. *Nature* 396, 466-469.
- Voronina, E., Seydoux, G., Sassone-Corsi, P., and Nagamori, I. (2011). RNA granules in germ cells. *Cold Spring Harb Perspect Biol* 3. 10.1101/cshperspect.a002774.
- Wagner, E., and Glotzer, M. (2016). Local RhoA activation induces cytokinetic furrows independent of spindle position and cell cycle stage. *J Cell Biol* 213, 641-649. 10.1083/jcb.201603025.
- Wang, J.T., and Seydoux, G. (2013). Germ cell specification. *Adv Exp Med Biol* 757, 17-39. 10.1007/978-1-4614-4015-4\_2.
- Wang, X., and Page-McCaw, A. (2018). Wnt6 maintains anterior escort cells as an integral component of the germline stem cell niche. *Development* 145. 10.1242/dev.158527.
- Weber, J.E., and Russell, L.D. (1987). A Study of Intercellular Bridges during Spermatogenesis in the Rat. *Am J Anat* 180, 1-24. DOI 10.1002/aja.1001800102.
- Wilkinson, H.A., Fitzgerald, K., and Greenwald, I. (1994). Reciprocal changes in expression of the receptor lin-12 and its ligand lag-2 prior to commitment in a *C. elegans* cell fate decision. *Cell* 79, 1187-1198. 10.1016/0092-8674(94)90010-8.

- Wilson, R.K. (1999). How the worm was won. The *C. elegans* genome sequencing project. *Trends Genet* 15, 51-58. 10.1016/s0168-9525(98)01666-7.
- Winkelmann, M., Pfitzer, P., and Schneider, W. (1987). Significance of polyploidy in megakaryocytes and other cells in health and tumor disease. *Klin Wochenschr* 65, 1115-1131. 10.1007/BF01734832.
- Winston, W.M., Sutherlin, M., Wright, A.J., Feinberg, E.H., and Hunter, C.P. (2007). *Caenorhabditis elegans* SID-2 is required for environmental RNA interference. *Proc Natl Acad Sci U S A* 104, 10565-10570. 10.1073/pnas.0611282104.
- Wolke, U., Jezuit, E.A., and Priess, J.R. (2007). Actin-dependent cytoplasmic streaming in *C. elegans* oogenesis. *Development* 134, 2227-2236. 10.1242/dev.004952.
- Wollert, T., Wunder, C., Lippincott-Schwartz, J., and Hurley, J.H. (2009). Membrane scission by the ESCRT-III complex. *Nature* 458, 172-177. 10.1038/nature07836.
- Woodruff, R.I., and Tilney, L.G. (1998). Intercellular bridges between epithelial cells in the *Drosophila* ovarian follicle: a possible aid to localized signaling. *Dev Biol* 200, 82-91. 10.1006/dbio.1998.8948.
- Wu, J.Q., Guo, J.Y., Tang, W., Yang, C.S., Freel, C.D., Chen, C., Nairn, A.C., and Kornbluth, S. (2009). PP1-mediated dephosphorylation of phosphoproteins at mitotic exit is controlled by inhibitor-1 and PP1 phosphorylation. *Nature Cell Biology* 11, 644-U451. 10.1038/ncb1871.
- Xia, Y., and Whitesides, G.M. (1998). Soft Lithography. *Angew Chem Int Ed Engl* 37, 550-575. 10.1002/(SICI)1521-3773(19980316)37:5<550::AID-ANIE550>3.0.CO;2-G.
- Xie, T., and Spradling, A.C. (1998). *decapentaplegic* is essential for the maintenance and division of germline stem cells in the *Drosophila* ovary. *Cell* 94, 251-260. 10.1016/s0092-8674(00)81424-5.
- Yabuta, Y., Kurimoto, K., Ohinata, Y., Seki, Y., and Saitou, M. (2006). Gene expression dynamics during germline specification in mice identified by quantitative single-cell gene expression profiling. *Biol Reprod* 75, 705-716. 10.1095/biolreprod.106.053686.
- Yamaji, M., Seki, Y., Kurimoto, K., Yabuta, Y., Yuasa, M., Shigeta, M., Yamanaka, K., Ohinata, Y., and Saitou, M. (2008). Critical function of *Prdm14* for the establishment of the germ cell lineage in mice. *Nat Genet* 40, 1016-1022. 10.1038/ng.186.
- Yamamoto, S., Bayat, V., Bellen, H.J., and Tan, C. (2013). Protein phosphatase 1ss limits ring canal constriction during *Drosophila* germline cyst formation. *PLoS One* 8, e70502. 10.1371/journal.pone.0070502.
- Yang, D., Rismanchi, N., Renvoise, B., Lippincott-Schwartz, J., Blackstone, C., and Hurley, J.H. (2008). Structural basis for midbody targeting of spastin by the ESCRT-III protein CHMP1B. *Nat Struct Mol Biol* 15, 1278-1286. 10.1038/nsmb.1512.
- Yang, P.Y., Humphrey, S.J., Cinghu, S., Pathania, R., Oldfield, A.J., Kumar, D., Perera, D., Yang, J.Y., James, D.E., Mann, M., and Jothi, R. (2019). Multi-omic Profiling Reveals Dynamics of the Phased Progression of Pluripotency. *Cell Syst* 8, 427-+. 10.1016/j.cels.2019.03.012.

- Yuce, O., Piekny, A., and Glotzer, M. (2005). An ECT2-centralspindlin complex regulates the localization and function of RhoA. *J Cell Biol* 170, 571-582. 10.1083/jcb.200501097.
- Yue, L., and Spradling, A.C. (1992). Hu-Li-Tai-Shao, a Gene Required for Ring Canal Formation during *Drosophila* Oogenesis, Encodes a Homolog of Adducin. *Gene Dev* 6, 2443-2454. DOI 10.1101/gad.6.12b.2443.
- Zalokar, M., and Erk, I. (1976). Division and Migration of Nuclei during Early Embryogenesis of *Drosophila-Melanogaster*. *J Microsc Biol Cell* 25, 97-+.
- Zamboni, L., and Gondos, B. (1968). Intercellular Bridges and Synchronization of Germ Cell Differentiation during Oogenesis in Rabbit. *Journal of Cell Biology* 36, 276-+. DOI 10.1083/jcb.36.1.276.
- Zellag, R.M., Zhao, Y., Poupart, V., Singh, R., Labbe, J.C., and Gerhold, A.R. (2021). CentTracker: a trainable, machine-learning-based tool for large-scale analyses of *Caenorhabditis elegans* germline stem cell mitosis. *Mol Biol Cell* 32, 915-930. 10.1091/mbc.E20-11-0716.
- Zhang, J., Zhang, M., Acampora, D., Vojtek, M., Yuan, D., Simeone, A., and Chambers, I. (2018). OTX2 restricts entry to the mouse germline. *Nature* 562, 595-599. 10.1038/s41586-018-0581-5.
- Zhang, N., Zhang, J., Purcell, K.J., Cheng, Y., and Howard, K. (1997). The *Drosophila* protein Wunen repels migrating germ cells. *Nature* 385, 64-67. 10.1038/385064a0.
- Zhang, Q., Vashisht, A.A., O'Rourke, J., Corbel, S.Y., Moran, R., Romero, A., Miraglia, L., Zhang, J., Durrant, E., Schmedt, C., et al. (2017). The microprotein Minion controls cell fusion and muscle formation. *Nat Commun* 8, 15664. 10.1038/ncomms15664.
- Zhou, K., Rolls, M.M., and Hanna-Rose, W. (2013). A postmitotic function and distinct localization mechanism for centralspindlin at a stable intercellular bridge. *Dev Biol* 376, 13-22. 10.1016/j.ydbio.2013.01.020.
- Zimmet, J., and Ravid, K. (2000). Polyploidy: occurrence in nature, mechanisms, and significance for the megakaryocyte-platelet system. *Exp Hematol* 28, 3-16. 10.1016/s0301-472x(99)00124-1.